THE UNIVERSITY
of EDINBURGH

A zebrafish model of demyelination and remyelination

Marja J Karttunen

PhD

University of Edinburgh

2017

I have read and understood The University of Edinburgh guidelines on plagiarism and declare that this thesis is the result of my own work, except where indicated by references. This thesis has been submitted to the University of Edinburgh for the degree of Doctor of Philosophy only.

Marja Karttunen

Lay Summary

Myelin is a fatty layer which surrounds many neurons in the nervous system. In the central nervous system (CNS; brain and spinal cord) myelin is produced by specialised cells called oligodendrocytes. Myelin helps axons relay electrical signals faster and provides them with nutrition. Loss of myelin (demyelination) is associated with damage to neurons, and is seen in many neurological diseases, notably multiple sclerosis (MS). Myelin sheaths can be restored, via a process called remyelination, and this is thought to protect neurons from damage and improve the health of the patients. However, in the later stages of MS, remyelination becomes increasingly inefficient and ultimately fails. It is therefore imperative to develop ways to enhance remyelination in such patients. In order to do so, we must first have a better understanding of how demyelination and remyelination unfold, and what factors affect remyelination.

Our laboratory uses the zebrafish as a model organism to study myelin development, damage and regeneration. At the larval stages, zebrafish are transparent, which enables us to directly observe phenomena such as interactions between cells and effects of drug treatments on cell types of interest. Importantly, zebrafish and humans share much of their genetic and cellular makeup, such that any discoveries made in zebrafish are likely to be relevant in humans.

In order to study the processes of demyelination and remyelination, we have developed a novel genetically manipulated zebrafish line in which we can selectively kill oligodendrocytes with a simple drug treatment, without affecting the overall health of the animal. In this system, two-thirds of all oligodendrocytes are deleted over two days. This leads to demyelination of two-thirds of neurons in the spinal cord approximately one week later. Two weeks after the end of the drug treatment, complete remyelination is achieved.

During the period of demyelination, I observe an increase in microglia and macrophages, cells of the innate immune system, in the spinal cord. This is thought to help clear away the debris left by damaged myelin, and help bring about the regeneration of oligodendrocytes and myelin. In order to further study the role of the

immune system in regeneration, I am using mutant zebrafish which lack microglia and macrophages.

Future studies will use the model I have characterised to address important questions regarding the effects of demyelination on the health of neurons. Moreover, the model can be used in drug screens in which chemical compounds are tested to identify those that can improve myelin repair. Such compounds would represent promising candidates for drug treatments in diseases such as MS.

Abstract

Myelin is a protective layer wrapped around axons which helps them conduct electrical signals rapidly, and provides them with metabolic support. In the central nervous system (CNS), myelin is produced by specialised glial cells called oligodendrocytes. Loss of myelin (demyelination) is associated with degeneration of axons and many neurodegenerative disorders, including multiple sclerosis (MS). The restoration of myelin sheaths by remyelination may protect axons and help functional recovery of patients, but achieving this requires better understanding of how the process unfolds at the cellular level.

To investigate the processes of de- and remyelination *in vivo*, I have characterised a transgenic zebrafish line in which expression of the bacterial enzyme nitroreductase (NTR) is driven under the myelin basic protein promoter, thus in myelinating glia. I treat larvae with the NTR substrate metronidazole (Mtz). The reaction between NTR and Mtz results in a toxic metabolite which selectively kills NTR-expressing cells.

The treatment with Mtz consistently ablates two-thirds of oligodendrocytes while not harming the animals otherwise. Myelin sheaths continue to deteriorate after the end of the treatment, such that seven days later, extensive demyelination is observed by electron microscopy. By 16 days after Mtz-treatment, robust recovery has occurred, with no discernible axon loss and myelin thickness restored to control levels. At this time point, oligodendrocyte numbers have also returned to control levels. During the demyelinated phase, I observe a striking increase in microglia and macrophages in the spinal cord.

In order to study the role of the innate immune system in recovery, I used a mutant line, irf8-/- which lacks a transcription factor essential for development of microglia and macrophages. I am in the process of determining the ability of these mutants to regenerate their oligodendrocytes and myelin; preliminary results suggest that they are able to restore their myelin sheaths fully, but seem to have a delay in regenerating their oligodendrocytes compared to wild-types.

The model I have established can be used in the future to better understand the consequences of demyelination to axon health, as well as chemical screening to

identify compounds that could accelerate the remyelination process or enhance the thickness of myelin generated during remyelination. Insights arising from such studies will be useful in designing strategies to reduce axon loss and improve myelin regeneration in demyelinating diseases.

Acknowledgements

First, I am immensely grateful to my one-of-a-kind supervisor Dave Lyons. Your all-round support from the meanest technical detail to the grandest theoretical concepts is second to none, and your humour, patience, kindness yet cut-to-the-chaseness and astounding intelligence combine to make you a world-class mentor and human being. Thank you so much.

Of course, I must thank the magnificent Lyons lab, past, present and honorary members, for your indomitable cheer and resourcefulness, both in solving scientific problems and hiding from them in the tea room. For the laughs, the rants, the birthday cards, and the cakes (especially the cakes). Truly, I wouldn't have lasted a year without your inexhaustible support and friendship.

I would like to thank Catherina Becker, Charles ffrench-Constant and Dirk Sieger for making the annual thesis committee meetings not only extremely helpful but also stimulating and even enjoyable. I am also grateful to members of the Becker and Sieger labs for fish, reagents and entertaining chats.

A big thanks goes to my past housemates Hannah, Laura F, Laura D, Rikesh and Maria: for the fish and chips, the pizza nights, the countless evenings of TV and movies of varying quality, the quotes and the emergency wine. It's been quite a ride since we first sat on the RS! And you guys, like the RS, have continued to provide solace and a safe haven when the world (lab) got rough.

My family: mum, dad, Erkki, Metsku and Toivo: ette olleet paikalla, mutta olitte läsnä koko ajan. Äidin tekemä seeprakala ja sen varapussi myeliiniä, isän kahvilähetykset, Erkin ”kyllä me sinusta vielä tohtori leivotaan!”– kaikki tämä ja loputon määrä muuta tukea on ollut minulle mittaamattoman arvokasta.

Finally, my partner Will, for keeping me not only fed and watered but also, somehow, sane and happy during the write-up period – thank you. Your support has been unwavering throughout, and I absolutely could not have done this without you. When I'm with you, every day is St Tott's.

Contents

Chapter 1: Introduction

1.1 Why myelin is important

When Aaron Ramsey scored that perfectly timed chip-in goal with the outside of his right foot to win the 2014 FA Cup Final for Arsenal, he was able to display that level of skill because his motor tracts were myelinated.

Indeed, **myelin** is a highly important component of the nervous system. A lipid-rich membrane wrapped spirally around axons, myelin is produced by specialised glial cells called **oligodendrocytes** in the central nervous system (CNS) and **Schwann cells** in the peripheral nervous system (PNS). **Figure 1** below, adapted from Sherman and Brophy (2005), illustrates how an oligodendrocyte wraps myelin around an axon. Although originally myelin was thought to function as little more than a static insulator of axons, not dissimilar to the plastic coating of electric wires, it is now well established that myelin plays a number of crucial roles in the development and function of the nervous system.

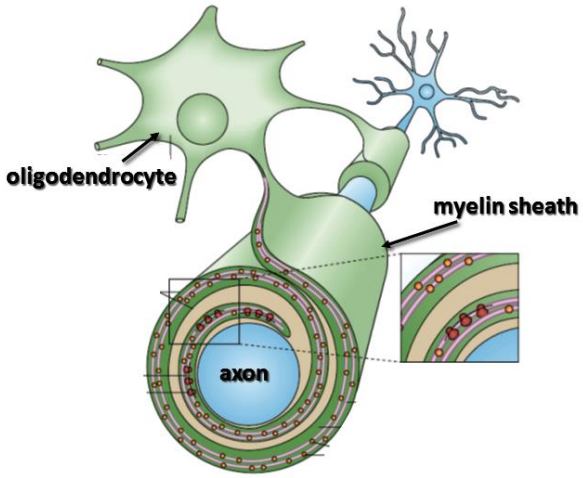

Figure 1. An oligodendrocyte wrapping myelin around an axon.

The first well-characterised role for myelin was that of accelerating the velocity of electrical conduction by axons (Rushton 1951). Without myelin, the principal way axons can increase their conduction velocity is to increase their cross-sectional size (calibre). Since nervous systems of animals are encased within bone, it would not be possible to increase the calibre of large numbers of axons indefinitely. Myelination of axons overcomes this problem by enabling saltatory conduction, whereby the electrical

impulse “jumps” (“*saltare*” being Latin for “to jump”) between segments of myelin, known as internodes. The impulse is propagated by the structures between internodes, called nodes of Ranvier, which are tightly clustered collections of ion channels and other proteins. In this way, saltatory conduction can dramatically increase the conduction velocity of the axon (Nave 2010). It could even be argued that this colossal increase in conduction speed without the necessity of growing the axons to cumbersome sizes is what made the evolution of complex nervous systems possible (Nave 2010).

In addition to enabling saltatory conduction, in recent years it has become abundantly clear that oligodendrocytes and Schwann cells actively communicate with axons throughout life, and play key roles in the maintenance of axon health and integrity (Trapp and Nave 2008). The first evidence that oligodendrocytes may play additional roles above and beyond merely wrapping axons came from studies of knockout mice lacking key myelin proteins. The first of these was a mouse which had been engineered null for proteolipid protein (PLP), a membrane protein thought to stabilise the ultrastructure of CNS myelin. These mice develop normally and assemble compact myelin of thickness appropriate to the size of the axon (Klugmann et al. 1997). However, on further investigation, they were found to display profound axonal abnormalities from six to eight weeks of age, with widespread axonal swellings and degeneration (Griffiths et al. 1998). These swellings were frequently observed in axons wrapped in apparently intact myelin. Notably, similar signs of degeneration were absent from *shiverer* mice, which lack another major myelin protein, myelin basic protein (mbp) and never assemble compact myelin sheaths in the first place (Readhead and Hood 1990). The authors reasoned that the event of becoming myelinated induces in the axon a dependency on support from normal myelinating glia.

Further evidence for this notion came from a study by Lappe-Siefke et al. (2003), who generated a mouse in which the gene encoding 2’,3’-cyclic nucleotide 3’-phosphodiesrerase (CNP), an enzyme found in mature oligodendrocytes as well as non-compacted regions of myelin sheaths was knocked out specifically in oligodendrocytes. CNP-null mice exhibited indistinguishable overall myelin protein patterns (with the exception of CNP) and lipid composition to wild-type controls, and

developed myelin which appeared by electron microscopy to have normal thickness and periodicity at 2.5 months of age. However, from four months onwards, the CNP-null mice began to show ataxia and hindlimb impairments and weight loss. These symptoms were associated with axonal swellings filled with microtubules, dense bodies, multivesicular bodies and mitochondria. Similar to the PLP-null mouse, many axons affected by swelling retained normal-looking myelin sheaths. In neither case was prominent loss of axons reported.

These studies provided compelling evidence that oligodendrocytes are intimately involved in maintaining axonal health and integrity over and above their role in wrapping myelin around axons.

In 2012, landmark papers by Fünfschilling et al. (2012) and Lee et al. (2012) delineated a key mechanism underlying this glial support of axons. The former found that mature oligodendrocytes lacking functional mitochondria were not noticeably affected by this deficit, and reasoned that once they have finished myelinating, oligodendrocytes may rely principally on the non-mitochondria dependent process glycolysis for their energy needs. Glycolysis produces lactate, which was previously known be metabolized by neurons (Pellerin and Magistretti 2012), and was shown to do so in these mice. This observation led the authors to propose an axon-glial metabolic coupling, whereby lactate derived from oligodendrocytes is purposely delivered to axons. Lee et al. supported this idea by specifying the lactate transporter monocarboxylate transporter 1 (MCT1) as the mediator of this coupling, and moreover demonstrated that inhibition of MCT1 resulted in neuronal death (as well as axonal swellings similar to those described previously) *in vitro* and *in vivo*. Recently, Saab et al. (2016) reported a mechanism by which oligodendrocyte lactate production is controlled by the electrical activity of the axon, via NMDA receptor signaling on oligodendrocytes. In this way, glycolysis in oligodendrocytes is matched to the needs of the axon and excessive lactate production is prevented.

Thus, the prevailing view now holds that oligodendrocytes actively “feed” axons. It is not difficult to accept that such an arrangement is necessary, given that axons are often long structures (up to 100cm in the corticospinal tract) and nutritional support from the cell body can be debilitatingly slow to transport to the more distal regions (Nave

2010). It would therefore be much more efficient for the axons to obtain necessary nutrients from the local environment, but the vast majority of the myelinated axon's membrane is, *ipso facto*, covered by myelin, and thus not in contact with the extracellular environment. That oligodendrocytes have been shown to solve that problem by providing nutrition to the axons they ensheath is therefore highly intuitive, and a perfect illustration of the close relationship between oligodendrocytes and axons which is essential to the proper functioning of the CNS (Simons et al. 2014).

It is also worth noting that as well as providing axons with nutrition, myelination also reduces the axon's energy requirement to propagate action potentials. This is because in unmyelinated axons, the maintenance of ion gradients by Na+, K+ -ATPase consumes a large proportion of the available ATP, whereas in myelinated axons axon ion currents are restricted to 0.5% of the axonal space and thus require far less ATP (Nave 2010). This difference in energy needs is reflected in the findings that unmyelinated axons typically contain more mitochondria than myelinated axons in physiological conditions (Barron et al. 2004) and that increased mitochondrial activity is observed in *shiverer* mice (Andrews et al. 2006).

1.2 Myelin is dynamically regulated throughout life

It is now well established that myelination in the CNS continues well into adulthood, possibly throughout life and moreover, far from being static once formed, myelin is a dynamic and malleable structure. This dynamic regulation is powerfully illustrated by evidence for experience-mediated plasticity in the white matter (which consists mainly of myelinated axons); this is emerging from studies finding increases to white matter volume when a new skill such as juggling or a foreign language is acquired (e.g. Scholz et al. 2009; Schlegel et al. 2012; Zatorre et al. 2012) or deficits following social isolation (Makinodan et al. 2012), which can be reversed following social re-integration (Liu et al. 2012). Further evidence for experience-based modulation of myelination comes from a recent study by Etxeberria et al. (2016) which demonstrated that long-term monocular deprivation led to shorter internodes on retinal ganglion cell

axons, which they suggested was the underlying cause of reduced conduction velocity of the optic nerve they observed.

What makes the dynamic nature of CNS myelin possible is the presence of oligodendrocyte progenitor cells in the adult brain (Nishiyama et al. 2014; Scolding et al. 1998). Although it has been known for some time that oligodendrocyte progenitor cells (OPCs) are present in the adult mammalian brain (ffrench-Constant et al. 1986; Nave and Trapp 2008), only in recent years it has become evident how widespread and multifunctional they can be. OPCs account for approximately 5% of all the cells in the adult brain (Pringle et al. 1992; Dawson et al. 2003), and are evenly distributed in every examined region across the CNS. These cells are identifiable by their expression of NG2 and PDGFRα, although their morphologies vary according to brain region (Dawson et al. 2003). Furthermore, OPCs continue to give rise to mature oligodendrocytes throughout adult life (Rivers et al. 2008), while also maintaining a steady population through homeostasis of proliferation, apoptosis and avoiding others (Hughes et al. 2013; Kirby et al. 2006) In fact, OPCs proliferate at surprisingly high rates even in fully myelinated regions such as the optic nerve in a 4-month old mouse (Young et al. 2013), suggesting ongoing myelin sheath remodelling in the adult brain by newly generated oligodendrocytes. This provides a possible mechanism for the experience-mediated white matter plasticity mentioned above. Indeed, a recent study by Yeung et al. (2014) demonstrated ongoing myelination in the adult human brain, mediated by *de novo* generation of new oligodendrocytes (particularly in the prefrontal cortex) as well as continued growth of existing mature oligodendrocytes in the corpus callosum. Furthermore, an interdisciplinary study by Snaidero et al. (2014), combining *in vivo* imaging and advanced electron microscopy indicated that pre-existing myelin sheaths in the adult could be stimulated to grow again upon activation of specific signalling pathways.

Importantly, in recent years, some of the functional roles of the widespread population of OPCs in the healthy brain have become clearer. For example, they have been shown to play crucial roles in learning new skills. McKenzie et al. (2014) report that not only did learning to run on a complex wheel (an apparatus with irregularly spaced rungs) stimulate OPC proliferation and differentiation, but prevention of this by conditional

knockout of the transcription factor myelin regulatory factor (Myrf) in adult OPCs significantly impaired the mice's ability to master the complex wheel. Strikingly, a follow-up study Xiao et al. (2016) revealed that the impairment in the conditional Myrf knockout mice was evident as early as 2.5 hours into training on the complex wheel. This was mirrored by the finding that training on the complex wheel induced production of newly differentiated oligodendrocytes (identified by novel marker Enpp6) within approximately 2.5 hours.

Further support for the notion that the transition of a single oligodendrocyte from premyelinating to myelinating status can be very rapid comes from a live imaging study by Czopka et al. (2013), who found that from the moment an oligodendrocyte extends its first myelin sheath, it has a limited time period of only 5-6 hours in which it initiates the formation of all of its future myelin sheaths. This lends credibility to the idea that OPC-mediated myelin remodelling can underlie the remarkably plastic properties we now know myelin to possess, and underlines the importance of the OPC population in responding to a variety of challenges in adult life (Richardson et al. 2011).

My PhD project will focus on the response of the OPC population to genetically induced oligodendrocyte death and loss of myelin, and explore the ability of this population to enable the regeneration of lost myelin.

1.3 Myelin in disease

Given the multitude of essential functions myelin plays, it is hardly surprising that its loss or damage (**demyelination**) is associated with a number of neurological conditions that afflict the CNS and PNS. These range from developmental diseases of the CNS such as prenatal periventricular white matter injury, which results from vulnerability of immature oligodendrocytes and is a common cause of cerebral palsy (Johnston et al. 2006) to leukodystrophies, which comprise a heterogenous group of inherited diseases where oligodendrocytes fail to either assemble or maintain myelin, resulting in various degrees of disability (Gordon et al. 2014). While leukodystrophies

are rare, two of the most commonly studied of them are Pelizaeus-Merzbacher disease (PMD) and vanishing white matter disease. The former is caused by mutations to the PLP gene which typically results in toxic misfolded proteins, and manifests as various degrees of developmental delay, spasticity and intellectual disability (Gordon et al. 2014). Vanishing white matter disease, on the other hand, is a progressive disorder caused by mutations to the housekeeping gene eIF2B which leads to improper activation of the unfolded protein response and subsequently oligodendrocyte and myelin degeneration, manifesting clinically as severe cerebellar ataxia (Bugiani et al. 2010).

More recently, critical myelin deficits have also been identified in neurodegenerative diseases of the CNS, such as amyotrophic lateral sclerosis (ALS), where abnormal OPC differentiation and reduced myelination were reported both in presymptomatic animals in a mouse model of hereditary ALS and post-mortem samples from ALS patients (Kang et al. 2013). White matter disorganisation is also reported in pre-symptomatic and symptomatic Huntington's disease, as well as a knockin mouse model expressing a mutant form of the huntingtin gene (Fennema-Notestine et al. 2004; Huang et al. 2015). Evidence is also emerging for a role in white matter abnormalities in mental health conditions such as schizophrenia (Najjar and Pearlman 2015) and autism (Deoni et al. 2015).

Here, however, I will focus on multiple sclerosis (MS), as it is the most prevalent non-traumatic neurological condition affecting young adults in Europe and North America, and moreover has a well-established myelin pathology. It is also important to note that several debilitating myelin pathologies exist in the peripheral nervous system, and I will address these in the context of Schwann cell biology in **Chapter 5**.

1.4 Multiple sclerosis

Multiple sclerosis is a disease which affects about one in 1000 individuals in the UK, and 1 in 500 in Scotland (Franklin and ffrench-Constant 2008). Its clinical manifestation can vary greatly between patients, but common symptoms include

muscle weakness, fatigue, vertigo, ataxia, focal sensory loss, muscle spasms, cognitive deterioration and psychiatric disturbances (Love 2006). The clinical picture of MS can also change considerably over the course of the disease within the same individual.

80% of MS patients initially present with a relapsing-remitting disease course, (RRMS) whereby episodes of severe clinical disability alternate with periods of remission and relative health (Compston and Coles 2008). After an interval, which again can vary between individuals but tends to span decades, about 65% of relapsing-remitting MS patients typically deteriorate into a phase of uninterrupted disease progression, (Compston and Coles 2008) termed secondary progressive MS, (SPMS) where recovery from relapses is diminished and clinical disability accumulates. In contrast to RRMS, about 10-20% of patients experience an unremitting disease course, known as primary progressive MS (PPMS) where irreversible neurological deficits accumulate from disease onset (Lassmann 2012; Lassmann et al. 2007). In both of these cases, progression typically commences around 40 years of age (Confavreux et al. 2000). In addition, during transition from RRMS to SPMS, some patients present with new relapses even during continuous clinical deterioration. This variant is referred to as relapsing progressive MS (Lublin and Reingold 1996; Lublin et al. 2014).

MS affects three times as many women as it does men (Compston 2000), and most patients are between 15 and 55 years of age at the time of disease onset (Love 2006). The diagnosis is made on the basis of the array of clinical symptoms but is often aided by laboratory data such as magnetic resonance imaging (MRI) revealing focal abnormalities in white matter (McDonald et al. 2001).

The heterogenous nature of the clinical profile of MS is reflected in the underlying pathology, where MS is characterised by lesions of varied size, shape and number, distributed in varied regions in the CNS, typically cerebral cortex, cerebellar white matter, brain stem, optic pathways and spinal cord, among others (Love 2006). Several different lesion types have been described by pathologists and researchers, but the exact nomenclature and subdivisions between lesion types has yet to reach consensus between researchers (Lucchinetti et al. 2000; Breij et al. 2008; Dutta and Trapp 2014).

However, in broad terms, the lesions can be divided into four main categories (Lassmann et al. 2012):

- *Active demyelinating lesions*: Highly abundant immune cells, both T lymphocytes of the adaptive immune system and macrophages and microglia of the innate immune system. Complex architecture, including zones of phagocytosis, prephagocytosis and often zones of remyelination.
- *Slowly expanding lesions* (also known as *chronic active lesions*): lesion centre is devoid of myelin and shows axon loss. Lesion edge contains microglia and macrophages, often with myelin fragments within them
- *Inactive lesions*. Devoid of myelin, showing profound axon loss. Infiltrates of T cells are rare, and fewer microglia and macrophages are seen than earlier lesion types.
- *Remyelinated lesions, "shadow plaques"*: Areas of regenerated myelin. Levels of inflammation are similar to those in age-matched controls, and axon loss is limited.

The lack of consensus regarding the exact classification of the lesions highlights the complexity of the cellular nature of the disease, whereby different lesions contain different combinations of adaptive immune cells, innate immune cells, dying oligodendrocytes, myelin debris, repaired myelin and intact and degenerating axons. Due to the heterogeneity of both the lesions and the patients at different time points, it has been challenging to define cause-effect relationships between immune infiltration, myelin injury and axon degeneration, and to delineate the cellular correlates for the progression of the disease (e.g. Trapp and Nave 2008; Frischer et al. 2009; Lassmann et al. 2001).

1.5. The role of the immune system in MS

Although the exact mechanisms of the cause of the disease are still being elucidated, the prevailing view of MS aetiology holds, in broad terms, that self-antigens (typically myelin components) bound to major histocompatibility complex II (MHCII) antigen-presenting cells (such as dendritic cells and macrophages) are mistakenly identified as being foreign by reactive T cells. These T cells become activated against the presented self-antigens, cross the blood-brain barrier and infiltrate the CNS where they attack myelin sheaths (Chastain and Miller 2012). Damage is further exacerbated by their expression of inflammatory cytokines and reactive oxygen species, as well as activation of other immune cells, notably B cells, monocyte-derived macrophages and microglia (Münzel et al. 2013). Thus, MS results from an aberrant autoimmune response to myelin antigens. Evidence for this autoimmune trigger for disease has come from a variety of sources, the chief of which I will outline below. (In this section, I will focus predominantly on the role of the adaptive immune system, but I will return to discuss the important role of the innate immune system in **Section 1.10.1**.)

Perhaps the most compelling evidence for an autoimmune basis for MS derives from pathological analyses of MS lesions themselves, in particular those obtained from RRMS patients, where peripheral infiltrates containing clonally expanded CD8+ T cells and, to a lesser extent, CD4+ T cells are consistently found (e.g. Booss et al. 1983; Gay et al. 1997; Lucchinetti et al. 2000; Lassmann et al. 2007). In addition, macrophages and microglia containing myelin debris are frequently seen in MS lesions (Lucchinetti et al. 2000).

Furthermore, several studies have reported that myelin antigens, including MBP and PLP, are present in the cervical lymph nodes of MS patients, contained within macrophages (Fabriek et al. 2005; de Vos et al. 2002). Importantly, the myelin antigens were located directly juxtaposed to T cells, suggesting that T cell priming against myelin antigens could occur in the lymph nodes (de Vos et al. 2002).

Some of the early evidence for the role of the immune system in MS came from genetic studies. MS has a genetic component: while the risk to the general public in Europe and North America is approximately 0.1%, this rises to 2-3% if one has a parent with

MS (Compston 1999). Monozygotic twins have a concordance rate of 25%, compared to 5% in dizygotic twins (Willer et al. 2003). This familial increase in risk suggests that it is possible to inherit a susceptibility to acquire MS.

From the earliest studies in the 1970s (Jersild et al. 1972) to recent times, the only genetic locus consistently associated with MS was that of the major histocompatibility complex, (Oksenberg et al. 2004) implying that dysregulation of the immune system conferred increased risk of acquiring MS. However, the list of candidate loci has expanded exponentially in the last decade, since the sequencing of the human genome made it possible to undertake large-scale genome-wide association studies (GWASs). As an example, Sawcer et al. (2011) carried out a GWAS involving over 9,000 cases of MS patients of a similar ethnic background, and reported 29 novel susceptibility loci (albeit all with effect sizes smaller than those associated with MHC). Among these, genes that influence T cell proliferation and maturation were disproportionately represented. The authors concluded that such an overrepresentation strongly suggests that the critical disease mechanisms involve immune dysregulation.

Thus, while the above is by no means intended as a comprehensive review of the evidence that MS involves an autoimmune attack on the CNS, it serves to highlight the breadth of investigations which all point to a profound role of the adaptive immune system in MS. Indeed, all of the currently available treatments for MS act to suppress the activity of the adaptive immune system in one way or another.

1.6. EAE as a tool for developing drug treatments for MS

Instrumental in the development of many current treatments for MS has been the widely used animal model known as experimental autoimmune encephalomyelitis (EAE; Baxter 2007). In this model, rodents are inoculated with myelin antigens (typically parts of myelin oligodendrocyte protein MOG or myelin basic protein MBP) which induces an autoimmune attack on the CNS. Although wide variation exists, depending on factors such as the specific myelin component chosen, the strain of

rodent used, in broad terms EAE induces a relapsing-remitting disease characterized by T cell infiltration in the CNS, which results in demyelinated lesions and neuronal damage (Robinson et al. 2014). Given the premise that MS is likely driven by an autoimmune attack of myelin, numerous researchers have used the broadly similar phenotype of EAE to study the cellular and molecular basis of the disease process. From such studies, a plethora of factors to alter the course and severity of EAE have been identified. Indeed, all currently approved MS treatments have been tested on EAE at some point during their development (Kremer et al. 2015).

In order to illustrate how EAE has been used to discover and test treatments for MS, I will briefly describe the development of the drug glatiramer acetate. Glatiramer acetate, a random copolymer, was encountered serendipitiously by a group of researchers at the Weizmann institute in Israel, investigating the immunological properties of synthetic polymers and copolymers which presented with similar amino acid structure as MBP. The researchers reasoned that such a polymer should induce EAEv, but instead, they found that their polymers were protective against EAE (Teitelbaum et al. 1971) The most effective of these was Copolymer 1, now referred to as glatiramer acetate; preclinical research showed that, unlike most modifiers of EAE, it was capable of ameliorating EAE in several mouse strains, guinea pigs, rabbits and two kinds of monkeys (Teitelbaum et al. 1997). The mechanism of action of glatiramer acetate was thought to be stimulation of suppressor T cells and inhibition of MBP-activated T cells. Clinical trials showed glatiramer acetate to be well tolerated (for at least two years) and to moderately but significantly reduce the rate of relapses compared to placebo (Bornstein et al. 1987; Johnson et al. 1995; Johnson et al. 1998).

The drug became licenced in 1996 in the USA and in 2001 in the EU (Johnson 2014) but studies continued to elucidate its mechanism of action. Reviewed by Aharoni (2013), glatiramer acetate ameliorates EAE in a multitude of ways, including competition for the binding of antigen presenting cells, antagonism of particular T-cell receptors and biasing several classes of immune cells towards anti-inflammatory responses.

Several similarly immunomodulatory drugs are currently in use, and I have summarised them in the table below.

Table 1.				
Drug name	**What it does**	**Status**	**Does it affect disease progression?**	**Recent reference**
Beta-interferons	Inhibits T cell proliferation, shifts cytokine production towards anti-inflammatory, reduces migration of immune cells across blood brain barrier	In use in UK	No evidence to date	(Dhib-Jalbut and Marks 2010) (Ziemssen et al. 2015)
Glatiramer acetate	Reduces antigen presentation and stimulates T cell secretion of anti-inflammatory cytokines	In use in UK	Currently being trialled for slowing disease progression and enhancing remyelination	(Aharoni 2013)
Natalizumab	α4 integrin antagonist. Prevents T cells from crossing blood brain barrier	In use in UK	No; clinical trial failed to show significant effect on primary or secondary endpoints	(Rudick et al. 2006); NCT01416181
Fingolimod	Prevents T cells from exiting lymph nodes	In use in UK	Currently being trialled for slowing disease progression	(Mantia et al. 2016)
Daclizumab	Suppresses T cell activity via activation of natural killer cells	In trial	No evidence to date	(D'Amico et al. 2015)
Teriflunomide	Pyrimidine synthesis inhibitor; has anti-proliferative and anti-inflammatory effects	Approved by FDA and European Medical Agency	Trials continue to test effects on relapses and disease progression	(He et al. 2016)
Laquinimod	Inhibits T cell infiltration within CNS	In trial	Currently being tested for reducing relapses as well as	(Thöne and Linker 2016)

			slowing disease progression	
Alemtuzumab	Destroys lymphocytes	In use in UK	Currently being trialled for slowing disease and remyelination	(Willis and Robertson 2016)
Dimethyl fumarate	Immunomodulatory; exact mode of function unknown	In use in UK	Trial for slowing disease and remyelination was stopped.	(Linker and Haghikia 2016; A. Williams (pers.comm.)

Thus, EAE has played a role in the development of a variety of the immunomodulatory drugs currently available for the treatment of MS. However, as (Vesterinen et al. 2010) point out, it is worth noting that many studies using EAE have not been optimally designed, for instance commencing drug administration at the same time as EAE induction. In such cases, the intervention may lower the severity EAE symptoms by preventing the disease from developing fully in the first place, rather than alleviating an existing disease. It is not clear how such a drug could be beneficial to patients in whom MS has already developed, and regrettably it is not currently possible to identify MS patients prior to the onset of the disease. With this in mind, it is imperative to always evaluate results from EAE studies with great care (Vesterinen et al. 2010).

1.7. Current MS treatments do not affect the progressive stage of the disease

The above described immunomodulatory treatments are often successful at reducing the rate of relapses during RRMS (Clegg and Bryant 2001). However, the evidence for their efficacy in altering disease progression is extremely limited (Vesterinen et al. 2010) and none of the treatments currently in use are targeted at repairing the damage already inflicted (Miron et al. 2011; Williams 2015). As a result, most patients still proceed to the progressive phase of the disease, where immunomodulatory treatments have proven ineffective (Vesterinen et al. 2010). Interestingly, one EAE study reported that even complete elimination of clinical relapses after only one relapse is insufficient to prevent long-term neurodegeneration (Hampton et al. 2013).

What, then, causes the progression of clinical disability? In the last few decades, the consensus has arisen that the primary cause of disability during the relapsing-remitting phase is inflammation and the consequent demyelination, but that in the progressive phase, axonal damage is the major cellular substrate for accumulating clinical disability (e.g. Kuhlmann et al. 2002; Lassmann et al. 2001; Franklin et al. 2012).

Axon pathology is observed in both early and late MS lesions, but is found at much higher levels in actively demyelinating lesions than chronic inactive demyelinated lesions (Ferguson et al. 1997; Trapp et al. 1998; Kornek et al. 2000; Kuhlmann et al. 2002). This pathology of axons, typically demonstrated as increased staining for amyloid precursor protein (APP) or SMI-32, is always concomitant with demyelination, evident from reduced myelin staining and appearance of myelin particles within macrophages. However, while axon pathology may not be a major feature of chronic MS lesions, *loss* of axons seems to be associated with the progressive stage of the disease: a number of longitudinal brain imaging studies in humans have revealed significant positive correlations between extent of axon loss and scores on the EDSS clinical disability scale (de Stefano et al. 1998; Ge et al. 2000). Indeed, using post-mortem tissue from severely disabled (paralysed) patients, Bjartmar et al. (2000) demonstrated a mean 68% loss of axons in the spinal cords of MS patients compared to healthy controls. In a review in 2012, Lassman and colleagues note that

diffuse global tissue injury is more pronounced in progressive than relapsing-remitting MS.

Related to the pathology of demyelinated axons is the common observation of increased mitochondrial content within axons in demyelinated lesions (Mahad et al. 2009; Witte et al. 2009). It is thought that, much like the increased mitochondrial content in *shiverer* mice which lack compact myelin, axons upregulate their mitochondria in order to meet the elevated energy needs associated with not being myelinated. However, the increased mitochondrial content may not remain adaptive; mitochondria dysregulation and damage are associated with axonal degeneration (Dutta et al. 2006; Trapp and Stys 2009).

Bearing in mind the evidence presented in **Section 1.1**., detailing the pivotal role myelin plays in maintaining axonal health and integrity, it is not surprising that demyelination in MS lesions can lead to drastic adaptations and ultimately pathology and loss of axons. However, very importantly, the reverse logic also holds true – that *re*generation of myelin may *prevent* axon damage and loss. Indeed, as alluded to above, another prominent feature of post-mortem MS brains is the presence of **remyelination** – that is, the restoration of myelin sheaths onto naked axons. This is evident as focal, sharply demarcated areas of lighter myelin staining that surround normal-appearing white matter, known as shadow plaques (Lassmann 1983). Evidence for remyelination is observed in MS tissue of all ages and disease phases, although partial remyelination on the rim of lesions is more common than shadow plaques (Prineas and Connell 1979). In some cases, remyelination can be extensive: Patani et al. (2007) report that in two patients who had been suffering from MS for over 20 years, 95% of the lesions examined were fully or partially remyelinated (22% and 73%, respectively). Crucially, remyelination is associated with a more favourable outcome for patients with MS: Patrikios et al. (2006) found that patients who died older (i.e. survived longer) had more shadow plaques that those who died younger. Furthermore, shadow plaques are associated with minimal axon pathology compared to demyelinated lesions (Kornek et al. 2000; Kuhlmann et al. 2002).

Thus, remyelination appears to have protective effects on the axons and be associated with an improved outcome for the patients. This stands to reason, given that

remyelination presumably restores saltatory conduction as well as the oligodendrocyte-mediated nutritional support to axons. In addition, being ensheathed in myelin likely protects axons from bystander immune mediated damage (Patani et al. 2007). In this way, remyelination is considered a highly desirable outcome for MS patients, and promoting this endogenous process presents an attractive therapeutic goal alongside existing immunomodulatory therapies.

Remyelination restores compact myelin to axons, but does not achieve the relationship between axon circumference and myelin circumference (g ratio) that is normally observed; newly generated myelin sheaths are thinner than those seen on never-demyelinated axons (Blakemore 1974). Another well-known feature of remyelination is that the newly generated internodes tend to be shorter than those found in controls (Blakemore and Murray 1981). The mechanistic basis for these differences remain to be understood, but in any case they do not seem to prevent remyelination from restoring normal conduction velocity to axons (Smith et al. 1979 – discussed in greater detail below).

Remyelination, like developmental myelination, can be carried out by oligodendrocytes. Remyelination is thought to occur via *de novo* differentiation of oligodendrocytes, rather than regrowth of myelin from pre-existing oligodendrocytes. This is based on the findings that mature oligodendrocytes do not seem capable of generating new myelin sheaths (Crawford et al. 2016), although the possibility that oligodendrocytes could exhibit unexpected behaviours in pathological circumstances cannot yet be categorically ruled out.

Remyelination is made possible by the presence of oligodendrocyte progenitor cells in the adult CNS. As detailed above in **Section 1.2.**, OPCs are a highly active population, distributed across the brain (Dawson et al. 2003) and capable of giving rise to new oligodendrocytes throughout life (Rivers et al. 2008). In fact, numerous studies have reported finding OPCs present either within or close by demyelinating MS lesions (Scolding et al. 1998; Wolswijk 2002; Maeda et al. 2001; Chang et al. 2002). Furthermore, a fate-mapping study in an experimental model of demyelination specified that the newly arising oligodendrocytes indeed derive from OPCs (Zawadzka et al. 2010). Intriguingly, the same study also showed that OPCs can also give rise to

myelinating Schwann cells. In the healthy nervous system, Schwann cells are normally associated with myelinating peripheral nerves, but they have previously been shown to also carry out remyelination in the CNS of MS patients and EAE mice (Snyder et al. 1975; Itoyama et al. 1983).

Thus, the adult CNS demonstrably possesses the *capacity* for remyelination. However, remyelination tends to become increasingly inefficient in MS patients as the disease progresses (Goldschmidt et al. 2009) which is thought to directly contribute to the progressive loss of axons and accumulating clinical disability, as discussed above. The reasons for the failure of remyelination over time are likely to be manifold and involve a complex interplay between the OPCs and the lesion environment (Franklin 2002). It is of the utmost importance to understand why remyelination fails in MS, if we are to overcome this failure and promote remyelination as a therapy (Franklin and ffrench-Constant 2008). However, it is extremely difficult to extrapolate clear conclusions using information from MS lesions alone, owing to their heterogenous nature and the multitude of cell types found within them (T cells, macrophages, microglia, astrocytes, oligodendrocytes, OPCs, axons). MS lesions constitute a snapshot representing a single time point, with no certainty as to how old the lesion is or in what order the cell types found within it arrived and how the cellular composition of the lesion may have changed over time. This makes it extremely difficult to disentangle the effects that the cell types may have on one another, or what cell type might be prominent in what phase of disease (demyelination or remyelination).

Similarly, EAE is not an ideal system for detailed studies on how remyelination occurs and fails, since demyelination and remyelination often occur simultaneously, and always against a backdrop of vicious inflammation (Dubois-Dalcq et al. 2005). This makes it very difficult to determine whether any given therapy acts by lessening demyelination, rendering the lesion environment less hostile to remyelination, or genuinely enhances the process of remyelination. Moreover, the widespread presence of the induced inflammation in EAE can mask any beneficial effects of the innate immune system, potentially giving rise to mistaken conclusions that inflammation is purely destructive to myelin (McMurran et al. 2016).

Finally, many observers have reported that the hyperactive inflammation associated with EAE can directly injure axons even in the absence of demyelination (Nikić et al. 2011). Although it is possible that such injury occurs in MS as well as EAE, this further blurs the line between cause and effect and renders EAE a patently unsuitable system for modelling the relationship between demyelination and axonal damage, or remyelination and axonal protection.

For these reasons, additional animal models of demyelination and remyelination are required. Simpler models where demyelination, remyelination and the presence of the immune system can be disentangled can prove invaluable for understanding demyelination and remyelination in and of themselves, and this information can subsequently be used when studying these processes in an inflammatory context such as EAE or MS. A thorough understanding of the reciprocal interactions between demyelination, the immune response and remyelination is essential for developing novel remyelinating therapies to work efficiently alongside existing immunomodulatory treatments.

Not surprisingly, then, several highly relevant models have been developed and used to great effect to learn more about demyelination, remyelination and the impact the immune system has on these. In the sections below, I will describe the key models and the insights that have been gleaned from them.

1.8. Toxin-based models of demyelination and remyelination, and what we have learned from them

Some of the most informative models of de- and remyelination have been focal toxin-based models, whereby a chemical is stereotaxically injected into a chosen location within the CNS to specifically destroy glia and myelin, and ideally leave the axons intact (Blakemore and Franklin 2008). A slightly different but widely used toxin is cuprizone, which is systemically introduced into the animals within their chow. I have summarised the most commonly used gliotoxins in the table below.

Table 2.			
Name (mode of action)	**Method of delivery**	**Pattern of lesions**	**Timeline and nature of remyelination**
Lysolecithin (membrane solubilising agent) Also known as lysophosphatidyl choline, LPC	Stereotaxic injection	Single lesion in location of choice: typically in dorsal funiculus of the spinal cord, cerebellar peduncle or corpus callosum.	At 14 days post lesion (dpl), small patches of remyelination are evident but restricted to lesion edges. At 21dpl, increased patches but still chiefly on edges. At 6 weeks post-lesion, extensive remyelination, predominantly by oligodendrocytes.
Ethidium bromide (DNA intercalating agent)	Stereotaxic injection	Single lesion in location of choice: often caudal cerebellar peduncle or dorsal funiculus	At 14dpl, only rare signs of remyelination. At 6 weeks, a significant proportion of axons remains demyelinated. Oligodendrocyte remyelination is restricted to rim, some Schwann cell remyelination near the core. Some axons remain demyelinated even at 3.5 – 6 months post lesion.
anti-galactocerebroside with complement (antibodies against major sphingolipid myelin constituents)	Stereotaxic injection	Single lesion, typically in dorsal funiculus of the spinal cord, cerebellar peduncle or corpus callosum	Some discrete patches of oligodendrocyte remyelination at14d pl. At 6 weeks, most lesions resembled ethidium bromide lesions, albeit with less Schwann cell remyelination. At 8 weeks, all lesions are extensively remyelinated, predominantly by oligodendrocytes.
Cuprizone (copper chelator)	Systemic; fed to animals in within their food	Multifocal: typically corpus callosum, internal capsule, thalamus white matter, cerebellar peduncles.	Cuprizone is fed for five weeks. Signs of demyelination appear at 3 weeks post-lesion, and remyelination from 5 weeks (some observed earlier). Schwann cell remyelination is rare. Recent adaptations to protocol include co-treating with rapamycin to inhibit concurrent remyelination and feeding cuprizone for 12 weeks.

References: (Woodruff and Franklin 1999; Blakemore and Franklin, 2008; Matsushima and Morell 2001; Blakemore 1972; Sachs et al. 2014; Bai et al. 2016)

The focal toxin models and cuprizone share the advantage of causing primary oligodendrocyte and myelin loss, whereby the death of oligodendrocytes and degradation of myelin are achieved without involvement of the adaptive immune system. This has allowed researchers to study remyelination and its requirements and consequences in a relatively isolated environment (Blakemore and Franklin 2008).

Studies using focal toxin-induced demyelination have been instrumental in establishing that remyelination is indeed beneficial for the function and health of demyelinated axons. In one of the first indications of this, Smith et al. (1981) demonstrated that action potential conduction was blocked in LPC-injected cats during the demyelinated phase, but restored to levels comparable to control animals by spontaneous remyelination. Later, Jeffery and Blakemore (1997) showed that ethidium bromide -injected rats exhibited motor deficits while walking on a narrow wooden beam, but that these deficits were corrected by spontaneous remyelination. If remyelination was prevented by use of X ray irradiation, the motor performance of the rats did not recover.

It also seems that remyelination attenuates the elevated energy requirements of demyelinated axons: Zambonin et al. (2011) found the mitochondrial content of remyelinated axons to be significantly lower than that of demyelinated axons following lysolecithin and ethidium bromide -induced lesions (albeit still higher than that of never-demyelinated axons). This suggests that demyelination prompted the need for additional energy supplies within the axon, and that this was at least partially alleviated by remyelination. Restoring the axon's energy production to levels approaching normal is extremely important since, during energy shortages, the Na^+ /K^+-ATPase sodium pump which maintains the axon's membrane potential can become underpowered and result in an influx of sodium ions. Such a sodium influx is particularly likely to occur in demyelinated axons, where sodium channels are distributed far more extensively than in myelinated axons. Accumulating levels of sodium ions within an axon may result in dysfunction of the sodium-calcium exchanger, causing importation of dangerous concentrations of calcium ions, and ultimately trigger axon degeneration (Craner et al. 2004; Trapp and Stys 2009; Franklin et al. 2012). Thus, remyelination can protect the axon by preventing the

energy shortage from developing in the first place, and reclustering sodium channels at nodes of Ranvier (which is regularly seen following remyelination in toxin-based models (Zhang et al. 2011; Kaya et al. 2012).

Compelling evidence that remyelination protects axons from degeneration comes from a study by Irvine and Blakemore (2008). They demonstrated that if remyelination was prevented (again by means of X-ray irradiation) in cuprizone-demyelinated aged mice, significantly more axons underwent degeneration than if spontaneous remyelination was allowed to proceed. Importantly, axonal degeneration was prevented in the X-irradiated mice by transplantation of OPCs which remyelinated the denuded axons. This key experiment further underlines the concept that oligodendrocytes and myelin are integral fjor axonal health and survival. Moreover, the demonstration that spontaneous remyelination can indeed protect axons from degeneration strengthens the foundation of the pursuit of remyelination as a neuroprotective therapy for MS. Since the human brain does possess the capacity for remyelination in MS, promotion of remyelination may be a more attainable goal than protection of the axons directly, although studies aiming to directly protect axons in MS are being pursued (Franklin et al. 2012), but will not be dealt with in detail here.

1.9. How to promote remyelination?

Thus, data emerging from toxin-based models of demyelination clearly indicate that remyelination restores conduction and function to demyelinated axons, may aid in reducing their energy needs, and, crucially, protects them from degeneration. Naturally, with this in mind, considerable effort has been exerted by the research community to identify factors that can be used to enhance endogenous remyelination.

In order to enhance remyelination, it is helpful to understand why it tends to fail in MS. While a plethora of factors associated with the lesion environment certainly plays a key role (as I will discuss below), much focus has been on the behaviour of the OPCs. The failure of remyelination can be broadly divided into two branches: failure of OPC *recruitment* (including proliferation and migration to lesion sites) and failure of OPC

differentiation (Franklin and ffrench-Constant, 2008). As discussed above, OPCs are frequently found in MS lesions, suggesting that their failure to differentiate into mature myelinating oligodendrocytes could be the primary deficit. On the other hand, a quantitative study estimated that in about 30-37% of lesions, OPCs were rare or absent, (Lucchinetti et al. 1999; Boyd et al. 2013) arguing that recruitment failure can also play a part in remyelination failure. Indeed, studies have shown that overexpressing Sema3F or downregulating Sema3A *in vivo* can increase OPC recruitments and subsequently enhance remyelination following LPC-induced demyelination (Piaton et al. 2011; Boyd et al. 2013).

In addition, there is also some evidence that some OPCs differentiate into mature oligodendrocytes yet still fail to initiate remyelination of the naked axons. For instance, Kuhlmann et al. (2008) observed mature NogoA-expressing (i.e. mature) oligodendrocytes in both active and chronic MS lesions, positioned adjacent to demyelinated axons, and Lindner et al. (2015) reported MBP-expressing (i.e. mature) oligodendrocytes interacting with axons but failing to assemble myelin sheaths in active MS lesions.

However, it is difficult to ascertain whether these were newly generated or pre-existing mature oligodendrocytes.

Thus, the failure of OPCs present in the CNS to become functional myelinating oligodendrocytes may occur at any stage during OPC lineage progression. Consequently, it is important to understand the molecular signals that regulate every aspect of oligodendrocyte development, as molecules shown to affect oligodendrocyte recruitment, differentiation and myelination could be pharmacologically targeted to enhance the lineage progression and ultimately remyelination.

The literature covering research on signals that regulate developmental myelination and remyelination is vast. Hundreds of researchers have worked on the topic for several decades, and much fundamental knowledge has been accumulated. This literature has been extensively reviewed by numerous authors, including, but by no means limited to, Emery (2010); Fancy et al. (2011); Kotter et al. (2011); Emery and Lu (2015); Mathews and Appel (2016). For the purposes of this Introduction, I will

simply conclude that the wealth of knowledge garnered regarding the molecular mechanisms of developmental myelination has greatly informed the study of the molecular mechanisms of remyelination; indeed, it seems that much of remyelination constitutes a recapitulation of the process of developmental myelination (Fancy et al. 2011). Very importantly however, it is also clear that fundamental distinctions exist between remyelination and developmental myelination, particularly with regard to the role of the innate immune system in clearing myelin debris and creating a molecular environment conducive to remyelination (to be discussed in detail below).

However, it is important to keep in mind that despite our increasing knowledge of the molecular signals governing oligodendrocyte development, myelination and remyelination, the path from being a promising new molecule found to affect oligodendrocyte development to being a viable drug candidate for use in promoting remyelination in MS patients is not always straightforward. Here I will take the opportunity to describe in detail the progression of one molecule, LINGO-1, from being discovered as a regulator of myelination/remyelination, through to an antibody designed to inhibit its function, to being tested as a possible treatment for MS. With this section, I hope to illustrate both the power of combining multiple animal models of MS for testing potential therapeutic targets, as well as how far we still have to go to develop approved and functional regenerative therapies for MS.

LINGO-1 (leucine-rich repeat and immunoglobulin-like domain-containing nogo receptor-interacting protein 1) is a membrane protein expressed by both neurons and oligodendrocytes. It was originally discovered by scientists at Biogen Idec who were studying the ways in which CNS myelin inhibits regrowth of transected CNS axons. Specifically, they were investigating a pathway consisting of myelin components (MAG and OMgp) which, when interacting with a receptor complex on neurons (comprising the Nogo-66 receptor and the p75 neurotrophin receptor), was known to inhibit neurite outgrowth, an effect mediated by RhoA). They found that the coexpression of Nogo-66 and p75 on non-neuronal cells was insufficient to activate RhoA, implying that other proteins are involved in its activation on neurons. It was while surveying several uncharacterised CNS-specific proteins for their ability to bind the Nogo-66 receptor (NgR1) that they discovered LINGO-1 and found it to function

as a part of the NgR1 complex (Mi et al. 2004). LINGO-1 was found to be present in all CNS areas examined, and more strongly in neonatal than adult brains (peaking at P1, but still present at P7). Together with NgR1 and the p75 receptor, LINGO-1 could activate RhoA when transfected onto non-neuronal cells. When a dominant-negative version of LINGO-1, lacking the cytoplasmic domain thought to mediate signalling, was transfected onto neurons, the inhibitory effect of myelin components on neurite outgrowth was abolished. The authors concluded that they had identified a novel protein important in regulating CNS function (Mi et al. 2004).

Knowing that LINGO-1 was involved in regulating the RhoA pathway, and that the RhoA pathway had previously been linked with oligodendrocyte differentiation (Liang et al. 2004), Mi et al. (2005) turned their attention to investigating the role of LINGO-1 in oligodendrocyte differentiation and myelination. They reported that LINGO-1 was expressed on mature oligodendrocytes, and that reducing endogenous LINGO-1 expression using a RNAi or lentiviral delivery of the dominant-negative LINGO-1, promoted oligodendrocyte differentiation *in vitro*. In the same vein, they found that inhibiting LINGO-1 by exogenous addition of specially manufactured antibody LINGO-1-Fc caused a dose-dependent increase in myelination in oligodendrocyte and neuron co-cultures. Finally, they generated global LINGO-1 knockout mice and observed an early onset of myelination in the spinal cords of knockout mice at postnatal day 1, in comparison to wild-type littermates, where myelination commenced around postnatal day 5.

Having demonstrated *in vitro* and *in vivo* that LINGO-1 is a negative regulator of oligodendrocyte differentiation and myelination, Mi et al. (2007) took the next step in guiding LINGO-1 towards becoming a treatment for MS, and tested how its regulation might affect disease course in EAE. This represented a novel challenge, as the interactions between LINGO-1 and components of the immune system had not previously been characterised.

To test the effects of blocking LINGO-1 function on EAE, they initiated MOG-induced EAE in the global LINGO-1 knockout mice. In the first instance, they used only the EAE score, which quantifies disease progression by measuring motor dysfunction, as a surrogate indicator of demyelination. Both wild-type and LINGO-1

knockout mice developed EAE symptoms, but the clinical score remained significantly lower in the knockouts throughout the experiment (Mi et al. 2007).

In order to exclude the possibility that the LINGO-1 knockout exerted its protective effects by modifying the generation and infiltration into the CNS of T cells, they isolated T cells from wild-type and LINGO-1 knockout mice following MOG immunization and measured their proliferation efficiency and ability to release cytokines (IL2, IL-4, IL-5, IL-6, IL-10, IL-13, IL-17, TNF-α, IFN-γ and granulocyte monocyte colony stimulating factor); these were not found to differ. In addition, MOG-immunized T cells which were adoptively transferred from knockout mice into wild-type mice induced EAE as normal, but T cells adoptively transferred from wild-type to knockout mice induced a markedly reduced EAE phenotype. This suggested that the LINGO-1 knockout did not affect the activity of the adaptive immune system.

Ultrastructural analysis of the demyelinated lesions indicated that the lower EAE scores did indeed correspond to fewer non-myelinated axons in the knockout animals. Since they do not say what time point the EM images represent, however, it is difficult to know whether this reflects increased remyelination or decreased demyelination. There are some thin myelin sheaths present in the knockouts, but so too are there several thickly myelinated large-calibre axons, suggestive of never having been demyelinated at all (Ludwin and Sternberger 1984).

Next, Mi et al. treated EAE mice with anti-LINGO-1 antibody, which was designed to bind specifically to LINGO-1 and block its function. They began local delivery of the antibody by osmotic pump at 3d after EAE induction and continued this for 36 days. At the end, they found the antibody treatment to significantly mitigate disease severity across all stages, as indicated by the EAE scores. Bolstered by this, they administered the antibody to animals already displaying EAE symptoms. After a two-week treatment, the anti-LINGO-1 treated animals showed lower EAE scores than controls. Importantly, the disease did not seem to be worsening at all in the antibody-treated group, but appeared stabilised.

Mi et al. next used diffusion tensor imaging (DTI) to assess axon function and integrity, which they assumed to be improved in the anti-LINGO-1 treated mice, given

their lessened EAE scores. DTI is an imaging technique based on the differential speed of water molecule diffusion through different tissues and is increasingly used to assess white matter changes in human neurological patients (Soares et al. 2013). The fractional anisotropy values were lower in control antibody-treated EAE mice, correlating with the demyelinated areas seen by toluidine blue staining. By contrast, high fractional anisotropy values were seen in anti-LINGO-1 treated EAE mice and control non-EAE mice, consistent with normal-looking histology. Indeed, increased luxol fast blue staining was seen in anti-LINGO-1 treated EAE mice compared to control antibody treated EAE mice. Furthermore, electron microscopy revealed many more thinly wrapped (presumably remyelinated) axons in anti-LINGO-1 treated EAE mice compared to control treated EAE mice.

In order to test whether LINGO-1 antagonism could enhance remyelination in established models of demyelination in the absence of adaptive immune system, Mi et al. (2009) administered the anti-LINGO-1 antibody to LPC-injected rats three days post-injection, (dpi) and at 7dpi saw an increase in mature oligodendrocytes in the lesions, accompanied by much smaller lesions than controls and more remyelinated axons by electron microscopy. This antibody-mediated improvement was abolished in the LINGO-1 knockout mouse. They also showed that lentiviral administration of DN-LINGO three days after LPC injection improved conduction velocity at 4 weeks post LPC, compared to control groups, which they attributed to the thicker myelin sheaths seen in the treated group (although DN-LINGO-1 treated animals do not reach control levels). Finally, they also found more myelinated axons following cuprizone intoxication, when anti-LINGO-1 antibody was administered at 2.5 and 3 weeks from start of cuprizone intoxication (Mi et al. 2009).

Following the success of LINGO-1 antagonism in improving remyelination in a variety of animal models of MS, a Phase I clinical trial called SYNERGY was launched in 2010. This was a randomised double-blind placebo-controlled study in which healthy human volunteers received a single-ascending dose of the antibody or a placebo and seven separate groups of RRMS patients received increasing doses of the antibody (or placebo) – each group receiving one dose, which was higher than that received by the previous group and found to be safe. After six months, safety,

tolerability and pharmacokinetics were assessed in all groups. The phase I concluded that the antibody was safe and well tolerated, and accordingly, the drug proceeded to Phase II trials (Mi et al. 2013).

The Phase II trials began in 2013. Four doses (3, 10, 30 and 100 mg/kg) were trialled, and both RRMS and SPMS patients were examined. The results of these Phase II trials have only become public in June 2016, and stated that the drug had missed its primary endpoint; that is, the treatment failed to improve physical or cognitive function in patients (Biogen website; MS Society website).

The full details of the Phase II trials are not yet available to the public, but Biogen have given assurances that they are still pursuing LINGO-1 as a remyelinating therapy for MS, and that some of the data from the Phase II trials indicate that the anti-LINGO-1 treatment increases conduction velocities as measured by visually evoked potentials, suggesting that the drug may promote remyelination (D. Lyons, personal communication). However, until the full details of the trial are made public, it is not possible to evaluate its success further.

In conclusion, then, LINGO-1 has been a promising novel candidate for a remyelinating therapy for MS, but unfortunately, has thus far not succeeded at achieving its main objective of improving the condition of MS patients.

Many factors may account for this apparent failure. Clinical trial design is a complicated issue, where the choices of the correct patient groups and outcome measures are key. Given the extremely heterogenous nature of MS, where patients with widely varying clinical profiles at the starting point display widely varying clinical progression over time, it is difficult to define a standard set of parameters demonstrate overall improvement in remyelination of the group. Human brain imaging using magnetic resonance imaging and DTI are often employed to obtain a measure of the deterioration and repair present in the patients' white matter. However, these techniques, although constantly improving, are not yet at a level where the degree of remyelination of individual lesions can be quantified in detail. Thus, subtle improvements in remyelination may be missed.

In addition, it is possible that the LINGO-1 antibody did not penetrate the blood-brain barrier sufficiently, limiting its availability in the CNS to ineffective quantities. Conscious of this potential pitfall, the conductors of the clinical trial attempted to overcome this problem by giving very high doses of the anti-Lingo antibody, and they did detect the antibody in the cerebrospinal fluid of the participants, suggesting that at least some antibody had entered the CNS. Nevertheless, it is difficult ascertain what an effective concentration in the CNS of human patients may be, so it is possible that the blood brain barrier penetration was insufficient (Mi, personal communication, 2013).

One general way to circumvent the problem of the blood-brain barrier permeability may be to load therapeutic molecules under trial into nanoparticles with surface-bound ligands which can be employed to target the nanoparticles to specific cells, in the case of Lingo, in principal OPCs. This would provide local high concentrations of the therapeutic cargo, and, equally importantly, avoid off-target effects outside of the CNS. This strategy was successfully employed in animal models by Rittchen et al. (2015) who used NG2-tagged nanoparticles to deliver leukemia inhibition factor (LIF), a known pro-remyelinating factor, to OPCs. Following LPC-induced demyelination of the corpus callosum, injection of targeted LIF-containing nanoparticles into the lesion significantly improved remyelination. Such data provide proof of concept that nanoparticles could become a valuable tool for delivering MS therapeutics to patients.

All in all, it cannot be emphasised enough that the narrative regarding LINGO-1 should not be taken as discouragement for the search for factors to promote remyelination, but rather as encouragement to study and understand the biology of demyelination and remyelination as fully as possible, while keeping in mind the challenges of successfully implementing laboratory findings in human patients.

1.10 Remyelination is more complicated than merely recapitulating oligodendrocyte differentiation from development

In the context of the search for factors that could enhance remyelination, there is a number of factors outwith the oligodendrocyte lineage itself that have been unequivocally shown to affect the success of remyelination. These factors include the activity of the innate immune system, the demyelinated axons themselves, and the age of the animal or patient. I will now describe the research that has unearthed and studied these factors and how they affect remyelination.

1.10.1. The innate immune system

The innate immune system, including monocyte-derived macrophages and microglia, which are the resident macrophages of the CNS, unquestionably plays a significant part in the pathogenesis of MS. This is evident in the consistent findings of macrophages and microglia in and around demyelinated MS lesions, frequently containing particles of myelin, indicating that they have been phagocytosing myelin material. Indeed, it is thought that macrophages are the proximate cause of myelin destruction in MS (Lampert and Kies 1967; Prineas 1975; Prineas and Parratt, 2012) and EAE (Fife et al. 2000; Heppner et al. 2005; Ajami et al. 2011). However, as I have alluded to above, evidence from toxin-based models of demyelination clearly indicates that the innate immune system is also critically important for remyelination (McMurran et al. 2016). The beneficial role of the innate immune system in remyelination is two-fold: it is required for clearing away the myelin debris generated as a byproduct of demyelination, and it is required for creating a pro-regenerative microenvironment.

In an early experiment on the response of the innate immune system to toxin-induced demyelination Ousman and David (2000) described a rapid influx of monocyte-derived macrophages into the CNS, as well as an activation of resident microglia, following LPC-induced demyelination. At four days post-LPC, many lesions were almost completely devoid of myelin debris, and fragments of myelin debris could be

detected within macrophages. The authors concluded that the primary purpose of the macrophage influx is to phagocytose myelin debris.

The importance of this debris clearance on remyelination was shown by Kotter et al. (2001), who demonstrated that if macrophage activity was inhibited, remyelination was impaired. The authors depleted macrophages in mice by use of a clodronate-liposome technique immediately before lysolecithin-induced demyelination, and observed reduced remyelination at 21 days post lesion (dpl). However, if clodronate liposome was administered at 8dpl, whereby normal macrophage activity was allowed during the first eight days following demyelination, no impairments to remyelination were observed. The authors reasoned that if myelin debris is not efficiently removed, it persists as a dense matrix within the lesion, and, essentially, constitutes a physical barrier to prevent OPCs from arriving at the lesion (Kotter et al. 2001).

The authors further underlined the importance of myelin debris clearance in a later experiment, where they experimentally injected purified myelin from uninjured rats to a demyelinated lesion to augment the naturally generated myelin debris, and found impaired remyelination compared to a control condition where purified liver membranes were added to demyelinated lesions (Kotter et al. 2006).

It is important to note that the clodronate liposome treatment depletes only macrophages, as the drug is injected intravenously and thus does not come into contact with microglia. The role of microglia in debris clearance is therefore not assessed by these experiments, although it is clear that microglia alone are not able to carry out sufficient phagocytosis of the debris. To distinguish between the responses of microglia and macrophages to EAE induction, a recent investigation by Yamasaki et al. (2014) used expression profiling and morphological distinctions between the two cell types, and presented evidence that microglia clear myelin debris following macrophage-initiated demyelination at the nodes of Ranvier. Thus, microglia are also capable of ingesting myelin debris.

The inhibitory effect of uncleared myelin debris on remyelination was not altogether unexpected, given that the role of myelin debris in inhibiting axonal regrowth is well documented (Vargas and Barres 2007; David and Lacroix 2003). Nevertheless, the

data described above established that myelin debris removal is a necessary prerequisite to successful remyelination.

Macrophage depletion experiments have also provided evidence that the innate immune system has a role above and beyond debris clearance. Kotter et al. (2005) employed the same macrophage depletion protocol, injecting the clodronate liposome on the day of demyelination, and examined its effects on OPC recruitment. They found that at 5dpl, there were significantly fewer OPCs at the lesion site, suggesting that their recruitment had been impaired. At 10dpl, the OPC numbers remained very similar, further suggesting that their differentiation, too, may be hindered. Moreover, further examination of the lesions by *in situ* hybridization indicated that the macrophage depletion had altered the expression of several molecules previously implicated in remyelination, including IGF-1 and TNF-β1. This suggests that macrophages are instrumental in creating a molecular environment which favours OPC differentiation and remyelination.

In order to address this role of inflammation on myelination independent of debris clearance, Setzu et al. (2006) used the adult rat retinal nerve fibre layer, which contains the unmyelinated proximal axons of the retinal ganglion cells before they become myelinated within the optic nerve. This location was chosen as it constitutes an *in vivo* milieu of unmyelinated axons of a suitable diameter for myelination. The researchers transplanted OPCs from neonatal rats into retinae, injected the animals with the potent inflammogen zymosan and subsequently assessed levels of myelination. The results showed that the rats injected with zymosan had 48 times more myelin than those where OPCs had been transplanted onto intact retinae or retinae in eyes with a lens injury. The authors then went on to perform a microarray to confirm that zymosan had indeed caused inflammation of the retina. This was the case, and moreover, factors frequently associated with oligodendrocyte development were shown to be upregulated following inflammation; the most prominent of these was TGF-β1. These data suggest that inflammation has the power to activate OPCs which would not otherwise proceed to differentiate and myelinate (as was the case in the control conditions).

A later study by Yuen et al. (2013) used the same retinal system to perform a transcriptional analysis of the retinal innate immune response following zymosan

injection, in order to generate a list of candidate cytokines which could be important in inducing myelination. From this analysis, they identified endothelin 2 as a potent positive regulator of both myelination and remyelination following lysolecithin-induced demyelination. Thus, activation of the innate immune system upregulates the expression endothelin 2, which in turn acts to enhance remyelination. This is one of many examples of the way the innate immune system modifies the lesion microenvironment to promote remyelination.

The evident dichotomy of microglia and macrophages as both deleterious and beneficial for myelin can be related to their ability to assume a variety of activation states, of which the polarization states M1 and M2 are examples (albeit greatly simplified ones; Miron and Franklin 2014). Although the activation states really sit at either end of a broad spectrum, the distinction between the two can be a useful conceptual tool (although some investigators dislike the distinction and even find it harmful, e.g. Ransohoff 2016) for understanding the diversity of microglia and macrophage behaviour. In general terms, the M1 polarization state is regarded as inflammatory, whereas the M2 polarization state is considered anti-inflammatory.

In order to investigate the roles of the two polarization states on remyelination following lysolecithin-induced demyelination, Miron et al. (2013) examined the prevalence of the M1 and M2 macrophages and microglia over the course of de- and remyelination. They found the M1 phenotype to be more prominent at 3dpl, but by 10dpl, when remyelination is getting underway, there was a shift towards the M2 phenotype. This shift represented both microglia and macrophages. The authors then tested whether the factors secreted by M1 or M2 microglia were able to promote oligodendrocyte differentiation *in vitro*, and found that only conditioned media from M2 microglia achieved that outcome. Next, they employed various pharmacological interventions to deplete either M1 or M2 cells *in vivo*, and found that depletion of M1 cells impaired proliferation of OPCs but not the latter stages, whereas by contrast, depletion of M2 cells impaired both proliferation and differentiation of OPCs as well as remyelination of axons (Miron et al. 2013). From these data, among others presented in the paper, the authors make a compelling case for M2 cells being causally beneficial for remyelination. They finally took a candidate approach and examined the activity

of Activin-A, a member of the TGF-β superfamily, since its receptor had previously been shown to be upregulated during remyelination (Huang et al. 2011) and is expressed on OPCs. The authors demonstrated that the pro-regenerative effect of M2 cells was mediated through Activin-A by showing that M2 conditioned media containing an Activin-A blocking antibody did not increase oligodendrocyte differentiation either *in vitro* or on *ex vivo* cerebellar slices (Miron et al. 2013).

Thus, the data I have described above converge to indicate that the innate immune system acts as an indispensable trigger to initiate the regenerative process following demyelination. This raises the possibility of targeting components of the inflammatory response, such as Activin-A, to improve remyelination. However, given that immunomodulatory drugs will likely always be used to reduce relapses in MS patients, a challenging aspect of developing remyelinating treatments for MS is to find ways to harness the regenerative power of inflammation without interfering with the suppression of the harmful activities of the adaptive and innate immune systems. This condundrum is highlighted in a study by Chari et al. (2006), where corticosteroids, commonly used to reduce relapses in MS patients, were shown to slow down (although not prevent) remyelination following ethidium bromide -induced demyelination.

1.10.2. The characteristics and functional activity of demyelinated axons

One aspect of a demyelinated lesion that has received comparatively little experimental attention is the demyelinated axon itself, and how it could influence its own remyelination. It is clear that axonal function is compromised by demyelination: the functional domains of the nodes of Ranvier, paranodes and juxtaparanodes are disorganised (Waxman 2006). Redistribution of the sodium channels across the axolemma leads to lower sodium channel densities and consequently to altered electrical conduction of the axons (Waxman 2006). In addition, as mentioned above, the mitochondrial content is often dysregulated in demyelinated axons, which can in some cases trigger axon degeneration (Trapp and Stys 2009) but even short of that, considerably alter the metabolic profile of the demyelinated axon. Together, these are

likely to disrupt the signalling that would take place between non-myelinated axons and OPCs under physiological conditions (Franklin and Gallo 2014).

Furthermore, demyelination may lead to re-expression of molecules which regulate myelination during development. For instance, the adhesion molecule PSA-NCAM is downregulated during developmental myelination, its disappearance from the axonal surface coincides with initiation of myelination such that it is not usually detected in the healthy adult brain (Charles et al. 2002). In contrast, PSA-NCAM is found on demyelinated axons within MS lesions. Notably, it is not found upon axons within shadow plaques (Charles et al. 2002). These observations suggest that PSA-NCAM expression could be an endogenous axonal inhibitor of remyelination.

Neuronal activity has been shown to be important in regulating developmental myelination (Demerens et al. 1996; Wake et al. 2011; Káradóttir et al. 2005; Kukley et al. 2007; Mensch et al. 2015). This naturally begs the question of whether it can do so during remyelination. Etxeberria et al. 2010 reported that within experimentally demyelinated lesions in the corpus callosum, there were transient synaptic connections between unmyelinated axons and OPCs. These connections disappeared as the OPCs differentiated into oligodendrocytes, suggesting that input from the axons initiated the differentiation process. However, since many axons in the corpus callosum are not myelinated in the first place, it was not clear whether these synapses were truly between OPCs and *bona fide* demyelinated axons.

To clarify this matter, a recent study by Gautier et al. (2015) studied the caudal cerebellar peduncle, a region where every axon is myelinated under physiological conditions. The authors used ethidium bromide to induce demyelination in this region, and demonstrated that recently demyelinated axons are capable of conducting axon potentials, albeit at a reduced rate compared to myelinated axons in control animals. The authors go on to show that these demyelinated axons form *de novo* synapses with OPCs and that synaptic vesicle release and electrical activity of the demyelinated axons can regulate the differentiation and remyelination potential of local OPCs. They further identified glutamate as regulator of remyelination; interestingly, the receptors involved differ according to the phase of remyelination (AMPA/kainate receptors are important during OPC recruitment and NMDA receptors during differentiation).

This study provided intriguing insights as to the role of the activity of an axon in influencing its own remyelination. However, the study also raises many further questions: how long can an axon retain its ability to conduct axon potentials after it has become demyelinated? How might the presence of myelin debris, or the factors secreted by the innate immune system, or the size of the lesion, affect the axon's ability to communicate with OPCs? These, and many more questions must be considered before the potential of neuronal activity in promoting remyelination can be exploited.

1.10.3. Age

One of the most profound factors correlating with the success of remyelination is the age of the patient; in a nutshell, remyelination, like regenerative processes in other tissues, is slower and less extensive in older compared to younger patients (Goldschmidt et al. 2009; Kuhlmann et al. 2008).

Age has also shown to be highly important factor governing remyelination efficiency in animal models. Gilson et al. (1993) reported that the extent of remyelination was drastically reduced in older compared to younger mice one month after lysolecithin injections, with many more demyelinated axons, thinner myelin sheaths on those axons that were remyelinated and more myelin debris present. The authors postulate that the poorer remyelination in older mice was due to a sluggish response from macrophages and astrocytes.

A later study by Shields et al. (1999) tested the hypothesis that it is the rate of remyelination that is adversely affected by age, not the ultimate extent. These researchers found, like the previous study, less remyelination in older animals at 4 weeks post lesion. However, when they allowed nine weeks to elapse before assessing remyelination, they found that remyelination in the old animals resembled that of young animals at 4 weeks post-lesion. They therefore concluded that in a toxin-based model of demyelination, ageing results in slower rates of remyelination, but the same extent of remyelination is eventually achieved by the older animals.

Interestingly, a demyelination model in adult zebrafish Münzel et al. (2014) demonstrated that remyelination is also impaired in zebrafish; following LPC-induced myelination, young adult zebrafish accomplished full remyelination in 28 days, notably with normal thickness myelin sheaths. In contrast, aged adult zebrafish showed much slower remyelination, with thin myelin sheaths both at 28 days post-lesions and at three months post-lesion. It is noteworthy that ageing impairs remyelination even in zebrafish, a model organism generally hailed for its remarkable capacity for CNS regeneration (Grandel and Brand 2013).

Further studies have clarified why remyelination is slower in older compared to younger animals. Sim et al. (2002) reported that in mice, the age-associated impairment in remyelination was due to both impaired OPC recruitment and differentiation; recruitment was slower in older mice compared to young, and once recruited to lesions, OPCs in old mice took longer to differentiate into mature oligodendrocytes. These authors also measured the latency between OPC marker expression and oligodendrocyte marker expression. This latency increased in older animals as the lesion aged, such that at 28dpl, the latency to differentiate was substantially higher in older animals than in young. This suggests that the closer to demyelination remyelination begins, the more efficient it will be, possibly because of the presence of inflammation and the associated pro-regenerative signals in the early compared to the late lesion. Indeed, similar speculations had been made regarding MS lesions (e.g. Wolswijk 2002) but the age of the lesion is very difficult to define for certain from post-mortem tissue; in this way, data obtained from simpler animal models can be used to interpret a more complex disease such as MS.

Furthermore, Hinks and Franklin (2000) found that the expression of pro-regenerative signals such as IGF-1 and TGF-β1 was both slower and lower in older compared to younger mice following lysolecithin-induced demyelination. In addition, the expression patterns of the growth factors closely mirrored the presence of microglia and macrophages within the lesions, in both young and old animals. This lends support to the hypothesis suggested by Gilson et al. (1993) that the response of macrophages is more sluggish in older animals than in young.

The above described studies shed light upon the *cellular* substrates of the age-associated decline in remyelination efficiency. Wishing to address the *molecular* correlates of this decline, and knowing that histone modification can affect the timing of oligodendrocyte differentiation (Shen et al. 2005), Shen et al. (2008) set out to test whether epigenetic modifications affect remyelination. The authors first explored the gene expression patterns following cuprizone-induced demyelination in young mice during remyelination, and identified a coordinated decrease in the expression of numerous transcripts inhibitory to oligodendrocyte differentiation. This decrease was characterised by recruitment of transcription-inhibiting HDAC isoforms to the promoter regions of the inhibitory genes. In aged mice, both this HDAC recruitment and the decrease of differentiation inhibition were conspicuously absent. These data suggest that aging is associated with a diminished intrinsic capacity to recruit HDACs to the relevant promoter regions.

A key study to address the combined effects of aging and innate immune system activity on remyelination was carried out by Ruckh et al. (2013). In this study, the authors made use of the heterochronic parabiosis technique, whereby the blood circulations of two individual mice were surgically joined together. By joining the circulations of old mice to those of young mice, and inducing demyelinated lesions in the old mice, the authors were able to test whether exposure to a youthful systemic milieu could entice the aged OPCs in the old animal to remyelinate more efficiently. The young animals' cells were ubiquitously labelled with GFP to aid their identification in the old animals' system. The results showed increased numbers of both proliferating OPCs and mature oligodendrocytes, as well as improved remyelination, in old mice paired with young mice, compared to old mice paired with old mice. Importantly, lesioned young mice did not show impairments in remyelination when paired with old mice, refuting the possibility that the old animal's systemic milieu is toxic to remyelination; thus it was the positive influence of the young system to the old animal's lesions that improved their remyelination. The authors examined the identity of the GFP+ cells found within the demyelinated lesions in the old animals, and found that they were not cells of the oligodendrocyte lineage, but predominantly macrophages. In order to test whether these macrophages were *necessary* for the improved remyelination, the authors used CCR2 null mice, in which

macrophage recruitment is blocked, as the young partners in heterochronic pairings. These pairings failed to rejuvenate the old animals' lesions, which accordingly showed poorer remyelination than old animals joined to wild-type young mice, although they still remyelinated better than old mice paired to old mice.

Further characterisation of the lesions in the heterogenic and isogenic pairings revealed that there were no differences in the production of key OPC-regulating factors (including IGF-1 and PDGF-1α) between the old animals in young-old and old-old pairings. There were also very few differences in the repair-relevant cytokines in the sera between the parabiotic conditions, suggesting that alterations to local microenvironment are more important that the contents of systemic circulation. The key role of the local microenvironment was further underlined by the finding that myelin debris was significantly more abundant in old mice in old-old pairing than in young-old pairings. This difference was abolished when CCR2-deficient mice were used as the young partners.

Thus, the results from Ruckh et al.'s work strongly suggest that young macrophages are more efficient at clearing myelin debris than old macrophages, and this adversely affects the efficiency of remyelination in older animals. Moreover, another key message from this study is that old and inefficient OPCs *can* be coaxed to differentiate and remyelinate well, as long as a suitable environment is provided. In this way, this study constitutes important additional rationale that exogenous interventions such as drugs can in principle enhance endogenous remyelination even in systems where it is usually impaired.

In order to better understand the reasons for this inefficient myelin clearance of old macrophages, Natrajan et al. (2015) explored the expression profiles of microglia- and monocyte derived myelin-phagocytosing macrophages in young and old healthy volunteers. One prominent differentially regulated pathway between the groups was the retinoid acid receptor X (RXR) pathway, which was upregulated in the young macrophages and downregulated in the old. The authors tested the effects of this pathway on myelin debris clearance by administering the RXR agonist 9-*cis* retinoid acid to young and old macrophages *in vitro*, and found that it made no difference in young mice but markedly more macrophages treated with 9-*cis* retinoic acid were able

to phagocytose myelin, compared to control. However, the treated old macrophages remained impaired compared to young macrophages, indicating that more factors are at play than RXR. Further experiments demonstrated that pharmacological inhibition of RXR activity in young macrophages impaired their ability to phagocytose myelin debris, and mice in whom RXRα had been conditionally knocked out in myeloid cells showed impaired myelin debris clearance following lysolecithin-induced demyelination. Finally, they isolated macrophages from young and old healthy volunteers as well as patients with MS, treated these with the RXR agonist bexarotene and observed increased myelin phagocytosis in the MS patient-derived macrophages treated with bexarotene. Thus, differences in the regulation of the RXR pathway represent one underlying difference between efficient young and inefficient old macrophages, and as such, could be pharmacologically targeted to improve myelin clearance and remyelination in patients with MS.

Although the RXR pathway appears to be an important regulator of macrophage activity, it is still not clear *why* the old macrophages are impaired at phagocytosing myelin debris. A recent report by Safaiyan et al. (2016) shed some light on this matter. In this study, the authors noted that there were more microglia in older compared to younger mice, and specifically, more microglia containing fragments of myelin. Further characterisation of these aged myelin-containing microglia revealed that accumulation of myelin fragments over time results in the formation on insoluble lipofuscin-like lysosomal inclusions within microglia. As the mice aged, these inclusions overloaded the microglia and diminished their capacity for further phagocytosis. The authors further demonstrated that following cuprizone-induced demyelination and the subsequent phagocytosis of myelin debris, the point of overload of insoluble lysosomal inclusions is reached at a much younger age than in healthy mice.

It is not difficult to appreciate the fundamental implications these findings could have on understanding the age-related dampening of the immune response and consequently remyelination in MS; as patients age and they develop more lesions, their microglia are faced with an increasing burden of myelin debris to phagocytose. Over time, more and more of the microglia become overloaded and therefore less able to cope with the

debris, leading to inefficient debris clearance and inhibited remyelination. However, intuitive though such a model may seem, at present it remains in the realms of conjecture, and further studies are required to empirically delineate the extent and role of overloaded microglia in MS.

1.11. Remyelination may not always rescue the demyelinated axon

While ample evidence (some of which has been discussed above) has converged to suggest that remyelination is a beneficial outcome for the axon, it is worth noting that there are cases in which remyelination has failed to prevent axon degeneration. Manrique-Hoyos et al. (2012) report a case where usual remyelination was accomplished by mice following cuprizone-induced demyelination, but six months after the last dose of cuprizone, the mice began to exhibit motor deficits similar to those they had exhibited during the demyelinated phase. Examination of the brains of these mice revealed profound axonal pathology, often within still (thinly) myelinated axons.

Manrique-Hoyos et al. hypothesise that the late-onset axon degeneration they observe stems from an altered composition of the newly generated myelin compared to normal myelin, and posit that this variant of myelin is not as proficient at keeping the axon healthy as normal myelin is. Thus, it is possible that remyelination, despite ostensibly restoring normal axon function, does not always return all of the advantages of being myelinated to their fullest extent; after all, it is well established that myelin generated during remyelination is thinner and has shorter internodes that developmentally produced myelin. These properties are thought to account for the slightly elevated energy needs of remyelinated, compared to never-demyelinated axons, evident in their slightly higher mitochondrial content (Zambonin et al. 2011). Perhaps this leaves the remyelinated axons underperforming in subtle ways, which over time can culminate in premature axon death.

However, the evidence for such a scenario is far from extensive, and in the case of Manrique-Hoyos et al., may even stem from residual toxic effects of cuprizone on axons (Münzel and Williams, 2013). Be that as it may, the weight of the evidence suggests that remyelination can restore much of the lost function of the axons and at least hold back degeneration, and as such is currently the best hope for preventing progression of clinical disability in MS. To this end, as emphasised above, it is paramount to understand the mechanisms of demyelination and remyelination and their interplay with the immune system as fully as possible.

1.12 Genetically induced models of oligodendrocyte ablation

Collectively, the data described above indicate that while it is helpful to understand the molecular regulators of oligodendrocyte development during normal development, the context in which remyelination must occur is very different, and therefore additional hurdles must be understood and overcome. Both EAE and especially the toxin-based models have been instrumental in accruing knowledge of this context and how it can be circumvented. However, the focal toxin models have their limitations, as the toxin can injure other cell types such as astrocytes and endothelial cells, and thus the responses of these cell types to oligodendrocyte death and demyelination cannot be studied specifically. In addition, the damage is restricted to a single lesion, which may not present as challenging to repair as a multifocal disease such as MS would. Cuprizone-induced demyelination can be erratic as to its location, and remyelination often starts while the animal is still being fed cuprizone, blurring the line between demyelination and remyelination. (It should, however, be mentioned that the latter problem can be circumvented by co-treating mice with rapamycin during cuprizone intoxication and increasing the time frame of cuprizone feeding to 12 weeks (Sachs et al. 2014; Bai et al. 2016).

Nevertheless, there is a need for a demyelinating model where the primary deficit is oligodendrocyte apoptosis, as this has been proposed as a potential mechanism of formation of some types of MS lesion (Barnett and Prineas 2004).

In recent years, several groups have created novel *in vivo* models of demyelination whereby oligodendrocyte death is genetically induced and can be temporally controlled by the experimenter. These models are based on placing a toxic element such as the diphtheria toxin fragment A (DTA) or the diphtheria toxin receptor (DTR) under the transcriptional control of an oligodendrocyte promoter, either PLP (Traka et al. 2010; Pohl et al. 2011), MOG (Locatelli et al. 2012) or MBP (Oluich et al. 2012). In the case of the first two, one transgenic mouse carries a Cre-dependent DTA transgene in the ubiquitously expressed ROSA26 locus, and another a tamoxifen-dependent PLPCreERT2 allele. The double transgenic offspring treated with tamoxifen show expression of DTA specifically in PLP-positive oligodendrocytes, and this DTA expression leads to cell death. In the case of Locatelli et al. (2012), DTR is expressed in a Cre-dependent transgenic mouse, which is crossed with a mouse exressing Cre under the MOG promoter. Oligodendrocyte death in induced by treatment with diphtheria toxin. Oluich et al. (2012) express DTR directly under the mbp promoter, and treat these mice with diphtheria toxin.

I have summarised the main features of these models in the table below.

Table 3.				
	Traka et al. (2010)	**Pohl et al. (2011)**	**Locatelli et al. (2012)**	**Oluich et al. (2012)**
Method of oligodendrocyte ablation	Mice expressing PLP-CreERT and Rosa26:DTA and EGFP. Disease induced by injection of tamoxifen at 5-7 weeks of age	Mice expressing PLP-CreERT2 and Rosa26:(DTA) and EGFP. Disease induced by injection of tamoxifen at 8-12 weeks of age	MOG:Cre and Cre-inducible strain expressing DTR + injection of DT at 8-10 weeks of age	MBP:DTR + injection of DT at 8-10 weeks of age
Clinical profile	Female mice have a severe disease and	From 21dpi, ataxia, tremors, motor deficits	Motor deficits from 35 – 42 dpi,	Progressive motor deficits form 9dpi,

	die before 21dpi. Males survive but show severe ataxia and tremors by 35dpi. This phenotype is attenuated by 70dpi	with muscle atrophy and weight loss. Three weeks later mice have to be culled.	including ataxia, loss of motor coordination, tremors, weight loss, culminating in paralysis and death.	becoming profound in the next 5-6d. Ataxic gait, hindlimb paralysis. Never survived past 17dpi.
Oligodendrocyte loss	~60% loss at 21dpi (although OPC proliferation has been occurring simultaneously so true extent of OL loss may be greater	Loss of 55 – 80% oligodendrocytes, depending on brain region. 30% of OPCs is also lost	60% loss in white matter areas at 35dpi. Some OPC increases at 21dpi.	26% loss of oligodendrocyte density at end point.
Demyelination	Begins at 21dpi, extensive at 35dpi, peaks at 56dpi. Extensive myelin vacuolation seen	Extensive vacuolation of myelin seen from 20dpi through to end stage at 39dpi	Myelin vacuoles and extensive demyelination apparent from 21dpi, fully demyelinated axons at 35dpi	Almost no demyelination at any point.
Axon damage/loss	No increases in APP staining during demyelination but mitochondrial abnormalities. Conduction block at 35dpi and slow conduction at 56dpi, restored to normal by 70dpi.	Progressive loss of neurofilament staining, and increases in APP and SMI-32 staining at end stage. Accumulation of organelles and brain atropy at end stage.	Sparse but widespread TUNEL+ NeuN neurons early after DTI treatment, widespread loss of neurofilament staining at 28dpi.	Low density of APP+ swellings, longer nodes of Ranvier, suggesting dispersal of sodium channels, dissociation of paranodal loops from axolemma

Immune response	Increases in microglia but no infiltration of macrophages or adaptive immune cells in the time frame analysed (up to 70dpi).	Increases in Iba+ microglia but no macrophages or adaptive immune cells; equally severe disease when Rag-/- mice were used, which have no functional lymphocytes	Increased microglia but no adaptive immune cells, even despite many manipulations to bias the system towards autoimmunity against the CNS.	Increased density of Iba+ microglia but no phagocytic morphologies. No adaptive immune infiltration even at end point
Remyelination	Extensive at 70dpi, but still more unmyelinated axons than controls	Very poor remyelination.	Some remyelination observed near end point	None required, since demyelination was so low.

Thus, despite engineered using similar reasoning, the different genetic mouse models of oligodendrocyte death present with very distinctive disease courses: Traka et al. find extensive oligodendrocyte and myelin loss, including myelin vacuolation, accompanied by large increases in CNS microglia. No axonal damage is detected however, and extensive remyelination is observed by 10 weeks post injection. In the other three, oligodendrocyte and myelin injury is equally or less extensive, but outcomes are much more severe, with the all mice in all three models succumbing before six weeks post-injection.

Many factors may account for the differences between the outcomes in these models, including age at disease onset, (Traka et al. induce oligodendrocyte death in slightly younger mice than the other groups) the strength of transgene expression, the proportion of recombined cells, and the exact mechanism by which oligodendrocyte death is brought about.

What is key to note, however, is that these different disease courses can give rise to completely opposing conclusions. As a striking example, Locatelli et al. conclude that primary oligodendrocyte death is unable to elicit and autoimmune response from the adaptive immune system even when the experimental parameters were skewed

towards generating such a response. However, in stark contrast, a study by (Traka et al. 2016) revealed that 30 weeks after apparently complete remyelination, mice develop a secondary demyelinating disease, accompanied by the clinical symptoms of motor deficits and weight loss, and eventually death. Further investigation found this secondary demyelinating disease to be caused by an autoimmune attack on the CNS by the adaptive immune system, which the authors carefully demonstrate to have been primed during the first episode of primary oligodendrocyte death. They posit that other models failed to observe this later autoimmune attack, because the mice in the other models did not succeed at remyelinating sufficiently in the first instance, and thus died before the adaptive autoimmunity could develop (Traka et al. 2016).

This raises the possibility that even the extensive adaptive immune system infiltration into the CNS that is characteristic of MS, and generally considered to be the initiating cause of the disease, could conceivably be initiated by primary oligodendrocyte death. In this way, the study by Traka et al. is a very striking example of the power of new models to yield critical insights and even radically change long-held views within the field.

In addition, the study by Traka et al. also serves to highlight how much there still is to learn about demyelination, remyelination and the immune system. For instance, the finding that secondary demyelination may occur as a result of an adaptive immune system attack underlines the point I have mentioned earlier, that even if we succeed at promoting endogenous remyelination, this would not negate the need for immunomodulatory therapies. On the other hand, these must not interfere with the role of inflammation in promoting remyelination.

Thus, there is still a need for novel models and approaches to testing factors to enhance remyelination. The genetic models described above are extremely relevant *in vivo* models in which the biology of demyelination and remyelination and the immune response can be carefully examined. However, experiments performed using these models are necessarily time-consuming and expensive, and as such, these models are not ideally suited for large-scale searches for remyelination-enhancing factors.

1.13. *In vitro* drug discovery models

One can imagine that models of myelination and demyelination exist on a spectrum of complexity, from the complex but highly relevant to disease, to the simplified and straightforward but perhaps less relevant. On such a spectrum, *in vivo* models such as EAE and the genetically induced models of oligodendrocyte death sit at one end, and at the other end would be *in vitro* systems involving cultured oligodendrocytes. Importantly however, by the same token, *in vitro* systems also sit at the opposite end of the spectrum of throughput efficiency; although simplified, they are readily amenable to extremely high throughput chemical screening, whereas *in vivo* models such as EAE and the genetically induced models are cumbersome and impractical by comparison. Thus, *in vitro* systems can be valuable tools for drug discovery.

In the last few years, several innovative *in vitro* screens have been published, which have identified several promising molecules for the enhancement of remyelination. Mei et al. (2014) took advantage of recent findings that cultured oligodendrocytes readily myelinate paraformaldehyde-fixed axons (Rosenberg et al. 2008) as well as inert nanofibers, as long as they are of an appropriate diameter (Lee et al. 2012), and form the premise that pseudoaxonal substrates can be sufficient to elicit concentric wrapping from oligodendrocytes. Given this, they designed conical micropillars which can be placed in multiwell plates and used as an inert scaffold for oligodendrocyte myelination. Such an arrangement is ideal for investigating cell-autonomous mechanisms of oligodendrocyte differentiation and myelination. Cultured OPCs were plated on the pillars, subsequent observations revealed that mature oligodendrocytes had arisen and wrapped myelin around the micropillars. This could be detected as concentric rings around the micropillars (Mei et al. 2014).

A drug reprofiling screen was then carried out on these OPC-micropillar cocultures. Reprofiling of drugs refers to the testing of drugs that have already been approved for one condition for another condition. Repurposing FDA-approved drugs bypasses the need for preclinical testing and Phase I clinical trials, since the drug has previously been shown to be safe, and thus speeds up the process of drug development (Dang et al. 2016). Since oligodendrocyte proliferation and differentiation in a limited population are mutually exclusive processes, Mei et al. were able to distinguish

between compounds which increased proliferation and those which increased differentiation. Upon completion of the screen, the authors reported finding a cluster of eight FDA-approved drugs with known antimuscarinic effects which significantly increased oligodendrocyte differentiation. The most effective among these were benztropine, a Parkinson's disease drug, and clemastine, an over-the-counter antihistamine. Notably, these drugs did not increase the *number* of oligodendrocytes, only the amount of myelin found wrapped around micropillars.

Since both benztropine and clemastine were already FDA-approved, had known bioavailability and importantly, were known to cross the blood-brain barrier, the authors considered them to represent promising candidates for remyelinating therapies. In order to test clemastine in an *in vivo* demyelinating context, they treated lysolecithin-demyelinated mice with clemastine, and subsequently observed improved remyelination at 14dpl, a week earlier than in non-clemastine treated mice. At this time point, 29% of examined axons remained unmyelinated in the controls, while only 9% of axons remained unmyelinated in clemastine-treated mice.

Following favourable results in Phase I clinical trials, clemastine is now being tested a Phase II trial called ReBUILD, with reducing the latency of visually evoked potentials in MS patients as the primary outcome measure.

In another extremely high-throughput chemical screen, Deshmukh et al. (2013) screened 100,000 compounds on primary rat OPCs, and also found benztropine to substantially increase OPCs differentiation. The authors then administered benztropine to mice with PLP-induced EAE at the time of EAE induction, and found the EAE scores of the benztropine-treated group to be dramatically lower than those treated with other frequently used MS therapies such as β-interferon. However, this is not a clinically relevant approach, as it is not possible to offer MS patients treatments *prior* to their disease onset (Vesterinen et al. 2010). Notably, when benztropine was administered to mice at the onset of first symptoms, the treatment showed a much reduced effect on the EAE scores, albeit still significant at the later stages. Adoptive transfer experiments indicated that benztropine did not affect the immune response in EAE animals. Finally, benztropine was shown to improve remyelination in both EAE and a cuprizone model of demyelination. Thus, benztropine too could also represent a

promising candidate for remyelinating therapies for MS, although its side effects are far more extensive than those of clemastine.

These examples illustrate how high-throughput screens in simplified *in vitro* systems can identify novel candidates for drugs to enhance remyelination and moreover, that any results can be rapidly translated to more clinically relevant contexts (such as experimental models of demyelination) and onwards to clinical trials. In this way, *in vitro* systems can constitute very powerful tools for drug discovery, as vast libraries of compounds can be screened, which naturally increases the probability of finding effective compounds.

However, it is important to keep in mind that the success of simplified *in vitro* systems does not negate the need for *in vivo* models of demyelination and remyelination; any promising candidates from *in vitro* screens must first be validated in an *in vivo* system before proceeding to clinical trials. In addition, over and above drug discovery for MS, there is an intrinsic value to *in vivo* animal models, where interactions between cell types can be studies in their natural contexts. Animal models also offer the possibility to genetically express specific mutations in cell types of interest and study their effects on diseases or other phenomena of interest. For instance, the finding by Ruckh et al. (2013) that exposure to youthful macrophages can entice aged OPCs to remyelinate better, but not if the youthful macrophages cannot be recruited to the lesion site because of loss of CCR2 function, has provided the field with fundamental insight into the interactions between different cells, and in so doing has guided towards relevant questions to ask in future research. Similarly, the revelation by Traka et al. (2016) that primary oligodendrocyte death can induce a secondary adaptive autoimmune attack on the CNS has questioned long-held views regarding the aetiology of demyelination in MS. Such pivotal insights could never have been obtained from *in vitro* systems.

The field of myelination and remyelination is well equipped with a wide variety of tools with different pros and cons to them. Nevertheless, an unmet need in field, until recently, has been the ability to follow cells in their natural environments over time, at single cell resolution and in an intact living animal. Fortunately, this is a need that can be met by generating a model of demyelination in zebrafish. Moreover, on the spectrum I mentioned above between complex/relevant and simple/less relevant

systems for drug discovery, zebrafish sit in the middle, allowing relatively high-throughput screens in an intact living animal. In this way, zebrafish are arguably an ideal system for drug discovery as well as high-resolution cellular analyses.

I will now outline the main advantages of using zebrafish as a model organism, and give examples of how they have been harnessed to benefit the research community.

1.15. Advantages of using zebrafish

While the bulk of the existing knowledge on myelination, demyelination and remyelination has been amassed using either rodent-based *in vivo* or *in vitro* models, or human post-mortem samples, in recent years a growing number of researchers has opted employ the zebrafish (*Danio rerio*) to address questions of development, injury and regeneration. The reasons why the zebrafish have become such a pre-eminent system for biological research are clear and manifold, as I will outline below.

First, zebrafish embryos are optically transparent, and remain so for approximately the first two weeks of life. This allows detailed imaging of dynamic cellular processes and events in a living animal (Lyons and Talbot 2015). Live imaging of particular cellular events is also greatly aided by the availability of an ever-growing list of transgenic lines in which cell types of interest are labelled with fluorescent reporter proteins, allowing them to be identified and followed with ease. For instance, a study from our lab made use of several transgenic lines which label developing oligodendrocytes and performed time-lapse imaging overnight to record the myelinating behaviour of individual oligodendrocytes. This method revealed that once an oligodendrocyte has begun to form myelin sheaths, it will form all of its future sheaths within a period of five hours (Czopka et al. 2013).

Furthermore, zebrafish embryos are easy to obtain in large number, as a single overnight pair mating can produce hundreds of eggs. The embryos develop rapidly, such that by three days post-fertilisation (3dpf), functional neural circuits and spontaneous swimming behaviour is observed, and by 5dpf, both the central and peripheral nervous systems are robustly myelinated (Almeida et al. 2011). It is easy to

appreciate how this swift acquisition of samples and their rapid development are advantageous for large-scale studies.

It is also important to note that many fundamental aspects of biology are well conserved between zebrafish and mammals. In the case of myelin, homologs of the many of the main protein components of myelin are found in fish myelin, including mbp (Nawaz et al. 2013) and PLP (Schweitzer et al. 2006). The notable exception to this similarity is myelin protein zero, which is expressed in CNS in the zebrafish, but is restricted to the PNS in mammals (Bai et al. 2011). However, the similarity of g ratios between fish and mammals is well established (Hahn 1978) as are the periodic nature of the myelin wraps, membrane packaging and lipid composition of myelin (Avila et al. 2007). Furthermore, the molecular pathways which control the exquisitely complex signalling between myelinating glia and axons have been shown to have striking similarities between fish and mammals. As reviewed by Monk and Talbot (2009), the transcription factors Olig1, Olig2, Sox10 and Nkx2.2 all function in a comparable manner in regulating myelination in zebrafish and mammals. Similarly, canonical signalling cascades such as Notch, wnt, Hedgehog and ErbB2/3 have all been demonstrated to operate in very similar ways in fish as in mammals (Preston and Macklin 2014).

Moreover, not only are the molecular regulators of myelination conserved between fish and mammals, but evidence has indicated that the cellular events occurring during oligodendrocyte lineage progession are very similar, too.

1.15.1. Genetic screening in zebrafish

The speed of development, ease of acquiring large numbers of progeny from single pair-matings and the high degree of conservation between fish and mammals have all combined to make zebrafish a pre-eminent model organism for carrying out large-scale forward genetic screens (Haffter and Nüsslein-Volhard 1996). In these screens, a potent mutagen, typically N-ethyl-N-nitrosourea; ENU) is used to introduce random point mutations in the germ line of a founder male individual. These mutations are bred to homozygosity over three generations, and identified from phenotypic analyses.

The first forward genetic screens in zebrafish were undertaken by Christine Nüsslein-Volhard and colleagues, and yielded over 4000 mutations resulting in abnormal embryonic and larval phenotypes (Driever et al. 1996; Haffter et al. 1996). Many of these were general developmental delays and were discarded, but over a thousand mutants were characterised. These have contributed vitally to our understanding of the development of the dorsoventral axis, notochord formation, and axon pathfinding (Granato and Nüsslein-Volhard 1996). These genetic screens substantially increased the use and appreciation of the zebrafish as a model organism.

More specific screens aiming to discover genes pertaining to particular biological processes of interest have subsequently been carried out. For instance, in a screen looking for defects in myelination in the Talbot laboratory at Stanford, 13 mutations were identified (Pogoda et al. 2006). Among these was Gpr126, a G protein coupled receptor which had not been previously implicated in myelination but was found to be essential for the initiation of Schwann cell myelination (Monk et al. 2009). This gene functions autonomously in Schwann cells and drives the differentiation of Schwann cells from promyelinating to myelinating phenotypes by elevating cyclic AMP levels in them. Further investigation revealed that it Gpr126 is equally indispensable for myelination in the mouse PNS (Monk et al. 2011). Moreover, a recent study demonstrated that Gpr126 mediates the effects of prion protein in maintaining PNS myelin homeostasis – which, if disrupted, results in a chronic demyelinating polyneuropathy (Küffer et al. 2016).

Another gene discovered in the forward genetic screen in the Talbot lab is KBP, which is required for axonal outgrowth and maintenance in both the CNS and the PNS (Lyons et al. 2008). Not only do axons in KBP mutants fail to reach the posterior end of the spinal cord, but the axons also show signs of degeneration from 2-3dpf onwards. Importantly, a mutation in KBP underlies the human neurological condition Goldberg-Shprintzen syndrome, which is characterised by intellectual disability and disruption to white matter tracts (Fryer 1998). In this way, insight gleaned from genetic screens in zebrafish can provide new information relevant to human disease.

Two forward genetic screens have also been performed in our laboratory, and the genes discovered are currently being investigated further.

1.15.2. Chemical screening in zebrafish

Since zebrafish embryos develop outside of the mother, they are easily accessible for experimental manipulation, such as injection of transgenic constructs or drug treatments. Drug treatments are particularly straightforward to deliver; in contrast to mammals, there is no need for injections, as compounds can simply be diluted in the fish water, where they will be absorbed into the animal (MacRae 2015). Testing potentially therapeutic compounds on embryonic and larval zebrafish is increasingly preferred to testing on cultured cells, as toxic or global side effects of the compounds are easier to intercept in an intact living system (Preston and Macklin 2014).

Drug screens have already been undertaken in zebrafish, and in some cases have yielded drug candidates which are currently in clinical trials for human use. The most notable of these is the case of prostaglandin E2 (PGE2), which I will briefly summarise here. North et al. (2007) screened three separate chemical libraries of compounds (over two thousand compounds altogether) and discovered that compounds that enhanced synthesis of PGE2 increased numbers of blood stem cells in the developing zebrafish aorta, and conversely, compounds that blocked PGE2 synthesis decreased numbers of blood stem cells. The authors went on to test the drug they had identified in a mouse system, and were able to demonstrate that the drug enhanced the engraftment of blood stem cells in mouse bone marrow transplants. This was the first molecule found to increase a stem cell pool, and as such, had implications for treatment of patients with bone marrow failure and recovering from bone marrow transplantation. Following further characterisation of the mechanism of action of the PGE2-enhancing drug in mice, human cells *in vitro* and nonhuman primates (Goessling et al. 2011), the drug proceeded to clinical trials. A Phase I clinical trial demonstrated the safety of the drug (Cutler et al. 2013) and the Phase II clinical trials for increasing the blood stem cell count in umbilical cord blood tranfusions following bone marrow transplanation are ongoing (Zon 2016).

Thus, PGE2 serves as striking example of the power of zebrafish drug screens to generate viable drug candidates for clinical trials. Zebrafish screens can also accelerate the process of drug discovery by e.g. reprofiling FDA-approved drugs for novel purposes. For instance, lefluonomide, originally an anti-arthritis drug, was identified

as a potential novel melanoma treatment using a zebrafish screen (White et al. 2011). Being a living system, the potential to discover novel effects of drugs is likely to be greater in zebrafish than in *in vitro* systems.

A drug reprofiling screen in zebrafish has also been carried out to search for compounds to increase myelination. Buckley et al. (2010) reprofiled 1120 compounds from the Prestwick Chemical Library and 50 compounds from other commercially available reprofiling libraries. The authors treated transgenic fish expressing GFP under the Olig2 promoter with the compounds and quantified the dorsally migrated Olig2-expressing cells, as this population largely represents cells of the oligodendrocyte lineage (although olig2 is also expressed in motor neuron progenitors and motor neurons). Compounds repeatedly altering the numbers of these cells were considered "hits" and investigated further by quantitative PCR of myelin basic protein to accurately assess the levels of increase in myelination.

This screen identified a number of compounds which altered the numbers of dorsally migrated olig2-expressing cells, including members of pathways not previously implicated in myelination (such as COX inhibitors) as well as established regulators of myelination (such as PPAR agonists and steroid hormones). However, the quantification of mbp transcripts did not correlate with the olig2+ cell counts, and thus the authors concluded that the compounds identified in their screen did not necessarily increase myelination. Nevertheless, they emphasise that the screening system this study established will prove a robust tool for future drug discovery.

Perhaps one of the reasons for the lack of correlation between olig2+ cell counts and the number of mbp transcripts is that mbp is expressed both in the CNS and the PNS, and the dorsally migrated population of oligodendrocytes in the spinal cord accounts for a relatively small proportion of all the mbp-expressing cells in the larvae. Therefore, increases in the dorsally migrated population of olig2+ cells would have to be very substantial for it to significantly increase the overall number of mbp transcripts. With this in mind, perhaps a better way to quantify increases in myelinating oligodendrocytes would be to use markers specific to mature oligodendrocytes, such as mbp.

In recent years, our laboratory too has incorporated drug screening in zebrafish to our repertoire. Work from other members in the lab has established screening protocols using transgenic fish in which oligodendrocyte cell bodies are labelled, such that any effects of compounds oligodendrocyte cell number can be directly visualised. Importantly, carrying out very large-scale drug screens on zebrafish has recently been made exponentially faster in our laboratory, owing to our recent acquisition and development of a novel high-throughput system for drug screening. This system comprises a liquid handling robot by the name of VAST (Vertebrate Automated Screening Technology) which, in essence, lifts embryos out of the wells of a multiwall plate, delivers them to an optically optimal glass capillary located below a lens belonging a spinning disk confocal microscope, rotates the capillary until the orientation of the embryo matches the pre-set lateral orientation, then sends a command to the spinning disk microscope to commence imaging. This microscope is capable of imaging the entire length and depth of the spinal cord in one minute. Using this system, trained members of our lab are able to screen through upwards of 350 animals per day and retain a record of each animal's myelin phenotype as well as its general health and morphology. Needless to say, this system has revolutionised our capacity for screening through extensive libraries of chemical compounds, and consequently our chances of identifying novel regulators of myelination.

Several candidates which increase oligodendrocyte numbers have already been identified, and are currently being characterised further. The identification of these candidates indicates that there is indeed scope for increase in the number of oligodendrocytes even during developmental myelination.

1.15.3. Why a zebrafish model of demyelination and remyelination would be beneficial

All in all, the availability of a wealth of transgenic tools and technological advances such as VAST, combined with the inherent benefits of transparency, high fecundity and rapid development, render zebrafish an exquisitely well placed tool for studying myelination events. It seems natural, then, that zebrafish should also serve extremely

well for studying demyelination and remyelination. However, as I have discussed above, remyelination occurs in a very different context to developmental myelination. Thus, in order to use zebrafish to study remyelination and the factors that affect it, it will be necessary to first induce demyelination in a larval zebrafish. It is for this reason that our lab undertook to develop a zebrafish model of de- and remyelination.

The value of a system where demyelination can be induced in larval zebrafish is easy to appreciate. The ability to visualise individual cells, be they oligodendrocytes, neurons, immune cells or any combination thereof, in a living intact system, multiple times over the course of de- and remyelination could become a vital asset for the community seeking to understand the complex cellular interactions which mediate de- and remyelination. This advantage of *in vivo* imaging, although of fundamental importance to the understanding of the effects of de- and remyelination on the axon, may be particularly pertinent to the imaging of something as rapid and dynamic as the immune response (for which a growing variety of transgenic tools exists; Sieger and Peri 2013).

A demyelinating fish model would also open up other possible avenues of investigation. For example, recent advances in genome editing technology such as crispr-cas make it relatively straightforward to knock out (or, indeed, in) specific genes, allowing the researcher to subsequently explore the effects of the manipulation on demyelination, the immune response, and remyelination. In addition, any novel genes pinpointed by the large-scale forward genetic screens as important regulators of developmental myelination can be tested for their role in remyelination by recreating the same mutation in a demyelinating fish.

Finally, inducing demyelination in larval zebrafish could enable screening for chemical compounds to improve remyelination, which, combined with VAST, could form the basis for remyelination screens in zebrafish in the future.

Crucially, such studies and screens necessarily require a robust and well-characterised zebrafish model of demyelination before they can be attempted. It is paramount to thoroughly understand the timing and extent of demyelination, as well as any spontaneous remyelination, in order to make informed decisions as to how best to use

the model. Therefore, my PhD project has chiefly focused on characterising my zebrafish model of demyelination and remyelination, with the aim of providing the field with a useful tool for demyelination and remyelination research. In addition to this characterisation, I have preliminarily explored some of the effects that the demyelinated state may have on the health of the axons as well as the role of the innate immune system in bringing about myelin repair in this model.

Chapter 2:

Materials and Methods

2.1. Generation of the mbp:mCherry-NTR transgenic line

This work was carried out by Ms Marieke Goedhart and Dr Tim Czopka prior to my arrival at the lab.

Ms Goedhart and Dr Czopka used the tol2kit (Kwan et al. 2007) to construct the plasmids required create the Tg(mbp:mCherry-NTR) line. First, they amplified the nitroreductase sequence from a 3' entry clone containing the sequence for bacterial nitroreductase using the following primers (including restriction sites):

HindIII_NTR_forward GACAAGCTTATGGATATCATTTCTGTCGCC and XhoI_NTR_reverse CAGACTCGAGGTTACACTTCGGTTAAGGTG.

The PCR products were then recombined with the 3' entry clone vector PDONRP2R-P3 (Czopka, unpublished). This vector also contained a SV40 late poly adenylation (poly-A) signal located directly 3' to its multiple cloning site. Poly-A signals are known to aid termination of transcription and improve transgene expression (Proudfoot 2011). This completed the generation of the 3' entry clone containing the NTR sequence.

The mbp:mCherry-NTR plasmid was generated by recombining the above described 3' entry clone containing the NTR sequence, a 5' entry clone containing the regulatory sequence for the myelin basic protein and the pME_mCherry fluorescent middle entry clone with the pDEST_Tol2_PA2 destination vector. This ligation was done using LR clonase II Plus (Invitrogen). The mbp:mCherry-NTR plasmid thus generated was then injected into fertilised wild type zebrafish eggs at the 1-8 cell stage (see **Section 2.6** below) to create embryos that expressed the transgene mosaically; that is, sparsely, in random locations along the length of the animal. These injected animals were allowed to develop into larvae, and at 5dpf they were sorted for transgene expression under a stereomicroscope. Those larvae that showed robust mosaic expression of the transgene were raised to adulthood, becoming the F1 generation. Only some individuals in the F1 generation contain the transgene in their germ lines; in order to identify the individuals that did, all F1 fish were outcrossed to wild type fish, and the progeny of

these crosses was analysed. Those F1 fish that contained the transgene in their germ lines produced fully transgenic offspring which expressed the transgene in every cell of the appropriate cell type (here, mature oligodendrocytes and Schwann cells). Such F1 fish were kept as founders of the new transgenic line. In order to propagate the line, the founders were outcrossed and the progeny, the F2 generation, was raised to adulthood. The generation of a stable transgenic line is illustrated in **Figure Methods 1** below, taken form Bin and Lyons (2016).

Figure Methods 1. Generation of a stable transgenic line.

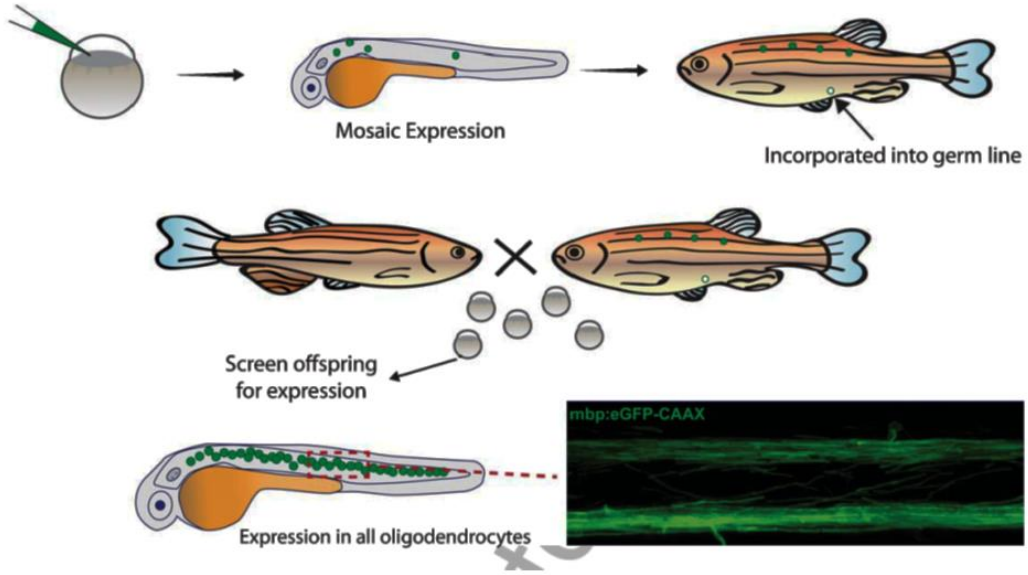

All experiments described in this thesis were performed on the members of the F2 generation and subsequent generations of this Tg(mbp:mCherry-NTR) line, either incrossed or outcrossed to different transgenic lines, as required. In Figures and legends, "Tg" before the line name denotes a stable, germline inserted transgenic line, whereas a transgene name indicates that a plasmid was injected, resulting in mosaic expression.

2.2. Maintenance of adult zebrafish

Adult zebrafish were used in these studies exclusively for breeding purposes; to obtain the fertilised eggs and subsequent embryos and larvae on which all experiments were performed. Adult zebrafish were maintained in a dedicated aquatic facility at the Queen's Medical Research Institute at 28.5°C and under a 14 hours light and 10 hour dark cycle. All husbandry was performed by the facility staff in accordance with UK Home Office regulations.

2.3. Transgenic zebrafish lines used

The transgenic or mutant zebrafish lines I have used throughout this project are listed in the table below.

Tg(mbp:mCherry-NTR)	Visualising and ablating oligodendrocytes and Schwann cells	This study
Tg(mbp:EGFP)	Visualising oligodendrocytes and Schwann cells	(Almeida et al. 2011)
Tg(mbp:EGFP-CAAX)	Visualising myelin sheaths	(Almeida et al. 2011)
Tg(mbp:nls-EGFP)	Visualising oligodendrocyte and Schwann cell nuclei	Unpublished
Tg(mpeg:GFP)	Visualising macrophages and microglia	(Ellett et al. 2011)
irf8 -/-	Lacking microglia and macrophages at early developmental stages	(Shiau et al. 2015)

2.4. Acquisition of fertilised eggs

Fertilised egg were obtained by natural spawning through pair matings and subsequently kept in petri dishes containing embryo medium (10mM HEPES-buffered E3 embryo medium; 500PM NaCl, 170 KCl PM, 330 PM CaCl2, 330 PM MgSO4) in a 28.5°C incubator.

2.5. DNA microinjections

If mosaic labelling of single cells was required, the fertilised eggs were microinjected with the appropriate DNA construct at the 1-8 cell stage. Eggs were injected with 1 nl of a solution containing 5-20 ng/µl plasmid DNA (depending on the plasmid in question), 12-20 ng/µl tol2 transposase mRNA, and 10% phenol red (to aid in visualising the successful injection). After injection, eggs were transferred to petri dishes containing embryo medium) and placed in a 28°C incubator.

2.6. Metronidazole treatment and maintenance of larvae post-treatment

5dpf larvae were anesthetised with tricaine (168µg/mL 3-amino benzoic acid ethyl ester, Sigma) and manually sorted under a fluorescent stereomicroscope, to identify larvae showing strong expression of the mbp:mCherry-NTR transgene, as well as any other transgene involved in the experiment. The 5mM solution of metronidazole (Mtz) was then prepared in 1% DMSO and embryo medium, and the selected larvae placed in 50ml petri dishes containing either the metronidazole solution or only 1% DMSO, and kept in a 28°C incubator for 48h. After 24h of treatment, the solutions were replaced with freshly prepared solutions. At the end of the 48h treatment, the larvae were transferred into one-litre nursery tanks at the aquatic facility, and maintained there for 1-16 days, depending on the experiment. During this time, they were fed by the facility staff according to established fish rearing protocols (Nüsslein-Volhard and Dahm, 2002; Westerfield, 2007).

2.7. Live imaging

For live imaging, living zebrafish larvae were anaesthetised in tricaine as above, and embedded in 1.3% low melting point agarose (Invitrogen). To align larvae for imaging, they were laid on their sides on the coverslip and gently pressed against the coverslips along the length of their trunk, in order to ensure they lay as close to the coverslip as possible. During imaging, larvae were surrounded by "tricained" embryo medium.

Confocal images were acquired using Zeiss LSM 710 or 780 confocal microscopes with a 20x air lens, with the exception of live imaging of single oligodendrocytes at 21dpf, which was performed on a Zeiss LSM 880 Airyscan microscope with a 10x air X lens.

All live images presented in this thesis represent lateral views of the spinal cord, with anterior towards the left and dorsal towards the top of the image. A stretch of approximately four somites was typically imaged, but figure panels show representative x-y areas cropped from the original images (see **section 2.8**. for details on live image processing).

2.8. Processing of live images

The majority of image processing was carried out using Fiji software (a distribution of ImageJ). This was mainly limited to global enhancements in brightness and/or contrast, and manipulating the colour schemes of images (e.g. changing the pseudocolouring of an image from green to grayscale). A small number of images was also processed in Adobe Photoshop CC 2015; this was again limited to global changes in brightness and contrast.

The images of single oligodendrocytes at 21dpf captured on the Zeiss 880 Airyscan microscope were all subjected to a post-magnification zoom of 1.8 and a 3D post-acquisition deconvolution using the Wiener filter.

For all figure panels, maximum intensity projections of z stacks were created (unless indicated otherwise), and representative x-y areas cropped. Figure panels were assembled using Adobe Illustrator CS5, Fiji and GraphPad Prism version 6.07.

2.9. Quantification of live images

All quantification of live images was performed using Fiji; either the cell counter plugin (for counting cells or subcellular components) or the region of interest plugin (for measuring lengths of myelin sheaths on individual oligodendrocytes).

All analyses of larvae at 17dpf or older was performed blinded to the treatment condition or genotype, if applicable. At time points earlier than 17dpf, it was overwhelmingly obvious from the images whether the animal in question belonged to the treated or the control group, so blinding was deemed superfluous in these cases.

2.10. Preparation of samples for electron microscopy

Preparation of zebrafish tissue for transmission electron microscopy was performed according to the following protocol.

1. Terminally anaesthetised larvae were immersed in primary fixative solution (4% paraformaldehyde, 2% glutaldehyde and 0.1M sodium cacodylate, pH 7.4).
2. As soon as possible, they were microwave-stimulated using a Panasonic microwave with “Inverter” technology: one minute at 100 Watts, one minute out of the microwave, one minute at 100 Watts, one minute out. Then the power setting was adjusted to 450 Watts, and samples were stimulated for 20 seconds, then taken out for 20 seconds.; this was repeated five times. During all microwave stimulation, the larvae were kept in an ice bath of 15°C ± 3°C to prevent them from overheating.

The microwave stimulation is highly recommended, as a brief interval of microwaving has been found to markedly improve quality of zebrafish tissue

fixation, although it is not known precisely what the underlying mechanism of this benefit is.

3. After microwave stimulation, samples were incubated in primary fix for 1-14 days at 4°C.
4. When ready to continue processing, samples were washed three times for ten minutes in 0.1M sodium cacodylate buffer and their heads were dissected away (another measure thought to improve quality of fixed tissue).
5. The beheaded samples were immersed in secondary fixative, (2% osmium tetroxide and 0.1M imidazole) and microwave-stimulated again: one minute at 100 Watts, one minute out, one minute at 100 Watts, one minute out. The power setting was changed to 450 Watts again and the samples stimulated for 20 seconds and taken out for 20 seconds; this was again repeated five times.
6. The microwaved samples were incubated on a shaker at gentle speed (~30rpm) at room temperature for at least three hours.
7. The samples were next washed five times for ten minutes in water.
8. Next, an *en bloc* stain was performed by immersing samples in aqueous saturated uranyl acetate (8% w/v) and microwave-stimulating them (450 Watts for one minute, out for one minute, 450 Watts for one minute).
9. An ethanol concentration gradient series (50%, 70%, 95% and 100% EM grade ethanol) was then prepared for the dehydration steps. After being immersed in each new concentration of ethanol, the samples were microwave-stimulated for 45 seconds at 250 Watts, and incubated on a shaker at room temperature for ten minutes. At 100% ethanol, the samples were microwave-stimulated for one minute at 250 Watts, taken out for one minute and stimulated again at 250 Watts for one minute. This was repeated three times.
10. The samples were then subjected to an acetone dehydration: immersed in fresh EM grade acetone, they were microwave-stimulated at 250 Watts for one minute, out for one minute, stimulated at 250 Watts for one minute, and incubated on a shaker at room temperature for ten minutes.
11. During the acetone dehydration, a pre-infiltration solution consisting of 50% acetone and 50% EMbed 812 resin (Electron Microscopy Sciences) was

prepared. The samples were left in this solution overnight on a shaker at room temperature.

12. The next day, the 50/50 solution was replaced by 100% EMbed 812 resin, and the samples were left to incubate in this in the hood overnight, with the lids of the tubes open to allow residual acetone to evaporate.
13. Finally, the samples were aligned in EMbed-filled silicone moulds and baked at 65°C for at least 72h to solidify the resin into blocks. A small piece of paper was also embedded in the blocks to identify the samples.

These blocks were trimmed down using razor blades (Agar Scientific) until somite 16 was reached. This was readily identifiable as it is also the location of the urogenital opening (see **Figure Methods 2**); this ensured that sections were always obtained from comparable regions in every animal. From this region, transverse 70nm thick silver sections were cut on a Reichert Jung Ultracut microtome (Leica) or a Leica UCT ultracut, kindly made available to me by Dr D Sherman) using a Diatome diamond knife. Sections were stretched and flattened using chloroform, lifted using a magic loop (Agar Scientific) and placed on electron microscopy grids with hexagonal grid pattern (200 Mesh Grids, Agar Scientific).

Figure Methods 2. Schematic of a zebfafish larva to show where sections were cut for TEM.

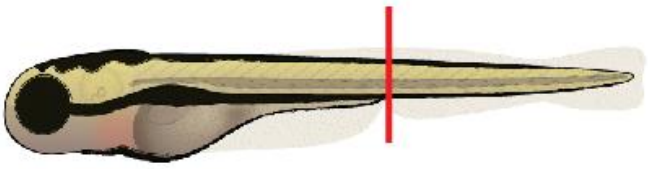

Subsequently, sections on grids were stained, first for five minutes with a 1:1 solution of EM grade ethanol and saturated uranyl acetate, washed in 50% ethanol, 50% water.

Finally, sections on grids stained with Sato's lead stain. This was prepared according to the following recipe:

0.2g lead citrate

0.15g lead nitrate

0.15g lead acetate

1g sodium citrate

48.2 ml boiled and cooled Millipore-filtered water

1.8 ml 5M NaOH prepared from the boiled and cooled Millipore-filtered water.

The lead citrate was heated on a hot plate in the hood until it changes colour from bright white to a dull gray. Then all ingredients were combined in a beaker while stirring, and the stain aliquoted into 1ml syringes.

Sections on grids were stained with this Sato's lead stain for five minutes, then washed in water and stored until imaging.

TEM imaging was performed at the University of Edinburgh Electron Microscope Facility, located in the Daniel Rutherford Building at King's Buildings campus. The images presented in Chapter 3 and most of Chapter 5 were captured using a Phillips CM120 Biotwin transmission electron microscope. This was then replaced by a Jeol JEM-1400 Plus electron microscope, and the images presented in Chapter 4 were captured using this new microscope. Image magnification ranged from 1600x to 7800x.

2.11. Processing and quantification of TEM data

An image of an entire transverse section of a 12dpf zebrafish spinal cord, cut at somite 16, is shown in **Figure Methods 3A**. Below, the schematic indicate the different regions of the spinal cord that are referred to throughout this thesis: dorsal and ventral tracts, and the left and right hemi spinal cords.

In the figure panels in this thesis, electron microscopy data for CNS studies is given as images of whole hemi-spinal cords, ventral tracts of one hemisphere (as defined in **Figure Methods 3B**) or individual tiles captured from ventral tracts. PNS data are

given as images of entire peripheral nerves (discussed further in **Chapter 5**). In order to create panoramic views of entire hemispinal cords, entire ventral tracts of one hemisphere or entire peripheral nerves, individual electron micrograph tiles were aligned using the automated photomerge tool in Adobe Photoshop CC. Any pseudocolouring on electron micrographs was applied using the lasso and bucket tools in Photoshop.

Counting of axons and other structures from electron micrographs was performed using Fiji. In my analyses of TEM images of the CNS, I focused exclusively on axons of a "myelinateable" size. This was defined as the size of the smallest myelinated axon in a control animal within the same experiment. When discussing unmyelinated or demyelinated axons, I refer only to axons that by their size would be *expected* to be myelinated.

Measurements of axon and myelin perimeters for obtaining g ratio data was done on Photoshop: I used the lasso tool to trace around the outer rim of the axon, and recorded the perimeter of my tracing using the measurements tool. I then traced around the outer rim of the myelin sheath, and recorded the perimeter of this too. From the perimeters, I calculated the diameters of the axon and the myelin, by dividing the perimeter value by π (employing the formula for perimeter of a circle $C = 2\pi r$, where r denotes radius). The g ratio was calculated using the formula below:

$$\text{g ratio} = \frac{\text{diameter of axon}}{\text{diameter of myelin}}$$

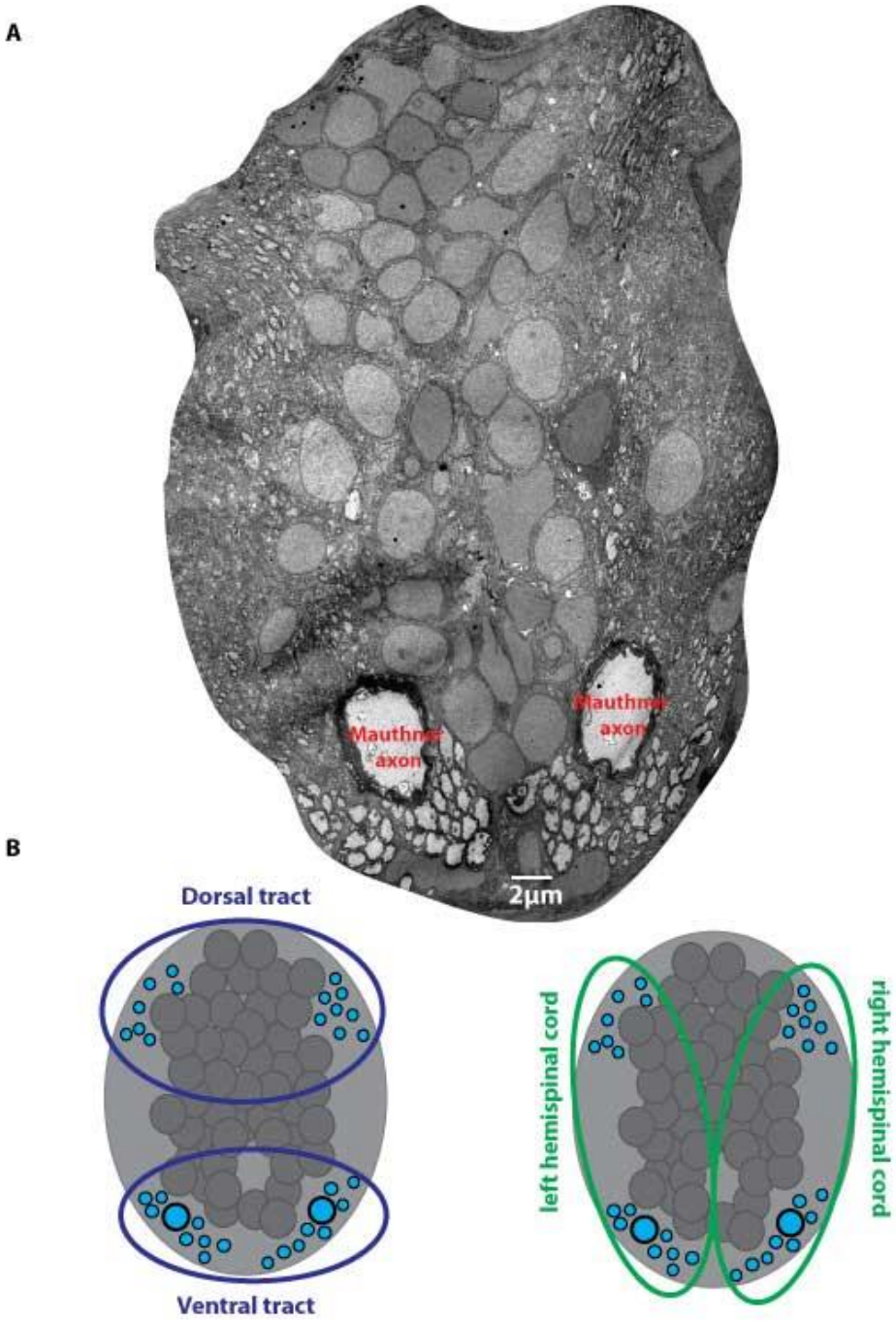

Figure **Methods 3.** TEM image interpretation.

2.12. Preparation of cryosections

In order to prepare cryosections, terminally anaesthetised larvae were fixed with 4% paraformaldehyde in PBS overnight at 4°C. They were then washed with PBS, and transferred to a 30% sucrose solution in PBS. Initially, the samples floated on the surface of the sucrose solution, but over the course of 24h gradually sank to the bottom. Once they had done so, they were aligned in silicone moulds containing optimal cutting temperature (OTC) medium (Scigen) and immediately snap frozen in 2-methylbutane (Sigma) immersed in liquid nitrogen. Cryoblocks were stored at -80°C until cutting.

Cutting was performed using a Leica CM3050S cryostat, kindly made available to us by the Brophy laboratory. 14µm thick sections were cut starting at somite 5, which is located just posterior to the swim bladder. This region was chosen because it was readily identifiable using anatomical clues under a stereomicroscope. In order to avoid sampling the same oligodendrocyte twice, sections were cut as follows: five Superfrost Plus (Thermo Scientific) slides were numbered 1-5. The first section was collected onto slide 1, then a section was cut but discarded, and the second section was collected into slide 2, and so forth. After slide 5 had received its first section, the next section was again collected onto slide 1. In this way, 8 x 14µm = 112µm came between the first and second (and second and third, etc) section on each individual slide. Since the diameter of an oligodendrocyte cell body is on average 5µm, I could be confident that when imaging any one slide, each oligodendrocyte was only represented once. A total of five sections were collected on each slide. The cryosections were stored at -80°C until staining and imaging.

2.13. Hoechst staining, imaging, and analysis of cryosections

Prior to imaging, the cryosections were stained with Hoechst (Thermo Scientific) to label nuclei. Cryosections were incubated with 1 mg/ml (1:1000 times dilution in PBS)

Hoechst for 10 min and subsequently washed with 0.02% Triton-X (Arcos) in PBS and finally with PBS (Lonza).

Cryosections were imaged on Zeiss LSM 710 or 780 confocal microscopes with a 40x oil immersion lens, using a post-magnification zoom of 2. The 405nm channel was used to visualise the blue Hoechst staining, and the 568nm channel to visualise the endogenous mCherry signal from the mbp:mCherry-NTR transgene. Four sections were imaged per larva.

Analysis of cryosections was carried out on Fiji. The two colour channels were merged using the merge channels plugin, and the number of oligodendrocytes was counted from each section, such that any Hoechst-expressing nucleus that clearly colocalised with mCherry signal was counted as an oligodendrocyte. Once all four sections originating from the same larva had been counted, a mean was calculated; this represented the number of oligodendrocytes in that larva.

2.14. Acridine orange staining

For labelling cells undergoing cell death *in vivo*, living larvae were incubated with 3µg/µl acridine orange (Sigma) at 28°C for ten minutes. The larvae were then washed in embryo medium for ten minutes at least three times, and subsequently mounted and imaged. The 488nm laser was used to excite the samples.

2.15. Genotyping for irf8

Larvae were genotyped for irf8$^{-/-}$ according to (Shiau et al. 2015) following extraction of genomic DNA by a standard protocol. Briefly, each larva was placed in 50µl of 50µM NaOH, and boiled at 98°C for 10 minutes. They were then neutralised by 10% tris-HCl (pH 8) and subsequently subjected to PCR. A 289 bp long fragment in irf8 exon 1 was amplified using primers:

5’-ACATAAGGCGTAGAGATTGGACG-3’ and

5’-GAAACATAGTGCGGTCCTCATCC-3’. (Shiau et al. 2015)

The PCR product was then digested with restriction enzyme Ava1 (New England Biolabs). The wild type PCR product is cleaved into two fragments (196bp and 93bp) whereas the mutant PCR product is not cleaved at all, as the mutation disrupts the Ava1 cut site. These were visualised by standard electrophoresis on 3% agarose gels containing 5% ethidium bromide.

Larval fin clips

In cases where phenotypic analysis was performed through TEM or imaging of cryosections, entire larvae could not be genotyped. In such cases, fin clip biopsies were taken from the larvae prior to fixation, and genotyping was carried out on the biopsies. Larval fin clipping protocol was performed using the protocol from Wilkinson et al. (2013). Briefly, this involves anaesthetising the larvae in tricaine and 3% Tween-20, laying in them on a square of parafilm, cutting a small clip of the tail fin with a sharp blade and transferring it to a PCR strip using a P20 pipette.

2.16. Statistical analysis

All statistical analyses were done in GraphPad Prism version 6.07. Statistical tests were chosen according to experimental design as specified in the figure legends. Direct experimental comparisons of treatment and control group were analysed by student’s t-tests (under the assumption of normality distribution), whereas experiments with more than two variables were analysed by ANOVA. Data are given as means ± standard deviations, with error bars representing standard deviations throughout the thesis. In every figure, N represents the number of larvae.

Chapter 3:

Characterisation of a zebrafish model of demyelination and remyelination

3.1. Introduction

In **Chapter 1**, I discussed why remyelination is considered an attractive therapeutic goal for treatment of MS and why many researchers opt to study demyelination and remyelination in simplified animal models; in short, because in such models it is possible to separate demyelination, immune infiltration, axon pathology and remyelination in time, enabling researchers to study the cause-effect relationships between them.

In order to study these processes *in vivo*, we have generated a transgenic zebrafish model in which we can specifically ablate oligodendrocytes in living larvae. Given the amenability of zebrafish to repeated high-resolution live imaging, a demyelinating zebrafish model could allow researchers to perform the kind of precise analyses of the dynamic cellular interactions that have thus far remained inaccessible in rodent models: for instance, it could be possible to follow a single axon over time as it undergoes demyelination and remyelination, and relate its health status to its myelination status. Experimenters could also attempt interventions, both delaying and speeding up remyelination, and examine the effects of these on the axon's health in terms of organelle transport, mitochondrial activity and calibre. These are crucial issues to consider, as it is currently not known how soon following demyelination a single axon begins to show pathology, and how far the pathology can proceed before it becomes irreversible by remyelination.

A zebrafish model of demyelination could also enable researchers to study factors affecting the success of remyelination at the level of single cells. For example, it would be interesting to ask how the electrical activity of individual demyelinated axons affects their chances of being remyelinated. Of course, a larval demyelinating zebrafish could also provide a disease-relevant screening platform for high-throughput chemical screening to identify compounds which could promote remyelination, and to subsequently elucidate how such compounds exerted their effects at the cellular level, thus providing insight to the mechanisms of remyelination.

Given the exciting potential of the larval zebrafish as a model of demyelination and remyelination, it is not surprising that other groups have developed such models in parallel to us. During the course of my PhD studies, two such models have been published: the first by Chung et al. (2013), with a follow-up study by Kim et al. (2015), and the second by Fang et al. (2014). I will discuss how these models and their findings compare with my model at the end of this chapter.

In addition, an *in vivo* model of demyelination and remyelination was developed in *Xenopus laevis* tadpoles by Kaya et al. (2012). Although *Xenopus* tadpoles share many of the benefits regarding live imaging with zebrafish, I would suggest that the zebrafish is better suited for studying demyelination and remyelination. This is because at the developmental stage when Kaya et al. start the metronizaole treatment, only 7% of the axons the *Xenopus* optic nerve are myelinated. In the zebrafish spinal cord, on the other hand, there are tracts that are well documented to be robustly myelinated from 4dpf onwards (Kimmel et al. 1982; Brösamle and Halpern 2002; Almeida et al. 2011). This means that the majority of the denuded axons seen in these tracts following a demyelinating treatment can be taken as *bona fide* demyelinated axons, and thus the majority of axons found to be myelinated at later stages can be taken to be *re*myelinated. In contrast, with the *Xenopus* optic nerve having so few myelinated axons to begin with, most of the myelinated axons observed at a corresponding stage are more likely to have been myelinated as part of the normal developmental process.

Another advantage of the zebrafish for studies of demyelination and remyelination is that a far greater selection of transgenic tools exists for zebrafish than for *Xenopus* (Bin and Lyons, 2016). This enables more complex live imaging of cellular interactions to be carried out in zebrafish.

For these reasons, I believe there remains a need in the field for a zebrafish model of demyelination and remyelination. Furthermore, in order to perform elaborate cellular analyses, it is essential that the demyelinating model is well understood. To this end, I undertook to thoroughly characterise a zebrafish model of demyelination and remyelination, which had been generated shortly prior to my arrival at the lab. In this chapter, I characterise the time course of demyelination and remyelination in this model, and consider the effects of demyelination on axon health.

3.2. The Tg(mbp:mCherry-NTR) line

3.2.1 The nitroreductase/metronidazole system enables inducible cell-type specific cell ablation

In order to selectively ablate mature oligodendrocytes (and Schwann cells; see Chapter 5 of this thesis) in living zebrafish larvae, I employed the nitroreductase/metronidazole system. This system was initially introduced to the zebrafish field by (Pisharath 2007) for the purpose of ablating pancreatic beta cells, and has since been used by a number of research groups to ablate hepatocytes, cardiomyocytes (Curado et al. 2007), male germ cells (Hsu et al. 2010), oocytes (White et al. 2011), rods (Choi et al. 2011) and motor neurons (Ohnmacht et al. 2016), among others.

In this system, the *E. Coli* enzyme nitroreductase (NTR) is expressed using a specific promoter for a cell type of interest; in my case, the regulatory sequence upstream of the gene encoding myelin basic protein (mbp), which is itself a major structural component of myelin, expressed in both mature myelinating oligodendrocytes and Schwann cells. The nitroreductase coding sequence is often fused to that of a fluorescent reporter, so that NTR-expressing cells can be easily identified within the animal. The expression of NTR by itself has no effect on the larva (Pisharath 2007) but when treated with the nontoxic prodrug metronidazole (Mtz), NTR reduces Mtz and converts it to a potent DNA interstrand cross-linking agent (Curado et al. 2007). This causes cell death of the NTR-expressing cell types. Thus, the nitroreductase/metronidazole system enables the researcher to ablate cells in a cell-type specific and temporally controlled manner. The research published to date using the nitroreductase/metronidazole system reports finding no bystander effects on other cell types.

3.2.2 Characterisation of the stable Tg(mbp:mCherry-NTR) transgenic line

Prior to my arrival in the lab, Ms Marieke Goedhart and Dr Tim Czopka had generated a stable transgenic line Tg(mbp:mCherry-NTR), whereby nitroreductase, fused to the fluorescent reporter protein mCherry, was expressed under the control of the mbp promoter (Almeida et al. 2011). (For further details regarding the generation of the transgenic constructs and the stable line, see **Chapter 2**, and **Figure 2A** and **B**. below). A whole-larva view of a Tg(mbp:mCherry-NTR) larva at five days post fertilisation is shown in **Figure 2B**, both as a brightfield and a fluorescent image, depicting the distribution of the transgene expression. Arrows point to the dorsal and ventral tracts of the spinal cord and the posterior lateral line, which is a prominent peripheral nerve.

Using this line, Dr Czopka carried out some preliminary characterisation and found that a two-day treatment with 5mM metronidazole (Mtz) was sufficient to ablate oligodendrocytes without causing detectible adverse effects on the larvae.

When I joined the lab, I wished to quantitatively assess the extent of oligodendrocyte ablation in the Tg(mbp:mCherry-NTR) line. Prior to testing this however, it was pertinent to first check how many oligodendrocytes in the larvae expressed the mbp:mCherry-NTR construct. To this end, I compared the number of oligodendrocytes in Tg(mbp:mCherry-NTR) larvae to that in Tg(mbp:EGFP) larvae. Tg(mbp:EGFP) is a well-established oligodendrocyte reporter in zebrafish (Almeida et al. 2011). I generated double transgenic larvae expressing both transgenes and counted the numbers of oligodendrocytes from both the mCherry and the GFP channels from a four-somite stretch of the spinal cord. This analysis showed that there was a mean of 72.56 ± 16.44 cells in the GFP channel and a mean of 72.11 ± 15.60 cells in the mCherry channel. A t test found this difference to be non-significant, $p = 0.954$ (**Figure 2C**). Thus, the expression of the mbp:mCherry-NTR transgene colocalises completely with the expression of another oligodendrocyte marker which we have used as a gold standard for studying myelinating oligodendrocytes (Almeida et al. 2011; Czopka et al. 2013).

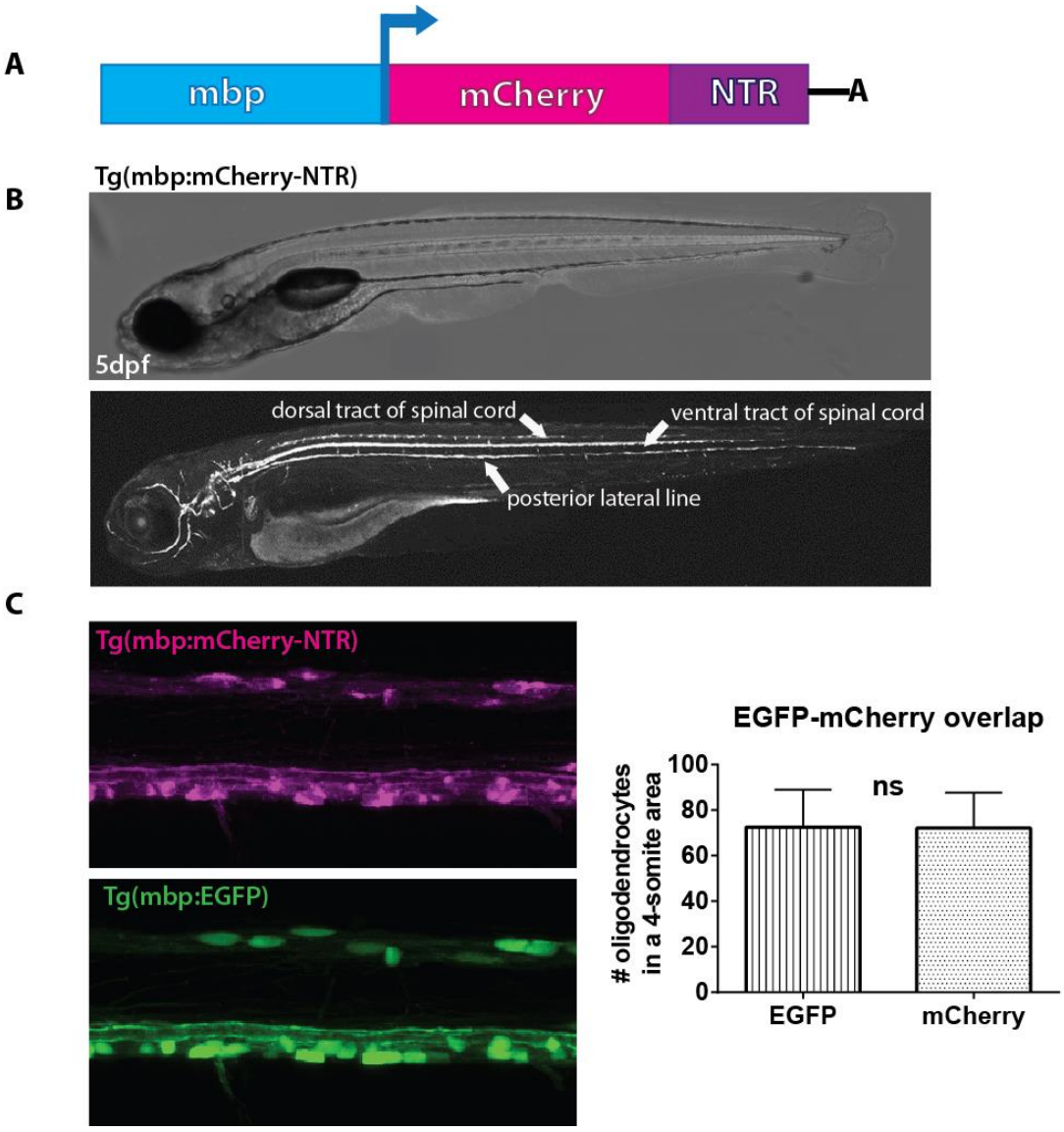

Figure 2. Characterisation of the Tg(mbp:mCherry-NTR) line.
A. Schematic of the mbp:mCherry-NTRpA construct, showing the nitroreductase enzyme fused to the fluorescent reporter mCherry, under the control of the myelin basic protein (mbp) promoter. **B**. Lateral view of the transgene expression in a 5dpf Tg(mbp:mCherry-NTR) larva. The dorsal and ventral tracts of the spinal cord, as well as the posterior lateral line, are labelled. **C**. Lateral views of both mCherry and GFP channels of a double transgenic Tg(mbp:mCherry-NTR);Tg(mbp:EGFP) larva at 7dpf, demonstrating that the mbp:mCherry-NTR transgene is expressed in all the same cells as the mbp:EGFP transgene. n = 9.

Next, I wished to ascertain whether the two-day treatment with 5mM Mtz alone caused any non-specific effects on oligodendrocytes. To check this, I used another transgenic

line, Tg(mbp:nls-EGFP), which labels oligodendrocyte nuclei, but importantly, does not express nitroreductase, and therefore should not be affected by the Mtz-treatment. I treated these larvae with 5mM Mtz for two days and then counted the numbers of oligodendrocytes to assess any effects on them. The result of this assessment is shown in **Figure 3**; I found no difference in oligodendrocyte numbers between Mtz- and vehicle (DMSO)-treated larvae, with 83.33 ± 8.20 oligodendrocytes in DMSO-treated and 87.92 ± 13.64 in Mtz-treated Tg(mbp:nls-EGFP) larvae, which was again found to be non-significant ($p = 0.324$). Thus, Mtz-treatment alone does not seem to be detrimental to oligodendrocytes that do not express nitroreductase.

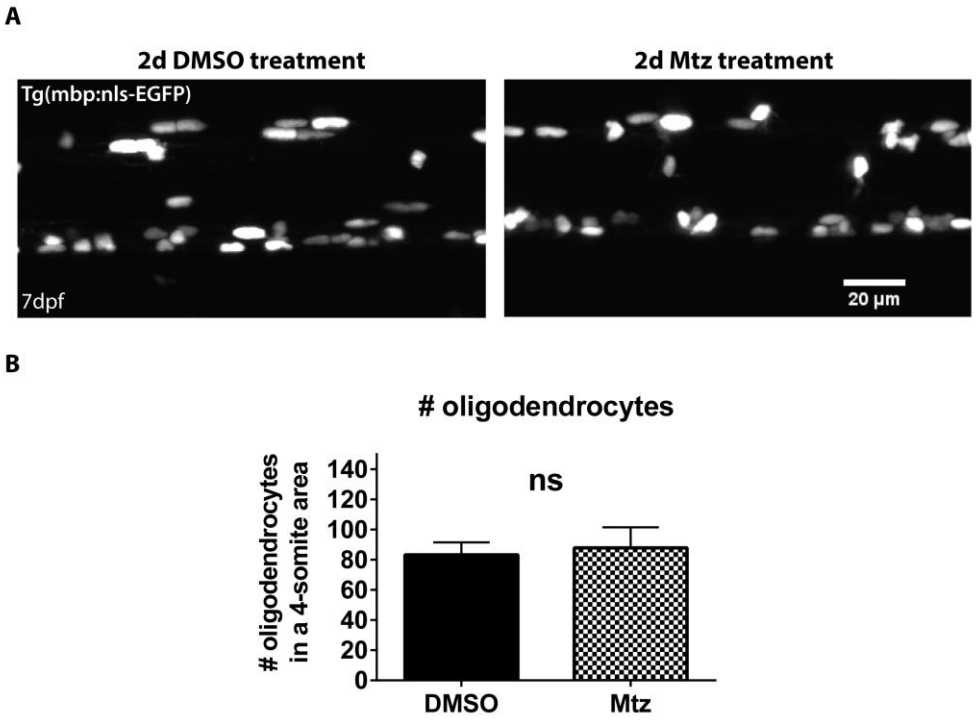

Figure 3. Metronidazole treatment does not ablate oligodendrocyts in non-Tg(mbp:mCherry-NTR) larvae. A. Lateral views of spinal cords of 7dpf Tg(mbp:nls-EGFP) larvae, treated with either DMSO (left) or Mtz (right). **B**. Quantification shows that oligodendrocyte numbers do not differ between DMSO- and Mtz-treated larvae when the animals do not express nitroreductase: the mean number of oligodendrocytes 83.33 ± 8.20 in DMSO-treated animals was and 87.92 ± 13.64 in Mtz-treated animals. A t test found this difference non-significant ($p = 0.324$). n = 12 for DMSO, 13 for Mtz.

3.3. Oligodendrocyte ablation using the Tg(mbp:mCherry-NTR) line

3.3.1. A two-day treatment with 5mM Mtz ablates two-thirds of oligodendrocytes in Tg(mbp:mCherry-NTR) larvae

I then proceeded to assess the proportion of oligodendrocytes ablated by the two-day 5mM Mtz-treatment that Dr Czopka had preliminarily indicated to result in ablation of oligodendrocytes. We chose to start the Mtz-treatment at five days post fertilisation (5dpf) as it is well documented that there are specific populations of large-calibre axons in the ventral and dorsal tracts of the spinal cord which are known to be myelinated at this stage (Kimmel et al. 1982; Brösamle and Halpern 2002; Almeida et al. 2011; Koudelka et al. 2016) which meant that we could in principle interpret the majority of non-myelinated axons following Mtz-treatment as demyelinated, rather than never-myelinated, depending, of course, on the efficiency of cell ablation and demyelination.

In order to quantitatively evaluate the degree of oligodendrocyte loss, I crossed the Tg(mbp:mCherry-NTR) line to the Tg(mbp:EGFP) line, because the GFP signal is cleaner than the mCherry signal (compare the images in **Figure 2C**) and thus renders the quantification of oligodendrocyte numbers more reliable than counting from the mCherry channel. I treated the double transgenic larvae with 5mM Mtz or the vehicle DMSO from 5dpf to 7dpf and subsequently imaged them using the GFP channel. Analysis of these images revealed that Mtz-treated larvae exhibit a drastic reduction in the numbers of recognisable oligodendrocyte cell bodies; yellow arrowheads indicate some of the remaining oligodendrocyte cell bodies. I counted the numbers of these remaining cell bodies, and found that the mean number of oligodendrocytes was reduced from 85.71 ± 2.1 in DMSO-treated larvae to 27.48 ± 2.1 in Mtz-treated larvae, amounting to a 68% decrease on oligodendrocyte numbers **Figure 4B**. A t-test found this difference significant, $p < 0.0001$.

I also counted the remaining oligodendrocyte cell bodies in the dorsal and ventral tracts separately, in case one of them experienced a more extensive loss of oligodendrocytes than the other. I found that in the dorsal tract, the mean number of oligodendrocytes

was reduced by 68% from 34.14 ± 1.3 in DMSO-treated larvae to 10.9 ± 1.2 in Mtz-treated larvae, $p < 0.001$. Similarly, in the ventral tract, the mean number of oligodendrocytes was reduced by 68% from 51.57 ± 1.3 in DMSO-treated larvae to 16.57 ± 1.3 in Mtz-treated larvae, $p < 0.0001$ **Figure 4B**.

In order to see whether a similar degree of oligodendrocyte ablation could be achieved with an even shorter treatment with 5mM Mtz, I also counted oligodendrocytes in Tg(mbp:mCherry-NTR) larvae after a one-day treatment, and compared the numbers (**Figure 4C**) with those that remained after a two-day treatment. This indicated that there was a mean of 34.10 ± 7.72 oligodendrocytes after a one-day treatment, compared to a mean of 26.0 ± 5.69 after a two-day treatment, $p = 0.0085$. Thus, a two-day treatment with metronidazole results in a significantly greater loss of oligodendrocytes, and was established as the protocol to use. Since Dr Czopka had seen evidence of non-specific toxic effects of Mtz following treatments longer than two days (data not shown), increasing the treatment duration to ablate even more oligodendrocytes was not considered a viable option.

Thus, a two-day treatment with 5mM Mtz results in loss of 68% of oligodendrocytes in the spinal cord, both the ventral and the dorsal tracts. As with any biological phenomenon, there is a degree of variability in the oligodendrocyte numbers, but the level of variation is similar in the control and Mtz-treated conditions, as is evident in the nearly identical standard deviations in the different conditions.

In addition to this loss of oligodendrocytes, Mtz-treated Tg(mbp:mCherry-NTR) larvae appear to have developed larger, less dense-looking structures between the remaining oligodendrocyte cell bodies, indicated with red arrowheads. For a further discussion of these, see **Section 3.3.3**. below.

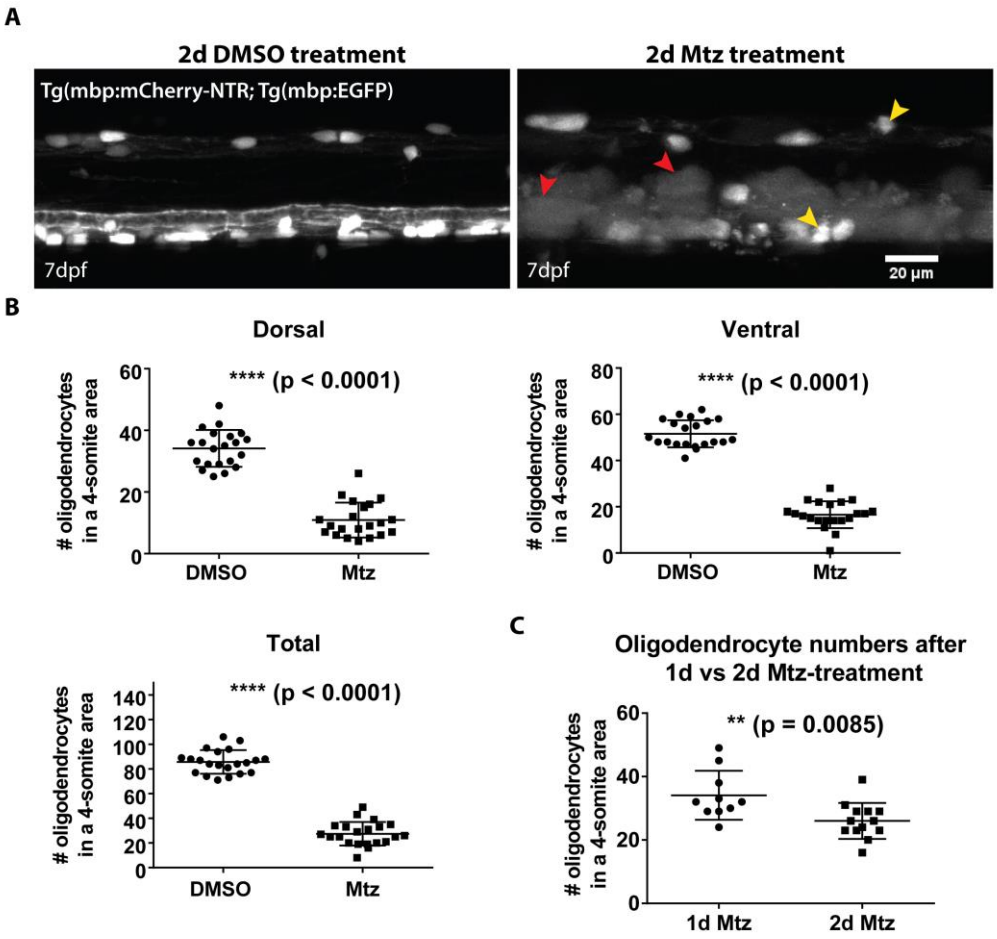

Figure 4. A two-day treatment with metronidazole treatment ablates two-thirds of oligodendrocytes in Tg(mbp:mCherry-NTR) larvae. A. Lateral views of spinal cords of 7dpf Tg(mbp:mCherry-NTRpA);Tg(mbp:EGFP) larvae, treated with either DMSO (left) or Mtz (right). The DMSO-treated larva looks normal, whereas the Mtz-treated larva has fewer oligodendrocyte cell bodies, and contains large mbp-expressing unidentified structures. Red arrowheads indicate these structures, and yellow arrowheads surviving oligodendrocyte cell bodies. **B.** Quantification of oligodendrocytes in the dorsal and ventral tracts, and the whole spinal cord, in DMSO and Mtz-treated larvae. In the dorsal tract, the mean number of oligodendrocytes are reduced by 68% from 34.14 ±1.3 in control to 10.9 ±1.2 in Mtz-treated animals ($p < 0.0001$), while in the ventral tract, the mean number of oligodendrocytes is reduced by 68% from 51.57 ± 1.3 in control animals to 16.57 ± 1.3 in Mtz-treated animals ($p < 0.0001$). Overall, the mean number of oligodendrocytes (dorsal and ventral combined) was reduced by 68% from 85.71 ± 2.1 in control to 27.48 ± 2.1 in Mtz, treated animals ($p < 0.0001$). n = 21. **C**. Comparison of oligodendrocyte loss between a one-day and a two-day treatment with Mtz shows that there is a mean of 34.10 ± 7.72 oligodendrocytes after a one-day treatment, compared to a mean of 26.0 ± 5.69 after a two-day treatment, $p = 0.0085$. n = 10 for one-day treatment, 13 for two-day treatment with Mtz.

3.3.2. Myelin sheaths are disrupted following metronidazole treatment in Tg(mbp:mCherry-NTR) larvae

To investigate how myelin morphology was affected following oligodendrocyte ablation, I crossed Tg(mbp:mCherry-NTR) fish with Tg(mbp:EGFP-CAAX) reporter fish, which expresses membrane-tethered GFP in all myelinating glia, and thus enables visualisation of myelin sheath morphology (Almeida et al. 2011; Czopka et al. 2013). I treated these larvae with 5mM Mtz from 5dpf to 7dpf, and subsequently imaged them. Representative images from control and Mtz-treated larvae are presented in **Figure 5**. and show general and severe disorganisation of the myelinated tracts in the Mtz-treated Tg(mbp:mCherry-NTR) larvae.

It is essential to note that the disorganised appearance of the myelin sheaths, as visualised by the Tg(mbp:EGFP-CAAX) line, cannot be taken to equate to demyelination *per se*. In order to visualise and quantitatively assess the actual myelination status of axons, it was necessary to perform electron microscopy, as described in detail in **Section 3.4**. below.

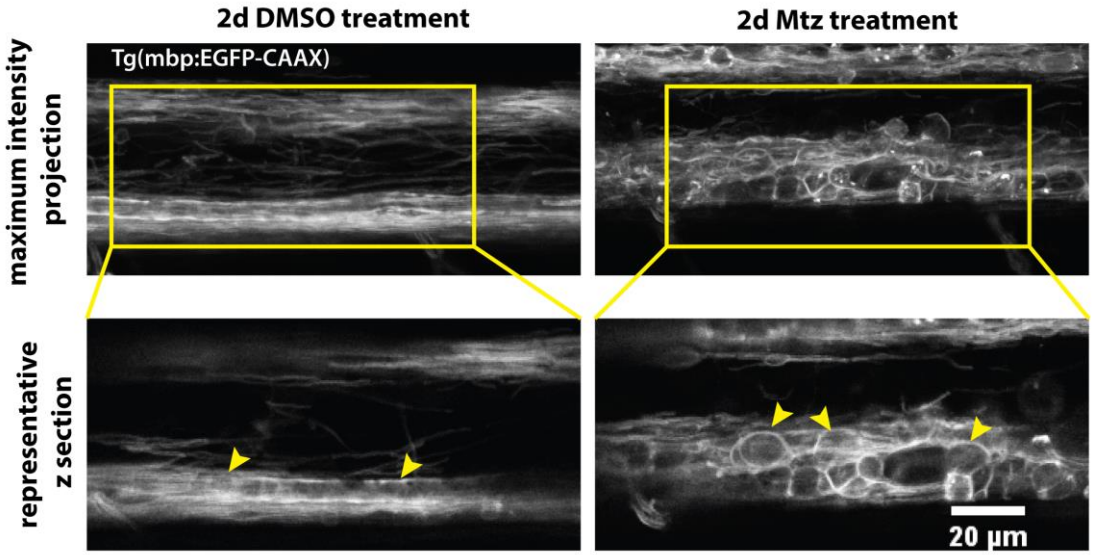

Figure 5. Myelin sheaths are severely disrupted following metronidazole treatment in Tg(mbp:mCherry-NTR) larvae. Representative confocal images of Tg(mbp:mCherry-NTR); Tg(mbp:EGFP-CAAX) larvae at 7dpf, following two-day treatment with DMSO (left column) or Mtz (right column). Top row: maximum intensity projections. Bottom row: representative single z sections to highlight the disrupted organisation of the myelin sheaths in the Mtz-treated, compared to control larva. Yellow arrowheads indicate normal myelin sheaths in the DMSO-treated larva, and presumptive "curled-up" myelin sheaths in the Mtz-treated larva.

3.3.3. Oligodendrocyte ablation results in appearance of cellular vacuoles

Previous studies have reported highly vacuolated tissue following genetic ablation of oligodendrocytes (Pohl et al. 2011; Traka et al. 2010; Locatelli et al. 2012). As I mentioned above, Mtz-treatment of Tg(mbp:mCherry-NTR) larvae results in the appearance of large, less dense-looking GFP-expressing structures in the spinal cord. These very striking features are consistently found in all Mtz-treated Tg(mbp:mCherry-NTR) larvae and warranted further investigation. To do this, I have employed a variety of tools to visualise the vacuoles in my line, including live imaging using a selection of transgenic markers, brightfield imaging and transmission electron microscopy (TEM). These analyses indicate that the large GFP-expressing structures I observe following oligodendrocyte ablation are fluid-filled vacuoles.

In **Figure 6A**, the vacuoles are shown using the Tg(mbp:EGFP) line, as before, while in **Figure 6B**, I visualised the vacuoles using the Tg(mbp:EGFP-CAAX) line. The images shown in **Fig**. **3.5B** were taken at five days post-treatment, and in the Mtz-treated Tg(mbp:mCherry-NTR) animal, a large vacuole can be seen spanning a large proportion of the height of the spinal cord, surrounded by a cluster of smaller vacuoles. Remarkably, the vacuoles are also clearly visible by brightfield microscopy (**Figure 6C**).

The full transgenic Tg(mbp:EGFP-CAAX) line is ideal for visualising the state of the spinal cord globally. For a better understanding of the nature of the vacuoles at the level of individual oligodendrocytes, I injected mbp:EGFP-CAAX plasmid into 1-8 cell staged embryos, which gives rise to mosaic labelling of single oligodendrocytes and all their myelin sheaths. As shown in **Figure 6C**, the morphology of oligodendrocytes in DMSO-treated animals does not change over the two-day DMSO-treatment. By contrast, single oligodendrocytes in Mtz-treated animals often have myelin sheaths that appear to be detaching and swelling up into a round bubble-like formation.

A recent study employing electron microscopy on high-pressure frozen tissue showed that appearance of vesicular membrane profiles in the innermost layers of the myelin sheath is the first stage in myelin sheath breakdown, and as the breakdown proceeds, the vesicular structures become increasingly prominent (Weil et al. 2016). The authors further showed that this disruption of myelin sheath organisation is triggered by loss of mbp. These observations are consistent with the idea that the vacuoles I see in fluorescent and brightfield microscopy are products of myelin sheath breakdown, although further live imaging and ultrastructural studies would be required for a comprehensive characterisation.

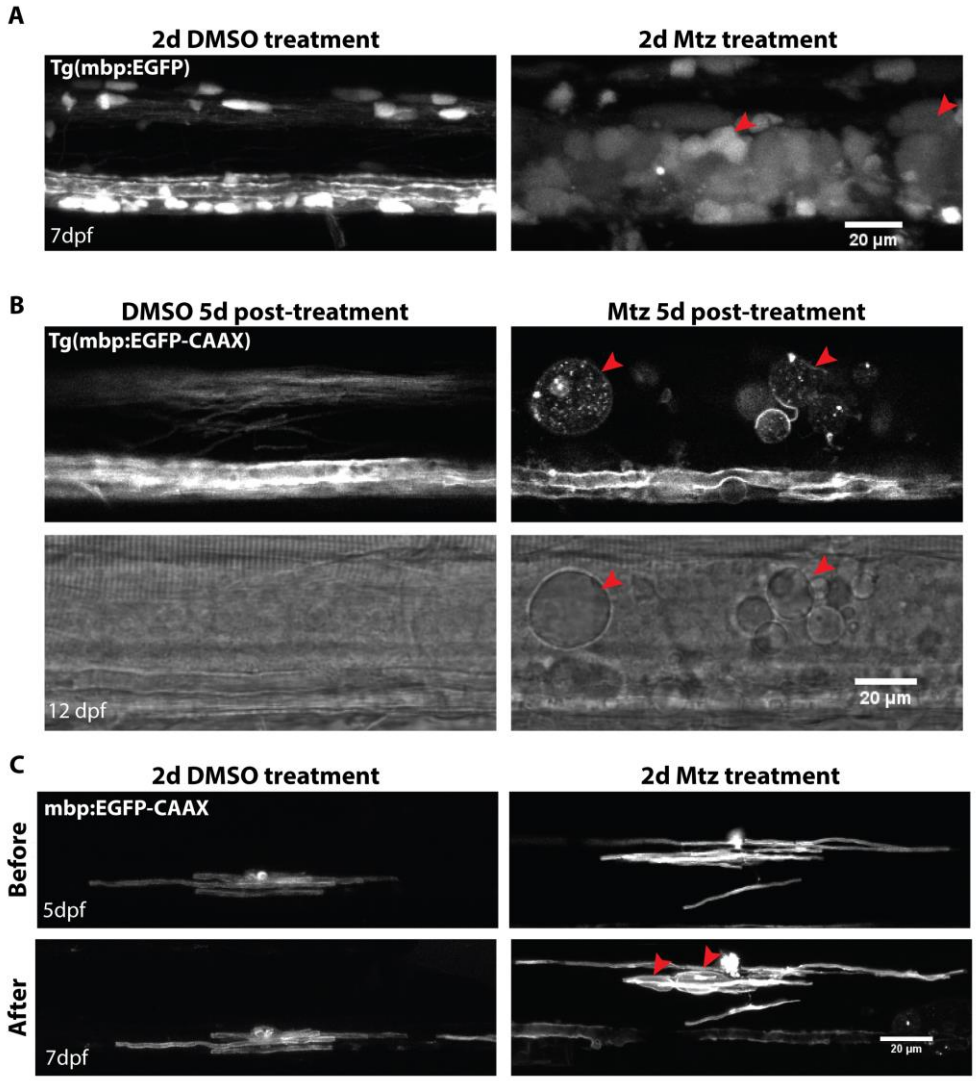

Figure 6. Vacuoles visualised by different methods. A. Lateral views of spinal cords of 7dpf Tg(mbp:mCherry-NTRpA);Tg(mbp:EGFP) larvae. The Mtz-treated animal (right) contains large mbp-positive structures (arrowheads) which are absent from the control animal. **B**. Lateral views of spinal cords of 11dpf Tg(mbp:mCherry-NTRpA);Tg(mbp:EGFP-CAAX) larvae. The GFP channel labelling myelin sheaths is shown. In the Mtz-treated animal (right) the myelin sheaths have formed vacuoles (arrowheads) which are absent from the control animal. **C**. Single oligodendrocytes labelled by injection of the mbp:EGFP-CAAX plasmid, before and after treatment with either DMSO or Mtz. The DMSO-treated cell remains unchanged, whereas some myelin sheaths on the Mtz-treated cell appear to be detaching from the axon and forming vacuoles (arrowhead).

Therefore, to better visualise the vacuoles I see in my model, and to compare them to vacuolated tissue reported by previous studies, I prepared Tg(mbp:mCherry-NTR) larvae for transmission electron microscopy (TEM), and cut transverse sections at

somite 16. **Figure 7** shows entire hemi-spinal cords of 11dpf larvae, treated with either DMSO or Mtz and sacrificed at 4 days post-treatment. The spinal cord in the Mtz-treated Tg(mbp:mCherry-NTR) larva contains large white, almost circular, structures which are entirely absent from the control animal. These structures presumably correspond to the vacuoles seen by confocal microscopy. Notably, the EM images indicate that some vacuoles can reach the size of neuronal cell bodies or the Mauthner axon (the largest axon in the zebrafish spinal cord, marked with a red letter M) while others are much smaller (inset). Based on the progression of "vesicularisation" from (Weil et al. 2016), it is possible that the different sizes represent vacuoles at different stages of myelin sheath breakdown.

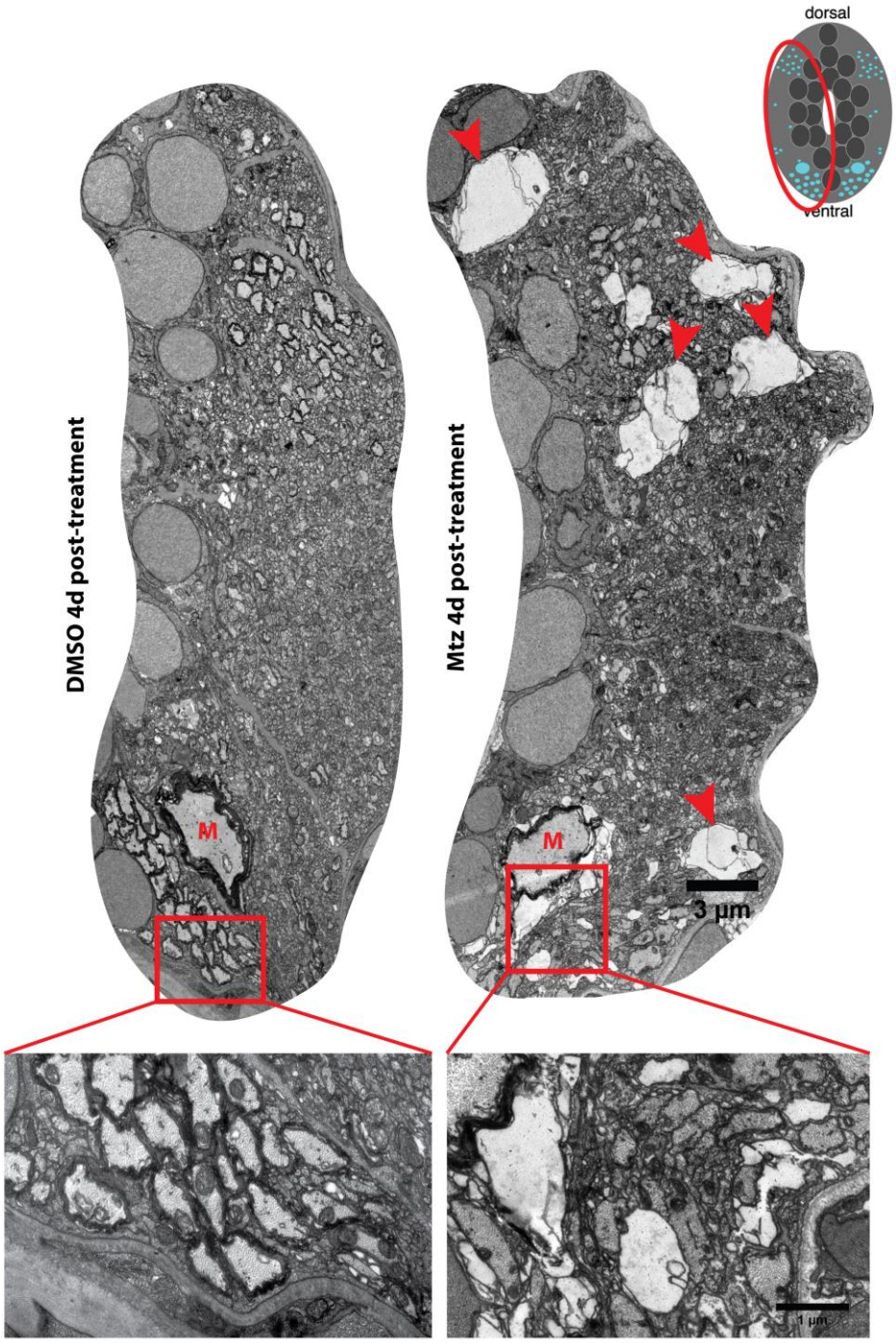

Figure 7. Vacuoles in the spinal cord as seen by TEM. TEM images of entire hemispinal cords of 11dpf Tg(mbp:mCherry-NTR) larvae, treated with either DMSO or Mtz, as indicated. **The schematic at the top right corner shows the structure of a whole spinal cord, in transverse section, and the red oval indicates the area where the TEM images are captured.** Red arrowheads on Mtz-treated larva indicate vacuoles and the red letters M indicate Mauthner axons.

As with the number of oligodendrocytes, a degree of variability in the severity of vacuolation exists between individual Tg(mbp:mCherry-NTR) larvae. **Figure 6C** above shows a relatively mildly affected oligodendrocyte, whereas **Figure 8B**. below is an example of a severely affected oligodendrocyte. Similarly, the electron micrograph of the spinal cord in **Figure 7** shows a relatively mildly affected phenotype, whereas the electron micrograph in **Figure 8A** is an example of a particularly strongly affected ventral spinal cord.

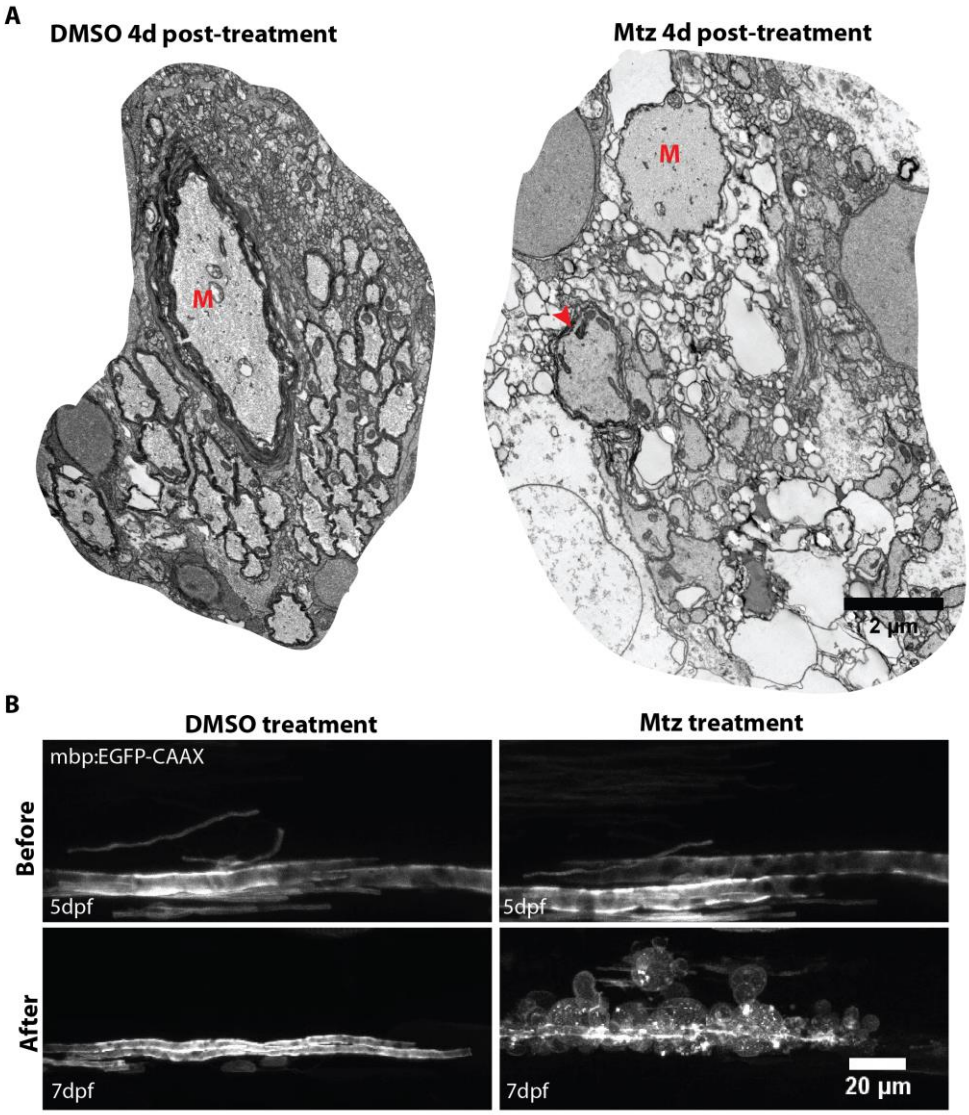

Figure 8. Examples of severely affected spinal cords and oligodendrocytes. A. TEM images of transverse sections of ventral spinal cords of 11dpf larvae, treated with either DMSO (left) or MTz (right). The tissue in the DMSO-treated animal looks normal, whereas in the Mtz-treated animal the spinal cord is filled with vacuoles and disrupted tissue. Red arrowheads indicate Mauther axon. **B**. Confocal images of a lateral view of spinal cords of 5dpf and 7dpf larvae, before and after either DMSO (left) or Mtz (right) treatment. A single oligodendrocyte is labelled in each, by injection of the mbp:EGFP-CAAX plasmid. The myelin sheaths of the DMSO-treated cell remain largely unchanged over two days, whereas those on the Mtz-treated cell appear to have detached and formed vacuoles

3.3.4. Oligodendrocyte numbers remain lower in Mtz-treated Tg(mbp:mCherry-NTR) larvae for at least seven days post-treatment

Thus far, the characterisation of the oligodendrocyte ablation in my Tg(mbp:mCherry-NTR) line has revealed that a two-day treatment with 5mM metronidazole ablates approximately two-thirds of spinal cord oligodendrocytes, and triggers the formation of vacuoles.

Having established these effects of the treatment, I was interested in what happens next; when I withdraw the metronidazole and replace it with normal embryo medium, does oligodendrocyte loss proceed further, or does the oligodendrocyte number begin to rise? If it begins to rise, does this occur immediately following Mtz-treatment, or after a delay?

It is now well documented that the vertebrate central nervous system is populated by oligodendrocyte progenitor cells throughout life (Dawson et al. 2003; Hughes et al. 2013). Indeed, in the zebrafish spinal cord, the number of oligodendrocytes rises throughout life (Park et al. 2007; Buckley et al. 2010). With these in mind, there was every reason to believe that zebrafish larvae would be able to generate new oligodendrocytes to replace those ablated. (It is important to note, however, that the continued production of oligodendrocytes is not likely to confound the analysis of de- and remyelinated axons, since the axon tracts I am interested in were already myelinated at 5dpf prior to the start of the Mtz-treatment; see **Section 3.4**. below for discussion of demyelination).

To find out when, if at all, the larvae begin to regenerate their oligodendrocytes, I carried out a time course experiment where I imaged larvae every day for the first seven days following withdrawal of the metronidazole treatment. I chose this time course, as at seven days post-treatment, the larvae are over 14 days old and have grown in size such that the thickness of muscle tissue renders high-resolution live imaging difficult after this point.

For reasons of larval health, it was not practical to image the same larvae over so many consecutive days, so the following data were obtained from imaging a different cohort

of larvae each day. In each larva, I imaged a four-somite long area of the spinal cord (approximately somites 8-11) and counted the oligodendrocytes from these images.

I again used the Tg(mbp:EGFP) line, crossed to my Tg(mbp:mCherry-NTR) line, to facilitate counting oligodendrocytes in live larvae. The results of this time course experiment are shown in **Figure 9**. Throughout the period of the first seven days following metronidazole treatment, the number of oligodendrocytes in the DMSO-treated larvae increases, with a mean of 69.94 ± 11.64 oligodendrocytes at 0d post-treatment and 92.15 ± 9.76, $p < 0.0001$. Interestingly, the number of oligodendrocytes in the Mtz-treated larvae does not decrease further from the end of the Mtz-treatment, and instead increases slightly over time, from a mean of 26.76 ± 7.20 at 0d post-treatment to 44.25 ± 11.57 at 7d post-treatment, $p = 0.0004$. Importantly, however, the number of oligodendrocytes in Mtz-treated larvae remains significantly lower than in DMSO-treated larvae throughout the seven-day period; at 7d post-treatment the mean number of oligodendrocytes was 92.15 ± 9.76 in DMSO-treated animals, compared to 44.25 ± 11.57 in Mtz-treated animals ($p < 0.0001$). Comparisons at other time points are detailed in the legend of **Figure 9**.

Thus, this timeline indicates that oligodendrocyte numbers are not restored to control levels in the first seven days following metronidazole treatment.

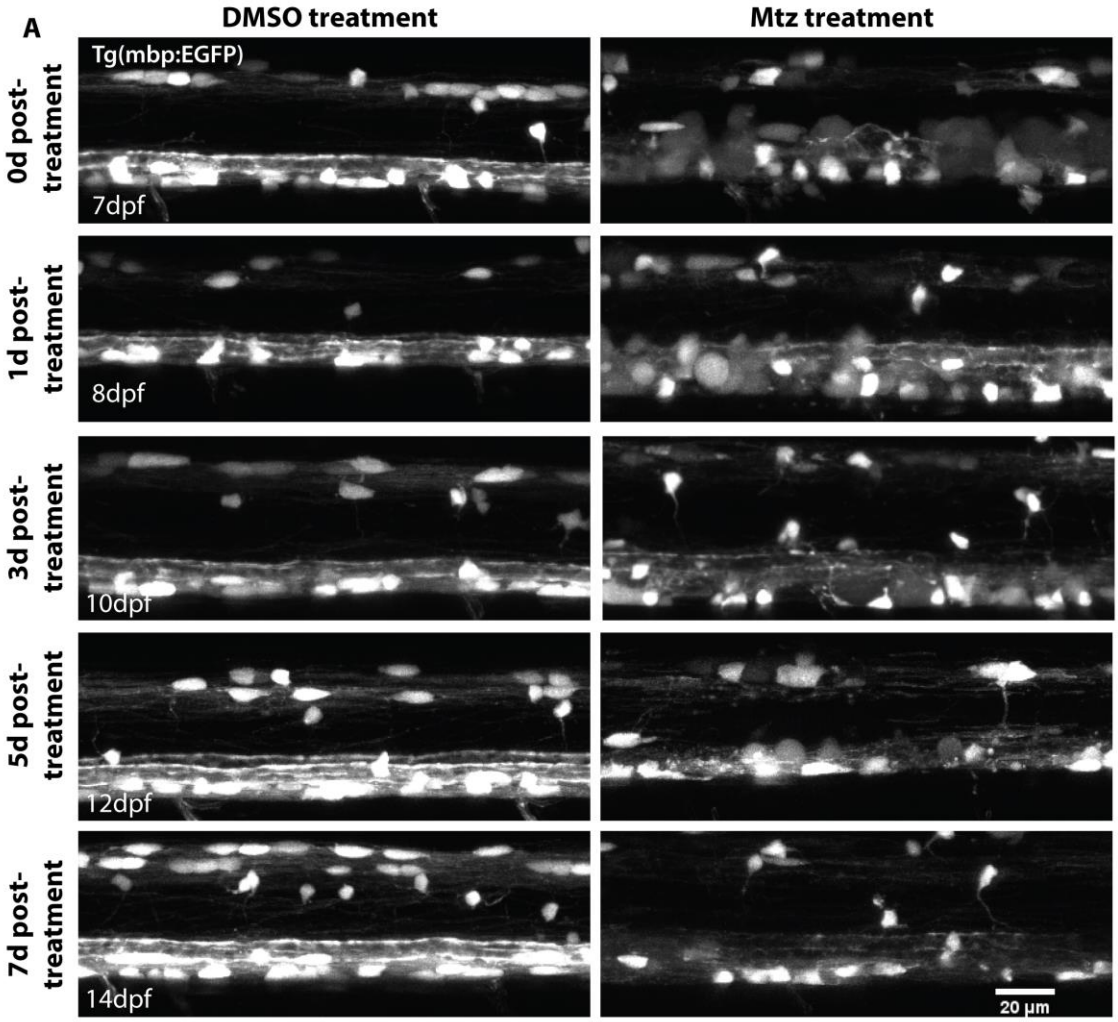
A
DMSO treatment
Mtz treatment
Tg(mbp:EGFP)
0d post-treatment
7dpf
1d post-treatment
8dpf
3d post-treatment
10dpf
5d post-treatment
12dpf
7d post-treatment
14dpf
20 µm

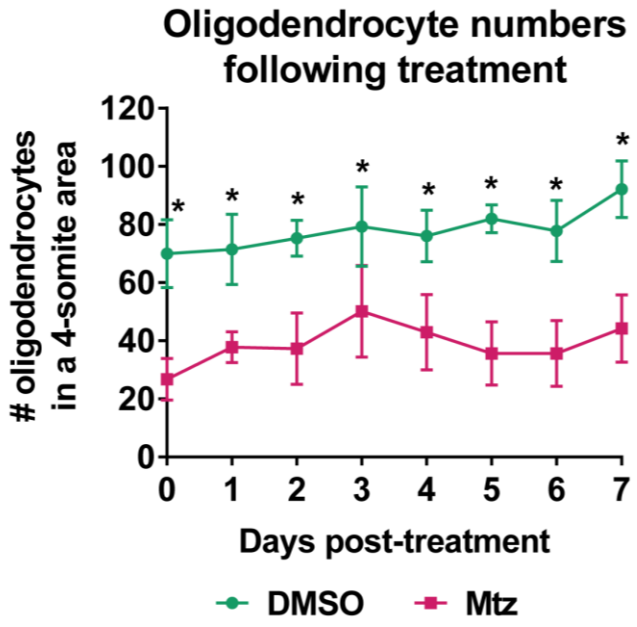
Oligodendrocyte numbers following treatment
oligodendrocytes in a 4-somite area
120
100
80
60
40
20
0
0 1 2 3 4 5 6 7
Days post-treatment
DMSO
Mtz

Figure 9. Oligodendrocyte numbers are not restored in the first seven days following Mtz-treatment. **A**. Representative images from the spinal cords of DMSO- and Mtz-treated larvae at the time points indicated. The number of oligodendrocytes in Mtz-treated larvae never approaches that in DMSO-treated larvae. **B**. Quantification of shows that oligodendrocyte numbers remain significantly lower in Mtz-treated compared to DMSO-treated animals throughout the first seven days after treatment. At 0d post-treatment, there is a mean of 69.94 ± 11.64 oligodendrocytes in control animals, compared to 26.76 ± 7.20 in Mtz-treated animals, $p < 0.0001$. At 1d post-treatment, there is a mean of 71.43 ± 12.09 oligodendrocytes in control animals, compared to 37.75 ± 5.34 in Mtz-treated animals, $p < 0.0001$. At 2d post-treatment, there is a mean of 75.29 ± 6.16 oligodendrocytes in control animals, compared to 37.22 ± 12.28 in Mtz-treated animals, $p < 0.0001$. At 3d post-treatment, there is a mean of 79.29 ± 13.71 oligodendrocytes in control animas, compared to 50.13 ± 15.78 in Mtz-treated animals, $p < 0.0001$. At 4d post-treatment, there is a mean of 76.08 ± 8.92 oligodendrocytes in control animals, compared to 42.95 in Mtz-treated animals, $p < 0.0001$. At 5d post-treatment, there is a mean of 81.92 oligodendrocytes in control animals, compared to 35.60 ± 10.88 in Mtz-treated animals, $p < 0.0001$. At 6d post-treatment, there is a mean of 77.78 ± 10.54 oligodendrocytes in control animals, compared to 35.64 ± in 11.30 in Mtz-treated animals, $p < 0.0001$. At 7d post-treatment, there is a mean of 92.15 oligodendrocytes in control animals, compared to 44.25 ± 11.57 in Mtz-treated animals, $p < 0.0001$. Statistical significances were determined by multiple t tests per row, without assuming equal standard deviations (Holm-Sidak method). n = no less than 7

3.4. Oligodendrocyte ablation results in extensive demyelination

3.4.1. Demyelinated axons are seen at 5d post-treatment

The gold standard for demonstrating demyelination is electron microscopy. In order to assess demyelination in the Tg(mbp:mCherry-NTR) larvae following Mtz-treatment, I prepared larvae for TEM at various time points during the first seven days following the treatment. As described above, for the first four days following withdrawal of the Mtz-treatment, significant myelin vacuolation was observed in the spinal cord. This extensive disruption to the overall architecture of the spinal cord made it difficult to assess demyelination. However, by 5d post-treatment, the extent of vacuoles diminished and the spinal cord cytoarchitecture appeared more intact. For this reason, I chose to quantify the extent of demyelination at 5d post-treatment.

In control animals at 12dpf, there are two notable populations of large calibre axons, one in the dorsal area and another in the ventral (see schematic in **Figure 10A**). In the control larvae, some non-myelinated large-calibre axons can be seen, pseudocoloured in turquoise, and likely represent axons soon to be myelinated. In stark contrast, in the Mtz-treated Tg(mbp:mCherry-NTR) larva, although the large calibre axons are present in the expected locations in the spinal cord, the vast majority lack distinct myelin sheaths (again pseudocoloured in turquoise; **Figure 10A**). **Figure 10B** shows higher magnification images of the ventral spinal cords of the same animals.

I have quantified the extent of demyelination in a number of ways **Figure 10C**. First, I counted the numbers of myelinated axons in the ventral spinal cord, and found that these were decreased from a mean of 58.33 ± 17.79 in control larvae to 12.75 ± 2.50 in Mtz-treated larvae, $p = 0.0034$. For this analysis, I considered any axon surrounded by more than one wrap of dark rim as myelinated. Next, I calculated the percentage of axons of a "myelinateable" size that was myelinated in control and treated animals. As a definition of "myelinateable" size in this case, I identified the smallest myelinated axon in a control animal, and defined its cross sectional size as the threshold for being of a "myelinatable" size. In the rest of this thesis, I will refer to axons of a "myelinateable" calibre simply as "large-calibre" axons. In this dataset, this threshold was a perimeter of 1 μm.

I then counted all axons of this size or larger in each animal, and calculated the percentage of those that were myelinated. This was reduced from 66.63 ± 8.0% in control animals to 16.90 ± 7.28% in Mtz-treated animals, $p = 0.0004$, amounting to a 75% decrease in percentage of myelinated axons in the ventral spinal cord.

Given the association of axonal damage with demyelination and the extent of tissue damage seen following the induction of oligodendrocyte death, I next wanted to quantify the total number of large calibre axons in control and Mtz-treated Tg(mbp:mCherry-NTR) animals. Perhaps surprisingly, the total number of large calibre axons did not differ between treated and control fish (87.67 ± 27.01 large-calibre axons in control animals, and 83.00 ± 28.65 in Mtz-treated animals, $p = 0.836$). Thus, the ablation of two-thirds of oligodendrocytes results in demyelination of 75% of the axons in the ventral spinal cord, but not in any loss of axons in this area.

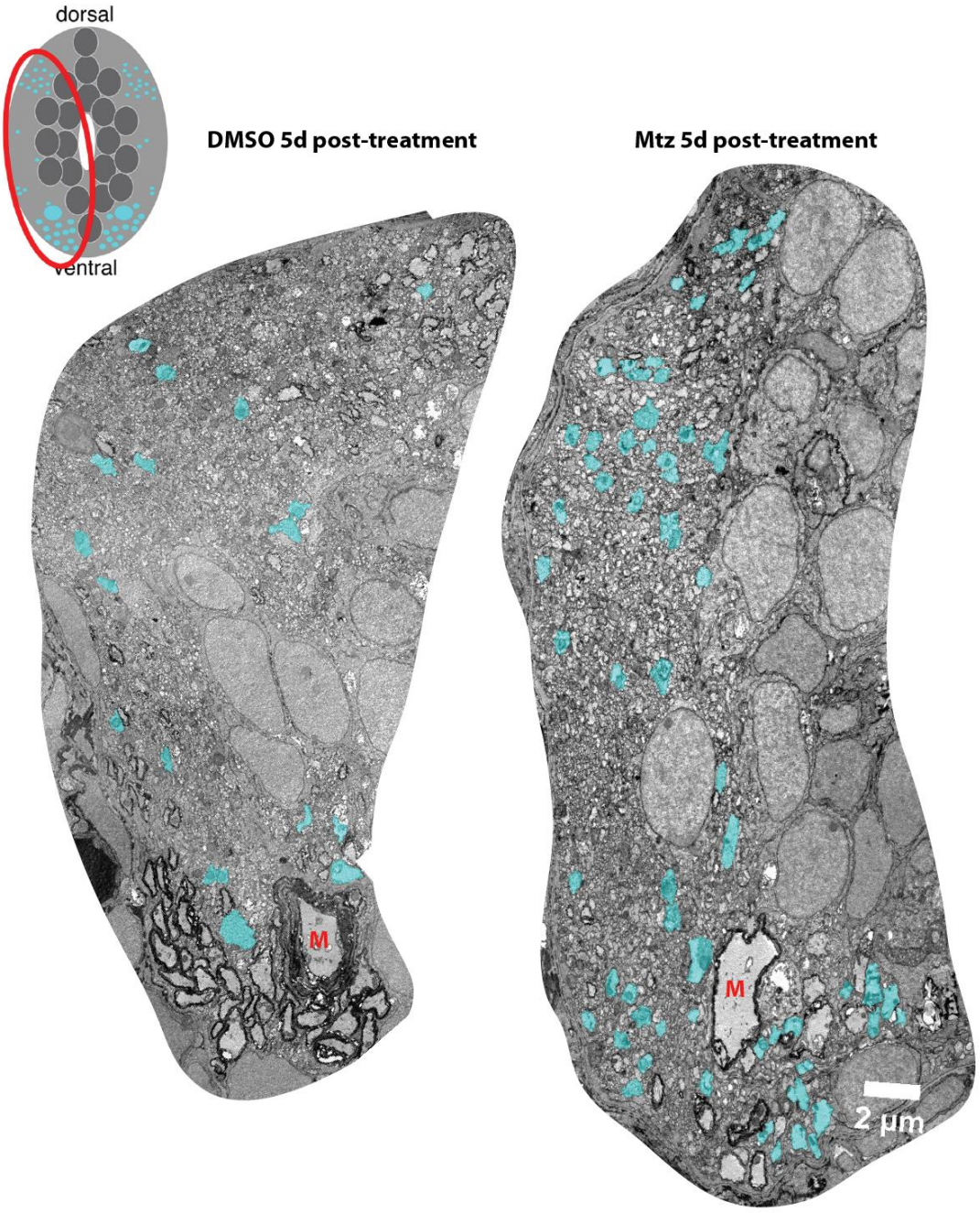

Figure continues overleaf

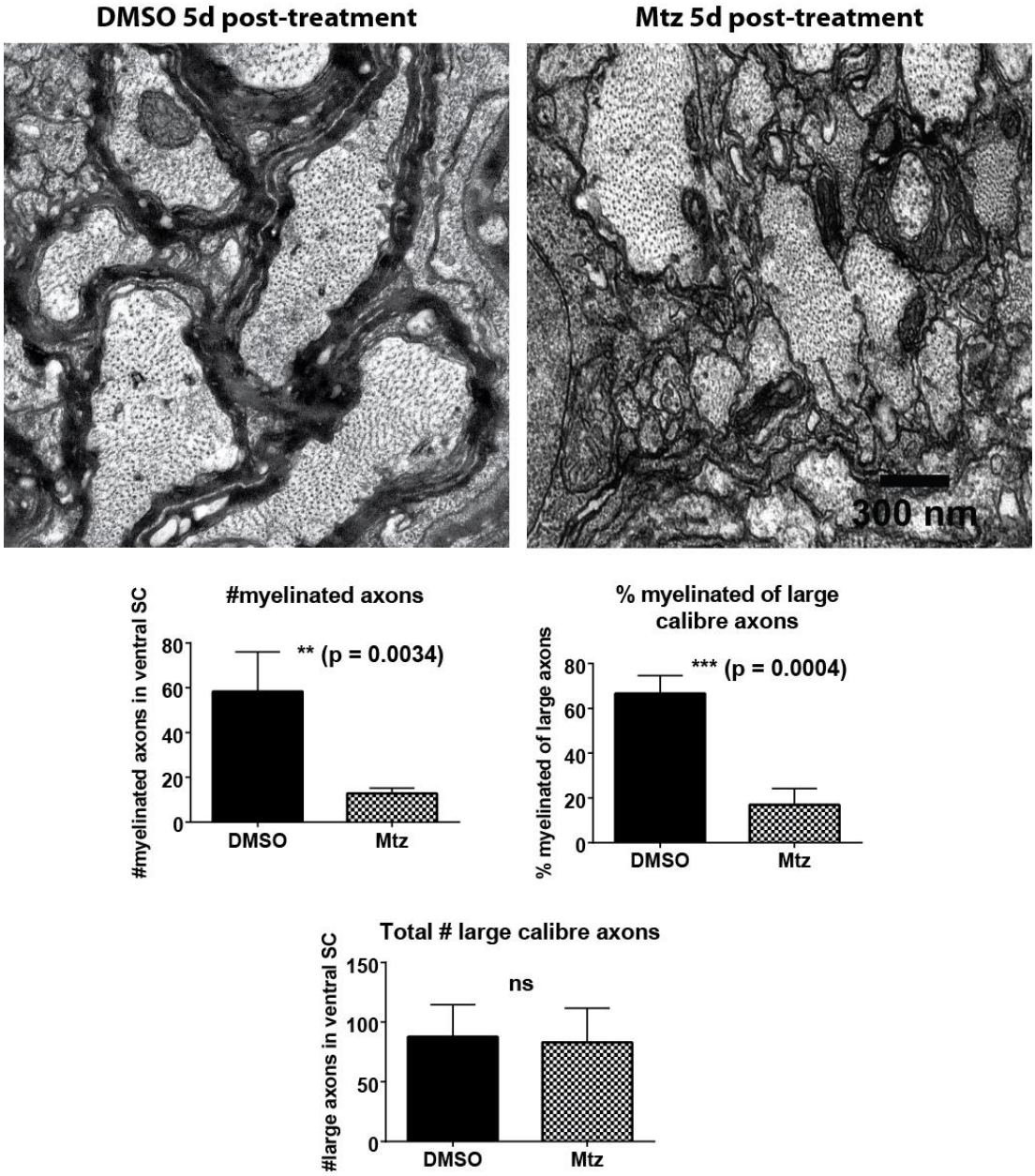

Figure 10. Extensive demyelination is observed at 5d post-treatment. **A** (previous page). Entire hemispinal cords of 12dpf larvae, treated with either DMSO (left) or Mtz (right). Red letters "M" indicate Mauthner axons. The schematic on the top left hand corner shows the structure of a whole spinal cord, and the red oval indicates the area captured in the TEM images. Large-calibre axons that are not myelinated are pseudocoloured in turquoise. **B**. Higher magnification images from the ventral spinal cord of the same larvae. The axons in the DMSO-treated animal are robustly myelinated, whereas in the Mtz-treated animal many axons are bare. **C**. Quantification shows that the total number of myelinated axons in the ventral spinal cord is reduced from 58.33 ± 12.75 in control animals to 12.75 ± 2.50 in Mtz-treated animals, $p = 0.0034$. The percentage of large-calibre axons that is myelinated is reduced from 66.63 ± 8.0% in control animals to 16.90 ± 7.28% in Mtz-treated animals, $p = 0.0004$. The total number of large-calibre axons does not differ

significantly between control and Mtz-treated animals (87.67 ± 27.01 in control animals, and 83.0 ± 28.65 in Mtz-treated animals, $p = 0.836$. $n = 3$ for DMSO, 4 for Mtz.

3.4.2. Axons remain demyelinated at 7d and 11d post-treatment

Having seen such extensive demyelination at 5d post-treatment, I next wished to determine how long axons remained demyelinated and when remyelination might commence. To this end, I prepared larvae for TEM at 7d and at 11d post-treatment, and assessed the myelination status of these animals. **Figure 11** shows representative images from ventral spinal cords of DMSO- and Mtz-treated animals at 7d and 11d post-treatment. It is clear from these images that spinal cords of Mtz-treated larvae still contain numerous demyelinated axons at both time points, whereas the vast majority of the axons in control animals at the same time points are myelinated.

To quantify this demyelination, I again counted the numbers of large-calibre myelinated and unmyelinated axons, and calculated the percentage of large-calibre axons that was myelinated. At 7d post-treatment, the percentage of myelinated axons was reduced from 59.46 ± 12.45% in control animals to 28.55 ± 11.54 % in Mtz-treated animals. At 11d post-treatment, the percentage of myelinated axons remains reduced in Mtz-treated animals, with controls having 72.05 ± 1.05% compared to 24.3 ± 10.66% in Mtz-treated animals. A two-way ANOVA found a significant main effect of treatment condition ($p < 0.0001$). Neither the main effect of time point ($p = 0.390$) nor the interaction ($p = 0.09$) were significant. The apparent decrease in percentage of myelinated axons between Mtz-treated animals at 7d and 11d post-treatment (28.55% to 24.3%) is not statistically significant ($p = 0.5227$).

I also counted the total number of large-calibre axons at these 7d and 11d post-treatment, and found that this did not differ between the time points or the treatment conditions: there was a mean of 85.4 ± 27.06 large-calibre axons in DMSO-treated larvae and 76.2 ± 20.79 in Mtz-treated larvae, while at 11d post-treatment, there was a mean of 89.5 ± 24.58 large-calibre axons in DMSO-treated animals and 87.25 ± 29.71 in Mtz-treated larvae. A two-way ANOVA found both main effects of treatment

condition ($p = 0.644$) and time point ($p = 0.542$) as well as the interaction ($p = 0.778$) non-significant (**Figure 11)**.

Overall, these data suggest that Mtz-treated spinal cords remains largely demyelinated until at least 11d post-treatment, but that this does not result in loss of axons. It is also worth noting that, as in the electron micrographs taken at 5d post-treatment, there are very few vacuoles present in the ventral spinal cords at 7d and 11d post-treatment.

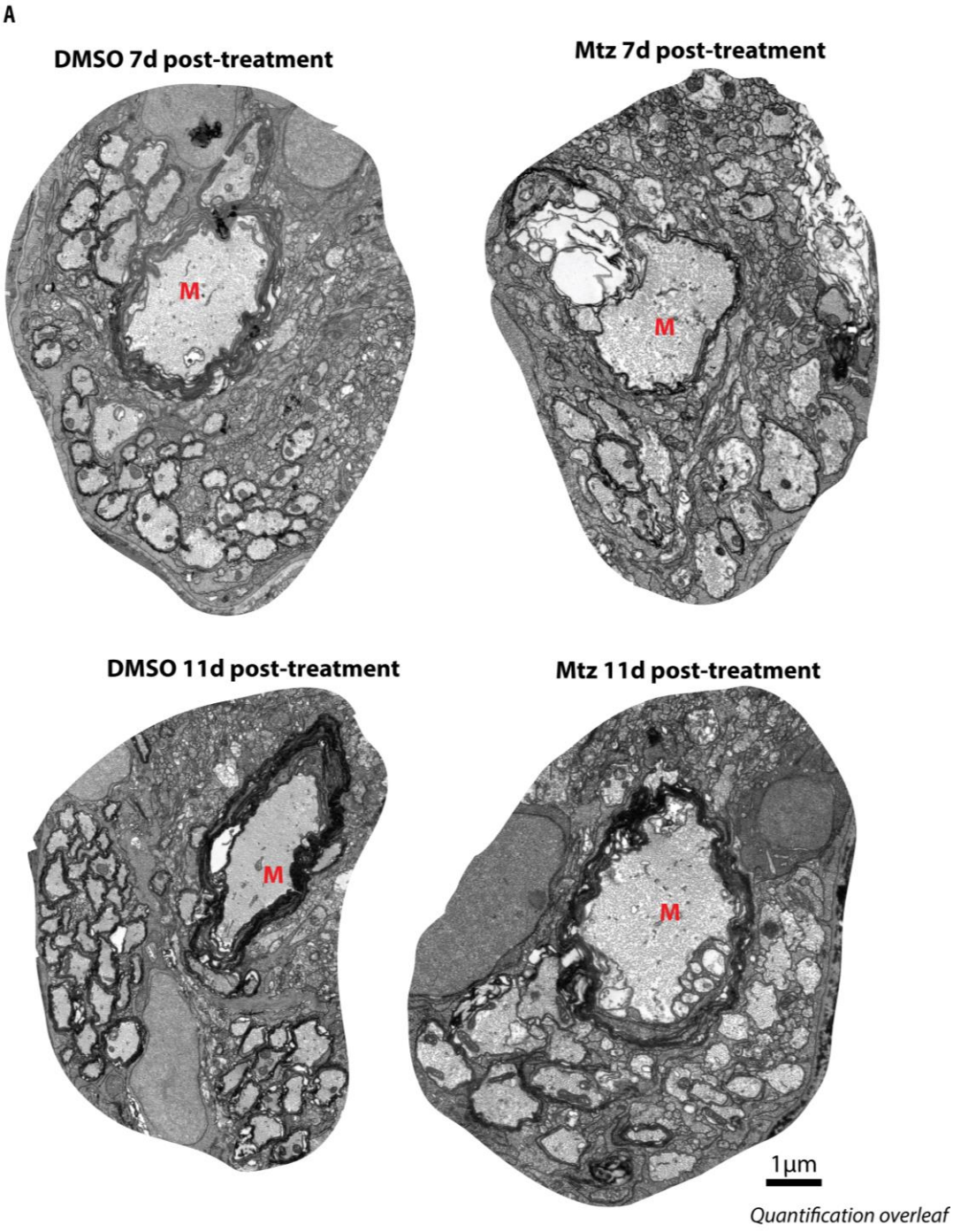

Quantification overleaf

B

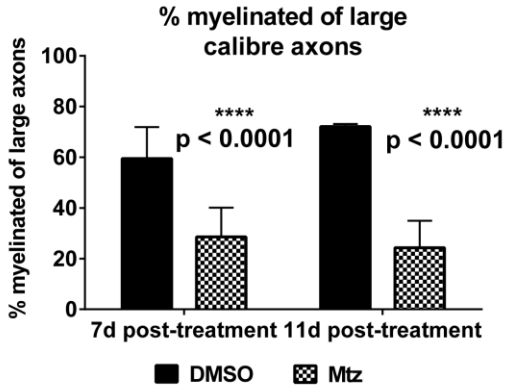

C

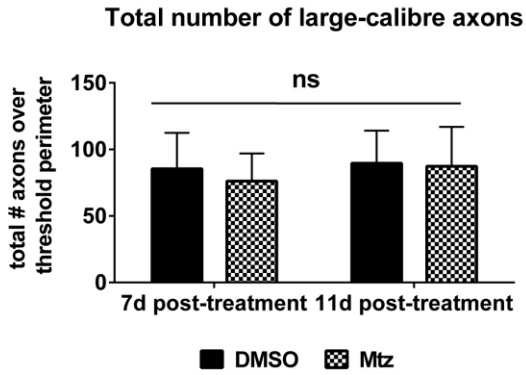

Figure 11. Axons remain demyelinated at 7d and 11d post-treatment. A. TEM images of ventral spinal cords of 14dpf and 18dpf larvae, treated with either DMSO or Mtz, as indicated. The Mtz-treated spinal cords at both 7d and 11d larvae still contain numerous demyelinated axons. **B**. Quantification reveals that at 7d post-treatment, the percentage of myelinated axons was reduced from 59.46 ± 12.45% in control animals to 28.55 ± 11.54 % in Mtz-treated animals. At 11d post-treatment, controls have 72.05 ± 1.05% myelinated of large-calibre axons, compared to Mtz-treated animals having 24.3% ± 10.66%. A two-way ANOVA finds significant main effect of treatment condition ($p < 0.0001$). Neither the main effect of time point ($p = 0.390$) nor the interaction ($p = 0.09$) were significant. The apparent decrease in percentage of myelinated axons between Mtz-treated animals at 7d and 11d post-treatment (28.55% to 24.3%) is not statistically significant ($p = 0.5227$). **C**. Quantification shows that there is no difference in the total number of large-calibre axons between the two time points or between control and Mtz-treated larvae: at 7d post-treatment, there is a mean of 85.4 ± 27.06 axons in DMSO-treated larvae and 76.2 ± 20.79 in Mtz-treated larvae, while at 11d post-treatment, there is a mean of 89.5 ± 24.58 axons and 87.25 ± 29.71 in Mtz-treated larvae. A two-way ANOVA finds both main effects of treatment condition ($p = 0.644$) and time point ($p = 0.542$) as well as the interaction ($p = 0.778$) non-significant. n = 5 at 7d post-treatment and 4 at 11d post-treatment.

3.5. Remyelination

3.5.1. Extensive remyelination is observed at 16d post-treatment

My electron microscopy data indicate that axons remain demyelinated for several days in Mtz-treated Tg(mbp:mCherry-NTR) animals. However, given that the zebrafish as a model system is renowned for its remarkable capacity for repair and regeneration, (Becker and Becker 2014) I considered it likely that the larvae would eventually be able to remyelinate at least some of their axons.

Therefore, following an amendment to our Home Office licences to allow analysis at later stages, I grew animals up for 16 days after withdrawal of Mtz-treatment. At this point, Mtz- and DMSO-treated animals had indistinguishable myelinated axons. **Figure 12** shows two hemi-spinal cords, from a control animal (left) and a Mtz-treated Tg(mbp:mCherry-NTR) animal (right). Quantification indicated that the number of myelinated axons was not different between treated and control animals (the mean number of myelinated axons was 80.88 ± 23.12 in control animals and 85.71 ± 22.01 in Mtz-treated animals, $p = 0.686$). Similarly, the percentage of large calibre axons that was myelinated did not differ significantly between treated and control animals (88.75 ± 7.09% of axons were myelinated in control animals and 82.86 ± 9.72% in Mtz-treated animals, $p = 0.199$). Finally, the total number of large-calibre axons did not differ significantly between treated and control animals either (there was a mean of 91.13 ± 25.39 large calibre axons in control animals and 104.0 ± 24.04 in Mtz-treated animals, $p = 0.334$). Thus, the data suggest that demyelinated axons undergo remyelination by 16d post-treatment and that the period of regeneration of myelin must take place between 11 and 16 days post-treatment.

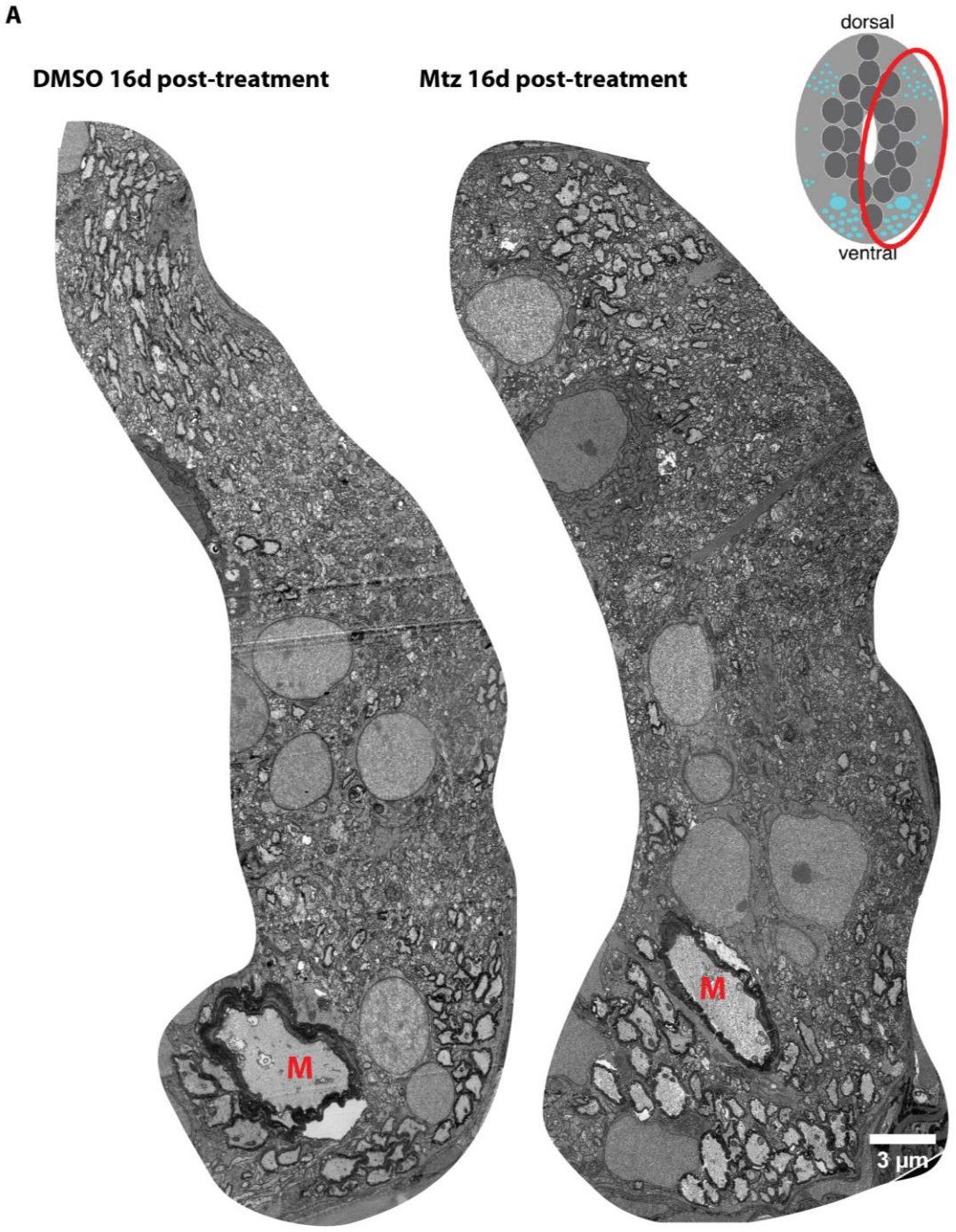

Quantification overleaf

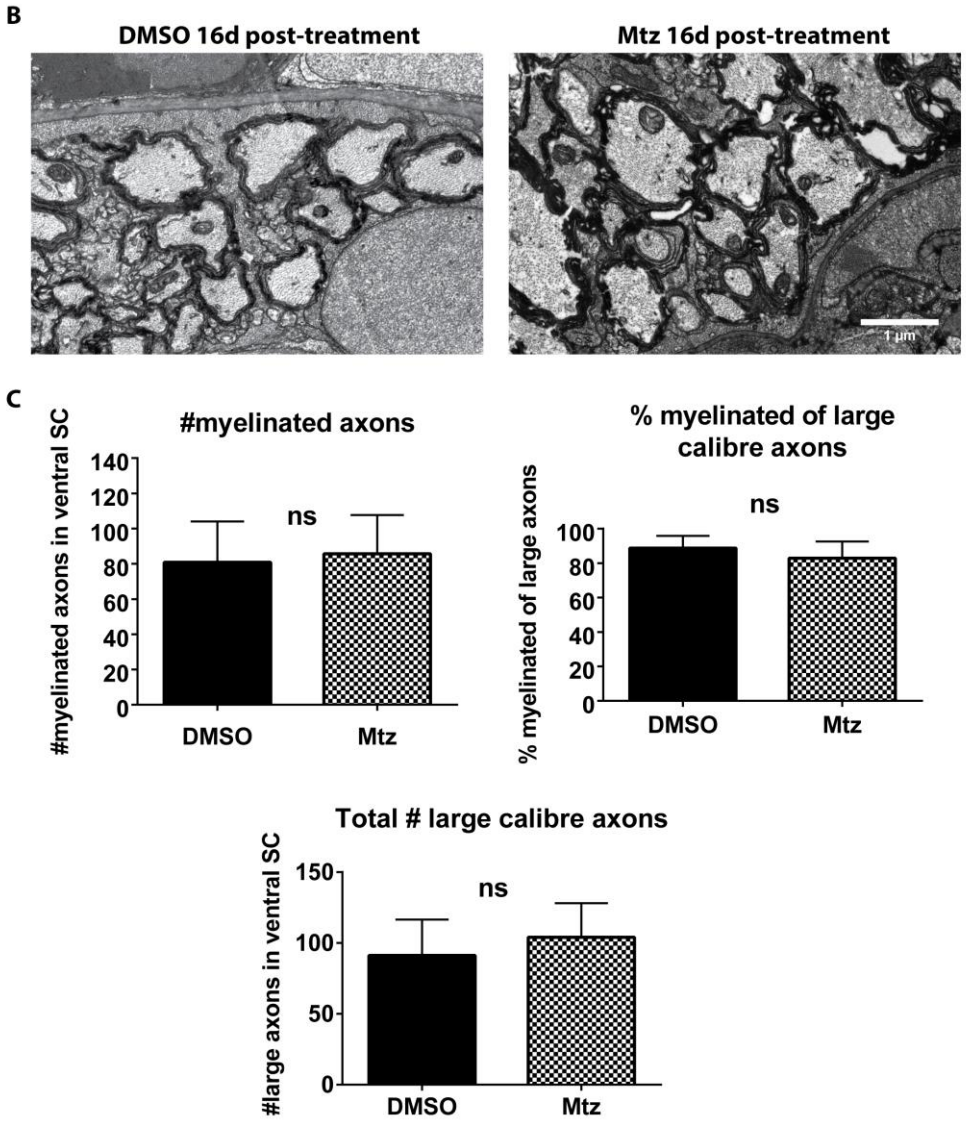

Figure 12. Remyelination is observed at 16d post-treatment. A. (previous page) Entire hemispinal cords of 23dpf larvae, treated with either DMSO (left) or Mtz (right). Both spinal cords appear robustly myelinated. **B**. Higher magnification images of the same spinal cords. **C**. Quantification shows that number of myelinated axons is not different between treated and control animals (the mean number of myelinated axons is 80.88 ± 23.12 in control animals and 85.71 ± 22.01 in Mtz-treated animals, $p = 0.686$). The percentage of large-calibre axons that is myelinated does not differ significantly between control and Mtz-treated animals (88.75 ± 7.09% in control and 82.86 ± 9.72% in Mtz-treated animals, $p = 0.199$). The total number of large-calibre axons does not differ between control and Mtz-treated animals either (a mean of 91.13 ± 25.39 in control animals and 104.0 ± 24.04 in Mtz-treated animals, $p = 0.334$). $n = 8$.

3.5.2. Regenerated myelin reaches the thickness of control myelin in Mtz-treated Tg(mbp:mCherry-NTR) animals

In the field of mammalian de- and remyelination, new myelin generated during remyelination is widely agreed to be thinner than myelin made during normal development (Blakemore 1973; Blakemore 1974). In fact, even in a model of adult zebrafish remyelination, the newly made myelin failed to reach the thickness of control myelin, although, interestingly, this was an age-dependent phenomenon with repair generating thinner myelin sheaths only in older animals (Münzel et al. 2014).

Therefore, I quantified myelin thickness at 16 days post treatment, by assessing the g-ratio:

$$\text{g ratio} = \frac{\text{diameter of axon}}{\text{diameter of myelinated axon}}$$

To determine the g ratios of the axons in this cohort, I first traced around the perimeter of the axon itself (inside the myelin sheath; blue tracing in **Figure 13A**) and then traced the outer perimeter of the myelinated axon (pink tracing in **Figure 13A**). I calculated the diameters from the perimeters and then calculated the ratio of the diameter of the axon to the diameter of the myelinated axon (see **Chapter 2**) for more details.

Figure 13 shows that there is no difference between the mean g ratios of control and Mtz-treated animals at 16d post-treatment (mean g ratio was 0.81 ± 0.042 in control animals and 0.82 ± 0.025 in Mtz-treated animals, $p = 0.671$). However, simply comparing g ratios without taking into account the sizes of the axons can be a crude and misleading measure, given that myelin thickness is known to vary with axon calibre (Blakemore 1973). In order to accommodate that, I plotted the g ratios I had calculated against the diameters of those axons. The resulting scatter plot, presented in **Figure 13**, clearly illustrates that there are no differences between myelin thicknesses between Mtz-treated and control larvae, regardless of the sizes of the axons. Thus, the data indicate remyelination restores myelin thickness to control levels in this model.

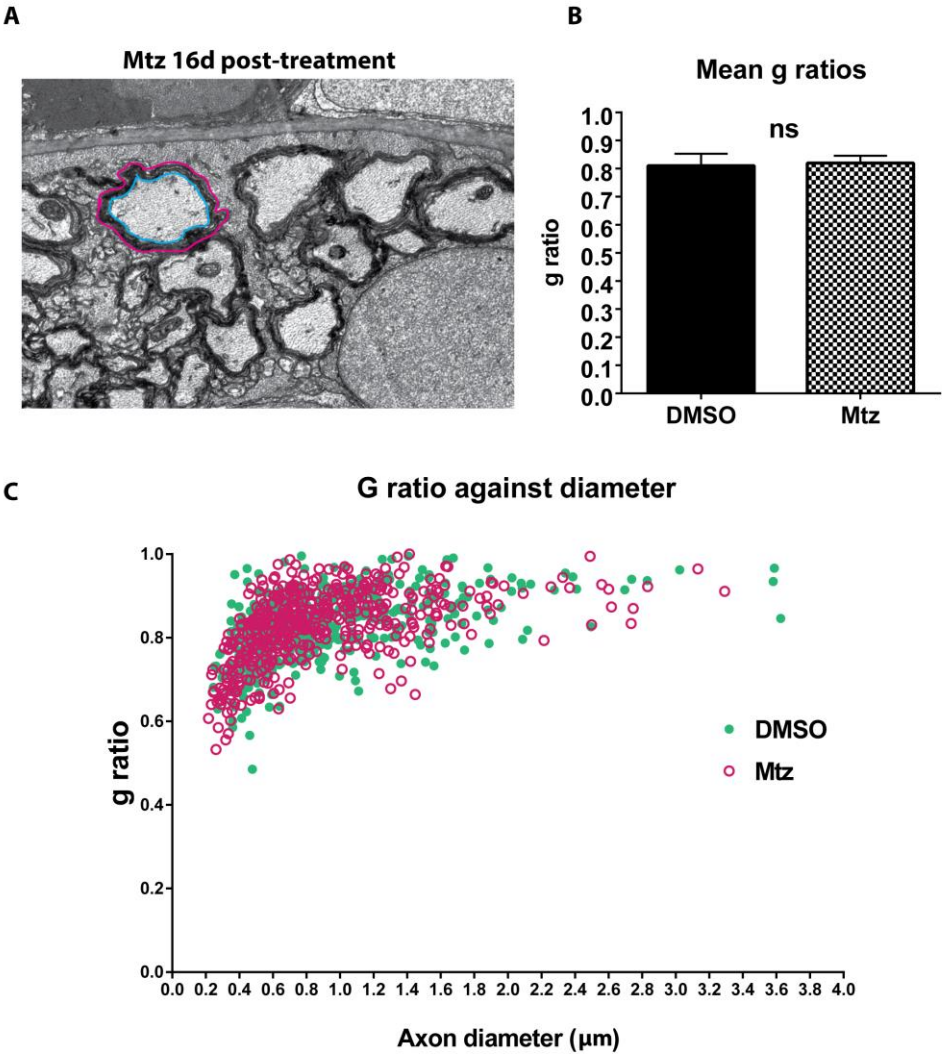

Figure 13. Remyelination restores myelin thickness to normal levels. A. Illustration of how g ratios were measured: the blue tracing indicates the perimeter of the axon, and the pink tracing the perimeter of the myelin. These were measured and divided by π to obtain diameters. Axon diameter was divided by diameter of myelinated axon to obtain g ratios. **B**. A comparison of the mean g ratios shows that the mean g ratio in control animals is 0.81 ± 0.042, and in Mtz-treated animals the mean g ratio is 0.82 ± 0.025, p = 0.671). C. G ratios plotted against axon diameters to illustrate the spread of myelin thicknesses over axons of different sizes. The population of axons in Mtz- and DMSO-treated animals is completely indistinguishable.

3.6. Oligodendrocyte number recovery

3.6.1. Oligodendrocyte numbers are restored to control levels by 16d post-treatment

Thus far, I have demonstrated that treating Tg(mbp:mCherry-NTR) larvae with 5mM Mtz from 5dpf to 7dpf ablates two-thirds of the oligodendrocytes in the spinal cord, as well as causing the appearance of cellular vacuoles. Oligodendrocyte numbers remain lower in Mtz-treated than in control animals for at least seven days following withdrawal of metronidazole. Electron microscopy indicates extensive demyelination, and this persists from 5 to 11 days post-treatment. However, by 16d post-treatment, Mtz-treated larvae achieve complete remyelination, where the Mtz-treated larvae are indistinguishable from controls in terms of the number and percentage of myelinated axons, as well as myelin thickness. This remarkable feat of successful replacement of lost myelin suggests that sufficient numbers of new oligodendrocytes are generated at some point to carry out the remyelination. However, intriguing questions remain over when these oligodendrocytes are produced, and whether the newly generated oligodendrocytes reach the numbers of control animals, or whether they fall short.

In order to address these questions, I carried out a time course experiment to quantify oligodendrocyte numbers during the period of peak demyelination through to recovery, i.e. between 7 and 16 days post-treatment. Owing to the increasing size of growing larvae during the recovery period, this experiment could not be completed to an acceptable standard by live imaging our available transgenic reporter. Therefore, I prepared cryosections from control and Mtz-treated Tg(mbp:mCherry-NTR) larvae at the different time points, and used the endogenous mCherry fluorescence to count oligodendrocyte numbers. Briefly, I cut four sections per animal, at least 100µm apart (to avoid imaging the same cell twice), stained these with Hoechst to label nuclei, and used the endogenous expression of the mbp:mCherry transgene to determine which nuclei belonged to oligodendrocytes. Representative images of these cryosections are shown in **Figure 14A**.

I counted the total number of oligodendrocytes on each section, and took the mean of oligodendrocyte number from the four sample sections to denote the relative number

of oligodendrocytes in each animal. The graph in **Figure 14B** shows that oligodendrocyte numbers are rising in both DMSO- and Mtz-treated larvae: oligodendrocytes in DMSO-treated larvae increase from 6.9 ± 0.44 at 7d post-treatment to 9.46 ± 2.21 ($p = 0.0282$) at 16d post-treatment, while oligodendrocytes in Mtz-treated larvae increase from 2.4 ± 0.23 at 7d post-treatment to 8.57 ± 2.58 at 16d post-treatment ($p < 0.0001$).

At the first three time points examined (i.e. 7, 10 and 14d post-treatment), there were significantly fewer oligodendrocytes in sections from Mtz-treated animals compared to DMSO-treated animals: at 7d post-treatment, there was a mean of 6.9 ± 0.44 oligodendrocytes in control sections compared to a mean of 2.4 ± 0.23 in Mtz-treated sections, $p < 0.0001$. At 10d post-treatment, there was a mean of 7.6 ± 0.75 oligodendrocytes in control sections compared to a mean of 4.04 ±0.47 in Mtz-treated sections, $p = 0.0012$. At 14d post-treatment, there was a mean of 9.88 ± 0.6 oligodendrocytes in control sections, compared to a mean of 7.3 ± 0.67 in Mtz-treated sections, $p = 0.0095$. However, at 16d post-treatment, oligodendrocyte numbers in Mtz-treated animals was no longer significantly different from that in control animals (9.46 ± 2.21 oligodendrocytes in control, and 8.57 ± 2.58 oligodendrocytes in Mtz treated animals, $p = 0.260$).

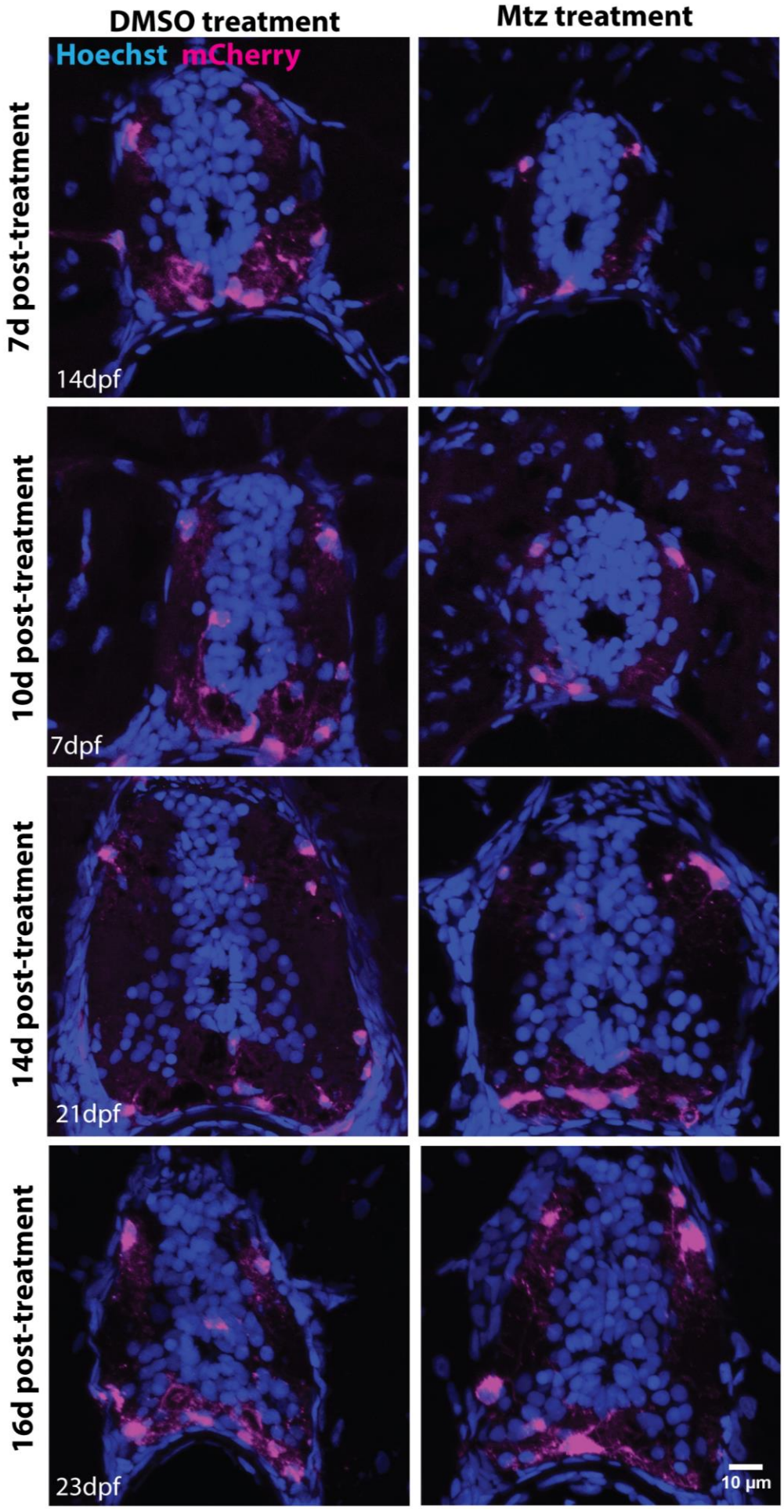

Quantification overleaf

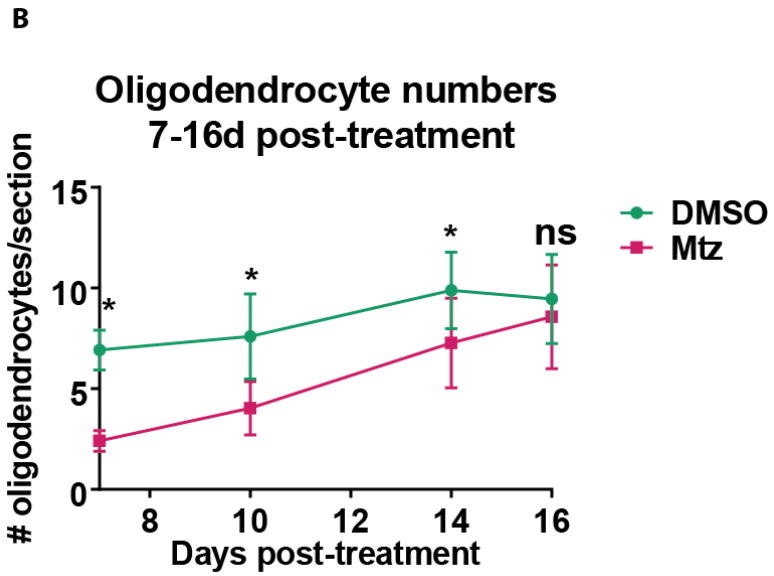

Figure 14. Oligodendrocyte numbers are restored to control levels by 16d post-treatment. A. (previous page) Representative images of cryosections stained with Hoechst to label nuclei, and showing endogenous expression of the mbp:mCherry-NTR transgene. Time points from 7d post-treatment to 16d post-treatment are shown, as indicated. At the first three time points, there are noticeably fewer oligodendrocytes in the Mtz-treated compared to control sections, whereas by 15d post-treatment, there seem to be similar numbers of oligodendrocytes in both conditions. **B**. Quantification of oligodendrocyte numbers between 7d and 16d post-treatment shows that there are significantly fewer oligodendrocytes in Mtz-treated compared to control sections at the first three time points: at 7d post-treatment, there is a mean of 6.9 ± 0.44 oligodendrocytes in control sections compared to a mean of 2.4 ± 0.23 in Mtz-treated sections, $p < 0.0001$. At 10d post-treatment, there is a mean of 7.6 ± 0.75 oligodendrocytes in control sections compared to a mean of 4.04 ±0.47 in Mtz-treated sections, $p = 0.0012$. At 14d post-treatment, there is a mean of 9.88 ± 0.6 oligodendrocytes in control sections, compared to a mean of 7.3 ± 0.67 in Mtz-treated sections, $p = 0.0095$. At 16d post-treatment there is a mean of 9.46 ± 2.21 oligodendrocytes in control sections and 8.57 ± 2.58 in Mtz-treated sections, $p = 0.260$. All significances were obtained using multiple t tests per row with a Holm-Sidak correction. n = no less than 5

Thus, it seems that Tg(mbp:mCherry-NTR) larvae are able to restore their oligodendrocyte numbers to control levels by 16d post-treatment. This is hardly surprising, as full remyelination is also observed at this time point.

3.7. Mitochondria within axons over the course of de- and remyelination

My characterisation of the model so far has demonstrated that treating Tg(mbp:mCherry-NTR) larvae with 5mM Mtz from 5dpf to 7dpf ablates two-thirds of the oligodendrocytes in the spinal cord. At 5d post-treatment, extensive demyelination is observed in the spinal cord, and this persists until at least 11d post-treatment. Complete remyelination is observed by 16d post-treatment. Oligodendrocyte numbers remain lower in Mtz-treated compared to control animals until 7d post-treatment, then slowly begin to rise and reach control levels by 16d post-treatment.

One of the striking features of the quantitative electron microscopy data described above is that at no point does there seem to be any loss of axons. While this can perhaps be largely attributed to the relatively rapid remyelination response, there is still a period of at least five or six days during which many axons remain demyelinated. This raises the intriguing question of whether the axons might undergo some adaptive changes in order to cope with the temporary loss of their myelin sheaths. Indeed, such adaptive changes are widely reported both in other experimental models of demyelination and post-mortem MS brains (e.g. Zambonin et al. 2011).

One such adaptive change known to occur acutely in demyelinated axons in mammals is changes to the distribution of mitochondria along the axons. Previous work has also demonstrated that demyelinated axons in MS patients contain many more mitochondria than equivalent axons in healthy controls (Mahad et al. 2009; Witte et al. 2009). Similarly, increased numbers of mitochondria are found at sites of demyelination in the cat optic nerve demyelinated by anti-galactocerebroside (Mutsaers and Carroll 1998). It stands to reason that axons, deprived of the metabolic support offered by oligodendrocytes and myelin, should attempt to bring in more mitochondria to meet their energy needs (Mahad et al. 2009; Zambonin et al. 2011). In order to investigate this possibility in my model, I quantified the numbers of mitochondria in both myelinated and unmyelinated axons, at 7d, 11d and 16d post-treatment in control and treated animals. For these analyses, I used the same sets of TEM images as I have already presented in the contexts of demyelination and remyelination.

3.7.1. Numbers of mitochondria within axons at the demyelinated stages (7d and 11d post-treatment)

I first investigated the numbers of mitochondria at the demyelinated stages, i.e. 7d and 11d post-treatment. To this end, I counted the numbers of mitochondria in large-calibre (defined as before, i.e. those with a perimeter over 1μm; see **Section 3.4.1**.) myelinated and unmyelinated axons, and divided them by the number of those axons to obtain a "mitochondria per axon" measure. I considered this a rational measure, given that the number of these large-calibre axons in Mtz-treated animals did not differ from that in control animals.

This analysis, shown in **Figure 15,** indicated that at 7d post-treatment, there was no significant difference in the numbers of mitochondria in axons between DMSO and Mtz-treated animals, nor between myelinated and unmyelinated axons: in DMSO-treated animals, there was a mean of 0.33 ± 0.14 mitochondria per axon in myelinated axons and a mean of 0.33 ± 0.13 mitochondria per axon, and in Mtz-treated animals, there was a mean of 0.55 ± 0.41 mitochondria per axon in myelinated axons and a mean of 0.41 ± 0.15 mitochondria per axon in unmyelinated axons. A two-way ANOVA found both the main effects of treatment condition ($p = 0.128$) and myelination status ($p = 0.453$), as well as the interaction between the two main effects, ($p = 0.463$) to be non-significant (**Figure 15A**).

Similarly, at 11d post-treatment, there were no differences between control and Mtz-treated animals or between myelinated and unmyelinated axons: in control animals, there was a mean of 0.26 ± 0.050 mitochondria per axon in myelinated axons and a mean of 0.43 ± 0.059 mitochondria per axon in unmyelinated axons, and in Mtz-treated animals, there was a mean of 0.32 ± 0.15 mitochondia per axon in myelinated axons and a mean of 0.34 ± 0.087 mitochondria per axon in unmyelinated axons. A two-way ANOVA again found no significant main effects of either treatment condition ($p = 0.830$) or myelination status, ($p = 0.073$) nor a significant interaction between the two ($p = 0.130$; **Figure 15B**).

Thus, even after approximately six days of demyelination, there does not seem to be any notable changes in the number of mitochondria within the spinal cord axons of these larvae.

It is important to note that at these stages, the unmyelinated axons found in control animals are large-calibre axons which may soon be myelinated as part of the developmental process, whereas unmyelinated axons in Mtz-treated animals comprise both “normal” unmyelinated axons and demyelinated axons. This presence of “normal” unmyelinated axons within Mtz-treated animals may mask a genuine increase in mitochondria in demyelinated axons, as “normal” unmyelinated axons and demyelinated axons are not possible to separate in the analysis. Thus, any genuine increase in mitochondria in demyelinated axons would have to be quite large in order to be detected. Post-hoc analyses indicate that the analysis described above is statistically underpowered even without considering the “normal” unmyelinated axons in Mtz-treated animals: a power analysis indicates that a sample size of 9 per group would have been required to be 80% certain of finding an effect if one existed, and the n numbers in this experiment are below that. Thus, it remains possible that the demyelination induced by the Mtz-treatment could lead to at least a small increase in mitochondria in the demyelinated axons, but the increase was not prominent enough to be detected in this experiment.

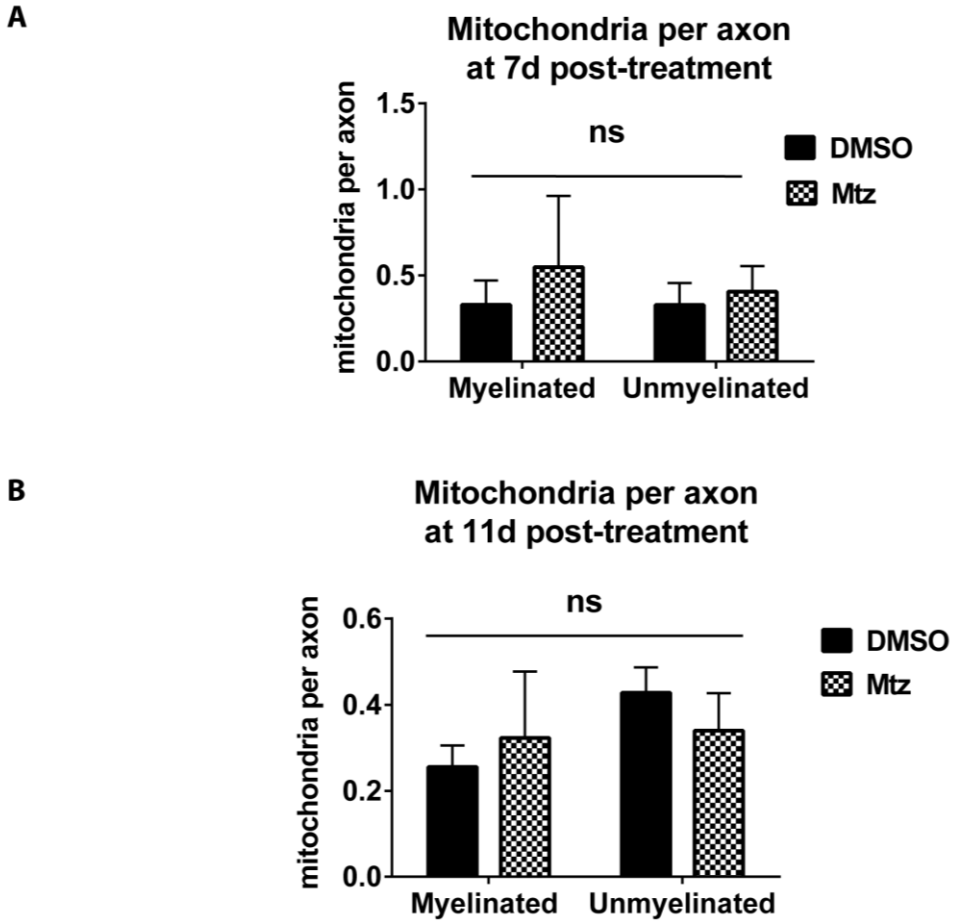

Figure 15. Numbers of mitochondria within axons at the demyelinated stages do not differ between control and Mtz-treated animals, or between myelinated and unmyelinated axons. A. Quantification of mitochondria numbers at 7d post-treatment found that in DMSO-treated animals, there was a mean of 0.33 ± 0.14 mitochondria per axon in myelinated axons and a mean of 0.33 ± 0.13 mitochondria per axon, and in Mtz-treated animals, there was a mean of 0.55 ± 0.41 mitochondria per axon in myelinated axons and a mean of 0.41 ± 0.15 mitochondria per axon in unmyelinated axons**.** A two-way ANOVA found both the main effects of treatment condition ($p = 0.128$) and myelination status ($p = 0.453$) as well as the interaction ($p = 0.463$) to be non-significant. n = 4 for DMSO, 13 for Mtz. **B**. Quantification of mitochondria numbers at 11d post-treatment shows that in control animals, there was a mean of 0.26 ± 0.050 mitochondria per axon in myelinated axons and a mean of 0.43 ± 0.059 mitochondria per axon in unmyelinated axons, and in Mtz-treated animals, there was a mean of 0.32 ± 0.15 mitochondia per axon in myelinated axons and a mean of 0.34 ± 0.087 mitochondria per axon in unmyelinated axons. A two-way ANOVA reveals that the main effects of both myelination status ($p = 0.0729$) and treatment condition ($p = 0.833$) and the interaction ($p = 0.1335$) are all non-significant. n = 4

3.7.2. Numbers of mitochondria within axons at the remyelinated stage (16d post-treatment)

Having established that there were no significant differences in numbers of mitochondria between unmyelinated and myelinated axons or between DMSO and Mtz-treated animals at the demyelinated stages (7-11d post-treatment), I went on to analyse axonal mitochondria numbers upon remyelination (16d post-treatment). It was still possible that at the demyelination stages, any adaptive changes to mitochondria distribution/density might not have had time to take effect, whereas at the remyelinated stage, any changes that might have sustained the axons through the presumably taxing period of demyelination may have accumulated, and thus could potentially still be observed. Indeed, Zambonin et al. (2011) report that, following lysolecithin-induced demyelination, mitochondria numbers remain elevated in remyelinated axons compared to never-demyelinated axons, long after remyelination is complete.

To test this possibility, I again counted mitochondria within myelinated and unmyelinated axons in control and Mtz-treated axons. The data are shown in **Figure 16.** At this time point, the data revealed two statistically significant results: first, that that there were more mitochondria in unmyelinated axons than in myelinated axons, and second, within unmyelinated/demyelinated axons, there were more mitochondria in Mtz-treated than in control animals: in myelinated axons, there was a mean of 0.32 ± 0.069 mitochondria per axon in control animals and 0.35 ± 0.12 in Mtz-treated animals, whereas in unmyelinated axons, there was a mean of 0.43 ± 0.098 mitochondria per axon in control animals and 0.55 ± 0.10 in Mtz-treated animals. A two-way ANOVA found significant main effects of both myelination status ($p < 0.0001$) and treatment condition ($p = 0.0319$). The interaction was not significant ($p = 0.229$; **Figure 16B**).

The mean of 0.32 ± 0.069 mitochondria per myelinated axon in control animals and 0.35 ± 0.12 in Mtz-treated animals ($p = 0.471$) suggests that remyelinated axons have similar numbers of mitochondria as normally myelinated axons. A power analysis indicates that an n number of over 39 animals per group would have been required to have an 80% chance of detecting an effect if one existed; thus, if there were a

difference in mitochondria numbers in myelinated axons between control and Mtz-treated animals, it would be so small as to be negligible.

In contrast, within unmyelinated axons there was a small but statistically significant increase in the mean number of mitochondria per axon in Mtz-treated animals compared to control (0.43 ± 0.098 mitochondria per axon in control animals and 0.55 ± 0.10 in Mtz-treated animals, $p = 0.0319$). As noted above, it is likely that the unmyelinated axons that are seen in treated animals at this stage will include axons that were demyelinated following oligodendrocyte ablation. This is because even in an animal undergoing remyelination, other axons are growing and being "normally" myelinated at the same time, meaning that some proportion of the newly generated oligodendrocytes will end up myelinating new, rather than demyelinated axons. It is even possible, as I have discussed in **Chapter 1**, that demyelinated axons are particularly unattractive to oligodendrocytes and thus *less* likely to be remyelinated than new axons are to be myelinated, and thus represent a relatively large proportion of those axons that remain unmyelinated at 16d post-treatment.

Thus, one interpretation of the finding that unmyelinated axons in Mtz-treated animals have more mitochondria than in control animals, is that the demyelinated axons, stripped of their myelin sheaths, required additional mitochondria to service their energy needs. This increase in mitochondria may have accumulated gradually and only become detectable at the stage when general remyelination is observed. However, this possibility could only be confirmed by following the same individual axons and their mitochondrial dynamics over time, or by having a method to differentiate between not-yet myelinated and demyelinated axons by electron microscopy.

It should also be noted that mitochondria in Mtz-treated animals may be elongated, which may result in one mitochondrion being counted more than once in a transverse section. It would be prudent to check for this possibility (by longitudinal EM sections or labelling mitochondria in living larvae) to be sure that there are more mitochondria in Mtz-treated compared to control animals at 16d post-treatment.

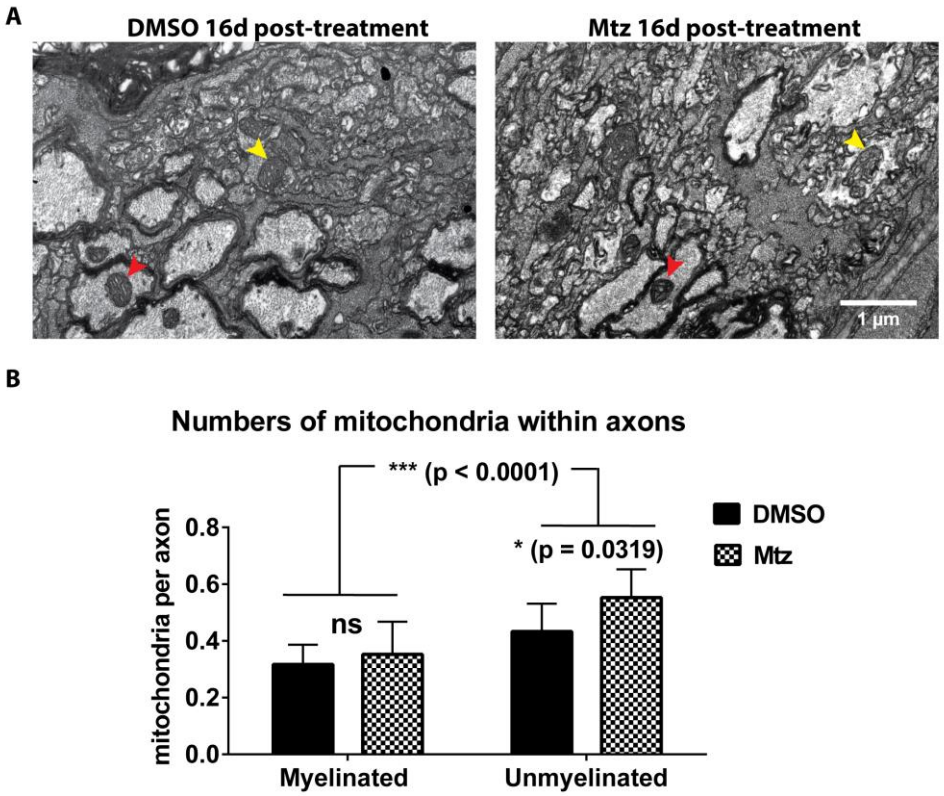

Figure 16. Numbers of mitochondria within axons at 16d post-treatment are greater in Mtz-treated than in control animals. A. TEM images from ventral tracts of spinal cords of 23dpf larvae. Red and yellow arrowheads indicate mitochondria in myelinated and unmyelinated axons, respectively. **B**. Quantification of mitochondria inside axons shows that in myelinated axons, there was a mean of 0.32 ± 0.069 mitochondria per axon in control animals and 0.35 ± 0.12 in Mtz-treated animals, whereas in unmyelinated axons, there was a mean of 0.43 ± 0.098 mitochondria per axon in control animals and 0.55 ± 0.10 in Mtz-treated animals. A two-way ANOVA reveals significant main effects of both myelination status ($p < 0.0001$) and treatment condition, (0,0319) but a non-significant interaction ($p = 0.229$). $n = 8$.

3.7.3. Mitochondria sizes during de- and remyelination

The above described discussion has focused solely on the *number* of mitochondria within axons. However, another important way in which a neuron can regulate its energy provision is by regulating the *size* of its mitochondria; indeed, increases in the sizes of stationary mitochondria have been reported in demyelinated axons *in vitro* (Kiryu-Seo et al. 2010). Therefore, in order to better understand the regulation of mitochondria during demyelination, I measured the areas of the mitochondria in control and Mtz-treated animals over the course of demyelination and remyelination,

3.7.4 Mitochondria sizes during demyelination

I first measured the areas of mitochondria within axons at the demyelinated stages (7d and 11d post-treatment). As shown in **Figure 17C**, at 7d post-treatment, there were no significant differences in sizes of mitochondria between control and treated animals, or between myelinated or unmyelinated axons (the mean area of a mitochondrion in a control animal was 0.054 ± 0.009 μm² in myelinated and 0.11 ± 0.054 μm² in unmyelinated axons, and the mean area of a mitochondrion in a Mtz-treated animal was 0.078 ± 0.068 μm² in myelinated and 0.091 ± 0.022 μm² in unmyelinated axons. A two-way ANOVA found both main effects of treatment condition and myelination status as well as the interaction non-significant ($p = 0.308$, $p = 0.226$ and $p = 0.451$, respectively).

I next measured mitochondrial sizes at 11d post-treatment, and found that there were no differences in mitochondrial sizes between Mtz-treated and control animals or between myelinated and unmyelinated axons (**Figure 17D**): the mean area of a mitochondrion in a control animal was 0.12 ± 0.026 μm² in myelinated and 0.18 ± 0.053 μm² in unmyelinated axons, and the mean area of a mitochondrion in a Mtz-treated animal was 0.16 ± 0.058 μm² in myelinated and 0.17 ± 0.027 μm² in unmyelinated axons. A two-way ANOVA found the main effects of myelination status ($p = 0.186$) and treatment condition ($p = 0.458$) and the interaction ($p = 0.252$) non-significant.

These data are consistent with the numbers of mitochondria at both 7d and 11d post-treatment time point, which were also not different between treatment conditions and myelination statuses.

A

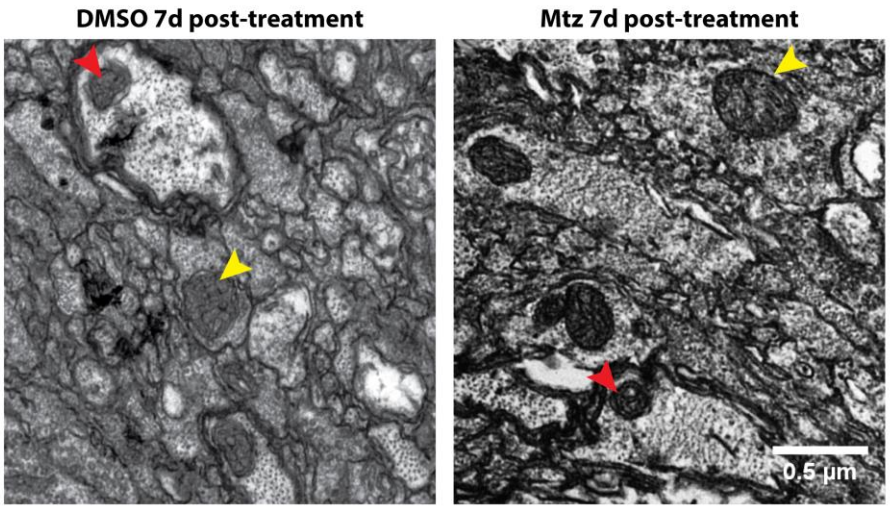

B

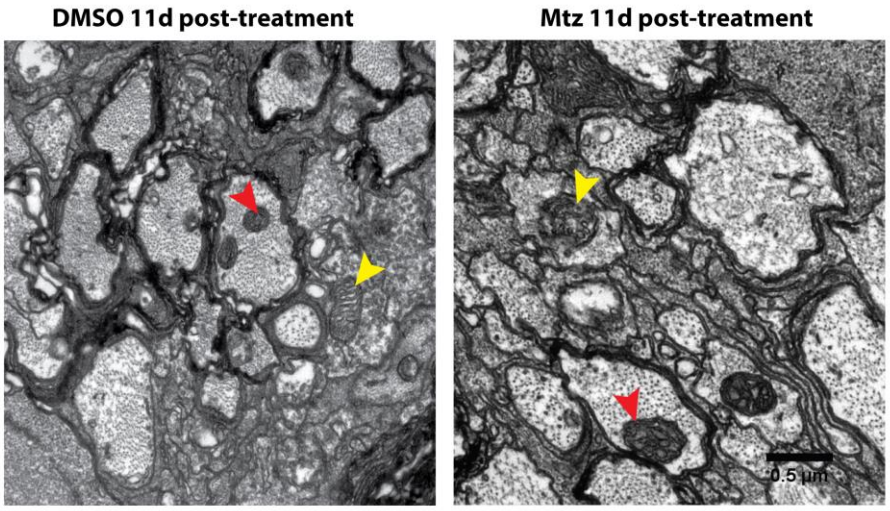

Quantification overleaf

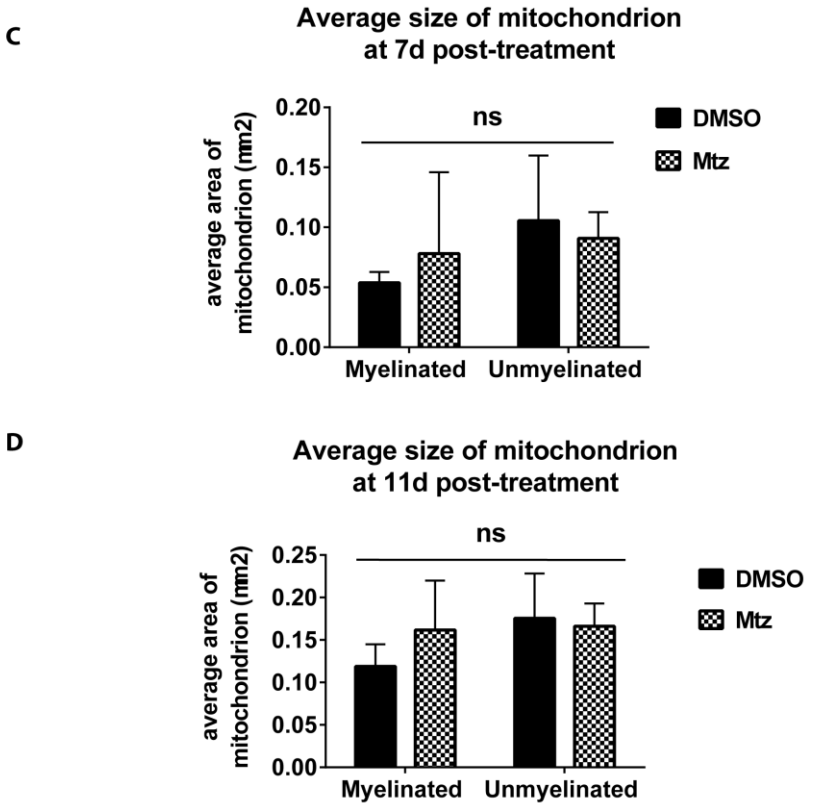

Figure 17. There are no differences in mitochondrial sizes between control and Mtz-treated animals or between myelinated and unmyelinated axons at the demyelinated stages. A, B: TEM images from ventral spinal cords from 14dpf and 18dpf larvae, respectively treated with either DMSO or Mtz, as indicated. Yellow arrowheads indicate mitochondria in unmyelinated axons, red arrowheads in myelinated axons. **C**. Comparison of mitochondrial areas at 7d post-treatment shows that the mean area of a mitochondrion in a control animal was 0.054 ± 0.009 μm² in myelinated and 0.11 ± 0.054 μm² in unmyelinated axons, and the mean area of a mitochondrion in a Mtz-treated animal was 0.078 ± 0.068 μm² in myelinated and 0.091 ± 0.022 μm² in unmyelinated axons. A two-way ANOVA shows that both main effects of treatment condition and myelination status as well as the interaction were non-significant ($p = 0.308$, $p = 0.226$ and $p = 0.451$, respectively). n = 3 for DMSO, 4 for Mtz. **D**. Comparison of mitochondrial areas at 11d post-treatment shows that the mean area of a mitochondrion in a control animal was 0.12 ± 0.026 μm² in myelinated and 0.18 ± 0.053 μm² in unmyelinated axons, and the mean area of a mitochondrion in a Mtz-treated animal was 0.16 ± 0.058 μm² in myelinated and 0.17 ± 0.027 μm² in unmyelinated axons**.** A two-way ANOVA found the main effects of myelination status ($p = 0.186$) and treatment condition ($p = 0.458$) and the interaction ($p = 0.252$) non-significant. n = 4

3.7.5. Mitochondria sizes at the remyelinated stage (16d post-treatment)

Regardless of the lack of evidence for mitochondrial size regulation during the stages of peak demyelination, I was interested to see whether there were changes in mitochondrial sizes at the remyelinated stage (16d post-treatment) as it was at this stage that I observed increased *numbers* of mitochondria within the unmyelinated/still demyelinated axons of Mtz-treated compared to unmyelinated axons of control animals.

To this end, I compared the mean areas of mitochondria between control and Mtz-treated and between myelinated and unmyelinated axons at 16d post-treatment. The results, shown in **Figure 18**, revealed two changes to mitochondrial size at the remyelinated stage: first, that mitochondria were on average larger in unmyelinated compared to myelinated axons, and second, that mitochondria were on average smaller in Mtz-treated compared to control animals, in this case in both myelinated and unmyelinated/still demyelinated axons.

The mean area of a mitochondrion in DMSO-treated myelinated axons was 0.10 ± 0.039 μm² and in Mtz-treated myelinated axons was 0.078 ± 0.012 μm^2. The mean area was 0.16 ± 0.029 μm² in DMSO-treated unmyelinated axons and 0.12 ± 0.033 μm² in Mtz-treated unmyelinated axons. A two-way ANOVA found a significant main effect of myelination status ($p = 0.0015$) as well as significant main effect of treatment condition ($p = 0.038$) but a non-significant interaction ($p = 0.598$).

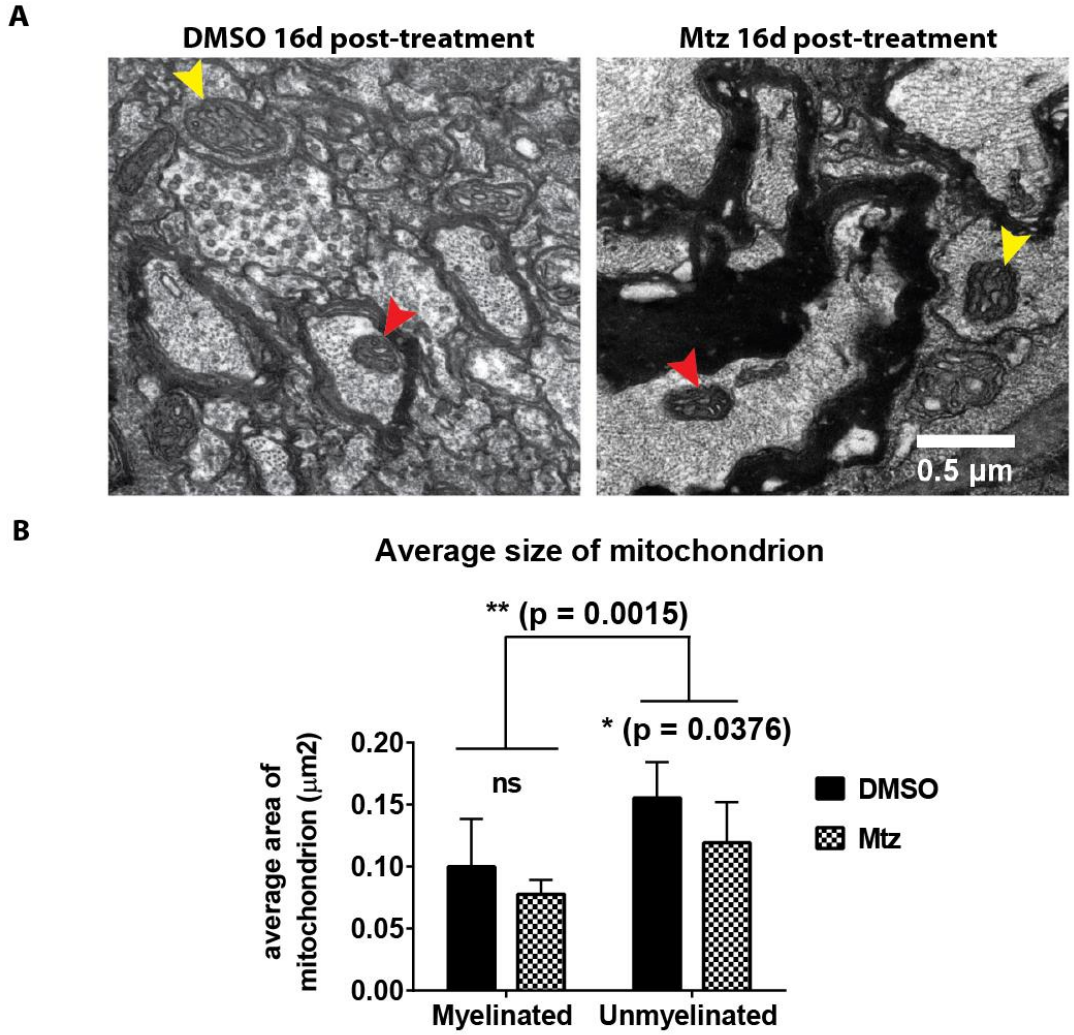

Figure 18. Mitochondria are larger in control than Mtz-treated animals at 16d post-treatment. **A**. TEM images from ventral spinal cords from 23dpf larvae, treated with either DMSO or Mtz, as indicated. Yellow arrowheads indicate mitochondria in unmyelinated axons, red arrowheads in myelinated axons. **B**. Quantification of the mean area of mitochondria shows that 1) mitochondria residing within unmyelinated axons are larger than those within myelinated axons, and that 2) mitochondria residing within DMSO-treated animals are larger than those residing within Mtz-treated animals: mean area of mitochondrion in DMSO-treated myelinated axons was 0.10 ± 0.039 µm² and in Mtz-treated myelinated axons 0.078 ± 0.012 µm², compared to 0.16 ± 0.029 µm² in DMSO-treated unmyelinated axons and 0.12 ± 0.033 µm in Mtz-treated unmyelinated axons). A two-way ANOVA found a significant main effect of myelination status ($p = 0.015$) and a significant main effect of treatment condition ($p = 0.0376$) and a non-significant interaction ($p = 0.5979$). Further investigation revealed that the main effect treatment condition was only significant in unmyelinated axons, $p = 0.0150$, while the difference between treated and control

animals in myelinated axons was not significant ($p = 0.251$). $n = 6$ for DMSO, 5 for Mtz.

Why are mitochondria smaller in Mtz-treated compared to control animals? One possibility is that in Mtz-treated animals, more mitochondria undergo fission. Mitochondrial fission, along with fusion, is an essential process in the regulation of mitochondrial homeostasis (Saxton and Hollenbeck 2012), and moreover, is known to occur when mitochondria are under stress or dysfunctional (Duvezin-Caubet et al. 2006). It could be, therefore, that over the demyelinated period, low levels of mitochondrial fission occur in axons due to the increased energy demands, but these only become detectable at the remyelinated stage, once they have accumulated. This is consistent with both the higher numbers of mitochondria and their smaller size in Mtz-treated animals at 16d post-treatment. (The earlier finding that there was no difference in mitochondria numbers in myelinated axons between control and Mtz-treated animals could reflect that axons that were remyelinated were already resolving the consequences of increased fission by downregulating the numbers of mitochondria, but those mitochondria that remained were still comparatively small).

Of course, the data presented above do not provide any direct evidence that mitochondrial fission is upregulated following demyelination in this model, but the possibility is intriguing nonetheless.

As for the finding that mitochondria are larger in unmyelinated than myelinated axons, this may simply reflect the generally higher energy needs of unmyelinated axons, which do not receive metabolic support from oligodendrocytes.

3.8. Axon calibre throughout demyelination and remyelination

3.8.1. Axon calibre does not change in Mtz-treated animals at the demyelinated stages (7d and 11d post-treatment).

Aside from upregulating their mitochondrial content, another adjustment a demyelinated axon may undergo is to vary its cross sectional size. Previous work has reported both abnormally small and abnormally large axons within demyelinated lesions; Prineas and Connell (1979) describe partially myelinated axons in post-mortem MS spinal cords, where the myelinated portion is wide and the bare portion noticeably more narrow, whereas Shintaku et al. (1988) find increased swollen axons in post-mortem MS spinal cords and Payne et al. (2012) show increased diameters of axons with decompacted myelin in rat optic nerves following transection. Furthermore, Münzel et al. (2014) recently saw an increased frequency of larger-calibre axons during demyelination in adult zebrafish following LPC-induced demyelination of the optic nerve.

Prineas and Connell (1979) speculated that following disintegration of the axon-myelin unit, the axon could no longer retain water as well as an intact unit, and thus the shrinkage of axons they observed could be explained as loss of water from the axon. Conversely, Shintaku et al. (1988) postulated that the removal of the myelin sheath might increase the permeability of the axolemma, which may result in increased influx of water. It is likely that both of these contrasting phenomena are at play, possibly depending on the type and age of lesion.

However, it also possible that increasing the calibre of the axon is an adaptive change, designed to help the axon keep functioning despite its denuded state; larger axons conduct nerve impulses faster (Hartline and Colman 2007) and could be less vulnerable to degeneration (Lovas et al. 2000). Given that the Mtz-treated larvae in my model do not display any overt behavioural disability during their period of demyelination (although this remains to be rigorously tested) it seems plausible that their axons might have adapted to becoming demyelinated by increasing their calibre.

In order to test this possibility, I measured the cross sectional sizes (perimeters) of the 26 largest axons in each ventral spinal cord at 7d and 11d post-treatment. These were axons with a perimeter of over 2µm (diameter 0.64 µm) which clearly stood out as the largest axons in the ventral spinal cords. At 7d post-treatment, of the 26 large-calibre axons, a mean of 22.67/26 (87%) was myelinated in control animals and a mean of 13.5/26 (52%) was myelinated in Mtz-treated animals at 7d post-treatment. At 11d post-treatment, of the 26 large-calibre axons a mean of 22.3/26 (85%) was myelinated in control animals and a mean of 10.3/26 (39%) was myelinated in Mtz-treated animals.

The measurements of the perimeters of these axons at 7d post-treatment revealed that there were no differences between control and Mtz-treated axons, nor between myelinated and myelinated axons: the mean perimeter of a myelinated axon was 3.76 ± 0.3 µm in a control animal and 3.16 ± 0.58 µM in a Mtz-treated animal; while the mean perimeter of the large unmyelinated axon was 3.88 ± 1.0 µm in a control animal and 3.70 ± 0.54 µm in a Mtz-treated animal. A two-way ANOVA found a non-significant main effect of treatment condition ($p = 0.1745$), a non-significant main effect of myelination status ($p = 0.2391$) and a non-significant interaction ($p = 0.4622$; **Figure 19C**).

The same situation prevailed at 11d post-treatment: there was no difference between control and Mtz-treated axons, nor between myelinated and myelinated axons: the mean perimeter of a myelinated axon was 3.5 ± 0.11 µm in a control animal and 3.69 ± 0.66 µm in a Mtz-treated animal, while the mean perimeter of an unmyelinated axon was 3.61 ± 0.3 µm in a control animal and 3.67 ± 0.78 µm in a Mtz-treated animal). A two-way ANOVA found a non-significant main effect of treatment condition ($p = 0.6362$), a non-significant main effect of myelination status ($p = 0.8681$) and a non-significant interaction ($p = 0.8136$; **Figure 19C**).

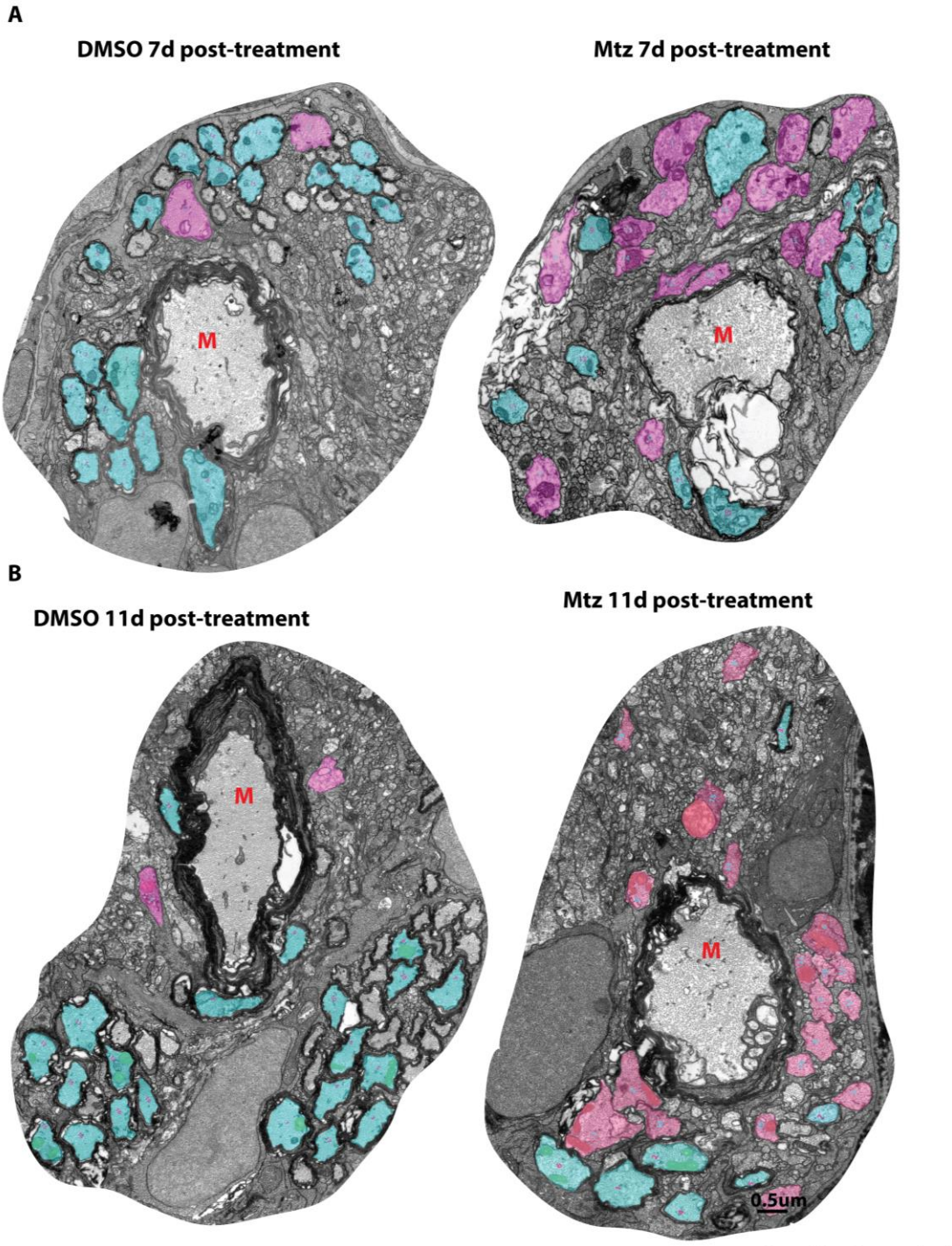

Quantification overleaf

C

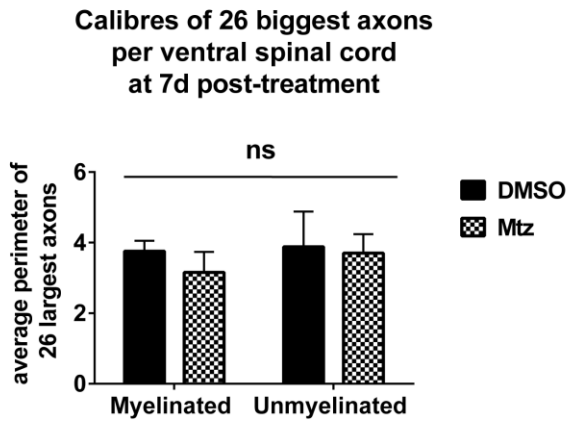

D

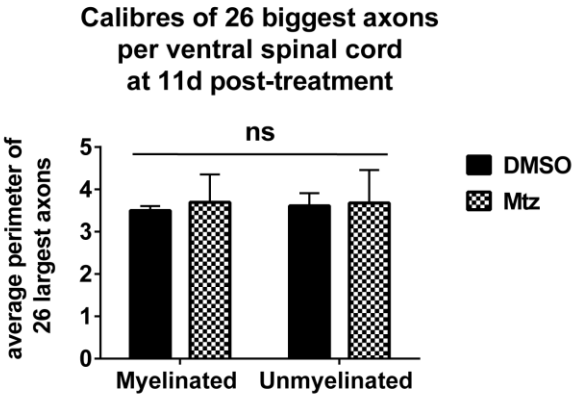

Figure 19. Axon calibre does not change during the demyelinated stages. A, B: TEM image from ventral spinal cords of 14dpf and 18d dpf larvae, respectively, treated with DMSO or Mtz, as indicated. The 26 largest axons are shaded; myelinated in turquoise, unmyelinated in magenta. **C**. Measurements at 7d post-treatment indicate that the mean perimeter of a myelinated axon is 3.76 ± 0.3 µm in a control animal and 3.16 ± 0.58 µM in a Mtz-treated animal, and that mean perimeter of an unmyelinated axon is 3.88 ± 1.0 µm in a control animal and 3.70 ± 0.54 µm in a Mtz-treated animal). A two-way ANOVA finds a non-significant main effect of treatment condition ($p = 0.1745$), a non-significant main effect of myelination status ($p = 0.2391$) and a non-significant interaction ($p = 0.4622$). $n = 4$ for DMSO, 7 for Mtz. **D**. Measurements at 11d post-treatment indicate that the mean perimeter of a myelinated axon is 3.5 ± 0.11 µm in a control animal and 3.69 ± 0.66 µm in a Mtz-treated animal; mean perimeter of an unmyelinated axon is 3.61 ± 0.3 µm in a control animal and 3.67 ± 0.78 µm in a Mtz-treated animal). A two-way ANOVA finds a non-significant main effect of treatment condition ($p = 0.6362$), a non-significant main effect of myelination status ($p = 0.8681$) and a non-significant interaction ($p = 0.8136$). $n = 4$.

3.8.2. Axon calibre is not different between control and Mtz-treated animals at the remyelinated stage (16d post-treatment).

From the above analyses of axon calibres at the demyelinated stages, I could be confident that the axons did not undergo any adaptive changes to their cross sectional sizes in response to being demyelinated. However, while investigating potential adaptive changes to the mitochondrial presence within axons, I had found hardly any changes during the demyelinated stages but did find increases in mitochondrial number and size in Mtz-treated animals at the remyelinated stage. Thus, it was possible that adjustments to axon calibre too would only become evident at this later stage. To address this possibility, I analysed the perimeters of the 26 largest axons in the ventral spinal cords of larvae at 16d post-treatment. I kept the number of axons analysed at 26 in order to remain consistent with analyses at the demyelinated stages, although it is plain from the images presented in **Figure 20A** that at these older stages, there are considerably more than 26 axons over the perimeter of 2µm in both control and treated animals.

The comparison of axon perimeters between control and Mtz-treated animals revealed that there was no difference between them: in control animals, the mean perimeter of a myelinated axon was 5.07 ± 0.78 µm and the mean perimeter of an unmyelinated axon was 4.1 ± 0.6µm, while in Mtz-treated animals, the mean perimeter of a myelinated axon was 4.89 ± 0.78 µm and the mean perimeter of an unmyelinated axon was 4.18 ± 0.31 µm. However, the myelinated axons in both conditions were larger than unmyelinated axons. A two-way ANOVA found a significant main effect of myelination status ($p = 0.0077$) but a non-significant main effect of treatment condition ($p = 0.87$) and a non-significant interaction ($p = 0.658$; **Figure 20B**).

These data suggest that axons in Mtz-treated animals do not at any point increase their cross-sectional size as an adaptation to becoming demyelinated. However, as I discussed in the context of mitochondria numbers in **Section 3.7.2**, it should be noted that amongst the observed unmyelinated axons in Mtz-treated animals, only 75% were demyelinated axons; the rest were “normal” unmyelinated axons. It therefore remains possible that the presence of these axons masked an increase in the sizes of the truly

demyelinated axons. However, even if this were the case, the increase in the sizes of demyelinated axons would have to be quite subtle in order to be masked by 25% of the unmyelinated axon population being “normal” unmyelinated axons.

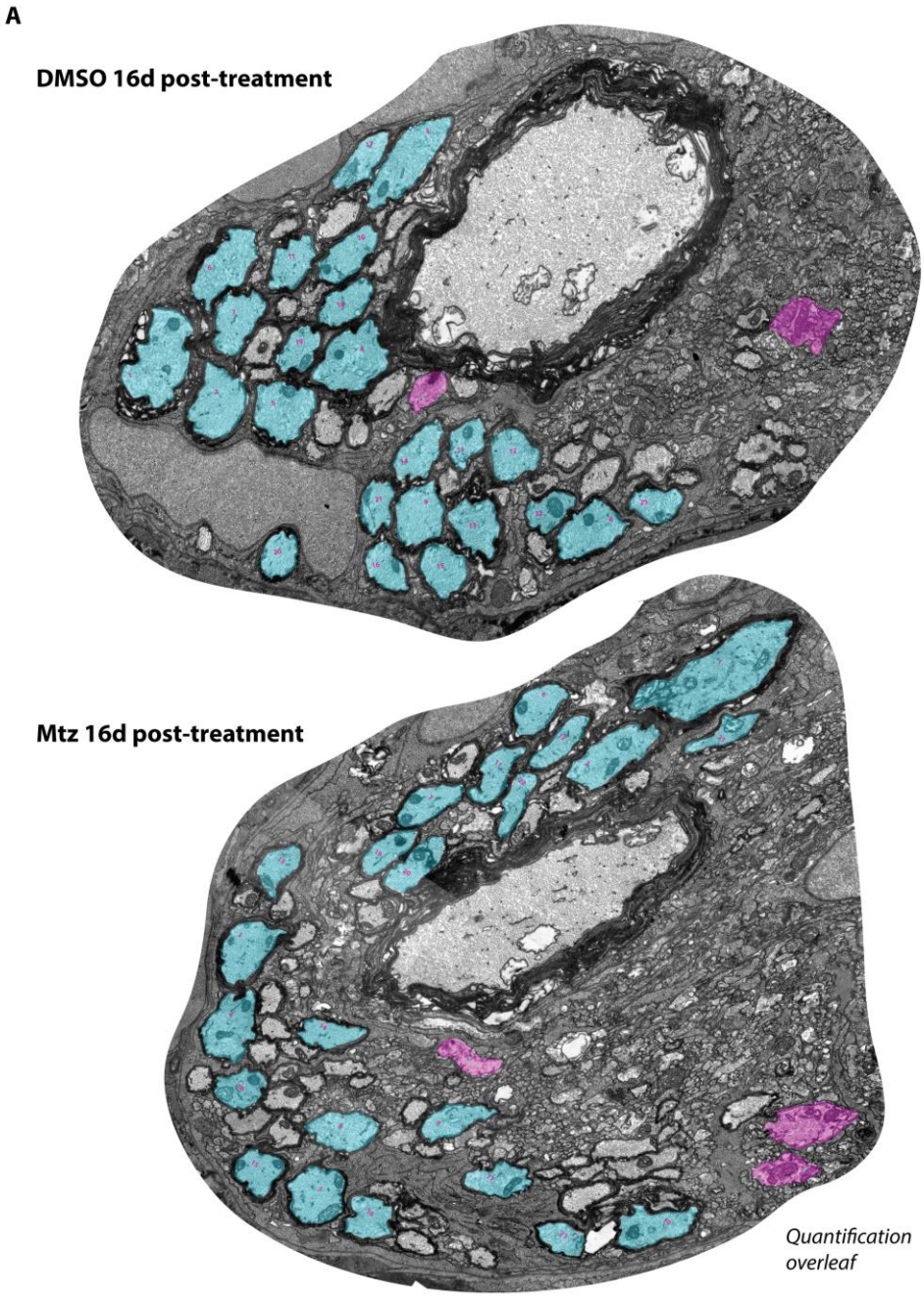

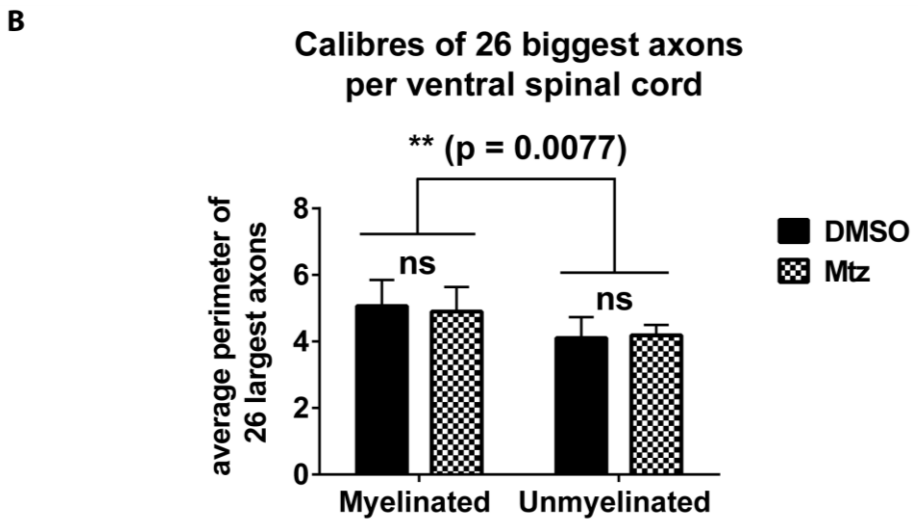

Figure 20. Axon calibres are not different between control and Mtz-treated animals at 16d post-treatment. A. TEM image from ventral spinal cords of 23dpf larvae, treated with DMSO or Mtz, as indicated. The 26 largest axons are shaded; myelinated in turquoise, unmyelinated in magenta. **B**. Measurements of the 26 largest axons revealed that the mean perimeter of a myelinated axon was 5.07 ± 0.78 µm in control animals and 4.89 ± 0.78 µm in Mtz-treated animals, while the mean perimeter of an unmyelinated axon was 4.1 ± 0.62 µm in control animals and 4.18 ± 0.31 µm in treated animals. A two-way ANOVA found a significant main effect of myelination status ($p = 0.0077$) but a non-significant main effect of treatment condition ($p = 0.872$) and a non-significant interaction ($p = 0.658$). n = 6 for DMSO, 5 for Mtz.

3.8.3. Myelinated axons grow in calibre through the period in which remyelination occurs

The data in **Figure 20** indicate that at 16d post-treatment, myelinated axons in both control and Mtz-treated animals are significantly larger than unmyelinated axons. Furthermore, when comparing the sizes of axons at 16d post-treatment to those at 11d post-treatment (18dpf), it appears that all axons, irrespective of myelination status or treatment condition, are larger in calibre at 16d post-treatment (23dpf). In order to assess this quantitatively, I plotted the sizes of myelinated and unmyelinated axons over time, and found that while indeed all axons increase in size from 11d to 16d post-treatment, the increase is more pronounced in myelinated axons, regardless of treatment condition (**Figure 21**).

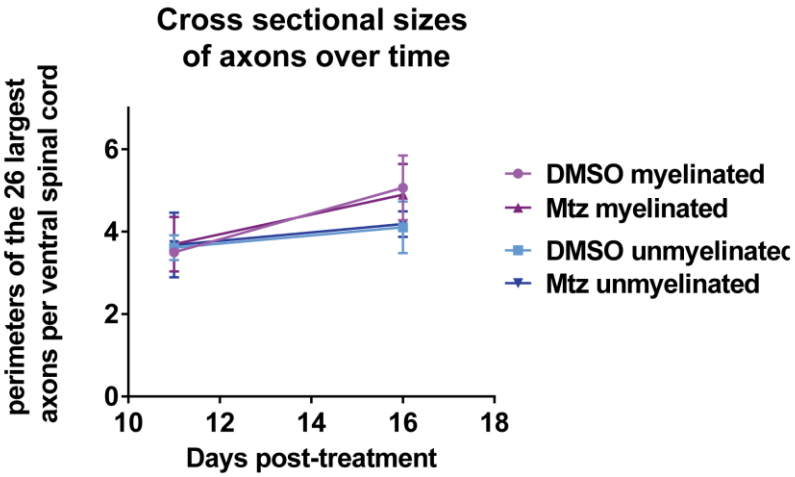

Figure 21. Radial growth is more pronounced in myelinated than in unmyelinated axons, regardless of treatment condition. Mean perimeters of the 26 largest axons (myelinated and unmyelinated) in control and Mtz-treated animals between 11d and 16d post-treatment. Myelinated axons are shown in shades of purple and unmyelinated in shades of blue. The slope of the increase in size is steeper in myelinated than in unmyelinated axons.

Thus, it seems that myelinated axons in both control and treated animals undergo something of a calibre growth spurt between 11d and 16d post-treatment; during the very interval when remyelination must occur in the Mtz-treated animals. In fact, it is possible that the developmental event of axon calibre growth at this age is an important *reason* for the success of remyelination in this system; perhaps an axon that is growing radially while being remyelinated is interpreted by the myelinating oligodendrocyte as being in a dynamic state, and thus promotes generation of a thick myelin sheath, resembling myelin made during normal development, when the axon is also growing radially. I will return to this intriguing possibility in the Discussion.

3.9. Discussion

In this chapter, I have characterised the main features of the Tg(mbp:mCherry-NTR) model of oligodendrocyte ablation, demyelination and remyelination. In this model, two-thirds of myelinating oligodendrocytes are ablated following a treatment with metronidazole between 5 and 7 days post-fertilisation, and at the same time, large cellular vacuoles are formed. Oligodendrocyte numbers remain lower in Mtz-treated compared to control animals for seven days following withdrawal of the Mtz-treatment, and during this time, axons undergo demyelination. Extensive demyelination is observed at 5d, 7d and 11d post-treatment, but no loss of axons is associated with this. At 7d post-treatment, the numbers of oligodendrocytes in Mtz-treated animals begins to climb, and reach control levels by 16d post-treatment. Complete remyelination is also observed at 16d post-treatment, with myelin sheaths restored to normal thickness.

The numbers of mitochondria within axons does not seem to be affected during the demyelination stages, but at the remyelinated stage, there are more mitochondria within the unmyelinated/demyelinated axons of Mtz-treated than control animals. At the remyelinated stage, mitochondria are also smaller in size in Mtz-treated animals compared to controls. These observations may reflect increased levels of mitochondrial fission in these axons, but this remains to be tested.

Axon calibres are not different between control and Mtz-treated animals (or between myelinated and unmyelinated axons). However, there is a clear growth in axon calibre during the period when remyelination occurs, suggesting the possibility that growth of axons in calibre may stimulate generation of thicker myelin sheaths during remyelination.

I will now discuss some pertinent topics arising from the material presented in this chapter.

3.9.1. Vacuolation following oligodendrocyte ablation likely represents myelin sheath breakdown

I showed in **Figures 6 - 8** that ablation of oligodendrocytes in this model results in severe disruption of the myelin sheath morphology, which manifests as bubble-like vacuoles. This phenomenon has been observed in nearly all other models of primary oligodendrocyte ablation (Traka et al. 2010; Pohl et al. 2011; Locatelli et al. 2012) but not in toxin-based models of demyelination. This is presumably because the injection of toxin directly causes the destruction of the myelin sheath, which thus does not undergo a gradual process of disintegration, whereby the lamellae of the myelin sheath split apart (Pohl et al. 2011). A recent study by Weil et al. (2016), which used high-pressure freezing techniques to preserve myelin close to its native state, indicated that the breakdown of myelin begins at the innermost layers and spreads outwards, which further supports the possibility that the early stages myelin sheath breakdown is often manifest as vacuolated (or, to use their term, vesicular) structures.

In addition, the appearance of the vacuoles when using the Tg(mbp:EGFP) line, which labels oligodendrocyte cell bodies, raises the possibility that some vacuoles seen in this model do not represent detached myelin sheaths but rather greatly swollen oligodendrocyte cell bodies. In speculation that I return to briefly in the Discussion of **Chapter 4**, it is possible that the mode of death these oligodendrocytes undergo involves disproportionate swelling prior to fragmentation.

In order to test this possibility, it would be highly interesting to follow single oligodendrocytes labelled with the mbp:EGFP-CAAX transgene (which would label individual oligodendrocytes and all their myelin sheaths) in a time-lapse movie; this would allow us to determine whether it is the myelin sheaths or the cell body, or both, which gives rise to the vacuoles.

3.9.2. Other zebrafish models of demyelination and remyelination

As I mentioned in **Section 3.1.**, during my PhD studies, two other models of demyelination and remyelination in larval zebrafish were published, the first by Chung

et al. (2013) with a follow-up study by Kim et al. (2015), and the second by Fang et al. (2014). Both make use of the nitroreductase/metronidazole system, but in different ways. Chung et al. use the GAL4/UAS system to express NTR in oligodendrocytes. This is a commonly used system which results in mosaic expression of the gene of interest (Davison et al. 2007). Chung et al. do not define what proportion of oligodendrocytes in their larvae express the transgene, and thus when they report loss of approximately 80% of oligodendrocytes, that means 80% of the *transgene expressing* oligodendrocytes, not the entire population. This means that it is difficult to estimate the true extent of oligodendrocyte loss in this model. Kim et al. (2015) report that remyelination has started to occur one day after withdrawal of metronidazole; they show increased oligodendrocyte numbers and increased thickness of the myelin sheath on the Mauthner axon (from fluorescent images). Moreover, they find more extensive remyelination in the same time frame following a one-day treatment with the anti-inflammatory drug sulfasalazine. Since in my Tg(mbp:mCherry-NTR) model, oligodendrocyte numbers remain relatively stable and low until 7d post-treatment, and demyelination is still widespread at 11d post-treatment, the speed of recovery in Kim et al.'s model seems surprising. It is possible that due to the mosaic nature of their transgene expression, they only ablate a small subset of all oligodendrocytes, and this limited extent of damage can be repaired relatively rapidly. However, if the extent of the oligodendrocyte ablation is indeed so limited, it renders the model less relevant for studying remyelination. For this reason, it may be preferable to simply express the nitroreductase enzyme under the mbp promoter, as our Tg(mbp:mCherry-NTR) line does.

Fang et al. (2014) use a very similar transgenic line to our Tg(mbp:mCherry-NTR) line, whereby the transgene is expressed directly under the control of the mbp promoter, except that they use GFP rather than mCherry as their reporter. Thus, in principle, this line should not have the problems associated with the varied mosaic expression of nitroreductase, as Kim et al. do. However, it is very difficult to assess how this model compares to mine, as they present only low-magnification images of live larvae where in the Mtz-treated animal, the GFP signal appears fainter than in the control, and quantify the extent of oligodendrocyte loss and demyelination only by showing that the amount of mbp expression is reduced by Western blot. Much of their

model characterisation focuses on the motor deficits they see following a five-day treatment with metronidazole, and are resolved seven days later. Although Fang et al.'s model characterisation is very preliminary, the observation that larvae show motor deficits following Mtz-treatment is an interesting one, and worth exploring in my model, too.

As noted in the Introduction to this chapter, a very similar model was also generated in *Xenopus laevis* by Kaya et al. (2012), but, as I have discussed above, the optic nerve where they assess demyelination is very sparsely myelinated at the start of the treatment, making it difficult to distinguish demyelinated axons from those that had not yet been myelinated, and remyelinated axons from those that were myelinated for the first time during the period of remyelination. In this regard, studying demyelination in the larval zebrafish spinal cord has the benefit that the majority of the large-calibre reticulospinal axons in the ventral spinal cord are known to be myelinated from 4-5dpf (Kimmel et al. 1982; Brösamle and Halpern 2002; Almeida et al. 2011; Koudelka et al. 2016).

3.9.3. The Tg(mbp:mCherry-NTR) larvae are still developing during stages demyelination and remyelination were examined.

However, despite the presence of well-defined myelinated tracts in the larval zebrafish spinal cord, it remains an important consideration that the animal is still developing and growing throughout the period of demyelination and remyelination that I examined. This prompts the question of whether the increase in oligodendrocytes and myelin I observe at 16d post-treatment, compared to 7d post-treatment for example, is truly a regenerative response, or whether it is simply a part of the ongoing developmental process, or a mix of both.

Undoubtedly, the developmental process is still underway, as is evident in the significant increases in oligodendrocyte number in control larvae both between 0 and 7 days post-treatment and 7 and 16 days post-treatment (**Figures 9** and **14**). The number of myelinated axons in the ventral spinal cords of control animals also

increases from a mean of 58.33 ± 12.75 axons at 5d post-treatment to a mean of 80.88 ± 20.23 at 16d post-treatment (**Figures 10** and **12**), an increase of just over 20 cells per animal in the four-somite long area of the spinal cord that I analysed. However, in all of these examples, the *rate* of increase in oligodendrocyte numbers and myelinated axons is considerably higher in Mtz-treated than in control animals; the slopes in of oligodendrocyte number increase are steeper for Mtz-treated animals than controls in **Figures 9** and **14,** and the number of myelinated axons increases from a mean of 12.75 ± 2.5 at 5d post-treatment to 85.71 ± 22.01 at 16d post-treatment, an increase of over 70 cells per animal, several times greater rate of increase than that seen in control animals. These sharp increases reflect the need of Mtz-treated animals to rapidly generate new oligodendrocytes and new myelin to replace those that were lost. That is, the Mtz-treated animals, while growing in size, were also actively restoring their oligodendrocyte populations following ablation, whereas the in control animals, the oligodendrocyte population was much more stable.

Thus, while the Mtz-treated animals are certainly undergoing normal development, additional regenerative processes are triggered by the oligodendrocyte ablation. It is also worth noting that oligodendrogenesis continues throughout adult life in mammals, too (Rivers et al. 2008; Young et al. 2013), so in a sense it could be argued that from the points of view of oligodendrocyte generation, most animals are developing well into adult life, albeit at a lower rate.

An important consequence of the ongoing development in the Tg(mbp:mCherry-NTR) larvae over the course of demyelination and remyelination is that, although there is a known population of myelinated axons in the ventral spinal cord from 4-5dpf, there are still also large-calibre axons that have yet to be myelinated throughout the ages that I have analysed. Thus, when considering electron micrographs taken at the demyelinated stage, it is not possible to determine with certainty whether any given non-myelinated axon is a demyelinated one, or one that has not yet been myelinated. Similarly, when assessing electron micrographs at the remyelinated stage, it is not possible to tell by looking at non-myelinated axons whether they are simply awaiting first myelination, or are long-term demyelinated. Furthermore, any given myelinated axon at the remyelinated stage may be either one that was not affected by the

oligodendrocyte ablation, (bearing in mind that one-third of oligodendrocytes on average remain unablated) one that was generated during the remyelinating period and myelinated for the first time, or genuinely remyelinated. These are important considerations, as the presence of "normal" unmyelinated axons which are included the same category as demyelinated axons, and "normal" myelinated axons which are included in the same category as remyelinated axons will naturally influence analysis of demyelination and remyelination. Indeed, this may go some way in explaining why I did not see more pronounced adaptive changes in the axons in response to being demyelinated.

However, given that the *majority* of the large-calibre axons in the ventral spinal cord are myelinated from at the stages I analyse them at, and that I ablate two-thirds of oligodendrocytes on average, then any given non-myelinated axon at 7d post-treatment is more *likely* to have been demyelinated than not-yet myelinated. Similarly, given that two-thirds of axons analysed in any one area are likely to have been demyelinated, then any myelinated axon at 16d post-treatment is more likely to have been remyelinated than "normally" myelinated for the first time during that period. However, the current lack of tools to unambiguously distinguish between unmyelinated and demyelinated axons, and between newly myelinated and fully remyelinated axons, by electron microscopy, is one that requires further consideration in this model.

One way to circumvent the problem of not knowing definitively which axons are demyelinated and which are "normally" unmyelinated would be to label single axons and the myelin sheaths along them in living larvae. Our lab has recently developed a fluorescent fusion protein that combines GFP with the axonal protein Contactin1A, which is localised along the length of axons prior to myelination, and to the nodal-paranodal region following myelination. This shift in localisation occurs because the GFP-Contactin1A is excluded from myelinated regions of the axon (Koudelka et al. 2016). Using this tool, it is possible to follow the same axons over the course of demyelination and remyelination, and in this way, changes in axon calibre, or mitochondrial dynamics (with the use of further transgenic labelling tools available to us) or other parameters could be observed in an axon which was known to be

demyelinated. By the same token, such an approach would also enable the remyelination of the same axon to be assessed definitively and directly. In general, identification or development of diagnostic markers that could better differentiate between demyelinated and unmyelinated axons would be of huge benefit to the field of remyelination research.

3.9.4. Individual axons in Tg(mbp:mCherry-NTR) animals are likely to be only partially demyelinated along their length.

Another important consideration when analysing the phenotypes of what appear to be demyelinated axons by EM is that a transverse section only depicts the myelination status of an axon at that precise point along its length. It therefore remains eminently possible that the same axon is myelinated at other locations along its length. Indeed, the Mtz-treatment *only* ablates two-thirds of the oligodendrocytes, which leaves a third of oligodendrocytes intact, and the internodes made by these oligodendrocytes presumably remain intact too. Since each axon is myelinated by multiple different oligodendrocytes, and there is no known preference for individual oligodendrocytes for specific axons, it seems far more likely that the majority of axons will, on average, become two-thirds demyelinated along their length, rather than there being two-thirds of axons that are completely demyelinated. This fact may go some way in explaining why the period of demyelination did not prompt a more pronounced adaptive response from axons; their energy needs were being served at intermittent locations along their lengths by the presence of normal myelin sheaths. Perhaps also the disorganisation of their functional domains (i.e. nodes of Ranvier, paranodes and juxtaparanodes) were not as pervasive as they would have been in a completely denuded axon. In this way, partial demyelination might have served to limit the extent of the dysregulation of sodium channel densities (Waxman 2006), or mitochondrial dysregulation (Trapp and Stys 2009) and thus contributed to the lack of axon loss that I see in this model.

It would be highly interesting to investigate extent and dynamics of partial demyelination further by using our transgenic tools that label individual axons and all the myelin sheaths along them; with these tools, one could follow the same axon over

time and see whether internodes were lost at around the same time or over a prolonged period, whether remaining internodes may elongate in order to cover some of the newly exposed axonal space, whether remyelination of the same axon occurs simultaneously all the way down its length or whether internodes are replaced gradually. Our lab has also developed fluorescent reporters to allow visualisation of nodes of Ranvier and paranodal domains that could be imaged during demyelination to see how they are affected by removal and replacement of myelin sheaths. In addition, longitudinal EM sections would allow minute comparisons of organelle content, calibre and other indications of axon health and function between demyelinated and remyelinated segments of the same axon.

3.9.5. Axons remain demyelinated for a limited period of time

Another possible reason why I did not observe any axon loss or notable pathology at any stage during demyelination or remyelination might be that the axons did not remain demyelinated for long enough to trigger adaptive or pathological responses; if we consider 5d post-treatment to be the beginning of peak demyelination, the axons were remyelinated within 11 days of that. By contrast, in the rodent models of primary oligodendrocyte ablation, axons remained demyelinated for several weeks, and pathological features only began to appear near the end stages, often six or seven weeks following the initial insult (Traka et al. 2010; Pohl et al. 2011; Locatelli et al. 2012) Indeed, in my model the only alterations to mitochondrial number and size I observe are present at the remyelinated stage, suggesting that they have accumulated over time. Mitochondrial dysregulation is often one of the first indications of axonal pathology (Trapp and Stys 2009) so the observation that even this is only evident at the remyelinated stage further highlights the mildness of the axon pathology in this model.

With this in mind, it would be of great interest to *prolong* the period of demyelination and assess the effects of this on axonal health and integrity. This may be achieved by increasing the duration of Mtz-treatment, or treating larvae for two days several times with a few days in between. In addition, one could attempt to inhibit remyelination by

molecular interventions, for example, pharmacologically dysregulating wnt signalling, or upregulating the expression of hyaluronan, or, both of which have been shown to delay remyelination in rodents (Fancy et al. 2009; Back et al. 2005) or treating the animals with the hedgehog inhibitor cyclopamine, which prevents oligodendrocytes developing (Tekki-Kessaris et al. 2001). With remyelination inhibited, it would be interesting to observe the effects of a more prolonged state of demyelination on axon health, in terms of organelle transport and accumulation, swellings, degeneration and motor functions. Moreover, the relationship between the *duration* of demyelination and axon health could be tested by varying the duration of the treatment to inhibit remyelination, and determining the point where the pathology becomes irreversible. Additional measures of axon health, such as immunostaining for SMI-32 or APP, common indicators of axon pathology, could be used to track the extent of axon pathology at different time points.

3.9.6. Axon calibre growth as a potential stimulator of myelin thickness growth

In the Tg(mbp:mCherry-NTR) model, I find that Mtz-treated larvae display normal myelin sheath thickness on their remyelinated axons. This is, at first sight, unexpected, as thinner myelin sheaths are generally considered the hallmark of remyelinated axons (Blakemore and RJM Franklin 2008). A potential insight into how the larvae achieve this comes from the observation in **Figures 20** and **21** that axon calibre grows during the 11d-16d post-treatment period when remyelination must take place in this model – and moreover, the calibre of myelinated axons grows at a faster rate than unmyelinated axons in both control and Mtz-treated conditions. As I mentioned in **Section 3.8.3**, these observations raise the possibility that the radial growth of the axon while it is being remyelinated signals to the remyelinating oligodendrocyte that the axon is dynamic, and thus promotes generation of a thick myelin sheath. That is to say, the remyelinating oligodendrocyte may interpret the ongoing radial growth as a sign that the axon is developing, and myelinate it accordingly.

If this were the case, it may go some way in explaining why myelin remains thin in rodent remyelination paradigms; demyelination is induced in animals in which radial growth of axons has presumably already finished, and thus the axons being remyelinated in these animals are static and do not promote radial growth of their new myelin sheaths. Indirect support for this hypothesis comes from the findings by Münzel et al. (2014), where it appears from their g ratio analyses that axons grow in calibre during the 28-day period between being lesioned and showing full remyelination in the young fish, which display full thickness myelin.

Furthermore, Powers et al. (2013) used an inducible remyelination reporter following spinal cord contusion in mice, which causes extensive demyelination of the spared axons, and assessed myelin sheath length and thickness for extended periods of time following remyelination. This analysis revealed that newly made myelin sheaths had reached normal myelin thickness at all time points examined (1, 3 and 6 months post-contusion). Crucially, their data clearly show that axon calibres had grown significantly between one and three months post-contusion, supporting the idea that radially growing axons receive thicker myelin sheaths. It is less likely that the causal relationship is the reverse, i.e. that the thicker myelin enabled the axon to grow radially, as data from our lab indicates that axon calibre is not affected by two separate treatments which completely prevent oligodendrocyte development (Lyons lab, unpublished).

Naturally, the hypothesis that axon calibre growth can promote myelin thickness growth needs to be experimentally tested. It would be paramount to test the hypothesis by inhibiting or enhancing radial growth of axons during demyelination and remyelination, and assess myelin thickness in such animals. However, very little is currently known about what regulates axon calibre growth in the CNS, so it may be difficult to specifically target this regulation. Alternatively, it may be possible to mimic the signalling between a radially growing axon and an oligodendrocyte by overexpressing the growth factor neuregulin1 on axons; it is thought in the context of the PNS that levels of neuregulin1 expression on axons correlate with their cross sectional size and as such, regulate myelination by Schwann cells (Nave and Salzer 2006). Thus, mere overexpression of neuregulin1 in axons may bypass the need for

actual growth in calibre, and promote generation of a thicker myelin sheath. This has been shown to be the case in the PNS (Michailov et al. 2004), but it is unclear whether the same regulation occurs in the CNS (Nave and Salzer 2006), although some studies have indicated that overexpression of neuregulin1 types I and III can promote myelin thickness on CNS axons (Brinkmann et al. 2008).

Nevertheless, if a method could be found to manipulate axon calibre growth in the CNS (or at least mimic such manipulation) in a demyelinated animal, it would be of the utmost interest to assess the effects of such a manipulation on myelin sheath thickness in remyelination.

3.9.7. Restoring full myelin thickness can be advantagenous

The above considerations on the potential effects of axon calibre on myelin thickness in remyelination are highly relevant to demyelinating diseases, as there is evidence to suggest that remyelination does not always fully rescue the demyelinated axon. As I mentioned in **Chapter 1**, Manrique-Hoyos et al. (2012) reported that following apparent remyelination from cuprizone-induced demyelination, the mice began to exhibit axon pathology and motor symptoms six months later. Degenerating axons were often found to be still ensheathed by thin myelin. The authors proposed that the newly made myelin was not as effective at maintaining axon health and integrity as normal developmental myelin is. Further support for this notion comes from the observations of Zambonin et al. (2011) that the mitochondrial content of remyelinated axons remains elevated compared to never-demyelinated axons, again suggesting that the new, thinner, myelin is not able to fully recapitulate the function of normal developmental myelin.

Thus, it could be advantageous to explore ways to not only enhance remyelination but also promote generation of full thickness myelin in the context of remyelination. Some evidence already exists that experimental manipulation in rodents can increase thickness of newly made myelin to normal levels; Fyffe-Maricich et al. (2013) showed that sustained activation of ERK1/2 signalling in oligodendrocyte lineage cells results in restoration of normal g ratios following lysolecithin-induced demyelination.

Since Tg(mbp:mCherry-NTR) larvae restore normal myelin thickness spontaneously, it could be informative to study the precise process by which they achieve the full remyelination: the regulation, behaviour and morphology of the newly generated oligodendrocytes, the effects of the activity of the neurons on these, and indeed the effects of axon calibre growth during remyelination on myelin thickness. With better understanding of how larval zebrafish in this model bring about complete remyelination, potential targets could be identified which could help to recapitulate the success of zebrafish in mammalian systems.

3.9.8. Future use of the Tg(mbp:mCherry-NTR) model

In the introduction to this chapter, I described the reasons why we felt a larval zebrafish model of demyelination and remyelination would be a beneficial tool for the field of remyelination research. Briefly, we believed that such a model could enable researchers to study the health and integrity of individual axons over the course of demyelination and remyelination, and relate the health of the axon to its myelination status. In addition, researchers could study oligodendrocyte morphologies during remyelination to see if each cell makes more myelin during remyelination than it would during developmental myelination (as I would expect them to, given that oligodendrocyte numbers in Mtz-treated animals remain short of control numbers, despite the animals achieving full remyelination) as well as how this morphology might be influenced by the activity or calibre of the demyelinated axon. We also anticipated that it could be a useful tool for chemical screening to identify compounds to enhance remyelination, and for testing the effects of novel genes found to affect myelination on remyelination.

Having now characterised the timing and extent of demyelination in the Tg(mbp:mCherry-NTR) model, it seems that it is amenable to ultrastructural analyses of certain indicators of axon health, such as their mitochondrial content or cross-sectional size, and that novel observations such as the possibility of axon calibre growth stimulating myelin thickness growth, can be made using this model. However, when studying remyelination in the Tg(mbp:mCherry-NTR) model, it is essential to

bear in mind the caveats I have discussed here, namely the ongoing developmental processes, the difficulty in definitely identifying demyelinated axons ultrastructurally, and the likelihood that any axon is only partially demyelinated. These issues chiefly arise from the fact that ultrastructural analyses allow examination of only onetime point, and thus could be circumvented by labelling individual oligodendrocytes and axons in a living larva, and imaging the same cells over time. For example, I could label individual reticulospinal axons and follow them over time, determine when during the development of the larva they stop growing in calibre, and induce demyelination after this time point, to see whether remyelination still results in full thickness myelin when the axons are no longer growing radially.

The above mentioned example, and indeed most experiments I have discussed here, involve imaging Tg(mbp:mCherry-NTR) larvae at during the period of demyelination and remyelination, when they are over 14 days old. On this point, one issue I have touched on briefly in this chapter is that live imaging of larvae gets progressively more challenging as the animals age and grow in size. This is because increased thickness and opacity of muscle tissue makes it more difficult to focus on the spinal cord and acquire high-quality images. Indeed, this is why I quantified oligodendrocyte numbers from cryosections rather than live larvae at 16 and 18d post-treatment. However, with appropriate adjustments to imaging protocols, including using tools better suited to deep tissue imaging, such as multiphoton microscopes, live imaging of demyelination and remyelination events can be carried out.

Furthermore, as I will discuss further in **Chapter 6** (General Discussion) I also believe that this will be a valuable tool for small-scale chemical screening and testing the effects of various manipulations on the overall extent and timing of oligodendrocyte regeneration and remyelination. In the next chapter, I introduce a set of experiments whereby I study the response of microglia/macrophages to oligodendrocyte ablation and test the effects of an irf8 mutation, which prevents microglia and macrophages developing during the early stages, on the success of oligodendrocyte regeneration and remyelination.

Chapter 4:

The response of the innate immune system to oligodendrocyte ablation

4.1. Introduction

4.1.1. The innate immune system plays a pivotal role in remyelination

In **Chapter 3**, I showed by electron microscopy that the Tg(mbp:mCherry-NTR) larvae achieve full remyelination within sixteen days from oligodendrocyte ablation. In this chapter, I test the hypothesis that the innate immune system is activated following oligodendrocyte ablation, and that this activation plays an important role in bringing about the successful remyelination that I see in this model. The reasoning underpinning this hypothesis stems from recent findings demonstrating that the innate immune system has important and beneficial effects on remyelination in rodent models, and furthermore that the innate immune system also has important and beneficial effects on CNS tissue regeneration in zebrafish models.

I will briefly recap the evidence for the role of the innate immune system in remyelination in rodent models, and then discuss what is known about its function in zebrafish CNS regeneration.

Despite the known involvement of microglia and macrophages in the pathology of MS and EAE (Lucchinetti et al. 2000; Ajami et al. 2011), it is now very clear that the innate immune system plays a critical role in bringing about remyelination (McMurran et al. 2016). As I detailed in **Chapter 1**, the innate immune system serves two major functions following demyelination: first, to remove the myelin debris generated as a by-product of demyelination. Phagocytic cells, namely CNS-resident microglia and monocyte-derived macrophages, are recruited to the lesion sites and engulf the myelin debris, thus effectively clearing the way for OPCs to be recruited to the lesion and give rise to remyelinating oligodendrocytes (Kotter et al. 2001; Kotter et al. 2006). If this clearance is hindered, for instance because the animal is aged (Ruckh et al. 2013; Safaiyan et al. 2016) or because important control mechanisms such as RXR signalling are disrupted (Natrajan et al. 2015), remyelination is impaired.

The second major function of innate immune cells in driving remyelination is their release of anti-inflammatory and pro-regenerative factors that regulate behaviour of cells of the oligodendrocyte lineage. Setzu et al. (2006) and Yuen et al. (2013)

demonstrated that upon experimental induction of inflammation in the absence of demyelination, a plethora of growth factors, transcription factors and cytokines were upregulated. A number of these, for example endothelin-2, were shown to induce myelination as well as improve endogenous remyelination following toxin-induced demyelination (Yuen et al. 2013).

This pro-regenerative activity is facilitated by the microglia and macrophages assuming a particular activation state, termed "M2 polarization state", distinct from the more inflammatory "M1 polarization state". While separation of the two states is clearly a markedly simplified and even arbitrary division, many researchers have considered the terms a pragmatic approach to understanding the numerous functions microglia and macrophages serve. Indeed, a study by Miron et al. (2013) examined the molecular phenotypes of microglia and macrophages during demyelination and remyelination, and found that a switch from the M1 to the M2 state drives efficient remyelination.

Thus, the two functions of myelin debris clearance and creation of a favourable lesion environment for remyelination make the innate system an indispensable component of the remyelination process. In recent years, the distinct functions performed by CNS-resident microglia and peripherally-derived macrophages in both myelin damage and remyelination are beginning to be elucidated (e.g. Yamasaki et al. 2014) but much remains to be clarified before their distinct roles are properly understood.

Interestingly, it is not just following demyelination and injury that the innate immune system is important. Recently, microglia have also been the focus of much attention for the roles they play in normal CNS development, from clearing apoptotic neurons to prevent the contents of dying cells affecting nearby healthy cells (Wakselman et al. 2008) to pruning synapses (Schafer et al. 2012) and secretion of growth factors to support neuronal survival (Ueno et al. 2013). There is also evidence to suggest that microglial activation promotes oligodendrocyte progenitor cell (OPC) proliferation in the subventricular zone in mice (Shigemoto-Mogami et al. 2014). These developmental roles may have important implications in studies where microglia function is inhibited, and thus are worth keeping in mind when interpreting the results of such studies.

4.1.2. Innate immune system in zebrafish development and injury

While the part played by the innate immune system in mammalian remyelination is now under intense scrutiny, less is known about interactions between the innate immune system and myelinating cells in the zebrafish. In the Tg(mbp:mCherry-NTR) model, spontaneous remyelination is very successful, so if the innate immune system performs a similar function in fish as it does in mammals, I would expect it to be activated and essential in bringing about remyelination.

In terms of development, the zebrafish innate immune system is well studied. Macrophages are the first leukocytes to arise in the developing embryo: they originate from the rostral end of the lateral mesoderm, then migrate to the yolk sac and differentiate there from 20 hours post-fertilisation (hpf; Herbomel et al. 1999). From 24hpf, macrophages begin to migrate out of the yolk sac and towards various tissues. Colonisation of the brain begins around 35hpf and by 60hpf, macrophages are distributed across the developing brain, with a notable cluster near the optic tectum (Herbomel et al. 2001). At this point, these cells downregulate the expression of the macrophage marker L-plastin, whereas macrophages in all other tissues and in blood circulation retain this expression. From 72hpf onwards, the macrophages in the brain begin to express apoe, confirming them as early microglia (Herbomel et al. 2001).

Peripheral macrophages, on the other hand, are found predominantly in the epidermis and blood circulation after the embryonic stages (Herbomel et al. 2001; Herbomel and Levraud 2005).

Similar to mammals (Hashimoto et al. 2013; Ajami et al. 2007), zebrafish monocyte-derived macrophages do not generally enter the CNS in the absence of injury or infection (van Ham et al. 2014). Interestingly, a recent live imaging study in zebrafish revealed that even microglial colonisation of the embryonic brain is partially triggered by apoptosis of neurons; if neuronal apoptosis was inhibited, fewer microglia were attracted to the brain, and if apoptosis was increased, more microglia migrated to the brain and remained there (Casano et al. 2016).

Also as in mammals, microglia perform a range of important functions during zebrafish development, including phagocytosing apoptosing neurons during development (Peri and Nüsslein-Volhard 2008; van Ham et al. 2012) and modulating the excitability of neurons to optimise network properties (Li et al. 2012).

Several studies have suggested a beneficial role of inflammation in CNS tissue repair in zebrafish. In general, adult zebrafish recover extremely well from CNS insults, including complete spinal cord transections and stab wounds to the telencephalon, such that function is restored (Becker and Becker 2014; Kroehne et al. 2011). Kyritsis et al. 2012 set out to test the role of inflammation in mediating this recovery. They first observed that microglia and macrophage numbers increase within hours of a stab wound to the adult zebrafish telencephalon, and remained elevated for several days. If this response was blocked by co-injection of the immunesuppressant steroid dexamethasone, generation of new neurons was reduced. The necessity of the immune response was not specific to the CNS; dexamethasone-treated fish were also unable to regenerate their caudal fins following clipping.

Next, Kyritsis et al. injected the inflammogen zymosan into the brains of the adult fish, and found that this induced an immune response highly reminiscent of that elicited by the stab wound. Moreover, zymosan injection in the absence of any wound was sufficient to induce proliferation of neuronal progenitors. The authors went on to perform a transcriptome screen to identify the molecular players that may be involved in the regenerative response, and showed that Cysteine Leukotriene Receptor 1 (cystlr1) was highly upregulated in the wounded hemisphere but not the contralateral one. They used pharmacological loss and gain of function experiments to confirm that signalling through cystlr1 was necessary and sufficient to promote neuronal progenitor proliferation. Importantly, zymosan injection in the absence of a lesion was shown to upregulate the same signalling pathways.

Thus, Kyritsis et al. (2012) provide strong evidence that an innate immune system response is required to achieve the remarkable regeneration of CNS tissue that is seen in zebrafish. This echoes the role proposed for the innate immune system in facilitating remyelination in rodent models, and moreover, gives rise to the possibility that the

innate immune system may be an important player in the remyelination process in zebrafish, too.

Kyritsis et al.'s study in adult zebrafish focuses chiefly on the signalling pathways that are upregulated in the wake of the innate immune response. For studies of the dynamic behaviour of the innate immune cells and their interactions with CNS tissue, larval zebrafish models are preferable. This is because, as the immune response to insult can be very rapid, with microglial activation commencing within minutes of the insult in some cases (Sieger et al. 2012), such cell behaviours are best explored using live imaging.

In an attempt to define the innate immune response to genetic ablation of neurons, van Ham et al. (2014) used the NTR/Mtz system to ablate neurons at 5dpf and observed the subsequent behaviour of transgenically labelled immune cell by live imaging. This showed that both microglia and macrophages carry out phagocytosis of debris while neutrophils and astrocytes were not involved. Furthermore, when debris clearance was complete about one week later, many monocyte-derived macrophages underwent apoptosis and were subsequently engulfed by microglia. Remarkably, over 80% of the larvae survived to adulthood and exhibited no sign of having had large proportions of their neurons ablated during their development. The authors posit that the brisk response of the innate immune system was the main reason for this swift and complete recovery achieved by the larvae. However, importantly, they did not include any experimental manipulation of the microglia and macrophage response, by enhancing or inhibiting it, and thus their conclusion remains a supposition that will be important to test in the future.

In an adult zebrafish model of demyelination where focal demyelination is induced in the optic nerve by direct application of LPC, Münzel et al. (2014) observed more 4C4-positive microglia at the lesion site in young fish, which succeed at restoring their myelin sheaths to full thickness, compared to old fish, which do not. This correlation again suggested that microglia contribute to the efficient myelin regeneration achieved by the young adult fish. However, again, this hypothesis was not experimentally tested in this study.

In stark contrast to the above studies implicating a positive role for the innate immune system following injury in the zebrafish, Kim et al. (2015) used a larval zebrafish model of demyelination (which I have discussed in the Discussion of **Chapter 3**) to suggest that the innate immune system may in fact be detrimental for remyelination. In this study, the authors administered the anti-inflammatory drug sulfasalazine, mainly used for in treatment of rheumatism and inflammatory bowel disease, to the larvae immediately following metronidazole withdrawal, and one day later, reported increased numbers of oligodendrocytes and increased thickness of the myelin sheath around the Mauthner axon compared to non-sulfasalazine treated larvae. They argued that this increase is due to the immunosuppressing effects of sulfasalazine, as the sulfasalazine treatment following Mtz-treatment reduced the number of apoe- and Cd11b-expressing microglia in the brains of the larvae. They also showed that a sulfasalazine treatment at 1dpf increased the proliferation of olig2-expressing cells, and suggested that sulfasalazine also promotes OPC proliferation following demyelination. Since they do not repeat this experiment in their demyelinating model, there is no way of knowing whether sulfasalazine would induce a similar increase in an injury context, or whether the increase has anything to do with suppression of the immune system.

However, the result reported by Kim et al. must be viewed in the context of their model. Neither demyelination nor remyelination is quantified in any other way apart from the thickness of the myelin around the Mauthner axon (and this from low-resolution confocal images rather than electron micrographs), rendering it difficult to evaluate the specific effects of a drug intervention. Furthermore, Kim et al. do not allow any time to pass between oligodendrocyte ablation and investigating demyelination, which (based on my own results) may not represent the full extent of the demyelination caused by the oligodendrocyte ablation. This calls into question whether the effect of sulfasalazine can be taken as remyelination; it is equally likely to suppress an ongoing immune attack on myelin and thus reduce the level of demyelination that occurs in the first place.

The authors acknowledge that their result contradicts much of what has been shown in rodent studies of remyelination, and postulate that the microglia and macrophages had

already carried out myelin debris clearance and secretion of pro-regenerative signals prior to sulfasalazine treatment, and thus the drug did not impede these essential functions. Instead, they argue, the drug protected the larvae from harmful effects of long-term immune presence in the spinal cord. However, since Kim et al. only treat their larvae with sulfasalazine for one day, it is not clear what they mean by harmful long-term exposure to microglia and macrophages. It is also doubtful whether the larvae would be able to clear all of their myelin debris prior to sulfasalazine treatment, as the sulfasalazine treatment commences immediately after Mtz-treatment, and some debris is clearly still present in the non-sulfasalazine treated larvae one day post Mtz-treatment. In general, the timeline of their model, as I have already discussed in **Chapter 3** is so rapid, with apparent remyelination occurring in one day, that it is difficult to relate events they report to those seen in other models.

All in all, then, while there is some compelling evidence that the innate immune system response is a necessary and beneficial event for CNS tissue repair in zebrafish, a systematic investigation of its role in the context of demyelination remains to be carried out.

4.1.3. The irf8 mutant zebrafish as a tool to disrupt macrophage and microglial development

Thus, evidence from mammalian systems strongly suggests that the innate immune system actively aids remyelination, whereas less clear evidence for its role is currently available in zebrafish models. In this chapter, I address the question of what role the innate immune system plays in remyelination in the Tg(mbp:mCherry-NTR) model.

I first describe the response of microglia and macrophages to oligodendrocyte ablation and show that it reaches its peak at four days post-treatment. I then demonstrate the immune response coincides with both the oligodendrocytes undergoing cell death and the reduction in the volume of the myelin vacuoles.

Next, I ask how remyelination in this model is affected if the development of microglia and macrophages were inhibited. To this end, I use the recently published irf8 mutant

fish (Shiau et al. 2015) in which the development of microglia and macrophages is impaired. The transcription factor irf8 (interferon regulatory factor 8) acts as a major determinant of macrophage/monocyte fate during hematopoiesis. In mammals, irf8 has been shown to be critical for macrophage lineage development; its deficiency in humans and mice causes a significant reduction of macrophage/monocyte development (Hambleton et al. 2011; Kierdorf et al. 2013).

Shiau et al. generated and characterised an irf8 null mutant zebrafish which has a frameshift mutation just 3' to the initiation codon in the irf8 gene, causing complete loss of function. Accordingly, the authors report a complete lack of macrophages at 2dpf (as shown by an absence of mfap4 RNA expression by *in situ* hybridization) and a complete lack of microglia at 3dpf – 6dpf (as shown by an absence of apoe RNA expression by *in situ* hybridization). In contrast, by showing excessive mpx RNA expression the authors demonstrate an extensive expansion of neutrophils as early as 1dpf. This was to be expected, as cell fate switching has been previously demonstrated in the zebrafish myeloid lineage: Li et al. (2011) showed increased output of neutrophils when irf8 was knocked down during early development, without affecting the overall number of primitive myeloid cells. Conversely, overexpression of irf8 leads to enhanced macrophage formation at the expense of neutrophil numbers.

By 2.5dpf, Shiau et al. show a small number of weakly mpeg-expressing cells in irf8 mutants, restricted to blood-forming regions in the tail. By 7dpf, irf8 mutants contained a few strongly mpeg-expressing cells in the head, and by 14dpf and 31dpf, they had around 50 mpeg-expressing cells in their head regions (but, notably, still less than half the number seen in their wild-type siblings). The authors concluded that the second wave of hematopoiesis in zebrafish is regulated by a different set of transcription factors and thus does not depend on irf8 function.

In order to test the effects of the irf8 mutation on remyelination in my model, I created irf8 null Tg(mbp:mCherry-NTR) larvae by crossing Tg(mbp:mCherry-NTR) fish with irf8 mutant fish and subsequently incrossing these heterozygous animals once they reached adulthood. I demonstrate that irf8 null larvae do not show deficits in early oligodendrocyte development up to 5dpf, and that their spinal cords contain very few microglia or macrophages at the time point when the immune invasion is at its peak in

wild-type larvae. Despite this, however, ultrastructural analysis of the spinal cord at 16d post-treatment reveals that irf8 null animals do not show any deficits in remyelination, although they do show a delay in oligodendrocyte number regeneration. In the Discussion of this chapter, I consider what might account for this lack of impairment, and posit that the function of microglia and macrophages is served by neutrophils, and/or the macrophages born in the second wave of hematopoiesis.

4.2. Timeline of microglia and macrophage response to oligodendrocyte ablation

4.2.1 Microglia/macrophage presence in spinal cord peaks at 4d post-treatment

As summarised above, cells of the innate immune system, notably microglia and macrophages, play a pivotal role in bringing about myelin regeneration in rodent models of demyelination, and if their activity is inhibited in some way, regeneration is compromised. Given the very successful myelin regeneration achieved by the Tg(mbp:mCherry-NTR) fish (**Figures 12** and **13**) following demyelination, it seemed likely that the innate immune system is actively involved in the process.

I therefore set out to investigate the response of the innate immune system to oligodendrocyte ablation and demyelination. The first step was to ask simply whether there was any detectible response from the immune system following oligodendrocyte ablation, and if there was, what would it consist of and when would it take place.

In order to study the behaviour of microglia and macrophages *in vivo*, I used the transgenic line Tg(mpeg:GFP), which labels both cell types (Ellett et al. 2011). Since both CNS-resident microglia and monocyte-derived macrophages express mpeg, it is not possible to separate the two populations using this line. For this reason, during most of this chapter, I will discuss microglia and macrophages as a single population. The undoubtedly important distinctions between microglia and macrophages will be considered further in the Discussion.

To investigate the microglia and macrophage response to oligodendrocyte ablation, I crossed Tg(mbp:mCherry-NTR) fish to Tg(mpeg:GFP) fish, treated the resulting double transgenic progeny with DMSO or metronidazole from 5dpf to 7dpf, as in **Chapter 3**. Using these larvae, I carried out a time course experiment whereby I imaged larvae at different time points during the first nine days following the withdrawal of DMSO- or Mtz-treatment. As before, for reasons of larval health, it was not practical to image the same larvae over so many consecutive days, so the following data were obtained from imaging different larvae each day. I quantified these data by counting the numbers of mpeg+ cells from a four-somite area of the spinal cord.

The data from this time course experiment are presented in **Figure 22A**. At the time of withdrawal of the DMSO or Mtz-treatment, there are very few mpeg-expressing cells in either condition; yellow arrowheads indicate one such cell in each larva. Counts indicated that there was a mean of 2.0 ± 1.73 mpeg+ cells in control animals and 2.0 ± 2.25 in Mtz-treated animals, $p = 1$. A similar situation prevails at 2d post-treatment, when there was a mean of 2.33 ± 2.02 mpeg+ cells in control animals and 4.14 ± 1.75 in Mtz-treated animals, $p = 0.022$. In contrast, at 3d post-treatment, noticeably more mpeg+ cells are seen in the spinal cord of treated animals, and indeed counts showed that there was a mean of 1.79 ± 2.39 mpeg+ cells in control, compared to 8.2 ± 3.69 mpeg-expressing cells in Mtz-treated animals, $p < 0.0001$. At 4d post-treatment, the number of mpeg+ cells in the spinal cord of Mtz-treated animals was elevated even further, with a mean of 3.17 ± 2.23 mpeg-expressing cells in control, compared to a mean of 10.92 ± 4.01 mpeg-expressing cells in Mtz-treated animals, $p = 0.00040$. From that time onward, the number of mpeg-expressing cells gradually decreases. The difference remains significant at 7d post-treatment (3.69 ± 1.7 mpeg-expressing cells in control, compared to 7.94 ± 2.38 mpeg-expressing cells in Mtz-treated animals, $p = 0.00032$) but by 9d post-treatment, the number of mpeg-expressing cells in Mtz-treated animals has become indistinguishable from that in control animals (3.00 ± 1.48 in control, compared to 4.22 ± 2.44 in Mtz-treated animals, $p = 0.18$).

Interestingly, the TEM data I described in **Chapter 3** indicated that during the first four days following the Mtz-treatment, there was a significant presence of vacuoles in the spinal cord, and this becomes much less pronounced from 5d post-treatment onwards; thus the beginning of the decline in vacuoles coincides with the peak of the immune presence in the spinal cord. Furthermore, the peak demyelination stages of 7-11d post-treatment occur after the microglia/macrophage presence in the spinal cord has attenuated.

A

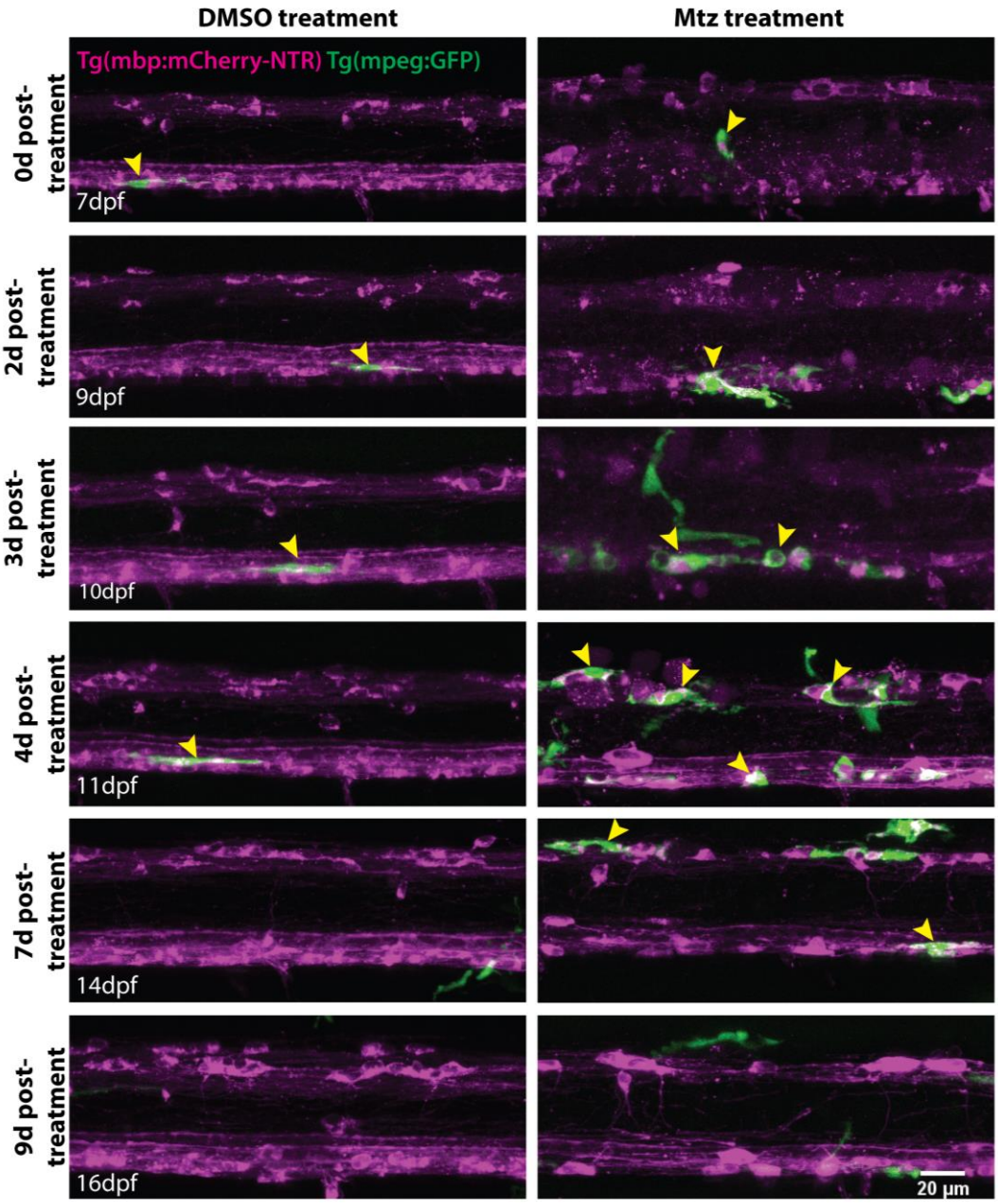

Quantification overleaf

B

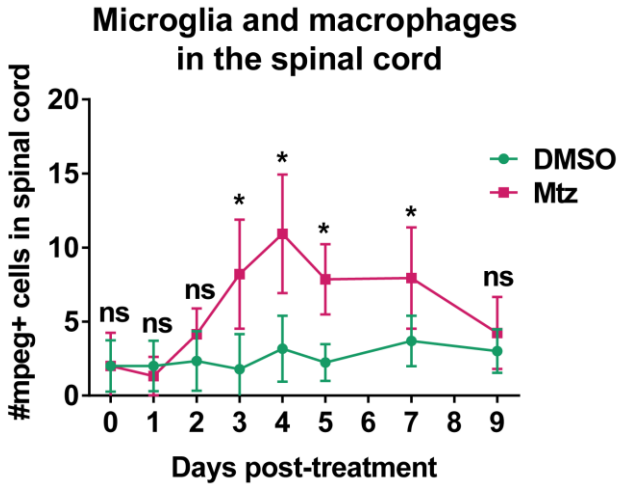

Figure 22. The number of microglia/macrophages in the spinal cord peaks at 4d post-treatment and declines by 9d post-treatment. A. Confocal images of spinal cords of larvae treated with either DMSO or Mtz, and at different time points, as indicated. Green cells are mpeg-expressing microglia and macrophages. Yellow arrowheads indicate examples of mpeg+ cells in contact with the spinal cord. **B**. Quantification of immune invasion by counting mpeg+ cells in contact with the spinal cord shows that from 3d post-treatment, there are significantly more mpeg+ cells in Mtz-treated compared to control animals (a mean of 1.79 ± 2.39 mpeg+ cells in control compared to a mean of 8.2 ± 3.68 mpeg+ cells in Mtz-treated animals, $p < 0.0001$). The immune invasion peaks at 4d post-treatment (a mean of 3.17 ± 2.22 mpeg+ cell in control, compared to a mean of 10.92 ± 4.01 mpeg+ cells in Mtz-treated animals, $p = 0.00040$). After that, the presence of immune cells in the spinal cord decreases gradually, until at 9d post-treatment there is no significant difference between control and Mtz-treated animals (3.0 ± 1.48 mpeg+ cells in control, compared to 4.22 ± 2.44 in Mtz-treated, $p = 0.18$). Statistical significance was determined using multiple t tests per row, with a Holm-Sidak method, without assuming equal SD between the groups n = no less than 9.

4.2.2 Microglia and macrophages phagocytose mCherry+ material

The above described timeline revealed that the immune response to oligodendrocyte ablation consists of drastically increasing the numbers of microglia and macrophages in the spinal cord, starting at 3d post-treatment, peaking at 4d post-treatment and then winding down gradually until at 9d post-treatment there is no longer a notable presence of microglia and macrophages in Mtz-treated compared to control spinal cords.

Having established the timeline of the immune response, I was interested in how active the microglia/macrophages in the spinal cord actually were. Were they merely present, or were they phagocytosing oligodendrocyte and myelin matter? In order to address these questions, I analysed the same dataset in greater detail, this time counting only those mpeg-expressing cells which clearly contained mbp:mCherry-NTR -expressing material. This analysis required careful examination of each individual z section to ascertain that the mbp+ material was *inside* the mpeg+ cell. The insets in **Figure 23A** show examples of such individual z sections (2µm in thickness) from confocal stacks where there are a number of magenta mCherry-expressing fragments within the microglia/macrophages cells.

The timeline produced by this analysis closely resembled the timeline of immune invasion, with the exception that the number of mpeg+ cells containing mCherry+ material was significantly higher in Mtz-treated compared to control animals already at 2d post-treatment (whereas this difference only became significant at 3d post-treatment in the overall timeline). In short, at 1d post-treatment, phagocytosis had evidently not begun and there was a mean of 0.92 ± 1.38 mpeg+ cells containing mCherry+ material in control animals and 0.81 ± 1.05 in Mtz-treated animals, which was not significantly different ($p = 0.822$). By 2d post-treatment, the number of mpeg+ cells containing mCherry+ material had increased such that there were 2.79 ± 2.16 cells in Mtz-treated animals compared to 0.75 ± 1.06 in control animals and ($p = 0.0066$). The number of mpeg+ cells containing mCherry+ material continues to climb at 3d post-treatment and peaks at 4d post-treatment, when there is an average of 9.23 ± 4.02 cells in Mtz-treated animals compared to 1 ± 0.89 cells in control animals ($p = 0.00014$). After this, the number begins to decrease gradually, such that at 7d post-treatment the number of mpeg+ cells containing mCherry+ material has come down to a mean of 4.75 ± 3.17 cells in Mtz-treated animals, and has a mean of 0.85 ± 0.90 cells in control animals ($p = 0.00018$). By 9d post-treatment, the number of cells in Mtz-treated animals has further decreased to a mean of 2.11 ± 1.96 cells, compared to a mean of 0.45 ± 0.69 cells in controls ($p = 0.017$), which was not deemed statistically significant. I had used the Holm-Sidak method recommended by GraphPad to determine significances of differences at multiple time points. This is a stringent system which analyses each row (encompassing one time point, divided into control

and treated) individually and does not assume equal standard deviations between groups. Despite having its alpha value set at 5%, the Holm-Sidak method did not find the p value of 0.017 statistically significant. However, a t-test between the control and Mtz-treated groups at 9d post-treatment found the difference significant ($p = 0.0173$). That being said, a lack of significant difference between control and Mtz-treated animals is to be expected from the trajectory of the curve in **Figure 23B**; it is clear that the number of mpeg+ cells containing mCherry+ material is on its way to being indistinguishable from controls.

This timeline of mpeg+ cells containing mCherry+ material strongly suggests that the immune cells which invade the spinal cord following oligodendrocyte ablation perform a "mopping up" function whereby they phagocytose damaged oligodendrocyte material and myelin debris. This interpretation is also supported by the observation that the cellular vacuoles, which remain prevalent for some days following withdrawal of the treatment, are much less prominent from 5-6d post-treatment onwards. It is not difficult to imagine that the gradual decrease of the vacuoles is a result of microglia and macrophages phagocytosing and digesting them, until such time as the vacuoles are largely depleted and the immune presence in the spinal cord can disperse.

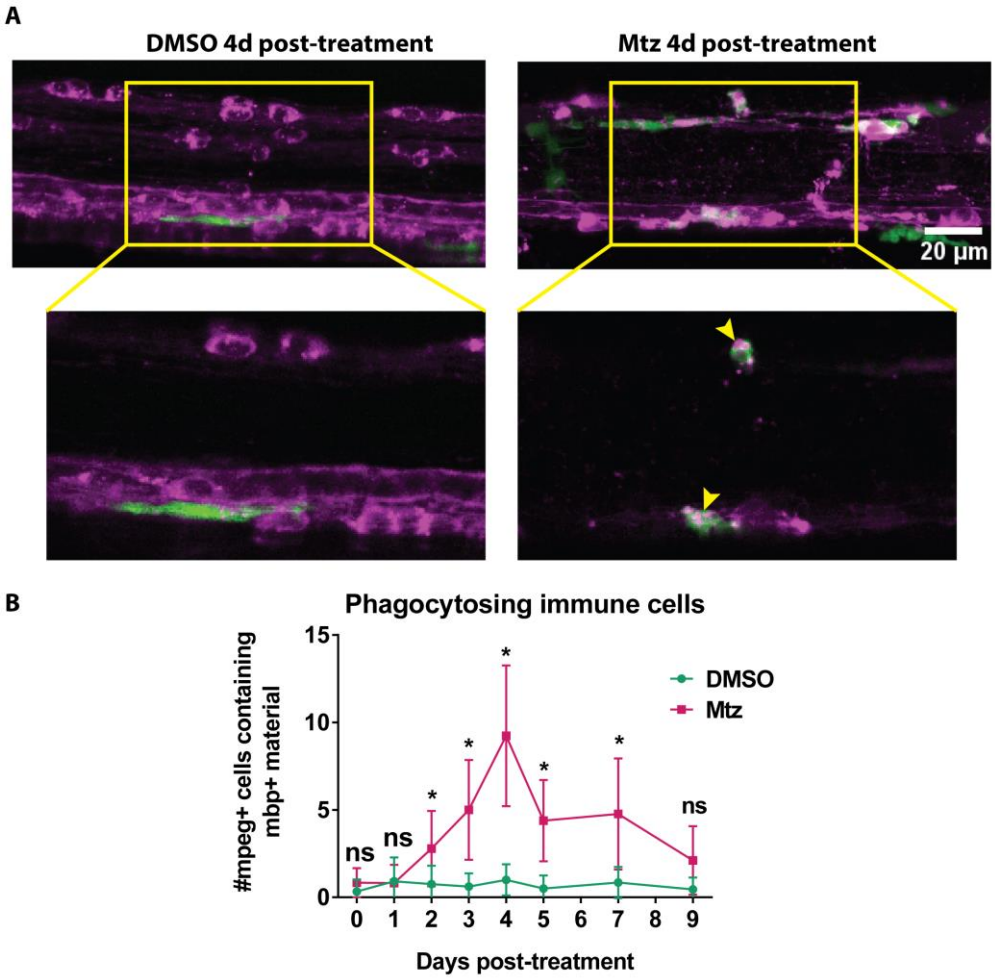

Figure 23. Phagocytosis reaches its peak at 4d post-treatment. A. Confocal images from 11dpf Tg(mbp:mCherry-NTR); Tg(mpeg:GFP) larvae, treated with either DMSO or Mtz, as indicated. Top panels are maximum intensity projections. Bottom panels (insets) are single z sections from the stack, at the location indicated by the yellow box. Yellow arrowheads indicate mhery+ material inside mpeg+ cells. **B**. Quantification shows that from 2d post-treatment onwards there are more mpeg mpeg+ cells containing mCherry+ material in Mtz-treated compared to control animals. At 1d post-treatment, there was a mean of 0.92 ± 1.38 mpeg+ cells containing mCherry+ material in control animals and 0.81 ± 1.05 in Mtz-treated animals ($p = 0.822$). By 2d post-treatment, there were 0.75 ± 1.06 mpeg+ cells containing mbp+ material in control animals and 2.79 cells in Mtz-treated animals ($p = 0.0066$). The number of mpeg+ cells containing mCherry+ material peaks at 4d post-treatment, when there is an average of 1 ± 0.89 cells in control animals compared to 9.23 ± 4.02 in Mtz-treated animals ($p = 0.00014$). After this, the number begins to decrease, such that at 7d post-treatment there is a mean of 0.85 ± 0.90 cells in control animals and a mean of 4.75 ± 3.17 cells in Mtz-treated animals ($p = 0.00018$). By 9d post-treatment, there is no longer a significant difference between control and treated animals, with a mean of 0.45 ± 0.69 cells in controls and 2.11 ± 1.96 cells in treated animals ($p = 0.017$). This was not deemed statistically significant by the Holm-Sidak method, with alpha set at 5%, as each row was analysed individually, without assuming a consistent SD. n = no less than 6, usually over 9.

4.3. Timeline of oligodendrocyte cell death

4.3.1 Acridine orange staining reveals oligodendrocytes undergoing cell death during the course of the immune invasion

The drastic increase in microglia/macrophage numbers in the spinal cord, and the observation that these cells readily ingest mCherry+ material, suggest that the oligodendrocytes affected by the Mtz-treatment and the degrading myelin sheaths express one or more "eat-me" signals to attract microglia and macrophages to them. Such signals are expressed on the surface of cells undergoing apoptosis (or another form of cell death; Hochreiter-Hufford et al. 2013). In order to test whether Mtz-treated oligodendrocytes were indeed undergoing cell death, I stained living DMSO- or Mtz-treated larvae with the vital dye acridine orange. This is a cell-permeable fluorescent cationic dye which intercalates into the double helix of DNA and thus enables visualisation of cells with compromised nuclear integrity and fragmented DNA. Acridine orange has previously been used to label dying cells in living zebrafish (Hammerschmidt et al. 1996; Paquet et al. 2009). By counting cells which were positive for both acridine orange (AO) and mbp:mCherry-NTR (**Figure 24A**) I could quantify oligodendrocytes undergoing cell death.

The results of this time course, shown in **Figure 24B**, revealed that cell death is detectable at the end of the Mtz-treatment (0d post-treatment): at this time point, there was a mean of 3.88 ± 1.25 AO+ mCherry+ cells in a four-somite area of the spinal cord in Mtz-treated animals, compared to 0.56 ± 1.01 per control animal, $p < 0.0001$. Over the course of the next few days, the number of AO+ mCherry+ cells continues to increase in Mtz-treated animals until at 4d post-treatment there is a mean of 6.5 ± 1.69 such cells in treated animals, compared to a mean of 0.4 ± 0.89 such cells in controls, $p < 0.0001$. Following this peak, the number of AO+ mCherry+ cells in Mtz-treated animals begins to decrease such that at 7d post-treatment, the numbers are indistinguishable between treated and control animals; a mean of 1.25 ± 1.16 cells in control and 0.86 ± 1.07 cells in Mtz-treated animals, $p = 0.51$.

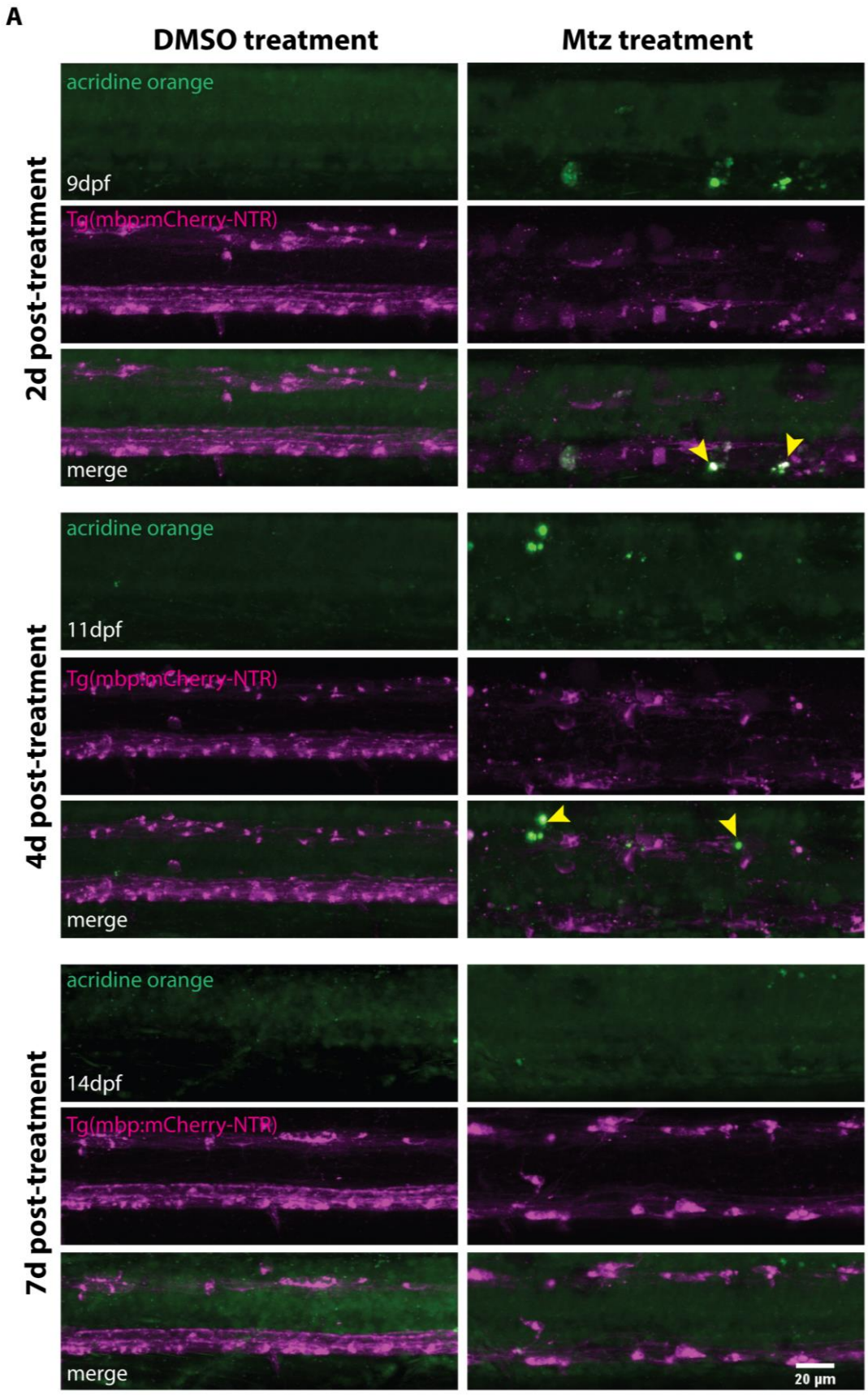
A
DMSO treatment
Mtz treatment
2d post-treatment
4d post-treatment
7d post-treatment
acridine orange
9dpf
Tg(mbp:mCherry-NTR)
merge
acridine orange
11dpf
Tg(mbp:mCherry-NTR)
merge
acridine orange
14dpf
Tg(mbp:mCherry-NTR)
merge
20 µm

B

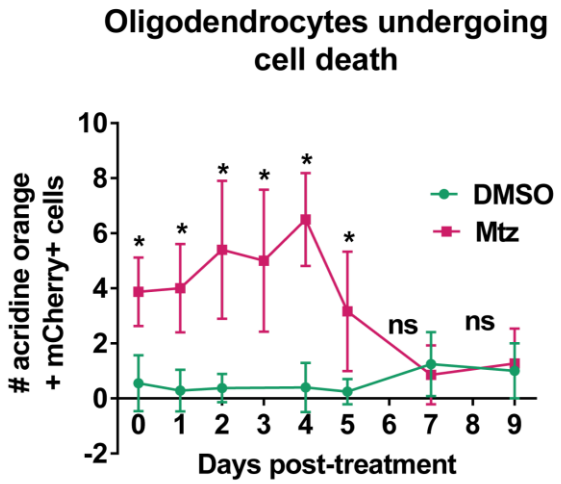

Figure 24. Oligodendrocytes in Tg(mbp:mCherry-NTR) animals undergo cell death following metronidazole treatment A. Confocal images of spinal cords of larvae treated with either DMSO or Mtz, and at different time points, as indicated. Acridine orange labels cells undergoing cell death in green. In the DMSO-treated animals, there is hardly any acridine orange signal, whereas in the Mtz-treated animals at 2d and 4d post-treatment, several bright green puncta can be seen, and these colocalise with mCherry (yellow arrowheads). **B**. Quantification of cells positive for both mCherry and acridine orange shows that there are significantly more oligodendrocytes undergoing cell death from 0d to 5d post-treatment: at 0d post-treatment, there was a mean of 3.88 ± 1.25 AO+mCherry+ cells per Mtz-treated animal, compared to 0.56 ± 1.01 per control animal, $p < 0.0001$. The number of AO+mCherry+ cells continues to increase in Mtz-treated animals until at 4d post-treatment there is a mean of 6.5 ± 1.69 such cells in treated animals, compared to a mean of 0.4 ± 0.89 such cells in controls, $p < 0.0001$. After this, the number of AO+ mCherry+ cells in Mtz-treated animals decreases such that at 7d post-treatment, the numbers are indistinguishable between treated and control animals; a mean of 1.25 ± 1.16 cells in control and 0.86 ± 1.07 cells in Mtz-treated animals ($p = 0.51$). n = no less than 8

Thus, it seems that following Mtz-treatment, oligodendrocyte cell death starts immediately (possibly even prior to withdrawal of the drug) and continues for a period of a week. This implies that some oligodendrocytes undergo cell death shortly after Mtz-treatment, while others succumb several days later. The reasons for these differences are not clear; perhaps those oligodendrocytes which expressed higher levels of the mbp:mCherry-NTR transgene were exposed to higher levels of the cytotoxic cross-linking agent and were therefore more vulnerable to cell death.

4.4. Impaired immune response in irf8-/- mutant animals

4.4.1 What happens to remyelination in an irf8 mutant fish?

The descriptive characterisation of the innate immune system's invasion of the spinal cord following oligodendrocyte ablation, and the evident phagocytic activities it performs, suggests that the innate immune system does indeed play an important role in clearing oligodendrocyte and myelin debris in Mtz-treated Tg(mbp:mCherry-NTR) animals. Extensive literature on the topic postulates that this clearance is a necessary prerequisite to effective oligodendrocyte regeneration and remyelination (Kotter et al. 2001; Kotter et al. 2006; Ruckh et al. 2012). With this in mind, and knowing that under physiological conditions, Mtz-treated Tg(mbp:mCherry-NTR) larvae are able to fully restore their myelin sheaths and even achieve normal myelin thickness , I hypothesised that at least some of this success is due to the activity of the innate immune system. This, naturally, prompted me to ask, what would happen to oligodendrocyte and myelin repair in this model, if the development of microglia and macrophages was impaired.

4.4.2 irf8 -/- mutant larvae have impaired development of microglia and macrophages

To impair the development of macrophages and microglia in the Tg(mbp:mCherry-NTR) larvae I used the recently published mutant zebrafish line, the irf8 mutant (Shiau et al. 2015). Irf8 is a transcription factor which acts as a major regulator of macrophage lineage development during hematopoiesis.

Shia et al. 2015 generated and characterised an irf8 null mutant zebrafish and reported a complete lack of macrophages at 2dpf and a complete lack of microglia at 3dpf – 6dpf. They also employ the Tg(mpeg:GFP) line and show at 2.5dpf a small number of weakly mpeg-expressing cells in irf8 mutants, restricted to blood-forming regions in the tail. By 7dpf, irf8 mutants showed a few strongly mpeg-expressing cells in the head, and by 14dpf and 31dpf, they had around 50 mpeg-expressing cells in their head

regions. In the tail region, the irf8 mutant larvae had around 10 mpeg-expressing cells at 31dpf.

Importantly however, even at 31dpf, the number of mpeg-expressing cells in irf8 mutants is still less than half of that seen in their heterozygous and wild-type siblings in their head regions, and less than a fifth in their tail regions. Furthermore, at 31dpf the authors were still unable to find any L-plastin positive microglia in the brain parenchyma of irf8 mutants (whereas there were many in their heterozygous and wild-type siblings).

Thus, even though some macrophages may have developed by the stages I am interested in (up to 23dpf), I was confident that the phenotype of the irf8 mutants was sufficiently prominent to considerably disrupt the immune invasion following oligodendrocyte ablation. Therefore, in order to investigate the effects of the irf8 mutation on oligodendrocyte and myelin repair in the Tg(mbp:mCherry-NTR) model, I crossed homozygous irf8 mutants to Tg(mbp:mCherry-NTR) fish and raised the resulting irf8 +/- progeny to adulthood. By incrossing these fish, I was able to obtain clutches where 25% of the animals were expected to be irf8 -/-, 50% irf8 +/- and 25% irf8 +/+, and all expressed the mbp:mCherry-NTR transgene.

4.4.3 irf8 -/- mutant larvae have normal numbers of oligodendrocytes at 5dpf.

Prior to embarking on studies regarding the effects of the irf8 mutation on oligodendrocyte and myelin regeneration, I wished to check whether the mutation had any adverse effects on early myelinating oligodendrocyte development. This was an important consideration, because microglia have been shown to play a part in regulating oligodendrocyte proliferation during development in mice (Shigemoto-Mogami et al. 2014) and it was possible that in their complete absence over the first five days of life, oligodendrocyte development may be compromised. If that were the case, it would make little sense to study oligodendrocyte and myelin regeneration in animals where these structured had not formed correctly in the first place.

To assess the level of oligodendrocyte development, I counted the numbers of oligodendrocytes from a four-somite stretch in the spinal cords of irf8 mutants and their siblings at 5dpf; the age when I start the metronidazole treatment.

These counts showed that there was no difference in oligodendrocyte numbers between animals that were wild-type, heterozygous or mutant for irf8: the mean number of oligodendrocytes in a four-somite area of the spinal cord was 70.38 ± 13.59 in irf8 +/+ animals, 74.10 ± 8.20 in irf8 +/- animals and 67.33 ± 12.47 in irf8 -/- animals. A one-way ANOVA found the difference between the genotypes to be non-significant ($p = 0.527$; **Figure 25B**). Since the oligodendrocytes were counted using the mbp marker, which is only present in mature oligodendrocytes, the observed normal number of oligodendrocytes can be taken to reflect both normal proliferation of OPCs as well as normal differentiation at least until the stages at which cell ablation was induced.

Thus, the irf8 mutation did not impair early oligodendrocyte development, and I was able to carry out oligodendrocyte ablation treatments in the knowledge that I was ablating a normal starting population of oligodendrocytes.

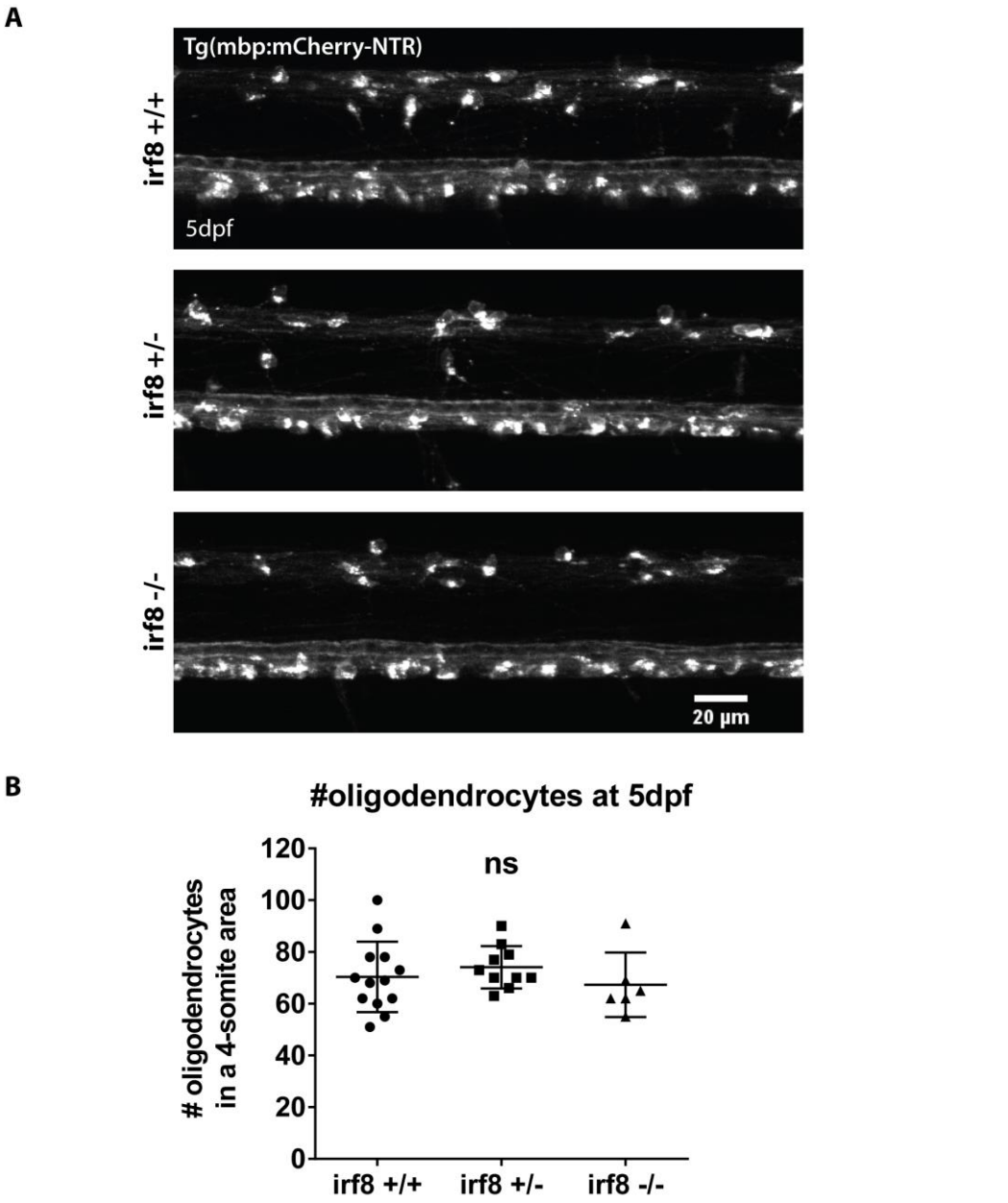

Figure 25. The irf8 mutation does not affect oligodendrocyte numbers at 5dpf. **A**. Confocal images from the spinal cords of 5dpf Tg(mbp:mCherry-NTR) larvae, wild-type, heterozygous or mutant for the irf8 gene, as indicated. **B**. Quantification shows that there is no difference in oligodendrocyte numbers between the genotypes: mean number of oligodendrocytes in four-somite area is 70.38 ± 13.59 in irf8 +/+ animals, 74.10 ± 8.20 in irf8 +/- animals and 67.33 ± 12.47 in irf8 -/- animals. A one-way ANOVA found the difference between the genotypes to be non-significant ($p = 0.527$). n = 13 for irf8 +/+, 10 for irf8 +/- and 6 for irf8 -/-.

4.4.4. irf8 -/- mutant larvae have very few mpeg-expressing cells in the spinal cord at the time point of peak immune invasion

Since Shiau et al. (2015) had reported that by 7dpf, there was a small number of mpeg-expressing cells in the head region of irf8 mutant larvae, and the immune attack I was seeking to disrupt occurs after this age, I was keen to establish that there was still a notable shortage of mpeg-expressing cells in the spinal cord following DMSO- or Mtz-treatment.

To this end, I created Tg(mbp:mCherry-NTR); irf8 +/-; Tg(mpeg:GFP) fish by crossing Tg(mpeg:GFP) fish with the aforementioned Tg(mbp:mCherry-NTR); irf8 +/- fish. The resulting progeny were either heterozygous or wild-type for irf8, so I genotyped these fish at a young age and only raised the heterozygotes to full adulthood. By incrossing these heterozygotes, I was able obtain clutches where, again, 25% of the animals were expected to be irf8 -/-, 50% irf8 +/- and 25% irf8 +/+, and furthermore, all were expected to express both the mbp:mCherry-NTR and mpeg:GFP transgenes.

In the following experiments, I will refer to irf8 -/- animals as mutants, and both irf8 +/+ and irf8 +/- animals as siblings, as all animals analysed in any given experiment originate from the same clutches.

I treated these larvae with DMSO or Mtz from 5dpf to 7dpf, then withdrew the treatment. At 4d post-treatment, the time point when I have shown the immune invasion to reach its peak in Tg(mbp:Cherry-NTR) animals wild-type for irf8, (**Figure 22**) I imaged the larvae and subsequently genotyped them. As is clear from the representative images shown in **Figure 26**, there were very few mpeg-expressing cells in the spinal cords of DMSO-treated siblings, a notable increase in Mtz-treated siblings, and hardly any in Mtz-treated mutant animals. I quantified this result by counting the numbers of mpeg-expressing cells in a four-somite stretch of the spinal cord and comparing the numbers between genotypes and treatment conditions. A one-way ANOVA found a significant overall difference between the groups ($p = 0.0008$), and subsequent individual t tests confirmed that there were significantly more mpeg+ cells in Mtz-treated siblings compared to Mtz-treated mutants (4.88 ± 4.01 cells in siblings compared to 0.80 ± 1.79 cells in mutants, $p = 0.0443$). In addition, as expected

from previous experiments, there were significantly more mpeg-expressing cells in Mtz-treated siblings than in DMSO-treated siblings ($p = 0.0003$). Unfortunately, of the 24 DMSO-treated larvae imaged over two experiments, only one was found to be an irf8 mutant. For this reason, no statistics involving DMSO-treated mutants could be performed.

Nevertheless, the immune presence in the spinal cords of Mtz-treated irf8-null larvae at the supposed peak immune invasion time point was entirely suppressed in the irf8 mutant. This was promising in terms of disrupting the debris clearance and potentially also myelin regeneration in this model.

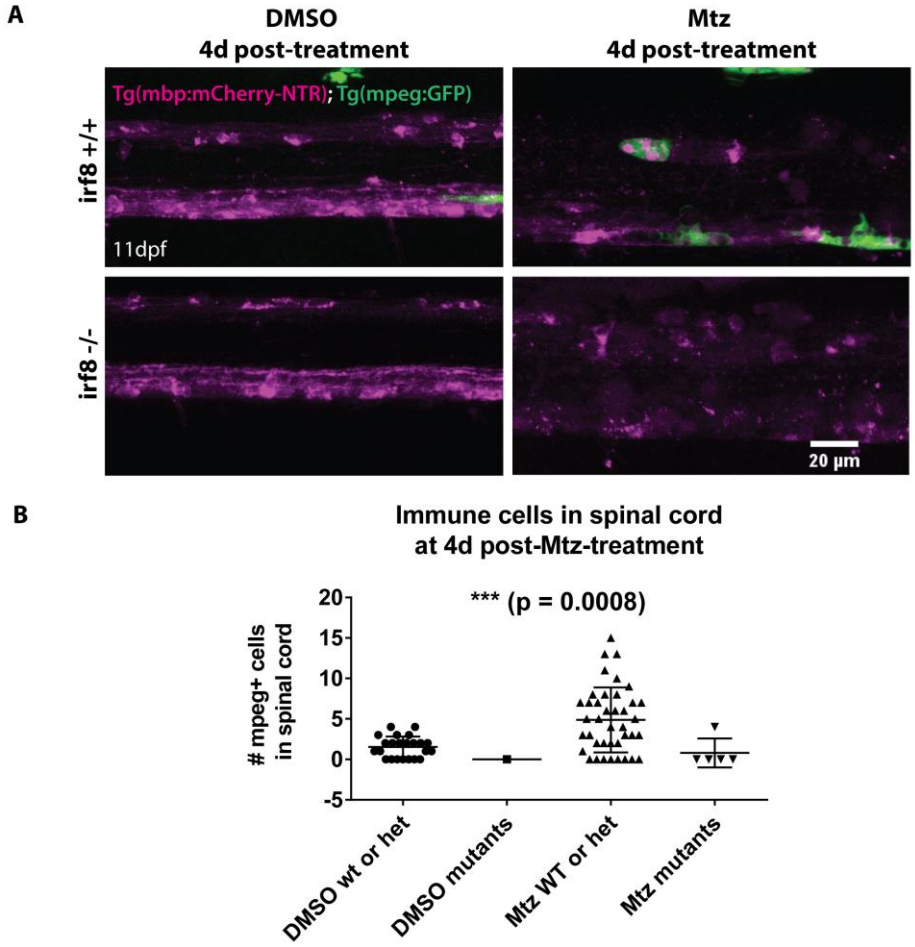

Figure 26. There are very few microglia/macrophages in the spinal cords of irf8 mutants at peak immune presence stage. A. Confocal images from spinal cords of 11dpf Tg(mbp:mCherry-NTR);Tg(mpeg:GFP) larvae, treated with DMSO or Mtz, and carrying wild type or mutant alleles of irf8, as indicated. There are few mpeg+ cells in the DMSO-treated animals, more in the Mtz-treated wild type animals, and none in the Mtz-treated wild type animals. **B**. Quantification of mpeg+ cells within the spinal cord was done by counting cells in a four-somite area. A one-way ANOVA revealed an overall difference between means of the different groups ($p = 0.0008$) and individual t tests confirmed that there are significantly more mpeg+ cells in Mtz-treated wild type or heterozygous animals than in Mtz-treated irf8 mutant animals (4.88 ± 4.01 cells in wt/het compared to 0.80 ± 1.79 cells in mutant, $p = 0.0443$). there were significantly more mpeg-expressing cells in Mtz-treated wt/het animals than in DMSO-treated animals of the same genotypes ($p = 0.0003$). There was no significant difference between DMSO-treated wt/het animals and Mtz-treated mutants (1.52 ± 1.31 cells in DMSO-treated wt/het animals, compared to 0.80 ± 1.79 in Mtz-treated mutants, $p = 0.304$). n = 23 for DMSO wt/het, 1 for DMSO mutant, 40 for Mtz wt/het and 5 for Mtz mutants. No statistics involving DMSO-treated mutants could be performed because of the n number of one.

4.4.5. Irf8 -/- mutant larvae are able to remyelinate their axons.

Having established that the irf8 mutation did not affect early oligodendrocyte development, but did significantly reduce the immune presence in the spinal cord following oligodendrocyte ablation, I was satisfied that this was a suitable model for studying the effects of disrupting the immune system on myelin repair.

To investigate the ability of irf8 mutants to remyelinate their axons following demyelination, I again incrossed the Tg(mbp:mCherry-NTR); irf8 +/- fish, treated the resulting progeny with DMSO or Mtz and then kept them in recovery tanks containing normal embryo medium for 16 days. At this time point, I took a fin clip biopsy from each larva for genotyping purposes, and fixed the animals for TEM processing. 16d post-treatment is the time point when I have previously shown normal Tg(mbp:mCherry-NTR) animals to have accomplished full remyelination; I was interested in whether irf8 mutants were able to achieve the same.

Examination of the TEM data strongly suggests that irf8 mutant animals are indeed able to remyelinate their axons: at 16d post-treatment, DMSO-treated siblings and Mtz-treated siblings and mutants all appeared indistinguishable from each other, with robustly myelinated axons populating the spinal cords (**Figure 27A**).

In order to quantify this apparent remyelination, I first counted the total numbers of myelinated axons in the ventral spinal cords (**Figure 27B**), and found them to not differ between the genotypes and treatment conditions: the mean number of myelinated axons was 167.30 ± 31.79 in the ventral spinal cords of DMSO-treated siblings, 157.50 ± 25.83 in Mtz-treated siblings and 133.50 ± 26.35 in Mtz-treated irf8 mutants. A one-way ANOVA found the differences between the groups to be non-significant ($p = 0.211$).

The number of myelinated axons can vary greatly with the overall sizes of the animals. To circumvent this, I compared the percentages of large-calibre axons that was myelinated (as before, the threshold for “large” axon was defined as the perimeter of the smallest myelinated axon found in a DMSO control animal). This comparison, too, yielded non-significant differences: the mean percentage of large-calibre axons that

was myelinated was 78.02 ± 2.80% in DMSO-treated siblings, 80.89 ± 2.52% in Mtz-treated siblings and 76.79 ± 10.15% in Mtz-treated irf8 mutants, p = 0.699 from a one-way ANOVA.

Finally, I also compared the total numbers of large-calibre axons, to detect any possible loss of axons or major differences in growth. The analysis indicated that there were no significant differences between the treatment conditions and genotypes: the mean number of large-calibe axons was 215.30 ± 46.32 in DMSO-treated siblings, 194.30 ± 28.14% in Mtz-treated siblings and 190.0 ± 46.11% in Mtz-treated irf8 mutants, p = 0.690.

Taken together, these analyses suggest that irf8 mutants are not impaired in repairing their myelin sheaths following demyelination.

However, it is essential to note that the total numbers of myelinated axons seen in this experiment (167.30 ± 31.79 in DMSO-treated siblings, 157.50 ± 25.83 in Mtz-treated siblings and 133.50 ± 26 in Mtz-treated mutants) are higher than those I had observed in the experiments in **Chapter 3** (80.88 ± 23.12 in control animals and 85.71 ± 22.01 in Mtz-treated animals), despite the animals being 23dpf in chronological age in both experiments. It is therefore possible that the larvae analysed in this experiment had grown relatively larger in the same period of time as those analysed in **Chapter 3**. Indeed, it is well known that fish can grow at very different rates over time, largely owing to husbandry-related reasons (McMenamin et al. 2016). If this was indeed the case, this cohort of animals may actually have completed their remyelination before the 16d time point. Thus, irf8 mutants may have experienced a delay in remyelination compared to their siblings, but caught up by 16d post-treatment. Therefore, it will be important to repeat this experiment and assess remyelination in irf8 mutants and their siblings at *earlier* time points and, and to normalise for remyelination based the total number of axons as well as chronological age.

In addition, in this dataset I did not check that demyelination was as extensive in irf8 mutant animals as it is in wild-type animals. Indeed, microglia and macrophages are thought to play key roles in instigating demyelination in MS and some animal models (e.g. Prineas et al. 2012; Yamasaki et al. 2014). It is therefore possible that

remyelination succeeded despite a disrupted immune response because the damage to be repaired was not as pronounced as it was in wild-types. This possibility should be addressed in future experiments.

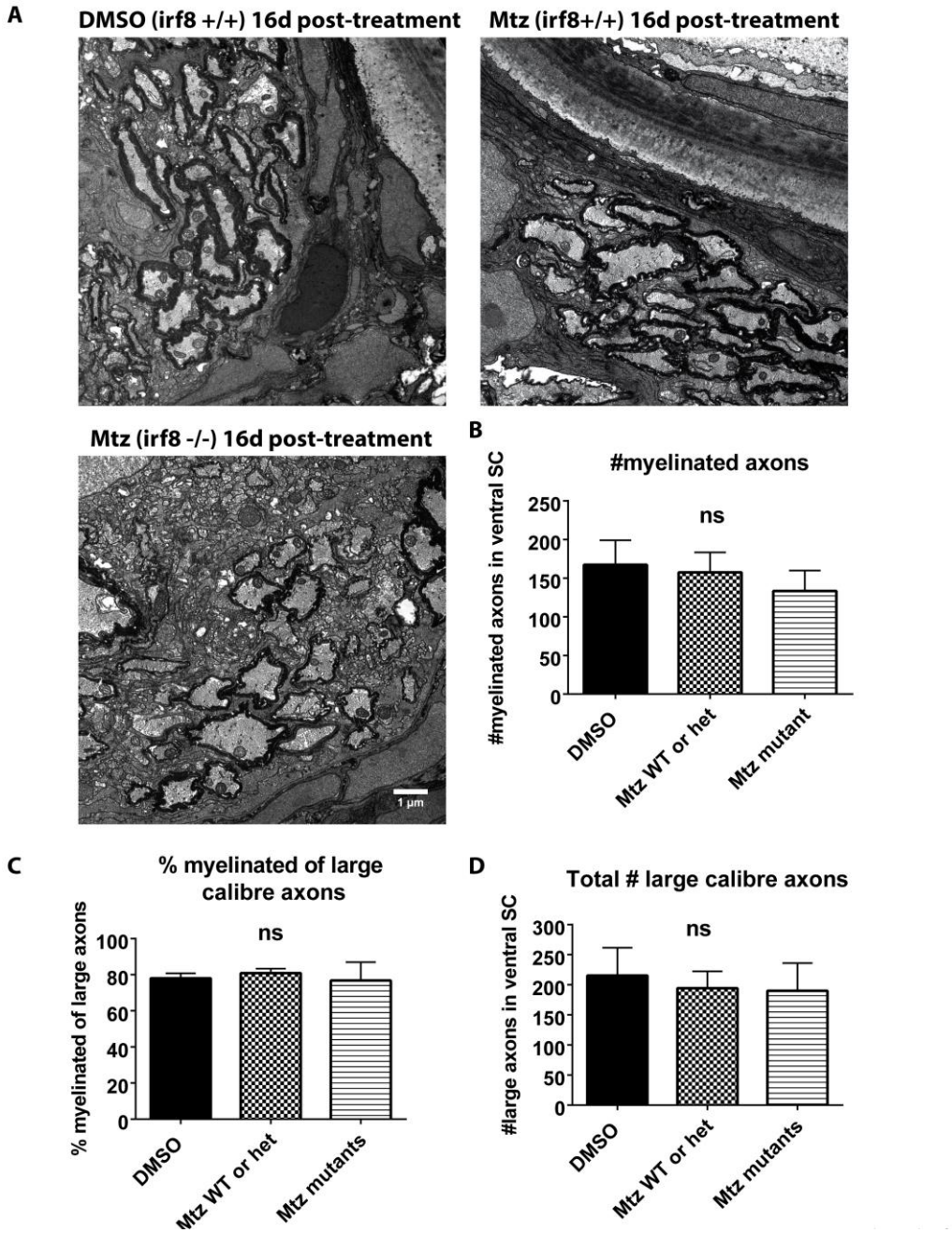

Figure 27. Irf8 mutants have remyelinated their axons by 16d post-treatment. **A**. TEM images of 23dpf larvae, treated with either DMSO or Mtz, and carrying either mutant or heterozygous alleles for irf8, as indicated. All three images show robustly myelinated ventral spinal cords. **B**. Counts of the total numbers of myelinated axons shows that there were no differences between the genotypes and treatment conditions: the mean number of myelinated axons was 167.30 ± 31.79 in DMSO-treated irf8+/+ and irf8 +/- animals, 157.50 ± 25.83 in Mtz-treated irf8+/+ and irf8 +/- animals and 133.50 ± 26.35 in Mtz-treated irf8-/- animals. A one-way ANOVA found the differences between the groups to be non-significant ($p = 0.211$). **C**. The percentages of "myelinateable" sized axons that was myelinated did not differ between the groups either: the mean percentage of was 78.02 ± 2.80% in DMSO-treated irf8+/+ and irf8 +/- animals, 80.89 ± 2.52% in Mtz-treated irf8+/+ and irf8 +/- animals and

76.79 ± 10.15% in Mtz-treated irf8-/- animals, p = 0.699. **D**. Comparison of the numbers of "myelinateable" sized axons found no differences between the groups: the mean number was 215.30 ± 46.32 in DMSO-treated irf8+/+ and irf8 +/- animals, 194.30 ± 28.14% in Mtz-treated irf8+/+ and irf8 +/- animals and 190.0 ± 46.11% in Mtz-treated irf8-/- animals, p = 0.690. n = 3 for DMSO wt/het, 5 for Mtz wt/het and 6 for Mtz mutants.

4.4.6. Irf8 mutants are able to restore their myelin sheaths to normal thickness.

Although the irf8 mutants seem able to remyelinate their axons following demyelination by 16d post-treatment, it was still possible that the disruption to their innate immune system would prevent them from achieving full myelin thickness. In order to test this possibility, I measured g ratios in the different groups.

Comparison of the mean g ratios showed that there was no difference between the three groups: the mean g ratio was 0.79 ± 0.017 in DMSO-treated siblings, 0.77 ± 0.01 in Mtz-treated siblings and 0.79 ± 0.43 in Mtz-treated irf8 mutants, p = 0.730 (**Figure 28B**).

G ratios are commonly expressed by plotting them against the axon diameters, since axons of larger diameters have been shown to have thicker myelin (Blakemore 1973). To check whether irf8 mutants too followed this pattern, I plotted the g ratios I had calculated against the diameters of the axons, and obtained the graph shown in **Figure 28C**. From this, it is very clear that the distributions of g ratios across different axon sizes is indistinguishable between the three groups.

These analyses provide compelling evidence that irf8 mutants are able to carry out full remyelination, exactly as their wild-type and heterozygous siblings are. However, as I mentioned above in the context of the numbers of myelinated axons, it is remains possible that the irf8 mutants are delayed in restoring full myelin thickness, but to determine this will require analysis at earlier stage.

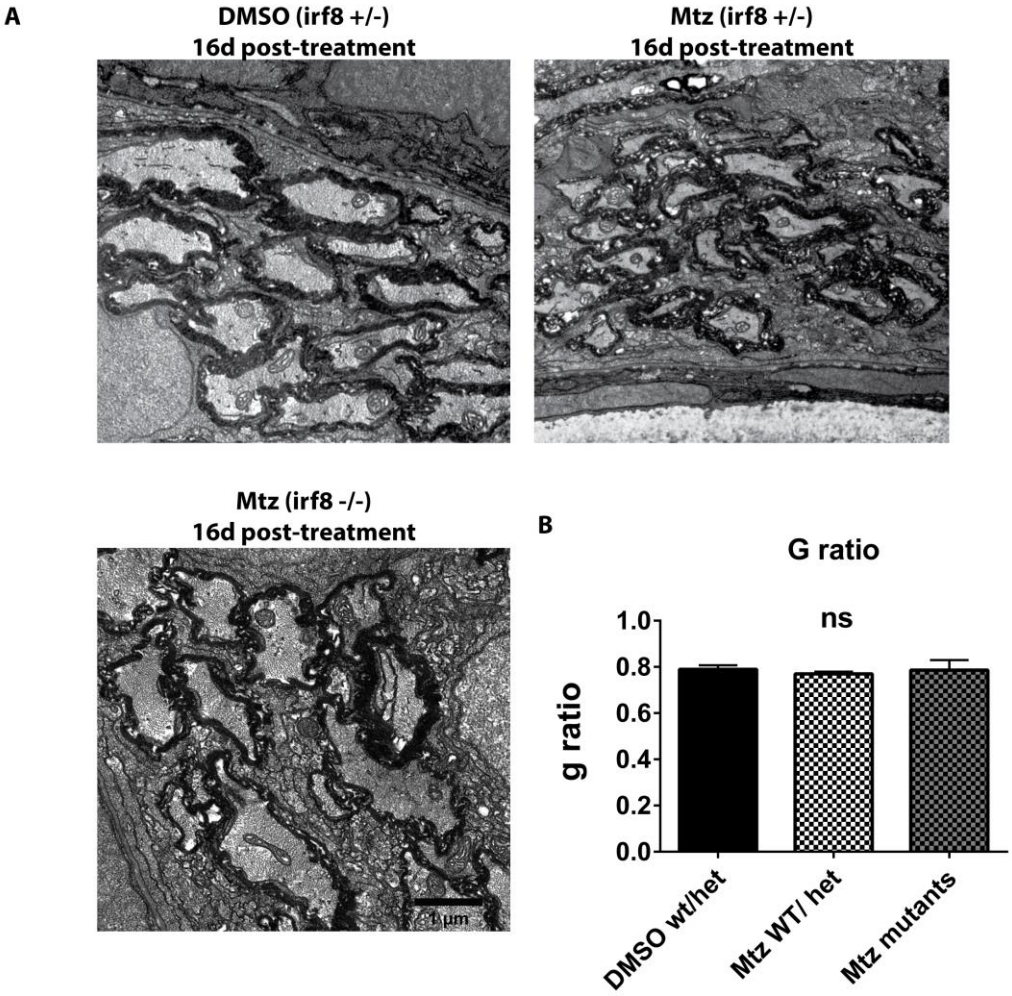
A
DMSO (irf8 +/-)
16d post-treatment
Mtz (irf8 +/-)
16d post-treatment
Mtz (irf8 -/-)
16d post-treatment
1µm
B
G ratio
ns
g ratio
1.0
0.8
0.6
0.4
0.2
0.0
DMSO wt/het
Mtz WT/ het
Mtz mutants
C
G ratios against diameter
g ratio
1.0
0.8
0.6
0.4
0.2
0.0
0.0
0.5
1.0
1.5
2.0
2.5
3.0
3.5
4.0
4.5
5.0
5.5
6.0
Diameter (um)
DMSO wt/het
Mtz WT/het
Mtz mutants

Figure 28. Irf8 mutants are able to restore their myelin to normal thickness. A. TEM images of 23dpf larvae, treated with either DMSO or Mtz, and carrying either mutant or heterozygous alleles for irf8, as indicated. The myelin sheaths in the images appear indistinguishable from each other. **B**. Comparison of the mean g ratios indicates that the mean g ratio was 0.79 ± 0.017 in DMSO-treated irf8+/+ and irf8 +/- animals, 0.77 ± 0.01 in Mtz-treated irf8+/+ and irf8 +/- animals and 0.79 ± 0.43 in Mtz-treated irf8-/- animals. A one-way ANOVA found the difference between the groups non-significant (p = 0.730). **C**. G ratios plotted against axon diameter. This analysis shows that there are no differences in the distribution of myelin thicknesses across different axon sizes between DMSO-treated irf8+/+ or irf8+/- animals, Mtz-treated irf8+/+ or irf8+/- animals or Mtz-treated irf8-/- animals. n = 3 for DMSO wt/het, 5 for Mtz wt/het and 6 for Mtz mutants.

4.4.7. Mtz-treated irf8 mutants are slower at replacing their oligodendrocytes than their Mtz-treated siblings.

Thus, the EM data above indicate that Mtz-treated irf8 mutants are able to remyelinate their axons with normal thickness myelin by 16d post-treatment, but it remains possible that they did this at a slower rate than their non-mutant siblings. In order to test the possibility that Mtz-treated irf8 mutants experience delays during the regeneration process, I assessed oligodendrocyte numbers at 14d post-treatment.

To do this, I incrossed the Tg(mbp:mCherry-NTR); irf8 +/- fish, treated the resulting offpsring with DMSO or Mtz and at 14d post-treatment, took a fin clip biopsy from each larva for genotyping purposes, and fixed the remainder of the larvae's bodies for cryopreservation. I prepared cryosections from these, stained them with Hoechst to label nuclei, and imaged their spinal cords, using the endogenous mCherry expression to label oligodendrocytes.

As before, I imaged four sections per animal, counted the oligodendrocytes on each section and took the mean of these four sections to represent the oligodendrocyte number for that animal. This analysis revealed that Mtz-treated irf8 mutants were behind in generating new oligodendrocytes compared to their wild-type Mtz-treated siblings (**Figure 29**).

Oligodendrocyte counts at 14d post-treatment showed that Mtz-treated irf8 mutants have fewer oligodendrocytes than their Mtz-treated siblings do (a mean of 7.27 ± 2.23 oligodendrocytes per section in siblings, compared to 4.39 ± 1.82 in Mtz-treated mutants, $p = 0.0165$). The Mtz-treated siblings, in turn, had significantly fewer oligodendrocytes than DMSO-treated siblings (which had a mean of 9.69 ± 2.19 oligodendrocytes, $p = 0.0378$) and DMSO-treated mutants (which had a mean of 10.33 ± 1.16 oligodendrocytes, $p = 0.0436$).

These data suggest that during the period of remyelination, the Mtz-treated irf8 mutants lag behind their Mtz-treated siblings in replacing their ablated oligodendrocytes.

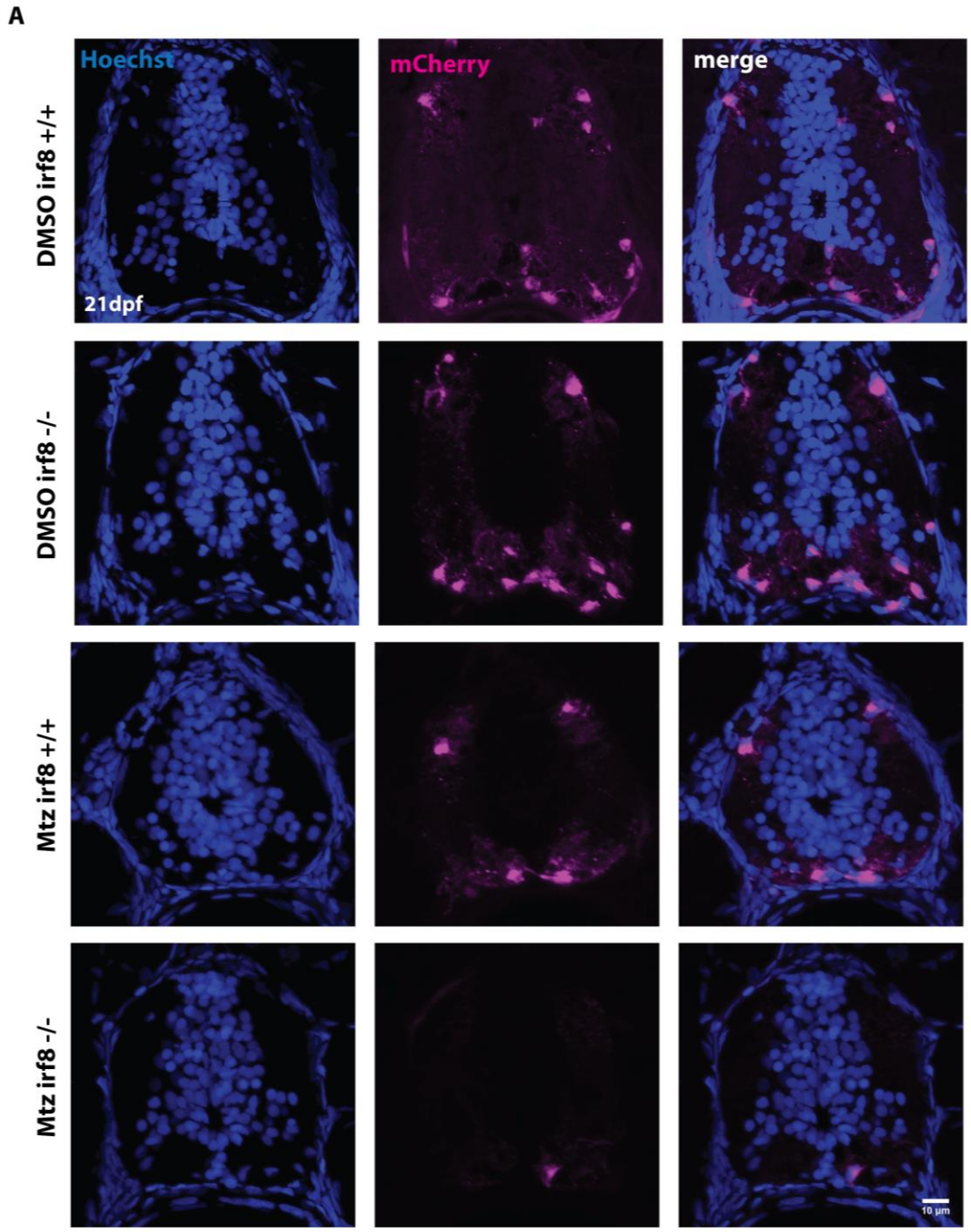

Quantification overleaf

B

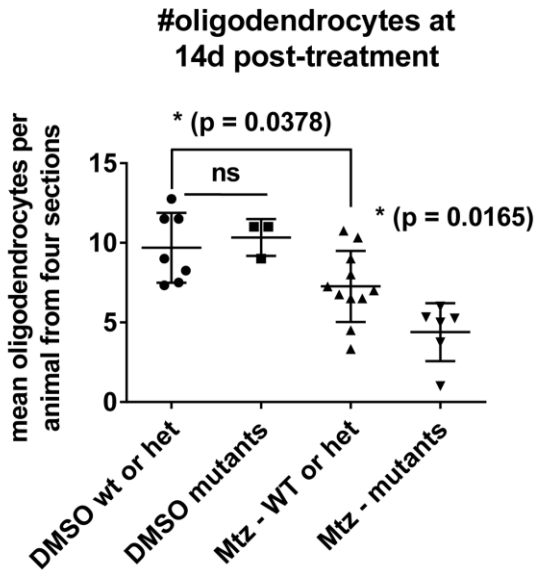

Figure 29. At 14d post-treatment, Mtz-treated irf8 mutants have fewer oligodendrocytes than Mtz-treated non-mutants. **A**. Confocal images of cryosections from 21dpf Tg(mbp:mCherry-NTR) larvae, wild-type, heterozygous or mutant for the irf8 gene, and treated with DMSO or Mtz as indicated. **B**. Oligodendrocyte counts indicate that there are fewer oligodendrocytes in Mtz-treated mutants than in Mtz-treated siblings: 7.27 ± 2.23 in siblings, compared to 4.39 ± 1.82 in Mtz-treated mutants, p = 0.0165. There are no differences between DMSO-treated irf8 mutants and siblings (a mean of 9.69 ± 2.19 oligodendrocytes in DMSO-treated siblings and 10.33 ± 1.16 in DMSO-treated mutants, p = 0.651.) There are more oligodendrocytes in DMSO-treated siblings than Mtz-treated siblings: 9.69 ± 2.19 compared to 7.27 ± 2.23 in Mtz-treated non-mutants, p = 0.0378. n = 7 for DMSO-treated non-mutants, 3 for DMSO-treated mutants, 11 for Mtz-treated non-mutants, and 6 for Mtz-treated mutants.

4.4.8. Oligodendrocyte numbers at 16d post-treatment

The finding that Mtz-treated irf8 mutant animals have fewer oligodendrocytes than their wild-type siblings at 14d post-treatment prompted me to ask whether this delay persisted to the full remyelination stage at 16d post-treatment.

To address this, I quantified the numbers of oligodendrocytes at 16d post-treatment. The dataset produced by the first two experiments is the same as I have presented in **Figure 14** (where, of course, I only included the wild-type animals). Thus, the data showed that oligodendrocyte numbers in Mtz-treated siblings do not differ from those

in DMSO-treated siblings (8.57 ± 2.58 oligodendrocytes in Mtz-treated, compared to 9.46 ± 2.21 oligodendrocytes in DMSO-treated, p = 0.103). The oligodendrocyte numbers were also not different between Mtz-treated siblings and Mtz-treated mutants (mean number of oligodendrocytes in Mtz-treated mutants was 8.17 ± 3.06, p = 0.835; **Figure 30**).

Thus, it appears that, despite showing a delay in oligodendrocyte regeneration at 14d post-treatment, irf8 mutants do catch up with their siblings by 16d post-treatment. It is important to note, however, that despite carrying out the experiment on three separate occasions, I was only able to find two irf8 null individuals among the Mtz-treated animals. This low n number means that further repetitions of the experiment are required before firm conclusions can be drawn.

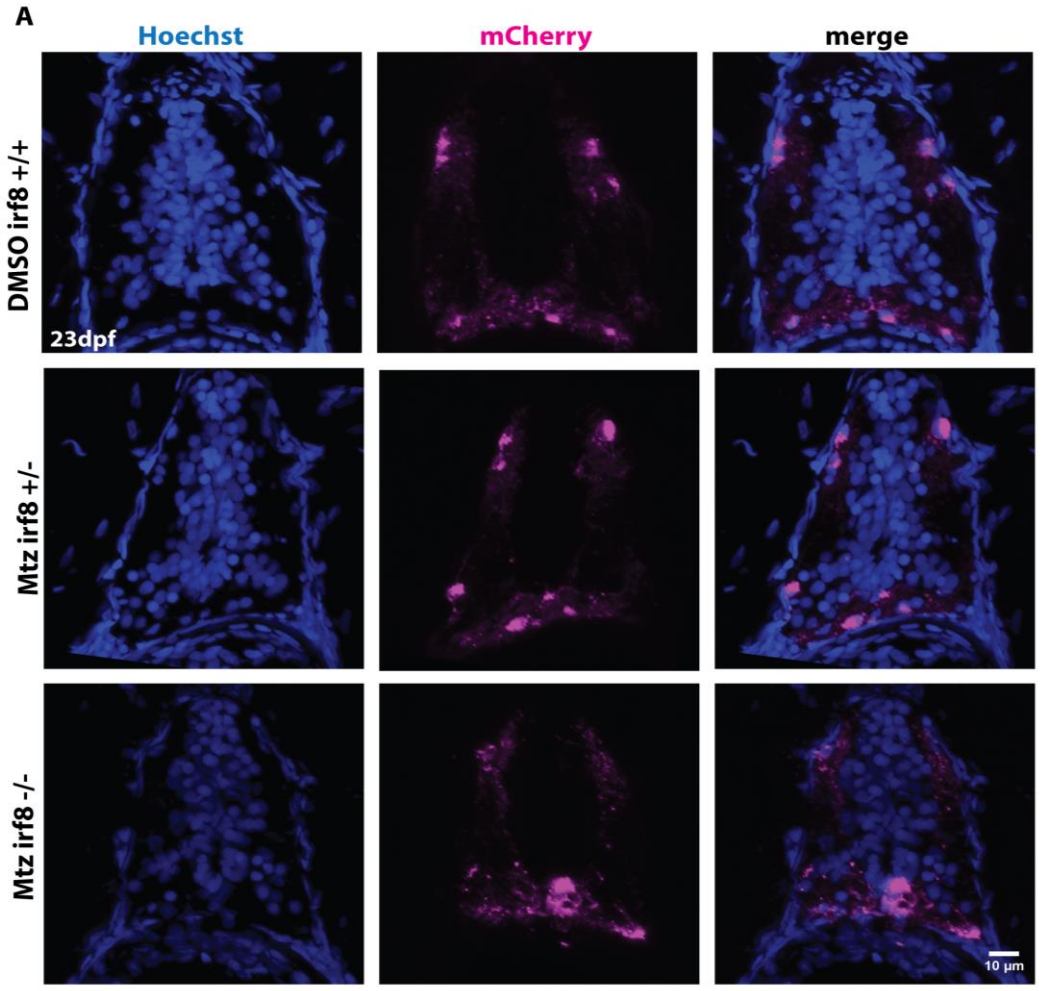

Quantification overleaf

B

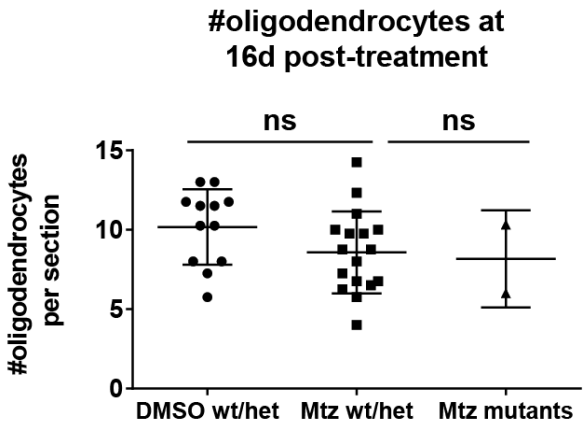

Figure 30. Oligodendrocyte numbers at 16d post-treatment in irf8 mutants and siblings. **A**. Confocal images of cryosections from 23dpf Tg(mbp:mCherry-NTR) larvae, wild-type, heterozygous or mutant for the irf8 gene, and treated with DMSO or Mtz as indicated. **B**. Counts of oligodendrocyte numbers from cryosections show that the numbers of oligodendrocytes do not differ between Mtz-treated siblings compared to DMSO-treated siblings (mean number oligodendrocytes from four sections is 10.17 ± 2.38 in DMSO-treated animals and 8.58 ± 2.58 in Mtz-treated animals, $p = 0.103$ from a t test). There is also no difference between the numbers of oligodendrocytes in Mtz-treated siblings compared to Mtz-treated mutants (mean number of oligodendrocytes in mutants is 8.17 ± 3.06, $p = 0.835$). n = 12 for DMSO wt/het animals, 17 for Mtz wt/het animals and 2 for Mtz mutants.

Thus, my analysis of remyelination and oligodendrocyte regeneration in irf8 mutant zebrafish suggests that overall, the mutants are able to achieve similar levels of remyelination and oligodendrocyte regeneration as their non-mutant siblings do by 16d post-treatment.

However, importantly, there appears to be a delay in oligodendrocyte number regeneration, and it remains possible that remyelination, too proceeds slower in the mutant animals. It is also worth keeping in mind that the initial demyelination may not have reached the same extent in mutants as it does in wild-types.

4.5. Discussion

In this chapter, I have described how the presence microglia and macrophages increases drastically in the spinal cord following oligodendrocyte ablation, peaking at 4d post-treatment and diminishing by 9d post-treatment. I provided evidence that these cells phagocytose myelin debris and as such, potentially play a role in disposing of the cellular vacuoles generated by the oligodendrocyte ablation.

Since the Tg(mpeg:GFP) transgenic line I used to track the presence of immune cells in the spinal cord labels both microglia and macrophages, it was not possible to distinguish between the two cell types in this system. However, recent evidence is converging to show that there are multiple important distinctions between microglia and macrophages, from distinctive transcriptomes (Hickman et al. 2013) to a number of recently discovered cell surface markers specific to microglia (Butovsky et al. 2014; Bennett et al. 2016). Moreover, depending on the model of demyelination used and other experimental parameters, specific depletions of microglia and macrophages have distinct roles in both demyelination and remyelination (Yamasaki et al. 2014; Lampron et al. 2015). With this in mind, it would be highly interesting to explore the nature of the immune presence in the Tg(mbp:mCherry-NTR) model further, for example by immunostaining larvae with the microglia-specific antibody 4C4 at different time points, to see whether their abundance relative to monocyte-derived macrophages fluctuates over time.

In an attempt to further understand the functional role of the increase in microglia and macrophages I observed, I used irf8 null animals to investigate what would happen to oligodendrocyte and myelin regeneration if the microglia and macrophage response were impaired. However, despite having very few microglia or macrophages present in the spinal cord during the peak immune presence stage, the irf8 mutants ultimately did not seem impaired at remyelinating their axons, achieving normal thickness by 16d post-treatment, exactly as their siblings do. The irf8 mutants do seem, however, to lag behind their siblings in regenerating their oligodendrocytes, at least at 14d post-treatment.

4.5.1. Irf8 mutants may have a delay in remyelination

It seems clear from the above summary that a discrepancy exists between the very prominent increase microglia and macrophages in the spinal cord following oligodendrocyte ablation, and the fact that prevention of this wave has ultimately so little effect on remyelination (although it does seem to cause a brief delay in regeneration of oligodendrocytes). Thus, it is pertinent to consider what might account for the eventual success of remyelination in the irf8 mutants.

First of all, as I mentioned in **Section 4.4.5**, the numbers of myelinated axons and all large-calibre axons were very high in this experiment, in fact almost double those seen in the remyelination experiment described in **Chapter 3**. This strongly suggests that the larvae in the irf8 experiment had grown rapidly during the same chronological time, and at 16d post-treatment were far ahead of the larvae in the first remyelination experiment, in terms of their developmental stage. This striking difference in growth rates between experiments is likely due to variations in the feeding regimen and other environmental parameters; it is well documented that zebrafish growth at the postembryonic stages is highly sensitive to environmental conditions (McMenamin et al. 2016).

With this in mind, it could be that 16d post-treatment was too late a time point to identify a significant delay in remyelination in the irf8 experiment, as it is possible that the wild-type Mtz-treated larvae had completed their remyelination earlier than 16d post-treatment. Thus, there might have been a delay in remyelination in irf8 mutants that I did not capture, because I assessed remyelination at a stage when irf8 mutants had caught up with their wild-type siblings. To test this, it will be important to assess remyelination in irf8 mutants and their siblings at several earlier time points, to determine whether this is the case, and if so, how substantial the delay is. In analysing the results of these experiments, I will need to normalise the number and percentage of myelinated axons against the total number of nuclei in the spinal cord as a proxy for the overall size of the animal. Previous investigators have also noted the importance of considering the growth of the animal, rather than chronological time, for post-embryonic staging in order to mitigate against the effects of variability (McMenamin

et al. 2016). It is important to emphasise that, as far as possible, in my experiments to date I did normalise for animal size by selecting animals of similar sizes for analysis.

The idea that comparing oligodendrocyte and myelin regeneration in irf8 mutants and their siblings at earlier time points may reveal a delay in regeneration is supported by the finding that at 14d post-treatment, Mtz-treated irf8 mutants have significantly fewer oligodendrocytes than their siblings (**Figure 29**).

It is important to note that even if further analyses do unearth a deficit in myelin regeneration in irf8 mutants at earlier stages, it can only be a delay, as the mutants achieve complete remyelination by the 16d post-treatment period analysed in this chapter. However, many factors found to inhibit remyelination cause a delay in remyelination rather than completely blocking it; for example, aged mice are much slower than young at remyelinating but eventually achieve the same extent (Shields et al. 1999) and high-dose corticosteroids, which modulate the activity of the immune system in a variety of ways, were shown to result in impaired remyelination at one month post-treatment, but by two months post-treatment, the corticosteroid-treated animals had reached the level of remyelination seen in control mice (Chari et al. 2006). With this in mind, the delay I observed in oligodendrocyte regeneration at 14d post-treatment strongly suggests that microglia and macrophages play an important role in oligodendrocyte regeneration in the Tg(mbp:mCherry-NTR) model.

However, even if the Mtz-treated irf8 mutants are slower at remyelinating than their siblings, it is still pertinent to consider what accounts for their ultimate success at remyelinating, despite ostensibily having a severely compromised population of microglia and macrophages.

4.5.2. How are irf8 mutants able to achieve full remyelination?

The simplest explanation for the ability of irf8 mutant larvae to remyelinate their axons is that, even though there were very few mpeg+ cells in the spinal cords of irf8 mutants at 4d post-treatment, the mutants might have been able to generate a larger population of macrophages during the intervening 12 days before the full remyelination stage at

16d post-treatment. Shiau et al. (2015) note that by 31dpf, irf8 mutants have approximately half as many mpeg+ cells as their wild-type and heterozygous siblings, owing to the definitive wave of hematopoiesis not requiring irf8 function. Interestingly, these cells are all monocyte-derived macrophages, since Shiau et al. show by a continued absence of apoe signal that the mutants do not develop microglia at any point. Perhaps this smaller population of macrophages is already present before 23dpf (the age of the animals at 16d post-treatment) and is able to cover enough of the responsibilities of the full population to allow remyelination to proceed. It would therefore be imperative to assess the numbers of macrophages at 16d post-treatment to see whether they had increased from 4d post-treatment. If they have, they could provide a simple explanation for the lack of remyelination failure.

Notably, Shiau et al. (2015) report a prominent expansion of the neutrophil population in irf8 null animals. This phenomenon had been reported previously; Li et al. (2011) found that levels of irf8 expression govern the balance between macrophage and neutrophil production in zebrafish. Neutrophils are the major pathogen-fighting cells of the innate immune system, and as such, naturally phagocytotic (Mayadas et al. 2014). They are also routinely recruited in the absence of inflammation (Keightley et al. 2014), but have previously been shown not to contribute to the phagocytosis of neuronal debris in zebrafish (van Ham et al. 2014). However, since in the absence of macrophages neutrophils are upregulated, it may be that under such circumstances, they proceed to take over the phagocytosing role of microglia and macrophages, and as such, pave the way to remyelination exactly as they would. In order to test this possibility, one could use the transgenic line Tg(mpx:GFP) (Renshaw et al. 2007) in which neutrophils are fluorescently labelled, and image the behaviour of neutrophils over the course of de- and remyelination in irf8 mutants and their siblings. If in irf8 mutants, neutrophils show a more pronounced presence in the spinal cord following oligodendrocyte ablation than their non-mutant siblings do, this would constitute evidence that neutrophils are carrying out the work of microglia and macrophages in their absence.

In this context, it is important to note that in previous work reporting impaired remyelination following macrophage depletion, the clodronate liposomes used to

deplete macrophages may also have affected neutrophils (Lee et al. 2011). Thus, it is possible that only by inhibiting both macrophages and neutrophils can debris clearance and subsequent remyelination be severely inhibited.

In this chapter, I have chiefly considered the microglia and macrophages absent from irf8 mutants as little more than biological "hoovers" whose only contribution to remyelination is to clear up the oligodendrocyte and myelin debris. However, in the Tg(mbp:mCherry-NTR) model, demyelinated axons are still prevalent at 11d post-treatment, that is, two days after the microglia/macrophage presence in the spinal cord has returned to control levels and the majority of the vacuoles have been removed. This suggests that remyelination does not proceed immediately following the departure of the vacuoles, and thus implies that more factors are involved in remyelination than merely removing the physical barrier of myelin debris. Indeed, it is well established that microglia and macrophages also play a more directly pro-regenerative role in response to demyelination. They are known to secrete cytokines and other factors essential for the inducing OPCs to differentiate and begin remyelination (Yuen et al. 2013; Miron et al. 2013). A compromised ability to mount this response, such as is the case in aged animals, is strongly associated with much diminished capacity for remyelination (Natrajan et al. 2015; Sim et al. 2002; Hinks and Franklin 2000).

The importance of the pro-regenerative signals from microglia and macrophages in oligodendrocyte differentiation is consistent with finding that oligodendrocyte number regeneration is delayed in irf8 mutants, where such signals would presumably be missing or present in much smaller amounts. However, irf8 mutants do eventually succeed at remyelinating their axons, which naturally raises the question of whether some pro-regenerative signals are present in these animals and if so, where they come from.

This consideration again raises the possibility that sufficient numbers of macrophages are generated as part of the second wave of hematopoiesis to enable remyelination. These new macrophages, not yet present at 4d post-treatment, could then secrete sufficient cytokines to stimulate differentiation of a sufficient number of

oligodendrocyte progenitor cells to carry out the task of remyelinating the denuded axons. As I have discussed elsewhere in this thesis, full remyelination does not appear to require a "full" set of oligodendrocytes, raising the possibility that a smaller number of oligodendrocytes can produce similar quantities of myelin as a larger population, if each individual oligodendrocyte makes more myelin per cell. In the same vein, it could be that a smaller population of macrophages may be able to secrete sufficient quantities of pro-regenerative signals to initialise the cascade of events which culminates in the successful remyelination observed in the irf8 mutants. However, the presumed smaller scale of this cascade in mutants compared to their siblings could be reflected in the observed delay in oligodendrocyte regeneration at 14d post-treatment, as well as in the potential delay in remyelination, as I have discussed above.

In addition, the possibility that some pro-regenerative signals are secreted by neutrophils should not be discounted. Accumulating evidence suggests that neutrophils, although not as extensively studied for their role in regeneration as macrophages have been, can indeed be instrumental for regeneration in some systems. For instance, Kurimoto et al. (2013) showed that antibody-mediated depletion of neutrophils resulted in strongly impaired axon regeneration following optic nerve crush in mouse. Furthermore, neutrophils are known to communicate closely with macrophages and direct them towards the pro-regenerative M2 polarization (Fadok et al. 1998). Thus, perhaps with the help of neutrophils, even a diminished population of macrophages can produce enough pro-regenerative signals to ultimately effect remyelination, even if it may be slightly delayed.

4.5.3. Oligodendrocytes may become vacuolated prior to dying

An interesting observation in this chapter is that oligodendrocytes continue to undergo cell death for several days after removal of the Mtz-treatment (**Figure 24**) and several days after the disappearance of recognisable oligodendrocytes. Indeed, the number of acridine orange positive apoptotic oligodendrocytes increases until 4d post-treatment, and decreases gradually from this point. This apparent increase in dying

oligodendrocytes seems to be at odds with the finding in **Chapter 3** that the number of viable oligodendrocytes remains relatively stable for the first seven days following metronidazole withdrawal; one might have expected the number of viable oligodendrocytes to show a corresponding dip at the point of peak oligodendrocyte cell death.

While it is difficult to know for certain why there is a disconnect between the number of viable cells and the number of dying cells, I would propose that many of the oligodendrocytes that are no longer detectable as viable oligodendrocytes at 0d post-treatment, do not immediately proceed to cell death, but first swell in size and in fact reflect appearance of vacuoles. Cellular swelling is a known feature of necrotic and necroptotic cell death (Degterev et al. 2008) which have been associated with oligodendrocyte death in EAE, cuprizone intoxication and even MS lesions (Ofengeim et al. 2015). These swollen oligodendrocytes may not yet have fragmenting DNA and thus would not be labelled by acridine orange. One imagines that over time, the swollen oligodendrocytes either deflate or begin to disintegrate, at which point they enter a cell death process and become detectible by acridine orange.

Moreover, the prediction that oligodendrocytes swell prior to entering a cell death programme may also help to account for the delay between observed loss of oligodendrocytes at 0d post-treatment and the increase in microglia and macrophage numbers in the spinal cord seen days after end of treatment. For example, it is conceivable that while the oligodendrocytes are swollen but not yet fragmenting, they do not express the "eat-me" signals on their surface which would attract microglia and macrophages to them. These signals may appear as the oligodendrocytes deflate or disintegrate, and thus elicit the strong response from microglia and macrophages that is observed in this model.

Of course, it must be emphasised that all of the above requires experimental investigation before it can be considered an explanation for how cell death occurs in this model. One way to assess this theory would be to time-lapse image individual oligodendrocytes continuously and determine whether their cell bodies swell and take on the appearance of vacuoles. In addition, immunostaining for common "eat-me"

signals such as the phospholipid phosphatidylserine at different time points may be informative to better understand the sequence of events.

4.5.4. Future/ongoing experiments

The main purpose of this chapter was to describe the response of microglia and macrophages to oligodendrocyte ablation in the Tg(mbp:mCherry-NTR) model and to assess what happens to oligodendrocyte regeneration and remyelination in irf8 mutants, in which this response is disrupted due to inhibited development of microglia and macrophages. The latter investigation suggested, unexpectedly, that the irf8 mutants are able to carry out full remyelination despite having very few macrophages and microglia (at least at the supposed peak immune presence stage at 4d post-treatment). The mutants are, however, delayed at regenerating their oligodendrocytes at 14d post-treatment. In order to better understand the nature of the impairment in the irf8 mutants, further examination of the immune response and remyelination in these mutants is warranted.

The first, and likely the most informative, of these will be to carry out EM analyses of irf8 mutants and their siblings at multiple earlier stages during remyelination, such as 9d, 11d and 13d post-treatment. These experiments will determine precisely if and when Mtz-treated irf8 mutants experience a delay in their oligodendrocyte regeneration and remyelination, compared to their siblings. In addition, it will be important to further assess oligodendrocyte numbers at 16d post-treatment to see whether the delay in oligodendrocyte regeneration observed at 14d post-treatment persists to the point of full remyelination. This would imply that irf8 mutants are able to perform full remyelination with an smaller population of oligodendrocytes than the wild-type Mtz-treated larvae (which, as I showed in **Chapter 3**, succeed in restoring their oligodendrocyte numbers to control levels).

Regardless of whether the analysis of irf8 mutants at earlier stages reveals a delay in remyelination or not, it will be highly interesting to investigate the numbers of macrophages at 16d post-treatment to see whether these have increased substantially from 4d post-treatment. If they have, it would certainly go some way in explaining the finding that irf8 mutants achieve remyelination by 16d post-treatment, even if they

show a delay in oligodendrocyte regeneration. In parallel, it will also be highly interesting to investigate the numbers of neutrophils in irf8 mutants. It is possible that in the relative absence of microglia and macrophages, neutrophils enter the spinal cord and carry out phagocytosis and potentially even secretion of pro-regenerative signals. If this were to be experimentally demonstrated, it would constitute fascinating evidence of the plasticity of the immune response. Furthermore, it will also be interesting to see whether neutrophil numbers decrease if and when the later population of macrophages arises.

It would also be important to develop a reliable method of quantifying vacuoles, and relate their extent to the immune response in both wild-type and irf8 mutant animals. If it could be formally demonstrated that the vacuoles decline after the time of peak immune presence in the spinal cord in wild type larvae, but remain in the spinal cord for longer in irf8 mutants, that would constitute persuasive evidence that the microglia and macrophages do indeed act to remove the vacuoles.

Finally, it would also be interesting to carry out gain of function experiments, and enhance the microglia and macrophage response, and subsequently assess the effects on remyelination. For example, if the inflammagen zymosan was injected into Mtz-treated Tg(mbp:mCherry-NTR) larvae at the point of Mtz withdrawal, would the increase in microglia and macrophages peak at 0d instead of 4d post-treatment, and might we then see complete remyelination already at 7d or 9d post-treatment? Such experiments may help define the sequence of events in oligodendrocyte ablation, demyelination, immune attack and remyelination. Alternatively, genetic overexpression of irf8 has previously been shown to lead to increased production of macrophages at the expense of neutrophil numbers (Li et al. 2011). It would be interesting to cross such irf8 fish to Tg(mbp:mCherry-NTR) fish and assess remyelination, to see whether neutrophils play any role in oligodendrocyte regeneration and remyelination.

Thus, the data presented in this chapter have raised as many questions as they have answered, and much remains to be done to understand the nature of the immune response following oligodendrocyte ablation in the Tg(mbp:mCherry-NTR) model.

Chapter 5:

Schwann cell ablation, demyelination and remyelination in the peripheral nervous system

5.1. Introduction

Numerous studies have shown that Schwann cells play key roles in maintaining the health and integrity of peripheral axons (Nave and Trapp 2008; Nave and Salzer 2006). Indeed, disruption to myelin in the peripheral nervous system (PNS) is involved in a number of human diseases. However, as I will discuss below, most currently available models of PNS demyelination are either specific models of genetically inherited peripheral neuropathies, or involve demyelination only as a secondary consequence of general injury to the nerve. In this chapter, I investigate the consequences of primary death of myelinating Schwann cells, which are also ablated in the Tg(mbp:mCherry-NTR) transgenic fish. The availability of a primary Schwann cell ablation model allows interesting questions to be addressed, including how myelin regeneration in the PNS compares to that in the CNS, the effects of Schwann cell loss on peripheral axons, the ability of the larvae to generate new Schwann cells to replace lost myelin, and the response of the innate immune system to primary Schwann cell death. I will mainly focus on an ultrastructural characterisation of the loss and regeneration of myelin in the peripheral nerve, and the effect these have on the peripheral axons, but I will also briefly consider the response of the innate immune system to Schwann cell loss.

5.1.1. Schwann cells have a different lineage origin and regulators from oligodendrocytes.

First, however, it is pertinent to mention some key aspects of Schwann cell biology and highlight the similarities and differences between Schwann cells and oligodendrocytes.

Schwann cells arise from the neural crest and migrate alongside axons as they elongate towards their targets (Jessen and Mirsky 2005). Once nerve outgrowth is complete, a process called radial sorting occurs, whereby immature Schwann cells choose individual large-calibre axons from large bundles, differentiate to pro-myelinating and then myelinating Schwann cells, and proceed to myelinate one segment of their chosen axon (Raphael et al. 2011). Thus, in contrast to oligodendrocytes, which can ensheath dozens of axons, each Schwann cell only myelinates one axon. Those Schwann cells

that do not associate with large-calibre axons remain ensheathing bundles of small-calibre axons, and are known as non-myelinating Schwann cells, or Remak cells. These cells serve a number of interesting functions (Jessen and Mirsky 2005; Nave and Salzer 2006), but will not be discussed further here. The Schwann cell lineage progression is illustrated in the figure below, taken from (Jessen and Mirsky 2005).

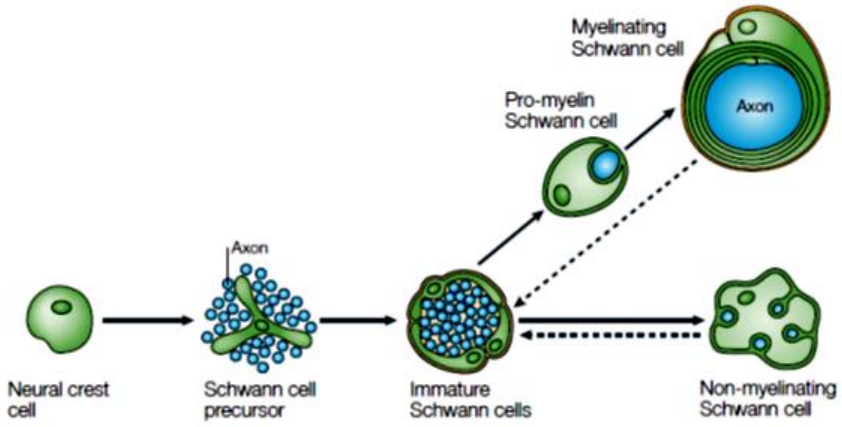

Figure 31. Schwann cell lineage development

A plethora of studies has elucidated many of the molecular signals that control the various stages of Schwann cell development and myelination, and these have been extensively reviewed elsewhere (Jessen and Mirsky 2005; Raphael and Talbot 2011; Glenn and Talbot 2013). The most extensively studied regulator of multiple stages of Schwann cell lineage progression is axonal neuregulin 1 (Nrg1) signalling through ErbB receptors on Schwann cells; as Schwann cells remain in close contact with axons throughout their specification, proliferation, directed migration, radial sorting and myelination, Nrg1 signalling controls virtually all these aspects of Schwann cell development (Nave and Salzer 2006; Newbern and Birchmeier 2010).

It is notable that the majority of the molecules involved in regulating Schwann cell development differ from those involved in oligodendrocyte development. A prime example of this is Nrg1: while disruption to Nrg1 signalling has been shown to result in peripheral nerves essentially devoid of Schwann cells and myelin in both rodents

and zebrafish (Riethmacher et al. 1997; Morris et al. 1999; Woldeyesus et al. 1999; Britsch et al. 1998; Lyons et al. 2005), its role in CNS myelination is less absolute. Brinkmann et al. (2008) generated multiple conditional Nrg1 and ErbB knockout mice but failed to detect any defects in oligodendrocyte differentiation or myelination in the brain, suggesting that Nrg1-ErbB signalling may be largely dispensable in the CNS. Subsequent work has raised the possibility that Nrg1-ErbB signalling can play a modulatory role in CNS myelination, such as mediating experience-dependent plasticity of myelination (Makinodan et al. 2012) or contributing to activity-dependent regulation of myelination (Lundgaard et al. 2013). Nevertheless, it is clear that this, and indeed other, crucial regulator(s) of Schwann cell development and myelination have very different roles in oligodendrocyte development and myelination.

5.1.2. Schwann cells are vital for axon health and development

Despite their differences in origin and molecular control, both Schwann cells and oligodendrocytes serve essential functions in the development and maintenance of their respective nervous systems. Indeed, much as oligodendrocytes provide axons with nutrients in the CNS (Fünfschilling et al. 2012; Lee et al. 2012), so too do Schwann cells provide peripheral axons with metabolic support. For example, (Beirowski et al. 2014) explored the role of the serine-threonine kinase LKB1 and its prime downstream target AMPK in mediating this support. They when they knocked LKB1 out specifically in Schwann cells, the mice displayed many symptoms of peripheral neuropathy, including an unsteady gait and hindlimb clasping. A closer inspection of the sciatic and femoral nerves of the knockout mice revealed widespread swellings and fragmentation of the axons. The authors suggest that LKB1 is an important regulator of major metabolic pathways in Schwann cells, and that Schwann cell metabolism is critical in supporting the integrity of peripheral nerve axons. This naturally raises the question of how peripheral axons might fare if they were to lose this support from Schwann cells; a question that I will address in this chapter.

Interestingly, Voas et al. (2009) showed that in ErbB2 and ErbB3 mutant zebrafish, which do not have any myelinating Schwann cells, the peripheral nerve contains a reduced number of axons, compared to their wild-type siblings. Moreover, in these mutants, the distribution of axon sizes in the peripheral nerve is more homogenous than in wild-type embryos, with fewer large-calibre and fewer very small axons (D. Lyons, pers. comm.). It is currently not clear whether these observations stem from disruptions to axon development or maintenance: it is possible that in the absence of Schwann cells, fewer axons grow in the peripheral nerve in the first place, or that the axons that do elongate fail to grow radially to the sizes seen in wild-types. Equally, it is also possible that axons develop normally, but in the absence of support from Schwann cells, axons may be lost, or large axons may shrink, or very small axons may swell, resulting in the observed "reverting to mean" phenomenon (D. Lyons, pers. comm.).

Nevertheless, these data highlight that Schwann cells are important in aspects of axon development and/or maintenance. One way to better understand the role of Schwann cells in axon maintenance would be to allow axons to develop normally in the company of Schwann cells, but subsequently ablate Schwann cells and examine the consequences on the axon's survival, size, mitochondrial content, and other parameters. Thus far, the tools to perform such experiments have not been available, but the Tg(mbp:mCherry-NTR) fish provides an excellent system in which to carry them out.

5.1.3 Neuropathies are diseases of the PNS

More evidence for the importance of Schwann cells in maintaining peripheral axon health comes from the fact that Schwann cell abnormalities are associated with severe diseases. Inherited neuropathies are largely caused by mutations in either Schwann cell or neuronal genes; in axonal neuropathies, axons are primarily affected, whereas in demyelinating neuropathies, the abnormalities are primarily found in Schwann cells (Suter and Scherer 2003).

Inherited neuropathies which do not occur as a part of a syndrome are referred to as Charcot-Marie-Tooth disease (CMT). CMT can be divided into two main categories based on conduction velocities in the forearm motor nerve: those patients in whom conduction velocity exceeds 38 m/s are classified as suffering from an axonal neuropathy (CMT2) whereas those in whom conduction velocity is less than 38 m/s are considered to have a demyelinating neuropathy (CMT1; Harding and Thomas 1980). Of these, CMT2 is more prevalent, and has an earlier age of onset than CMT1.

Both types of CMT are characterized by muscle atrophy and limb weakness, and various degrees of motor and sensory deficits, depending on the subtype and the particular mutation that caused the disease. Pathologically, CMT2 is associated with axonal degeneration and CMT1 with segmental demyelination and remyelination, evident in "onion bulbs", which are concentric "piles" of supernumerary Schwann cells around an incompletely remyelinated axon, thought to indicate repeated cycles of demyelination and remyelination (Suter and Scherer 2003). Despite the distinction between the two subtypes however, the phenotypes sometimes overlap, and secondary axon degeneration is observed in CMT1 (Krajewski et al. 2000).

The genetic causes of CMT are extremely heterogenous: over 900 mutations in 60 genes have been associated with the disease thus far (Bouhy and Timmerman 2013). For instance, a duplication of one allele of the peripheral myelin protein 22 gene causes a specific subtype known as CMT1A, whereas various missense mutations on the same gene cause more severe variants of the disease, evident from early infancy or even birth (Suter and Scherer 2003).

Research on CMT has centred on identifying the disease-causing mutations in human patients and creating transgenic mice bearing the identified mutations, so that disease mechanisms can be studied and potential treatments tested (Scherer and Wrabetz 2008). For example, in the case of the CMT1A subtype, it is known to be caused by overexpression of PMP22, and thus reduction of this expression is a high therapeutic priority. Two candidates, antiprogestin and ascorbic acid have been identified, and both can reduce levels PMP22 mRNA in the nerves and improve motor function in a PMP22-overexpressing rat (Sereda et al. 2003; Passage et al. 2004). Ascorbic acid

(vitamin C) was even taken to clinical trials as a treatment for CMT1A, but this failed to find a significant beneficial effect (Pareyson et al. 2011). Other mutations cause toxic gains of function and activate the unfolded protein response, prompting researchers to look for ways to interrupt this response (Khajavi et al. 2007; Pennuto et al. 2008). For demyelinating neuropathies caused by loss-of-function mutations in Schwann cells, very few therapeutic strategies exist at present but methods of restoring function to the missing gene are under investigation (Scherer and Wrabetz 2008).

Thus, despite the demyelinating phenotype of many CMT variants, the research to find ways to treat them has (understandably) focused on reversing the genetic anomaly rather than promoting remyelination by Schwann cells. Indeed, although the reported onion bulbs are considered evidence of spontaneous remyelination in CMT1, it is currently not even clear whether promoting Schwann cell remyelination could be beneficial for the patients. Better understanding of the effects of demyelination and remyelination on the health and function of peripheral axons may therefore open up new therapeutic possibilities; for instance, if correctly performed remyelination (as opposed to onion bulbs) were to be shown to protect the function of peripheral nerves, more research could be directed to develop ways to achieve this in CMT patients. The Tg(mbp:mCherry-NTR) model where Schwann cells are specifically ablated in peripheral nerves provides an opportunity to address the question of how loss of myelin might affect the health and function of the axon, and whether subsequent remyelination might reverse any changes seen during demyelination.

Other, non-inherited peripheral neuropathies exist in which myelination is affected, such as the autoimmune neuropathy Guillain-Barré syndrome (Martini and Willison, 2015). In these disorders, immune cells may attack either myelin or axons, leading to severe symptoms of neuropathy. Some Guillain-Barré patients show good recovery, and this outcome is associated with remyelination following resolution of the immune attack (Martini and Willison, 2015.). However, in these conditions, like in MS, the primary therapeutic target is the immune system, and no therapy for enhancing remyelination exists. Thus, again, the Tg(mbp:mCherry-NTR) model could prove useful as a model in which to test factors to promote Schwann cell remyelination and to determine whether these have beneficial consequences for the peripheral nerve and

the animal. Furthermore, since these autoimmune neuropathies can be mediated by an immune attack on Schwann cells and myelin, it would be interesting to study the relationship between immune cells, Schwann cells and the axon: for example, how do macrophages respond to primary Schwann cell death, do they play an equally important role in PNS regeneration as they do in the CNS? Such information would be important when designing interventions for the autoimmune neuropathies.

It seems, then, that despite many neuropathies where Schwann cell dysfunction or demyelination is either the primary cause or a major feature of the disease, little is known about how to promote Schwann cell remyelination in such cases, or whether it would even be beneficial to do so. It is natural that, given the well-recognised genetic or autoimmune causes of disease, the search for treatments should focus on targeting the causes. However, in some cases addressing some of the main symptom-causing features such as demyelination, could be equally effective in relieving the symptoms, as is seen in those Guillain-Barré patients who show good recovery. *In vivo* models of Schwann cell death and demyelination can help in developing such interventions by providing a platform in which to study the fundamental biology of the relationship between Schwann cells and the peripheral axons.

5.1.4. Most models of PNS regeneration involve injury to the entire nerve

Contrary the dearth of knowledge about Schwann cell repair in neuropathies, axonal repair in the PNS is extremely well studied. Indeed, the PNS is widely recognized for its superior capacity for regeneration, compared to the CNS. The vast majority of peripheral nerve repair studies inflict either a crush injury or a transection of the nerve. These methods produce injuries of differing severities and can be used to model different levels of human peripheral nerve injury (Wood et al. 2011). The crush injury is typically attained by applying a “crush” pressure across the nerve with forceps for a period of 30s (Bridge et al. 1994) and results in an injury where both the myelin and the axon in the nerve are disrupted, but Schwann cell basal lamina tubes are spared. By contrast, the transection injury involves a complete cut of all fibres, and is associated with a considerably worse recovery than the crush injury (Wood et al. 2011).

Following either kind of injury, the distal portion of the axons begins the process of Wallerian degeneration. This is an active process which in the PNS tends to take approximately 7- 14 days. Wallerian degeneration begins with fragmentation and degeneration of axons in the distal stump, with the precise mechanics depending on the type of injury inflicted: degeneration of the distal stump proceeds in an anterograde direction following nerve transection, and in the retrograde direction following a crush injury (Beirowski et al. 2005). Either way, this degeneration of axons results in myelin and axon debris at the injury site. The next step in Wallerian degeneration is an increase in blood-tissue barrier permeability, which enables an influx of macrophages and the consequent removal of the debris (Vargas and Barres 2007). This clearance is essential, as it removes the physical barrier to axon regrowth (Kang and Lichtman 2013).

The swift process of Wallerian degeneration in the PNS is considered a key reason why PNS injuries are followed by efficient recovery, and conversely, the inefficiency of Wallerian degeneration in the CNS is seen as an obstacle to repair following CNS injuries (Vargas and Barres 2007). Despite recent advances in understanding the genetic control of Wallerian degeneration (Conforti et al. 2014), the reasons for the stark contrast in the regeneration of PNS and CNS tissue remain to be fully understood. It would therefore be highly informative to be able to compare the responses of the CNS and the PNS in the same animal over time. This would be possible using a system such as the Tg(mbp:mCherry-NTR) fish, where oligodendrocytes and Schwann cells are simultaneously ablated, and the responses of both the glial cell types, axons and immune cells could be simultaneously studied.

One possible reason why the PNS shows more efficient recovery from injury than the CNS does is that Schwann cells play a key role in axonal regeneration (Jessen and Mirsky, 2005). Until recently, it was thought that upon becoming denervated as a result of axon injury, Schwann cells revert to an immature phenotype, downregulate myelin genes and upregulate many genes associated with early Schwann cell development (Arthur-Farraj et al. 2012). This apparent dedifferentiation is controlled by the transcription factor c-Jun; if the expression of c-Jun is blocked, Schwann cells fail to acquire the correct phenotype and functional recovery is severely impaired. Recent

data has adjusted this view to specify that the phenotype acquired by denervated Schwann cells following nerve transection is not a recapitulation of an immature phenotype but rather a distinct "repair phenotype" with a distinct expression profile, including glia-derived neurotrophic factor (GDNF), brain derived neurotrophic factor (BDNF) and vascular endothelial growth factor (VEGF) which are not expressed during normal development (Jessen and Mirsky 2016).

Interestingly, Stassart et al. (2012) found that following peripheral nerve crush in mice, Schwann cells began to express a neuregulin isoform not seen during normal development, Nrg1-III. A knockdown of Nrg1-III in Schwann cells did not affect developmental myelination but did severely impair myelination of newly regrown axons following crush injury. This observation is consistent with Jessen and Mirsky's data that a nerve injury induces a specific "repair" phenotype in Schwann cells. However, in the paradigms employed by these studies, the experimental injury is inflicted primarily on the axons, meaning that the majority of myelinating Schwann cells (not located at the precise site of crush or cut) remain relatively intact and able to assume the "repair" phenotype. It remains unknown whether, following primary Schwann cell injury, newly generated Schwann cells may acquire a similar "repair" phenotype.

Be that as it may, the "repair" Schwann cells proliferate and extend long cytoplasmic processes to reconnect the severed axon to its target. By doing this, "repair" Schwann cells form tracks, referred to as Büngner's bands, to guide regrowing axons to their targets (Gordon 2016). In this process, Schwann cells interact closely with a myriad of other cells and elements, including macrophages, extracellular matrix and blood vessels (Cattin and Lloyd 2016). In fact, recent evidence from Cattin et al. (2015) reveals that soon after nerve transection, a structure referred to as "the bridge" forms, initially composed of dense extracellular matrix and inflammatory cells, predominantly monocyte-derived macrophages, prior to the appearance of Schwann cells. This bridge is initially not vascularised and consequently becomes hypoxic. The macrophages within the bridge sense this hypoxia and respond by secreting VEGF. This response is both necessary and sufficient to initiate vascularisation of the bridge. The newly formed blood vessels reach across the bridge to the severed axon's target

and in so doing, constitute tracks for the Schwann cells to extend upon as they form Büngner's bands (Cattin et al. 2015). Consistent with this early role of macrophages is the observation in a live imaging study in zebrafish that macrophages arrive at the transection site even before the distal stump of the axon has fragmented (Rosenberg et al. 2012). These data highlight the complexity of the cell-cell interactions which mediate the successful peripheral nerve repair.

To add to the complexity, the "repair" Schwann cells also release cytokines such as TNFα, interleukin-1α, interleukin-1β and LIF, and thus are actively involved in recruiting monocyte-derived macrophages to the transection site to assist in the forming the bridge and to clear myelin and axon debris (Martini et al. 2008; Gomez-Sanchez et al. 2015; Cattin and Lloyd 2016). Furthermore, Schwann cells themselves are instrumental in phagocytosing myelin debris, which is an essential step for nerve regeneration (Stoll et al. 1989; Perry et al. 1995; Gomez-Sanchez et al. 2015).

It should be emphasised that, again, this active and coordinated response of Schwann cells, macrophages, blood vessels and a host of other cell types is observed following injury to the entire nerve. In contrast, it is not known at all what kind of response would follow primary Schwann cell death. The Tg(mbp:mCherry-NTR) model would allow researchers to address that question in a living system. One obvious difference is that in this model, myelinating Schwann cells are ablated and thus unable to assume a "repair phenotype". It would therefore be interesting to investigate whether the innate immune system would respond the same way to primary Schwann cell death as it does to an injury to the entire nerve, or would the response perhaps be delayed or weaker, in the absence of signals from damaged axons or "repair" Schwann cells? In addition, it would be highly informative to compare the immune response to primary Schwann cell death to the immune response observed following primary oligodendrocyte death in this model (described in **Chapter 4**), as this might shed light on the different rates of repair observed between the PNS and the CNS.

5.1.5. The need for a model of primary Schwann cell ablation

In conclusion, much is known about the complex interplay of cellular and molecular events which mediate peripheral nerve repair following injury to the nerve. As I have stressed, however, the models used to obtain these results have all inflicted damage primarily on the axons, and focused primarily on the regeneration of the axons. The importance of Schwann cell remyelination is often discussed (e.g. Stassart et al. 2012), but the phenomenon in question would perhaps be more accurately described as *de novo* myelination of the newly regrown axon. This is because "remyelination" implies former demyelination, i.e. an otherwise intact axon denuded of its myelin sheaths, which is not strictly the case in the current models of peripheral nerve injury. As I mentioned in **Chapter 1**, the phenotype and activity of a demyelinated axon may be very distinct from that of a newly growing axon, and thus may result in a distinct response from glial cells. With this in mind, then, very little is known about *bona fide* remyelination in the peripheral nerve.

The Tg(mbp:mCherry-NTR) model is, to my knowledge, the first system which allows us to study the consequences of primary Schwann cell death, PNS myelin loss and regeneration without the backdrop of an initial insult to the axon. As such, it is relevant for neuropathies where Schwann cell abnormalities are the primary cause of pathology, such as CMT1, or any condition where there is primary disruption to the myelinating Schwann cell itself. As I have alluded to above, it would be informative to study the effects that demyelination may have on the health and integrity of the peripheral axons, and whether remyelination can reverse these effects to the benefit of the function of the nerve and the animal. In addition, it would also be highly interesting to compare the demyelination and remyelination events, as well as the immune response, in the CNS and PNS in the same animal. Such a model may be particularly useful in zebrafish, which allows live imaging of all these events in the same animal over time.

5.1.6. Development and regeneration of the zebrafish peripheral nervous system

Several studies have used the zebrafish to study peripheral nerve regeneration. It is easy to appreciate the appeal of this system; the zebrafish peripheral nerve is a well-studied structure, and present on the surface of a transparent living animal, and thus lends itself extremely well for live imaging of dynamic events.

In zebrafish studies of peripheral nerve development and regeneration, much work has been carried out on the lateral line system. The anterior lateral line (aLL) and posterior lateral line (pLL) are sensory systems that detect changes in water currents, in the head and tail respectively. The aLL and pLL are comprised of discrete sensory organs called neuromasts, located throughout the skin and derived from ectodermal placodes that migrate from origins near the ear, the neurons that innervate the neuromasts and also project afferent axons into the brain, and the Schwann cells associated with the axons of such neurons (Ghysen and Dambly-Chaudière 2007). During development, axons of the pLL ganglion (cluster of neuronal cell bodies of the pLL) guide the Schwann cells as they co-migrate along the trunk of the embryo, in an interaction that requires Nrg1-ErbB signalling (Lyons et al. 2005; Perlin et al. 2011).

Figure 32A below illustrates the position of the pLL in a 5dpf larva, its appearance using the Tg(mbp:mCherry-NTR) and the Tg(mbp:nls-EGFP) transgenic lines. **Figure 32B** shows a transversal view of the pLL by TEM, and a schematic version of the pLL where the various components are labelled. A typical transversal view of the pLL contains a number of large-calibre myelinated axons, a population of small-calibre unmyelinated axons, occasionally a small number of relatively large-calibre unmyelinated axons, and Schwann cell nuclei closely adjacent to the axons.

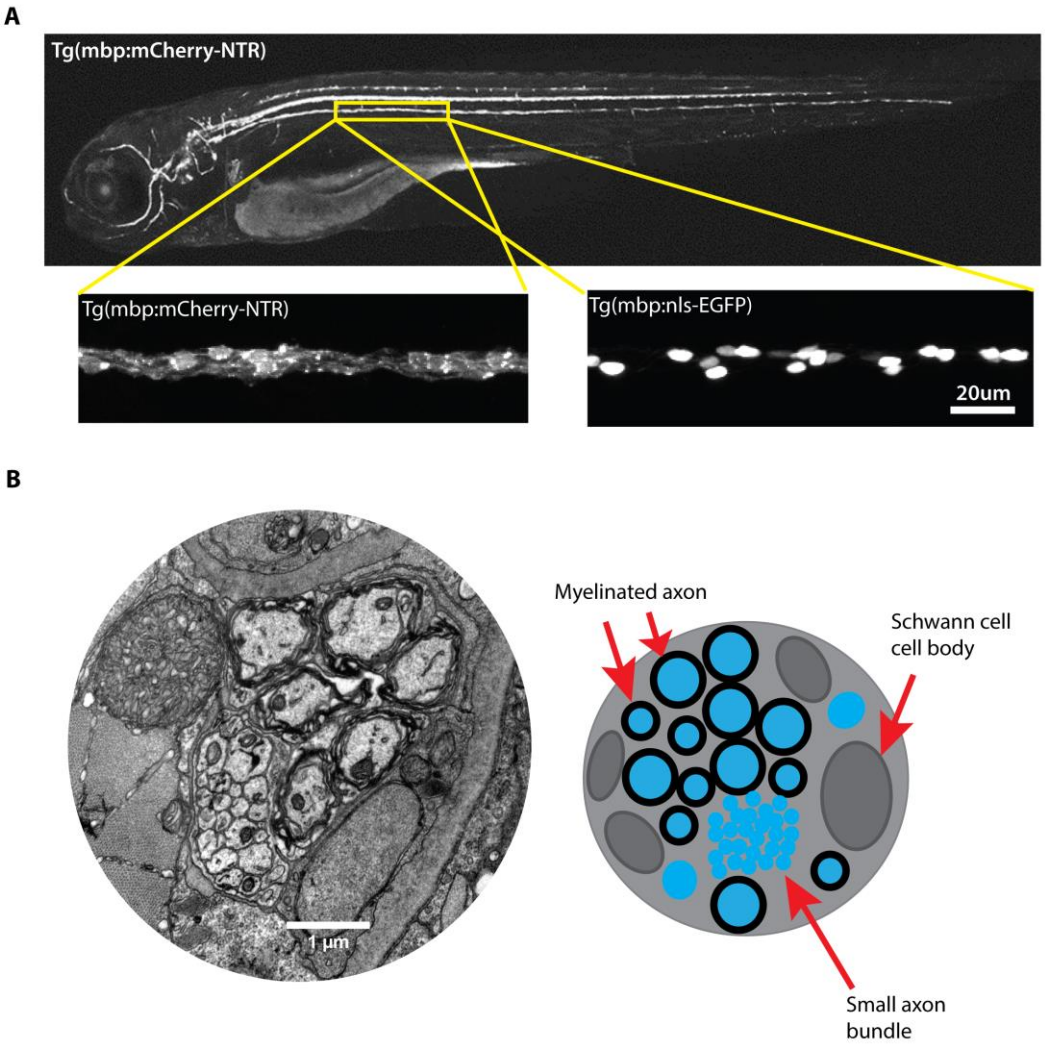

Figure 32. Zebrafish posterior lateral line nerve at 5dpf as seen by confocal and electron microscopy. A. Overview of an entire Tg(mbp:mCherry-NTR) larva at 5dpf. The yellow box denotes the area where the higher magnification images were taken. The left-hand image depicts the appearance of the pLL using the Tg(mbp:mCherry-NTR) line, while the right-hand image depicts the pLL using the Tg(mbp:nls-EGFP) line, which labels Schwann cell nuclei. **B**. An electron micrograph depicting a transverse view of the pLL at 5dpf. The schematic on the right-hand side indicates the large-calibre myelinated axons, the small-calibre unmyelinated axons and a Schwann cell nucleus.

The simple and well-understood structure of the pLL makes it an attractive system for studying regenerative events. Even more importantly, as I have discussed above, since peripheral nerve repair is a highly dynamic process, live imaging is an ideal method to study it.

For example, beautiful live imaging of pLL regeneration following by transection by laser microsurgery was performed by Xiao et al. (2015). These authors noted differential responses of Schwann cells to acute and chronic denervation: following nerve transection in both cases, some Schwann cell death was observed as a result of the surgery, but if the remaining Schwann cells received contact from axons by 24h post-transection, the loss of Schwann cells was halted. In contrast, if axons were ablated by directing the laser to the cell body, and Schwann cells remained denervated past 48h post-transection, they continued to undergo apoptosis. The same study also used laser ablation to kill subsets of Schwann cells adjacent to neuromasts, and severed the axons innervating that neuromast. In such cases, the axons failed to regrow to innervate the neuromast. Xiao et al. also noted that in ErbB2 mutant fish, which had failed to develop Schwann cells, axon regrowth was considerably slower than in wild-types and halted completely long before reaching its target. A similar observation was also made by Ceci et al. (2014) who pharmacologically prevented Schwann cells from migrating past somite 16, and then performed a transection anterior to that. The nerve regrew along the tracks formed by the Schwann cells until there were no more Schwann cells, at which point the nerve became misrouted and defasciculated and failed to reach its target.

These studies indicate that live imaging of nerve repair in the zebrafish pLL allows minute examination of local interactions between Schwann cells and axons, and their responses to genetic, pharmacological or surgical interventions. Importantly, the kind of imaging performed in these examples, revealing misrouted axons specifically in areas lacking Schwann cells, or the requirement for a local presence of Schwann cells, would be extremely challenging to conduct in mammalian systems. Naturally, the ability to follow individual axons and its interactions with other cell types over time as it undergoes Wallerian degeneration and subsequently grows out again could be fundamental to our understanding of how peripheral nerve regeneration unfolds. Of note, the zebrafish studies I mentioned show that Schwann cells play a key role in axon regrowth in zebrafish too, implying that the process of peripheral nerve repair is conserved between fish and mammals.

However, again, most of the currently used models of zebrafish pLL regeneration involve severing the entire nerve and examining the regrowing of axons and the responses of Schwann cells to losing their axonal contacts; I am not aware of any system where Schwann cells are killed while axons are spared. Yet, as I have discussed above, a model of primary Schwann cell death would enable researchers to address many important questions regarding the role of Schwann cells in maintaining peripheral axon health and the cellular events that follow Schwann cell death. Moreover, having such a model in zebrafish would have the advantages of live imaging and being able to follow CNS and PNS demyelination and remyelination at the same time.

Thus, despite human diseases where Schwann cell defects cause severe pathology, and the complete lack of knowledge of the consequences of primary Schwann cell death, contrasting to the extensive literature on axon injury in the peripheral nerve, so far there has been no model in which to study the effects of primary Schwann cell death. I propose that the Tg(mbp:mCherry-NTR) line could be a valuable addition to the arsenal of research tools for the study of peripheral nerve biology in injury, disease and repair.

5.1.7. Summary of this chapter

Therefore, in this chapter, I characterise the Schwann cell ablation model in the Tg(mbp:mCherry-NTR) line. I show that a two-day treatment with 5mM metronidazole ablates approximately half of the Schwann cells, and leads to demyelination of approximately half of the myelinated axons in the peripheral nerve one day later. I then outline the rapid remyelination of the pLL and ask whether de- or remyelination results in changes in the mitochondrial content of the axons. I show that unlike oligodendrocytes, Schwann cell numbers are restored to control levels by 5 days post-treatment. Finally, I describe the time course of response of the innate immune system to Schwann cell ablation.

5.2. Ablation of Schwann cells with metronidazole treatment

5.2.1 Metronidazole treatment of Tg(mbp:mCherry-NTR) larvae from 5dpf to 7dpf ablates approximately half of Schwann cells.

Given that the Tg(mbp:mCherry-NTR) line also expresses the transgene in Schwann cells, I assumed that the metronidazole (Mtz) treatment could also be used to ablate Schwann cells. However, since Schwann cells and oligodendrocytes differ in a number of important ways (see **Section 5.1.1**. above) it was possible that the effects of the treatment would not be identical.

To test this, I first tried the same 5mM Mtz-treatment from 5dpf to 7dpf as was used in **Chapters 3** and **4** to ablate oligodendrocytes. Starting treatment at 5dpf seemed rational, given the extensive myelination along the posterior lateral line (pLL) at this point.

As shown in **Figure 33A**, this Mtz-treatment regime causes damage to myelinating Schwann cells along the pLL. However, the cytoplasmic localisation and tendency of the mCherry reporter protein to cluster makes it very difficult to assess this damage quantitatively. To begin to address this problem, I crossed Tg(mbp:mCherry-NTR) fish with Tg(mbp:nls-EGFP) fish and carried out the experiment on the resulting double transgenic larvae. Tg(mbp:nls-EGFP) larvae express EGFP in their oligodendrocyte and Schwann cell nuclei, due to the inclusion of nuclear localisation sequence (nls) in the transgenic construct (Lyons lab; unpublished). **Figure 33B**, showing a four-somite stretch of the pLL, demonstrates that it is possible to reliably count Schwann cells using this transgenic line, even in the densely packed lateral line nerve. These counts (shown in **Figure 33C**) revealed that after a two-day treatment with Mtz, there was a roughly 53% decrease in Schwann cells in treated compared to control animals; a mean of 35.36 ± 4.72 Schwann cells in control, compared to a mean of 16.53 ± 5.18 in treated, $p < 0.0001$.

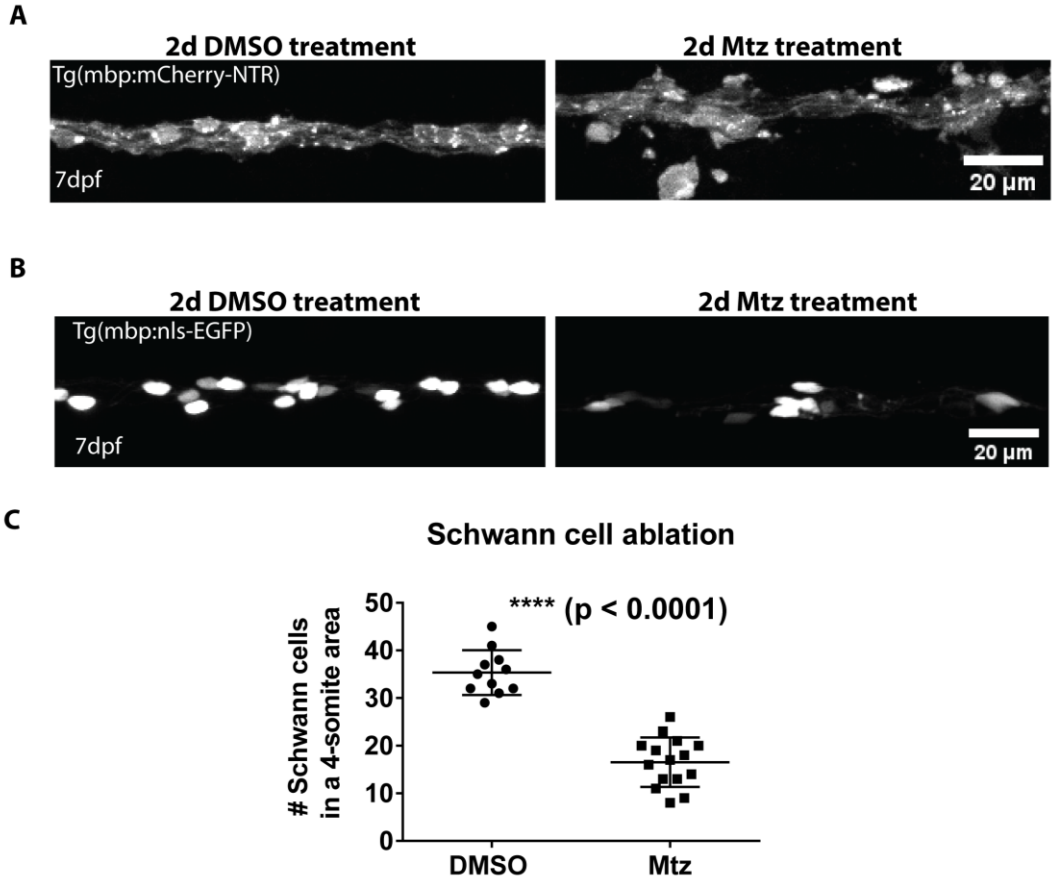

Figure 33. A two-day treatment with Mtz ablates approximately one-half of Schwann cells. A. Confocal images of four-somite long stretches of peripheral nerves of 7dpf larvae, treated with either DMSO or Mtz, as indicated. The Mtz-treated nerve appears disorganised and fragmented compared to the control nerve. **B**. PLLs of Tg(mbp:mCherry-NTR);Tg(mbp:nls-EGFP) larvae showing the mbp:nls-EGFP signal which labels Schwann cell nuclei. The number of nuclei is drastically reduced in the Mtz-treated animal. **C**. Quantification of Schwann cell ablation shows that Mtz-treatment ablates 53% of Schwann cells (reduction from 35.36 ± 4.72 to 16.53 ± 5.18 Schwann cells, $p < 0.0001$). n = 11 for DMSO, 15 for Mtz.

5.2.2. Schwann cell ablation causes disruption to myelin sheaths

Having discovered that a two-day metronidazole treatment ablates approximately half of the myelinating Schwann cell population, I was interested in how this ablation affected the myelin sheath morphology along the pLL nerve. I first addressed this by visualising the myelin sheaths using the Tg(mbp:EGFP-CAAX) line, as shown in **Chapter 3**. I crossed these fish with Tg(mbp:mCherry-NTR) fish and treated the progeny with Mtz (or DMSO) for two days. The results are shown in **Figure 34A**: in

the control animal, myelin sheaths along the lateral line nerve labelled with mbp:EGFP-CAAX have a typical elongated morphology. By contrast, in the Mtz-treated animal, myelin sheaths appear disorganised and myelinating Schwann cells seem to have become dissociated from the nerve, already at the time of Mtz withdrawal. One day later, Mtz-treated peripheral nerves appear fainter and thinner than their control counterparts (**Figure 34B**), suggesting that the Schwann cells and myelin sheaths continue to degrade after the Mtz-treatment is withdrawn.

Next, I prepared control and Mtz-treated larvae for transmission electron microscopy, in order to image the consequences of Schwann cell ablation on the myelination of PNS axons and on the underlying axons themselves.

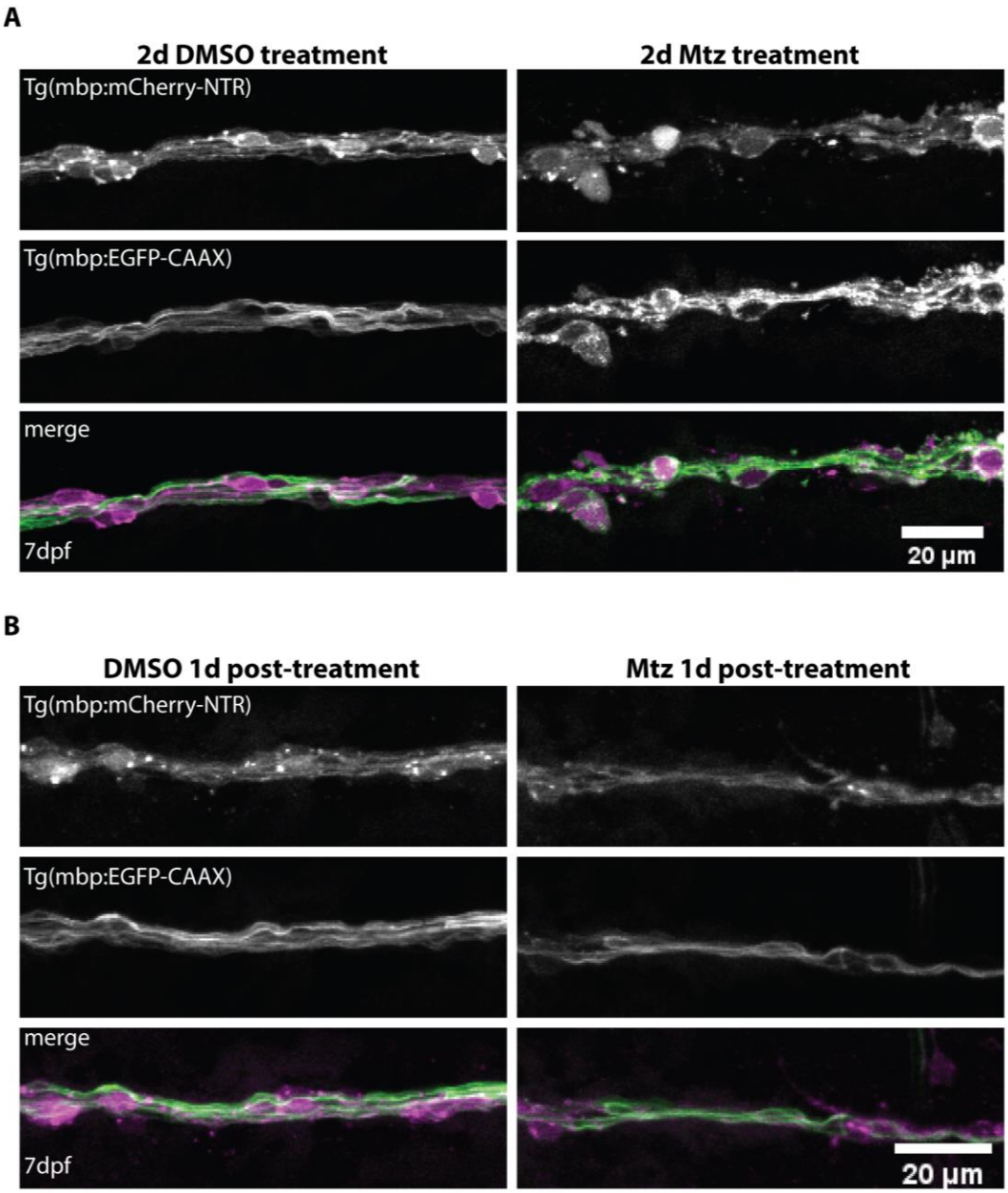

Figure 34. Schwann cell ablation causes myelin disruption. A. Confocal images of pLL nerves at 7dpf, in larvae treated with either DMSO or Mtz, as indicated. In the control nerve, the mbp:EGFP-CAAX transgene shows a smooth, continuous line. This organisation is disrupted in the Mtz-treated nerve. **B**. Confocal images of peripheral nerves at 8dpf, one day post-treatment. The Mtz-treated nerve appears fainter and thinner than the control nerve.

5.3. Demyelination in the pLL nerve

5.3.1. Approximately half of axons in the pLL nerve are demyelinated at 1d post-treatment

Since I had seen from live imaging that at 1d post-treatment, the mbp:EGFP-CAAX signal was growing fainter, I decided that this was an appropriate time point for investigating the myelination of peripheral axons at the ultrastructural level. I therefore prepared EM samples from 8dpf control and Mtz-treated larvae, and imaged their pLL nerves. Representative images are shown in **Figure 35A**. The DMSO-treated nerves displayed the expected structure of the pLL nerve at 8dpf: a population of large-calibre myelinated axons, a bundle of small-calibre unmyelinated axons, and a small number of large-calibre unmyelinated axons. By contrast, the organisation of the Mtz-treated nerves was disrupted: fewer myelinated axons could be seen, and many more large-calibre unmyelinated axons were present. The small unmyelinated axon bundle did not appear affected.

To quantify the effects of metronidazole treatment on PNS axons and myelin, I first counted all axons, and calculated the percentage of all axons that was myelinated, to assess any overall changes to the peripheral nerve structure. There was no difference in the total number axons between control and Mtz-treated animals, with a mean of 45.25 ± 20.39 axons in control animals and 45.00 ± 12.44 in Mtz-treated animals, $p = 0.981$; **Figure 35B**).

In contrast, when I counted the total number of myelinated axons, I found it significantly reduced in Mtz-treated, compared to control animals (a mean of 9.0 ± 4.69 myelinated axons in control animals, compared to 4.0 ± 1.67 in Mtz-treated animals, $p = 0.04$). This amounts to a 56% reduction in the number of myelinated axons within the pLL. By the same token, there was also a significant reduction in the percentage of myelinated axons: in the control animals, 19.75 ± 2.22% of all axons were myelinated, whereas in Mtz-treated animals, only 9 ± 3.23% of all axons was myelinated, $p = 0.0004$ (**Figure 35B**).

However, it can be argued that the bundle of small unmyelinated axons is not of much interest when assessing the effects of a demyelinating treatment, since these axons

would not have been myelinated in any case. Thus, in order to focus more clearly on demyelinated axons, I counted only those axons that by their size would have been expected to be myelinated. To this end, I took the perimeter of the smallest myelinated axon in a control animal as the threshold for a "myelinateable" size, which was approximately 1.2µm in perimeter. As before, I will refer to these axons as large-calibre axons. Analysis of these large-calibre axons showed that there was no difference in their overall number (a mean of 14.50 ± 8.96 in control and 13.50 ± 2.35 in Mtz-treated animals, p = 0.796; **Figure 35C**) The total number of myelinated large-calibre axons was the same as that of the total number of myelinated axons (**Figure 35B**), since all myelinated axons, by my definition, fall into the large calibre category. Accordingly, the percentage of large calibre axons that was myelinated was significantly lower in Mtz-treated than in control animals (**Figure 35C**): in control animals, 83.50 ± 19.12% of the large-calibre axons was myelinated, whereas in Mtz-treated animals, only 31.33 ± 9.18% of them was myelinated, p = 0.0004.

A

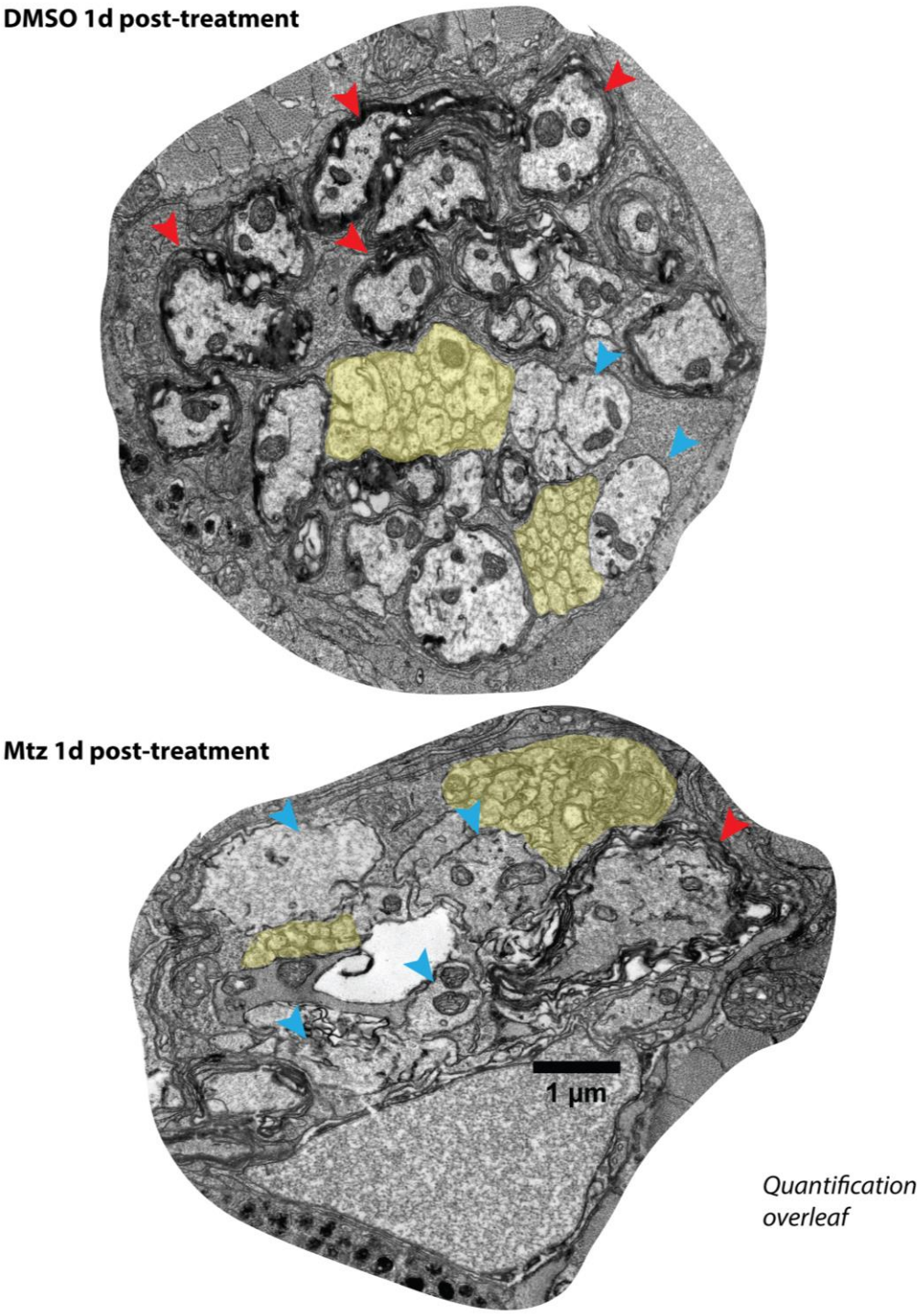

Quantification overleaf

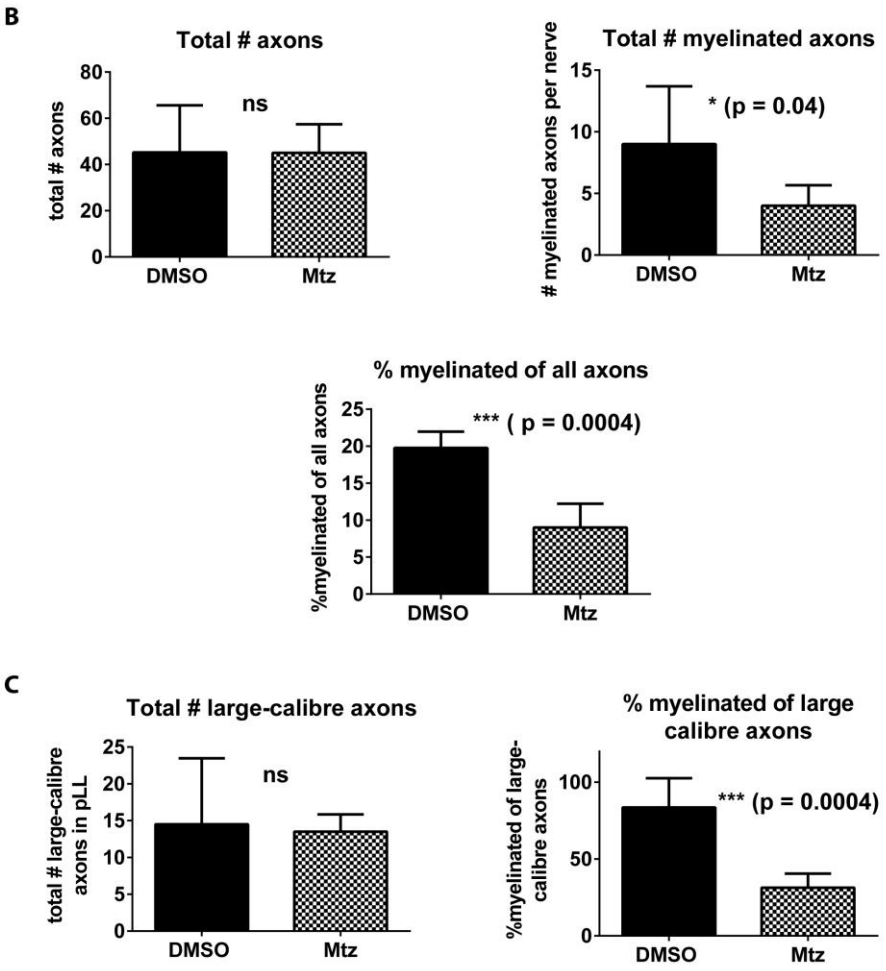

Figure 35. TEM shows extensive demyelination in pLL nerve at 1d post-treatment. A. TEM images of peripheral nerves of 8dpf larvae, treated with DMSO or Mtz as indicated. The DMSO-treated nerve has a number of large myelinated axons, (red arrowheads), some large unmyelinated axons (blue arrowheads) and a population of small unmyelinated axons (shaded yellow). **B**. Quantification shows that the total number of axons does not differ between Mz-treated and control animals (the mean number of axons is 45.25 ± 20.39 in control animals and 45.00 ± 12.44 in Mtz-treated animals, p = 0.981) but the number of myelinated axons is significantly lower in Mtz-treated compared to control animals (a mean of 9 ± 4.69 myelinated axons in control animals, compared to 4 ± 1.67 in Mtz-treated animals, p = 0.04). The percentage of all axons that is myelinated is also significantly lower in Mtz-treated animals compared to controls (19.75 ± 2.22% in control vs 9 ± 3.23% in treated animals, p = 0.0004). **C**. Quantification of large-calibre axons shows the same effect: total number of axons does not differ between treated and control animals (a mean of 14.50 ± 8.96 axons in control and 13.50 ± 2.35 in Mtz-treated animals, p = 0.796) but the percentage of large-calibre axons that is myelinated is significantly lower in Mtz-treated compared to control animals (83.5 ± 19.12% in control vs 31.33 ± 9.18% in Mtz-treated animals, p = 0.0004). n = 4 in control, 5 in Mtz-treated.

5.3.2. Peripheral nerve demyelination continues at 3d post-treatment

Having established that ablation of approximately half of the myelinating Schwann cells results in a corresponding demyelination of 56% of axons, I next wished to see whether the axons would remain demyelinated for the next few days. I therefore prepared EM samples from control and Mtz-treated larvae at 10dpf, i.e. three days post-treatment. Analysis of these larvae clearly showed that axons remain demyelinated at this time point; **Figure 36A** shows many more large unmyelinated/demyelinated axons in the Mtz-treated peripheral nerve compared to control. Quantification of all axons (**Figure 36B**) indicated again that there was no difference in the total number of axons between control and Mtz-treated animals, (the mean number of axons in control animals was 41.20 ± 6.57, and in Mtz-treated animals 46.60 ± 19.76, $p = 0.578$) but that the total number of myelinated axons was significantly lower in Mtz-treated compared to control animals (10.40 ± 1.67 myelinated axons in control animals, compared to 3.8 ± 1.30 in Mtz-treated animals, $p = 0.0001$). Consequently, the percentage of myelinated axons remained significantly lower in Mtz-treated than in control animals (25.80 ± 4.32% myelinated in control animals, compared to 8.6 ± 2.88% myelinated in Mtz-treated animals, $p < 0.0001$).

Next, I again performed another quantification focusing solely on large-calibre axons, in order to better understand the extent of the loss of myelin. This analysis (**Figure 36C**) showed that there was no difference in the total number of large-calibre axons between control and Mtz-treated animals, (the mean number of large-calibre axons was 13.20 ± 2.86 in control animals, and 11.80 ± 1.92 in Mtz-treated animals, $p = 0.391$) but there was a significant reduction in the percentage of these axons that was myelinated (80.80 ± 15.17% myelinated in control animals, compared to 35.40 ± 16.13% myelinated in Mtz-treated animals, $p = 0.0018$).

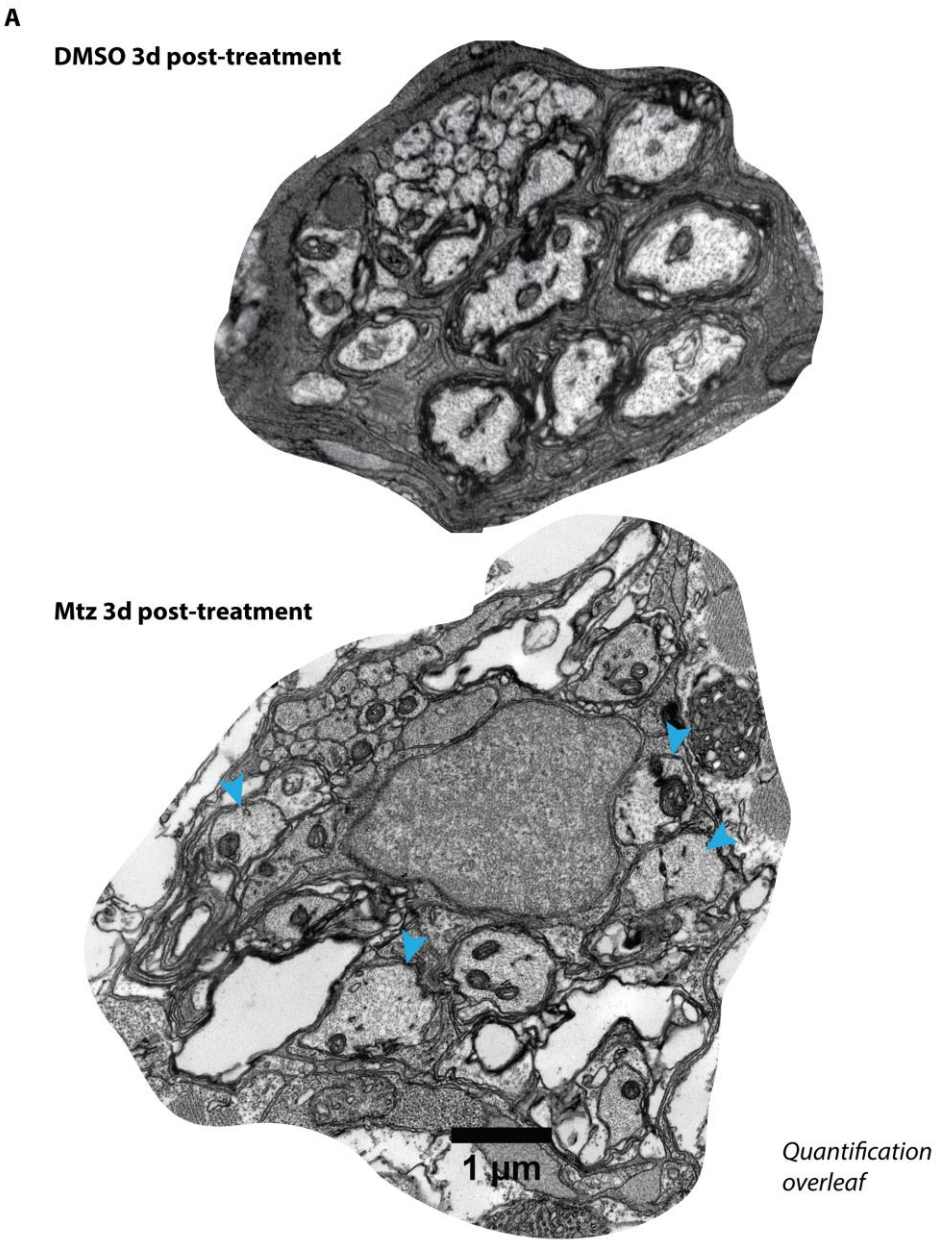
A
DMSO 3d post-treatment
Mtz 3d post-treatment
1 µm
Quantification
overleaf

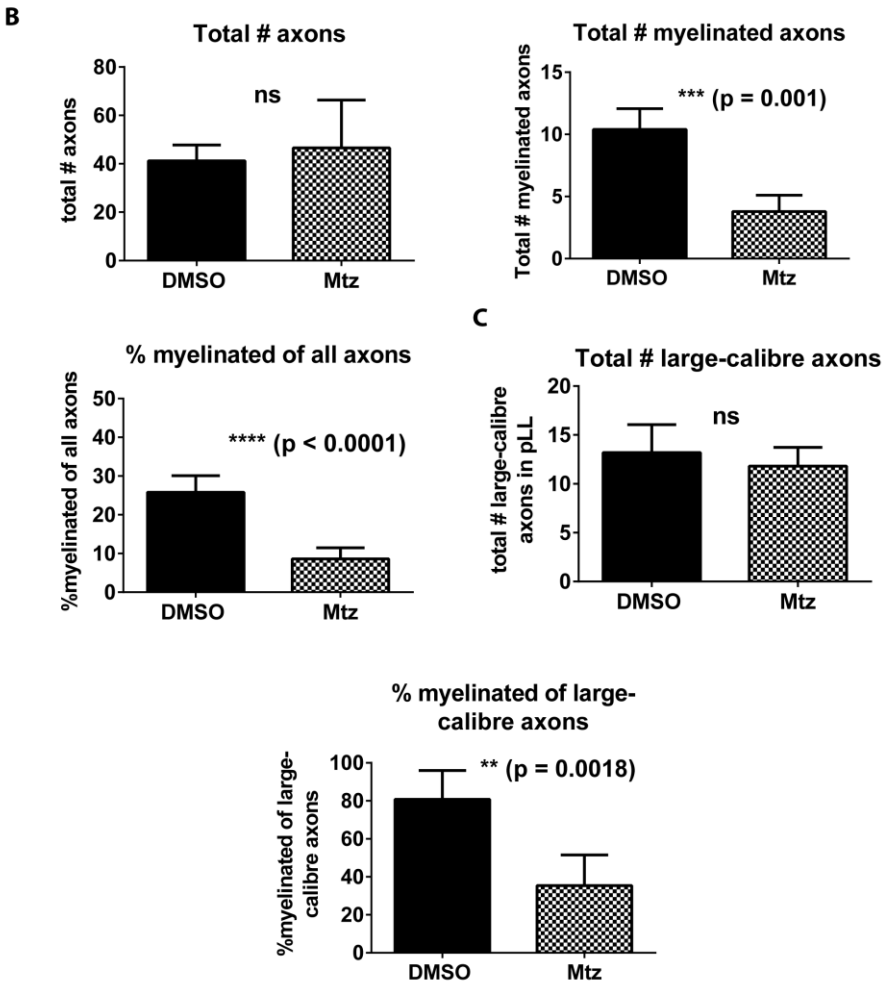

Figure 36. Demyelination continues in the pLL at 3d post-treatment. **A**. TEM images of peripheral nerves of 10dpf larvae, treated with either DMSO or Mtz as indicated. The DMSO-treated nerve appears organised and almost all its large axons are myelinated. In the Mtz-treated nerve, many large unmyelinated axons can be seen. **B**. Quantification of all axons shows that the total number of axons does not differ between Mz-treated and control animals (mean number of axons in control animals is 41.20 ± 6.57, and in Mtz-treated animals 46.60 ± 19.76, p = 0.578) but the total number of myelinated axons is significantly lower in Mtz-treated compared to control axons (10.40 ± 1.67 myelinated axons in control, compared to 3.8 ± 1.30 in Mtz-treated, p = 0.0001). The percentage of all axons that is myelinated is also significantly lower in Mtz-treated animals (25.80 ± 4.32% in control vs 8.6% ± 2.88% in treated animals, p < 0.0001). **C**. Quantification of large-calibre shows the same effect: total number of axons does not differ between treated and control animals, (mean number of large-calibre axons is 13.20 ± 2.86 in control animals, compared to 11.80 ± 1.92 in Mtz-treated animals, p = 0.391) but the percentage of large-calibre axons that is myelinated is significantly lower in Mtz-treated compared to control animals (80.80% ± 15.17% in control vs 35.40% ± 16.13% in Mtz-treated animals, p = 0.0018). n = 5.

5.4. Remyelination in the pLL nerve

5.4.1. By 7d post-treatment, axons in the pLL have undergone remyelination

Thus, a two-day treatment with metronidazole ablates approximately half of the Schwann cells, and this leads to demyelination of approximately one-half (56%) of pLL axons, which persists for at least the first three days following withdrawal of metronidazole. However, since I have already shown that the CNS undergoes full remyelination within sixteen days of the end of the treatment, there was every reason to expect the PNS to recover in full, too. Moreover, as detailed above in **Section 5.1**., the remarkable efficiency with which the PNS can repair and regenerate itself is well documented (Vargas and Barres 2007). With this in mind, I first asked whether the peripheral nerves had begun remyelination at 7d post-treatment.

I again addressed this question by electron microscopy. The data presented in **Figure 37A** demonstrated that at 7d post-treatment, peripheral nerves appear to have undergone full remyelination. The overall appearances of the control and Mtz-treated nerves were indistinguishable: both clearly contained a population of large-calibre myelinated axons as well as a bundle of small unmyelinated axons and a small number of large unmyelinated axons.

To quantify this apparent remyelination, I performed the same counts as before. Comparison of the total number of axons found no difference between control and treated animals (a mean of 91.17 ± 29.28 axons in control and 100.80 ± 41.95 in Mtz-treated animals, $p = 0.664$). There was also no difference in the total number of myelinated axons (a mean of 26.33 ± 8.47 myelinated axons in control and 25.00 ± 15.28 in Mtz-treated animals, $p = 858$) nor in the percentage of all axons that was myelinated (mean 29.00 ± 4.20 in controls and 23.60 ± 3.91 in Mtz-treated animals, $p = 0.0562$; **Figure 37B**).

Similarly, there was no difference between the numbers of large-calibre axons (a mean of 30.33 ± 6.45 in controls and 31.40 ± 15.03 in Mtz-treated animals, $p = 0.877$) and no difference between the percentage of these axons that was myelinated (a mean of 85.67 ± 13.22% in controls and 77.20 ± 14.92% in Mtz-treated animals, $p = 0.344$). It

therefore appears that the larvae have achieved a full recovery from demyelination by 7d post-treatment (**Figure 37C**).

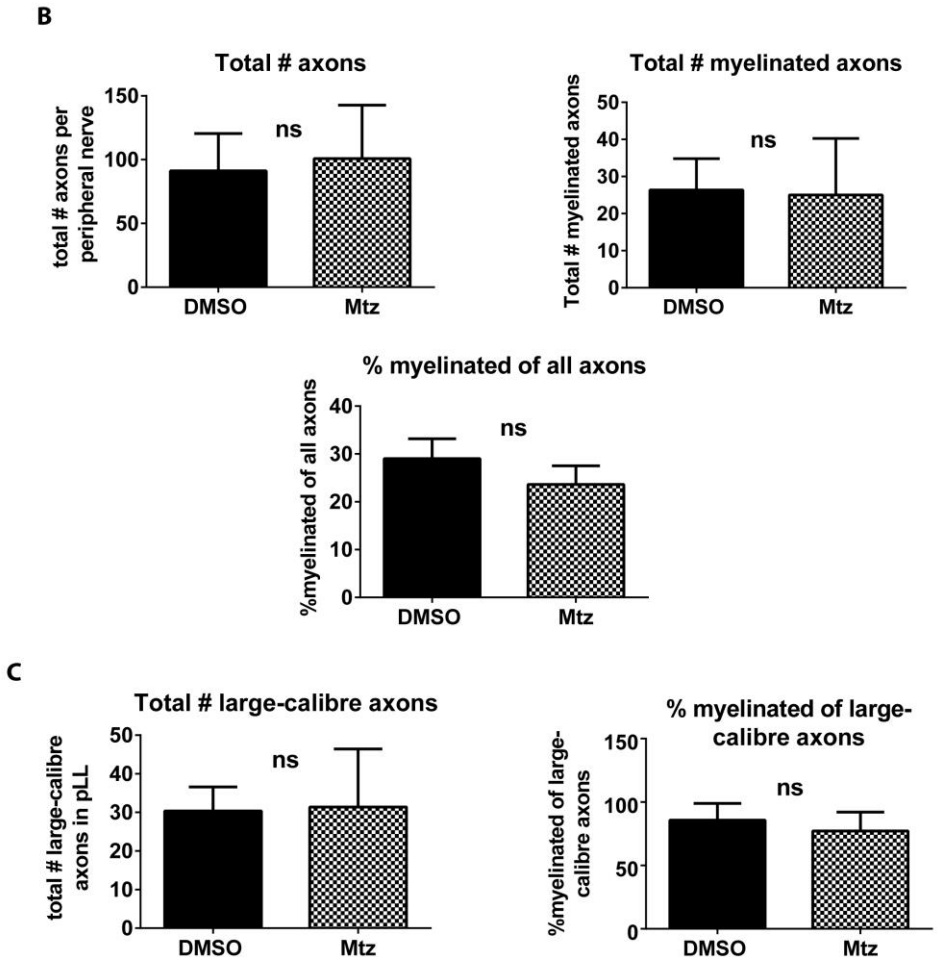

Figure 37. By 7d post-treatment, the pLL nerve has undergone remyelination. **A**. TEM images of peripheral nerves of 14dpf larvae, treated with either DMSO or Mtz as indicated. Both nerves appear organised and the majority of large axons is myelinated. **B**. Quantification of all axons shows that the total number of axons does not differ between control and Mtz-treated animals (the mean number of axons is 91.17 ± 29.28 in control and 100.80 ± 41.95 in Mtz-treated animals, p = 0.664). There is also no difference in the total number of myelinated axons (mean 26.33 ± 8.47 in control and 25.00 ± 15.28 in Mtz-treated animals, p = 858). Consequently, there is no difference in the percentage of all axons that is myelinated (mean 29.00 ± 4.20 in controls and 23.60 ± 3.91 in Mtz-treated animals, p = 0.0562). **C**. There are no differences in the total numbers of large-calibre axons (30.33 ± 6.45 in controls and 31.40 ± 15.03 in Mtz-treated animals, p = 0.877) or the percentage of them that is myelinated (85.67 ± 13.22% in controls and 77.20 ± 14.92% in Mtz-treated animals, p = 0.344). n = 6 for DMSO, 5 for Mtz.

5.4.2. G ratios of remyelinated axons are indistinguishable from g ratios of control axons

As with remyelination in the CNS, I was interested to see whether the newly generated myelin in the pLL achieved the normal thickness. To address this question, I measured g ratios of the myelinated axons in the pLLs of control and Mtz-treated larvae. The data presented in Figure 5.6B indicate that the g ratios in Mtz-treated larvae are not different from those in control DMSO-treated larvae (the mean g ratio was 0.72 ± 0.01 in controls and 0.73 ± 0.036 in Mtz-treated animals, p = 0.464).

I then plotted the g ratios against axon diameters to see whether there were any differences in the distribution of myelin thicknesses across different axon sizes, and found the distributions to be indistinguishable (**Figure 38C**). This suggests that the myelin thicknesses were similar between control and remyelinated axons across all axon sizes.

Thus, it appears that the Mtz-treated Tg(mbp:mCherry-NTR) larvae achieve full remyelination, complete with normal thickness myelin, by 7d post-treatment.

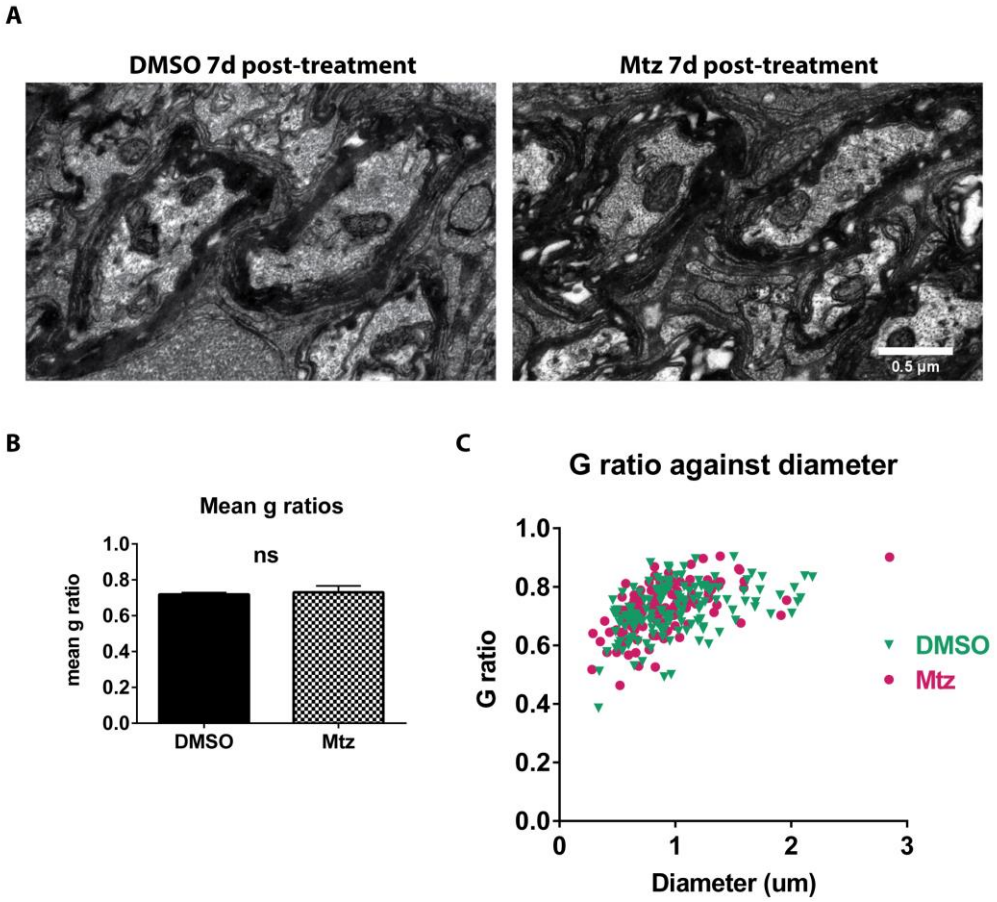

Figure 38. Remyelination restores myelin thickness to normal levels. A. TEM image from peripheral nerves of 14dpf larvae, treated with DMSO or Mtz, as indicated. **B**. A comparison of the mean g ratios finds no difference between control and Mtz-treated animals (mean g ratio of 0.72 ± 0.01 in control and 0.73 ± 0.036 in Mtz-treated animals, p = 0.4635). **C**. G ratios plotted against axon diameters show that there is no difference in the distribution of myelin thickness across axon sizes. n = 6 for DMSO, 5 for Mtz

5.5. Restoration of Schwann cell numbers

5.5.1. Schwann cell numbers are restored to control levels by 5 days post-treatment

Having established that Mtz-treated Tg(mbp:mCherry-NTR) larvae remyelinate their peripheral axons with normal thickness myelin by 7d post-treatment, I wished to know whether they had also restored their Schwann cells to control levels within this time. To address this question, I again crossed Tg(mbp:mCherry-NTR) fish to Tg(mbp:nls-EGFP) fish and treated the resulting double transgenic progeny with DMSO or Mtz. I then imaged the larvae at 0d, 1d, 3d, 5d and 7d post-treatment and counted the numbers of Schwann cells from a four-somite long stretch of the pLL at the different time points. The results, shown in **Figure 39**, indicated that there were significantly fewer Schwann cells in Mtz-treated compared to control larvae at 0d, 1d and 3d post-treatment, but by 5d post-treatment, the Mtz-treated larvae had caught up with their DMSO-treated siblings and had equivalent numbers of Schwann cells: at 0d post-treatment, there was a mean of 35.36 ± 4.72 Schwann cells in control animals, compared to 16.53 ± 5.18 in Mtz-treated animals, $p < 0.0001$. At 1d post-treatment, there was a mean of 34.64 ± 3.78 Schwann cells in control animals, compared to 13.57 ± 4.85 in Mtz-treated animals, $p < 0.0001$. Still at 3d post-treatment, there was a mean of 36.40 ± 3.97 Schwann cells in control animals, compared to 18.80 ± 7.01 in Mtz-treated animals, $p = 0.0012$. By 5d post-treatment, there difference between the groups was no longer significant, with a mean of 39.0 ± 10.23 Schwann cells in control animals and 38.94 ± 5.32 in Mtz-treated animals ($p = 0.984$). By at 7d post-treatment, both groups had increased their Schwann cell numbers to 47.77 ± 13.56 in control animals and 50.57 ± 9.62 in Mtz-treated animals ($p = 0.635$).

Thus, it seems that Tg(mbp:mCherry-NTR) larvae are able to restore their Schwann cell numbers to control levels by 5d post-treatment, and appear to carry out remyelination of the peripheral nerve with a complete set of Schwann cells.

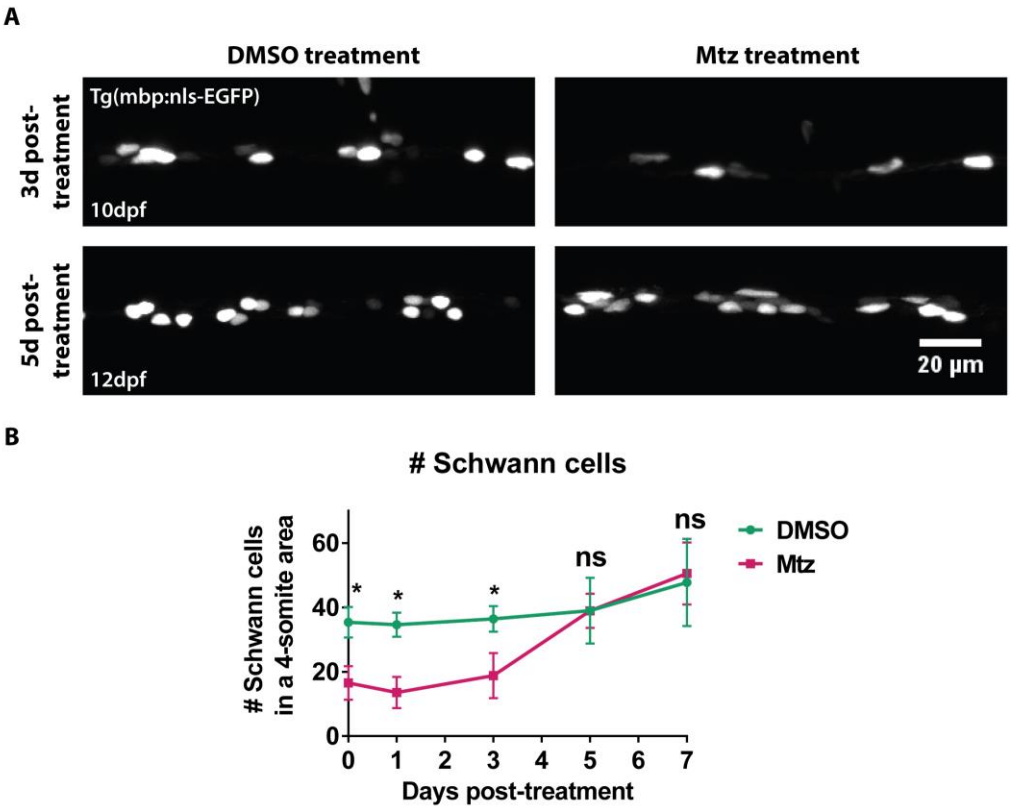

Figure 39. Schwann cell numbers are restored to control levels by 5d post-treatment **A**. Confocal images of the pLL from 10dpf and 12dpf control and Mtz-treated larvae, as indicated. **B**. Schwann cell counts indicate that there are significantly fewer Schwann cells in Mtz-treated compared to control larvae at 0d, 1d and 3d post-treatment, but no significant difference at 5d and 7d post-treatment. At 0d post-treatment, there is a mean of 35.36 ± 4.72 Schwann cells in control animals, compared to 16.53 ± 5.18 in Mtz-treated animals, $p < 0.0001$. At 1d post-treatment, there is a mean of 34.64 ± 3.78 Schwann cells in control animals, compared to 13.57 ± 4.85 in Mtz-treated animals, $p < 0.0001$. At 3d post-treatment, there is a mean of 36.40 ± 3.97 Schwann cells in control animals, compared to 18.80 ± 7.01 in Mtz-treated animals, $p = 0.0012$. By 5d post-treatment, there is a mean of 39.0 ± 10.23 Schwann cells in control animals and 38.94 ± 5.32 in Mtz-treated animals ($p = 0.984$) and at 7d post-treatment, there is a mean of 47.77 ± 13.56 Schwann cells in control animals and 50.57 ± 9.62 in Mtz-treated animals ($p = 0.635$). Statistical significance was determined using the Holm-Sidak method without assuming constant SD. n = no less than 5, usually over 10.

5.6. Mitochondria in pLL axons over demyelination and remyelination

5.6.1. There is no increase in mitochondria numbers at demyelinated stages

The above described results indicate that following Mtz-induced ablation of approximately half of Schwann cells, axons in the PNS undergo rapid demyelination, showing a 56% reduction in the number of myelinated axons by one day post-treatment. The larvae then mount a regenerative response, such that by 5d post-treatment, Schwann cell numbers have been restored to control levels and full remyelination is evident at 7d post-treatment, complete with myelin thickness restored to normal levels.

This timeline leaves a period of up to a week between the axons undergoing demyelination and having their myelin sheaths restored. Much like with demyelination in the CNS, I was interested to see whether this state of demyelination prompted any changes in the mitochondrial presence in the axons.

In order to investigate this possibility, I counted the numbers of mitochondria within axons at the different time points. For this analysis, I focused exclusively on the "large-calibre axons, (this was again defined as the size of the smallest myelinated axon in a control larva in the same experimental clutch) as changes in mitochondria within small axons that were never myelinated in the first place could not be attributed to the effects of demyelination. As shown in **Figure 40**, at 1d post-treatment, when 56% of the large calibre axons were demyelinated, I found no significant difference between Mtz-treated and control animals in the numbers of mitochondria inside these axons, whether myelinated or unmyelinated: the mean number of mitochondria within myelinated axons was 0.97 ± 0.56 in the peripheral nerves of control animals and 1.17 ± 0.89 in Mtz-treated animals, while the mean number of mitochondria in unmyelinated axons was 0.65 ± 0.69 in control animals and 0.29 ± 0.09 in Mtz-treated animals. A two-way ANOVA found the main effects of myelination status ($p = 0.055$) and treatment condition ($p = 0.779$) as well as the interaction ($p = 0.347$) non-significant (**Figure 40B**).

The result was very similar when I counted mitochondria within large-calibre axons at 3d post-treatment: although demyelination was still widespread at this time point, there were no differences between the numbers of mitochondria in control and Mtz-treated animals, or between myelinated and unmyelinated axons: the mean number of mitochondria within myelinated axons was 1.19 ± 0.53 in control animals and 1.72 ± 1.01 in Mtz-treated animals, while the mean number of mitochondria within unmyelinated axons was 0.97 ± 0.84 in control animals and 1.27 ± 1.56 in Mtz-treated animals. A two-way ANOVA found the main effects of myelination status ($p = 0.486$) and treatment condition ($p = 0.388$) as well as the interaction ($p = 0.815$) non-significant (**Figure 40C**).

Thus, it appears that there are no adaptive changes to the numbers of mitochondria during the demyelinated stages.

A

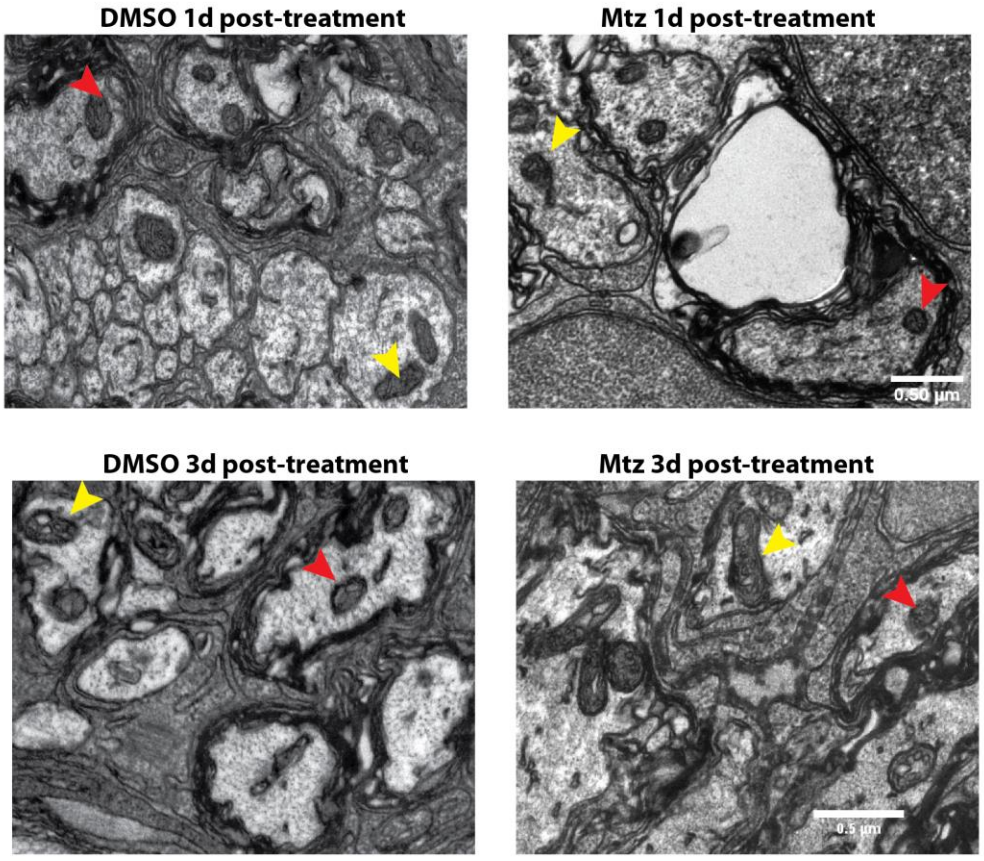

Quantification overleaf

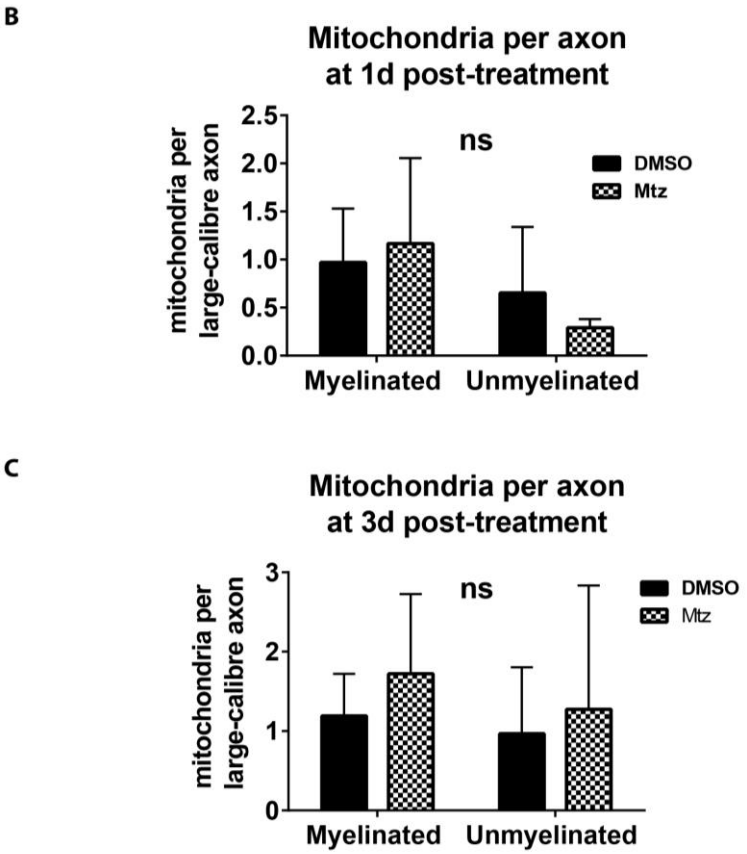

Figure 40. There are no changes in mitochondria numbers between control and Mtz-treated animals at the demyelinated stages. A. TEM images from peripheral nerves of 8dpf and 10dpf larvae (1d and 3d post-treatment, respectively), treated with DMSO or Mtz, as indicated. Red arrowheads indicate mitochondria within myelinated axons, yellow arrowheads within unmyelinated axons. **B**. Quantification of mitochondria numbers within large-calibre axons at 1d post-treatment shows that within myelinated axons, there is a mean of 0.97 ± 0.56 mitochondria in control animals and 1.17 ± 0.89 in Mtz-treated animals, while within unmyelinated axons the mean number of mitochondria is 0.65 ± 0.69 in control animals and 0.29 ± 0.09 in Mtz-treated animals. A two-way ANOVA finds the main effects of myelination status ($p = 0.055$) and treatment condition ($p = 0.779$) as well as the interaction ($p = 0.347$) non-significant. n = 4 for DMSO, 6 for Mtz. **C.** Quantification of mitochondria within large-calibre axons shows the mean number of mitochondria within myelinated axons is 1.19 ± 0.53 in control animals and 1.72 ± 1.01 in Mtz-treated animals, while the mean number of mitochondria within unmyelinated axons is 0.97 ± 0.84 in control animals and 1.27 ± 1.56 in Mtz-treated animals. A two-way ANOVA finds the main effects of myelination status ($p = 0.486$) and treatment condition ($p = 0.388$) as well as the interaction ($p = 0.815$) non-significant. n = 5 (scale bar = 0.5 μm)

5.6.2. There are no differences in the numbers of mitochondria between Mtz-treated and control animals at the remyelinated stage (7d post-treatment).

Counts of mitochondria within large calibre axons at the demyelinated stages (1d and 3d post-treatment) did not find any differences between Mtz-treated and control animals, or between myelinated and unmyelinated axons. In this regard, the results in the PNS closely resemble those seen in the CNS. With this in mind, and knowing there were intriguing differences in mitochondria numbers at the remyelinated stage (16d post-treatment in the CNS), I proceeded to count mitochondria in large calibre PNS axons at the remyelinated stage (7d post-treatment). This analysis showed that there are more mitochondria in myelinated than in unmyelinated axons, but that there are no differences between control and Mtz-treated animals (**Figure 41**): the mean number of mitochondria within myelinated axons was 0.91 ± 0.21 in control animals and 0.77 ± 0.18 in Mtz-treated animals, while the mean number of mitochondria within unmyelinated axons was 0.44 ± 0.37 in control animals and 0.48 ± 0.38 in Mtz-treated animals. A two-way ANOVA found the main effect of myelination status ($p = 0.0091$) significant, but the main effect of treatment condition ($p = 0.692$) and the interaction ($p = 0.500$) non-significant (**Figure 41B**).

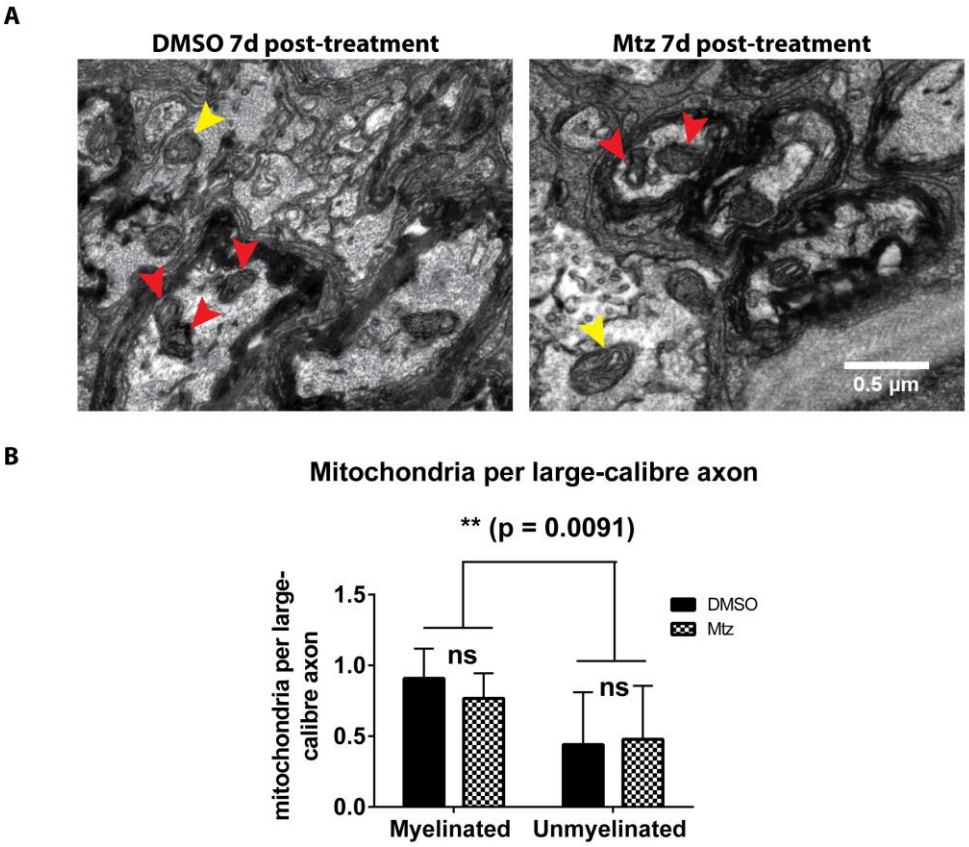

Figure 41. There are no differences in mitochondria numbers between control and Mtz-treated animals at the remyelinated stage. A. TEM images from peripheral nerves of 14dpf larvae, treated with either DMSO or Mtz, as indicated. Red arrowheads indicate mitochondria within myelinated axons, yellow arrowheads within unmyelinated axons. **B**. Quantification of mitochondria within axons of "myelinateable" sizes shows that the mean number of mitochondria within myelinated axons is 0.91 ± 0.21 in control animals and 0.77 ± 0.18 in Mtz-treated animals, while the mean number of mitochondria within unmyelinated axons is 0.44 ± 0.37 in control animals and 0.48 ± 0.38 in Mtz-treated animals. A two-way ANOVA found the main effect of myelination status ($p = 0.0091$) significant, but the main effect of treatment condition ($p = 0.692$) and the interaction ($p = 0.500$) non-significant. n = 6 for DMSO, 5 for Mtz.

5.6.3. The average size of a mitochondrion is not different between control and Mtz-treated animals at the remyelinated stage

Even though there were no differences in the numbers of mitochondria between control and Mtz-treated animals at 7d post-treatment, I was interested in whether there were differences in the sizes of mitochondria at this time point. This was a pertinent question because in the CNS, I had observed smaller mitochondria in Mtz-treated compared to control axons (and also smaller mitochondria in myelinated compared to unmyelinated axons) at the remyelinated stage.

I therefore measured the areas of mitochondria in myelinated and unmyelinated large-calibre axons in the pLLs of control and Mtz-treated animals. This analysis, shown in **Figure 42**, indicated that there were no differences in the sizes of mitochondria, either between control and Mtz-treated animals or between myelinated and unmyelinated axons: the mean area of a mitochondrion in a myelinated axon 0.075± 0.017μm² in control animals and 0.067 ± 0.023 μm² in Mtz-treated animals, while the mean area of a mitochondrion in an unmyelinated axon was 0.054 ± 0.012 μm² in control animals and 0.058 ± 0.022 μm² in Mtz-treated animals. A two-way ANOVA found the main effects of myelination status and treatment condition, as well as the interaction, non-significant ($p = 0.110$, $p = 0.815$ and $p = 0.506$, respectively).

Thus, it appears that there are no adaptive changes to the numbers or sizes of mitochondria during demyelination or remyelination in the pLL.

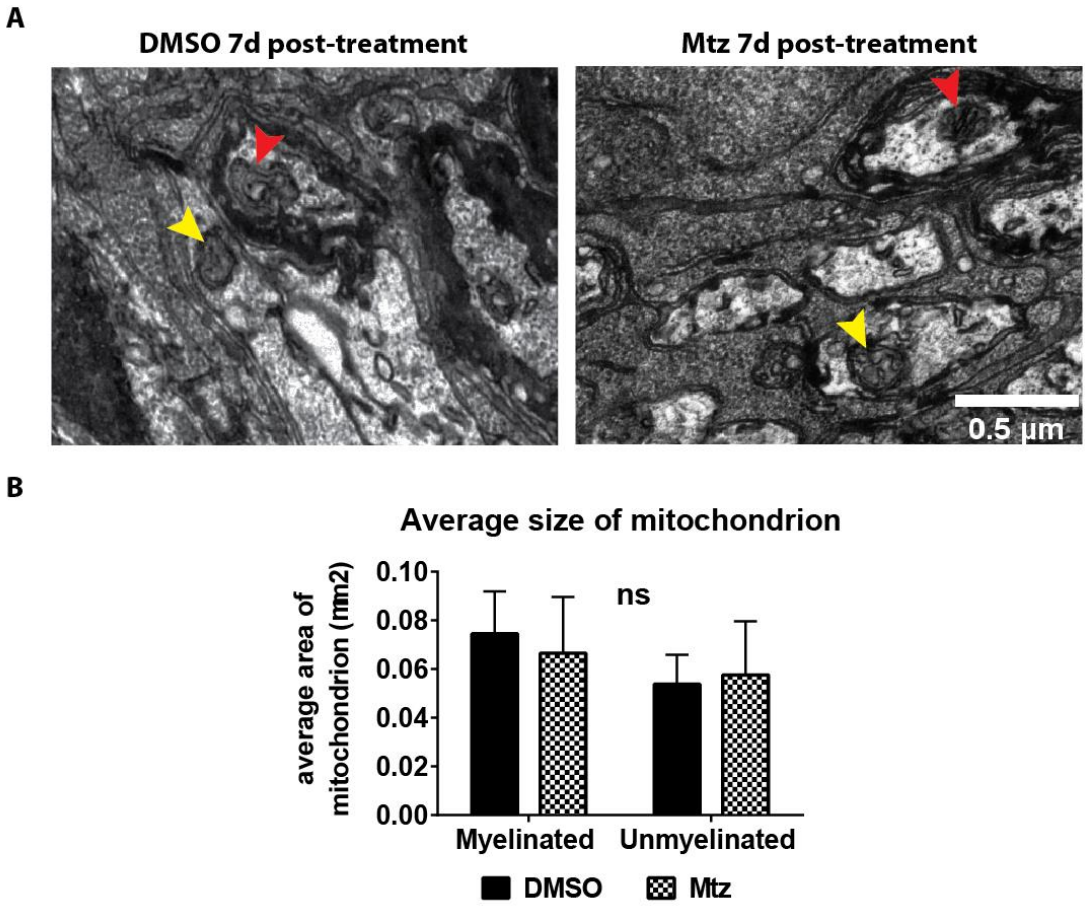

Figure 42. The average size of a mitochondrion is not different between control and Mtz-treated animals or myelinated and unmyelinated axons at 7d post-treatment. A. TEM images from peripheral nerves of 14dpf larvae. Red arrowheads indicate mitochondria within myelinated axons, yellow within unmyelinated. **B**. Comparison of the mean areas of mitochondria shows that there is no difference in mitochondrial size between control and Mtz-treated animals, nor between myelinated and unmyelinated axons: mean area of a mitochondrion in a myelinated axon is 0.075 ± 0.017µm² in control animals and 0.067 ± 0.023 µm² in Mtz-treated animals, while the mean area of a mitochondrion in an unmyelinated axon is 0.054 ± 0.012 µm² in control animals and 0.058 ± 0.022 µm² in Mtz-treated animals. A two-way ANOVA found the main effects of myelination status and treatment condition as well as the interaction non-significant ($p = 0.110$, $p = 0.815$ and $p = 0.506$, respectively). n = 6 for DMSO, 5 for Mtz.

5.7. Calibres of pLL axons at the remyelinated stage

5.7.1. Peripheral axon calibres do not differ between control and Mtz-treated animals or between myelinated and unmyelinated axons at 7d post-treatment.

Next, I was interested to see whether peripheral axons responded to becoming demyelinated by adjusting their cross-sectional sizes.

To compare axon sizes of control and treated larvae as well as myelinated and unmyelinated axons, I measured the perimeters of all "myelinateable"-sized axons in the peripheral nerves. The results, shown in **Figure 43**, indicated that there were no differences in axon size between either control and treated larvae or between myelinated and unmyelinated axons: the mean perimeter of a myelinated axon was 3.10 ± 0.26μm in control animals and 2.83 ± 0.30μm in Mtz-treated animals, while the mean perimeter of an unmyelinated axon was 2.64 ± 0.39μm in control animals and 2.64 ± 0.57μm in Mtz-treated animals. The lack of significant difference was supported by a two-way ANOVA, which found both the main effect of treatment condition ($p = 0.435$) and the main effect of myelination status ($p = 0.076$), as well as the interaction ($p = 0.448$) to be non-significant. Thus, it seems that pLL axons do not change in calibre in response to Schwann cell ablation.

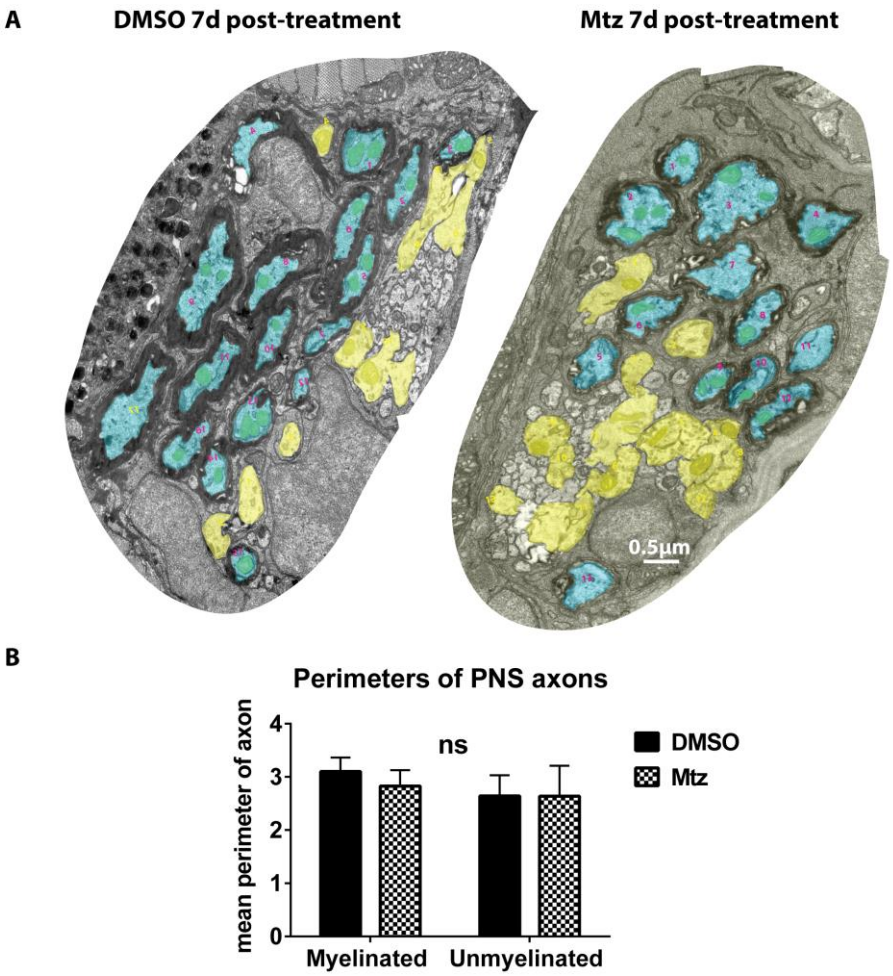

Figure 43. Axon sizes do not differ between control and Mtz-treated animals or between myelinated and unmyelinated axons at 7d post-treatment. A. TEM images of entire peripheral nerves of 14dpf larvae, treated with DMSO or Mtz, as indicated. Myelinated axons are shaded in turquoise and unmyelinated axons in yellow. **B**. Quantification of axon perimeters shows that there are no differences in axon sizes between control and Mtz-treated animals, or between myelinated and unmyelinated axons: the mean perimeter of a myelinated axon is 3.10 ± 0.26µm in control animals and 2.83 ± 0.30µm in Mtz-treated animals, while the mean perimeter of an unmyelinated axon is 2.64 ± 0.39µm in control animals and 2.64 ± 0.57µm in Mtz-treated animals. A two-way ANOVA found both the main effect of treatment condition ($p = 0.435$) and myelination status ($p = 0.076$) as well as the interaction ($p = 0.448$) to be non-significant. $n = 6$ for DMSO, 5 for Mtz.

5.8 Macrophage response in the PNS

5.8.1. Macrophage response to Schwann cell ablation begins at 1d post-treatment.

In **Chapter 4** of this thesis, I described the response of the innate immune system to oligodendrocyte ablation and CNS demyelination. To recap, an increase in mpeg-expressing microglia and macrophages in Mtz-treated larvae is observed at 3d post-treatment, peaks at 4d post-treatment and fades out by 9d post-treatment.

Given the findings in this chapter that the time course of demyelination and remyelination is more rapid in the PNS than in the CNS, one would expect that the immune response to Schwann cell ablation and PNS demyelination would also be swift and efficient. In addition, previous studies have also reported very rapid responses of macrophages to peripheral nerve injury in mammals and zebrafish (Cattin et al. 2015; Rosenberg et al. 2012), although these responses were elicited by injury to the entire nerve, so whether a similar response would follow primary Schwann cell death was not known.

In order to investigate how macrophages response to Schwann cell death, I carried out a time course experiment. I again crossed Tg(mbp:mCherry-NTR) fish to Tg(mpeg:GFP) fish and treated the resulting double transgenic progeny with either DMSO or Mtz. I then imaged a subset of larvae directly after the treatment, and others at various time points post-treatment. Representative images from the different time points are presented in **Figure 44A**: these images suggest that while there was a notable baseline presence of mpeg+ cells in the PNS even in control animals, from the very first time point, there were more mpeg+ cells in Mtz-treated than in control animals. From 1d post-treatment to 4d post-treatment, many immune cells can be seen in direct contact with the lateral line (red arrowheads).

As in the spinal cord images, it is important to note that in a maximum intensity projection, such as the images shown in **Figure 44A**, an immune cell may appear to be in contact with the pLL, but upon viewing each z section on its own, the two structures may turn out not to be in the same focal plane. For this reason, I quantified the numbers of immune cells by counting the mpeg+ cells that overlapped with the

lateral line in individual 2µm thick confocal z sections. As before, the counts were made from images depicting a four-somite long stretch of the pLL. The resulting timeline (**Figure 44B**) indicated that at 0d post-treatment, there was a mean of 3.40 ± 1.84 mpeg+ cells in contact with the pLL in control animals and 5.40 ± 1.84 in Mtz-treated animals, $p = 0.045$. At 1d post-treatment, however, the number of mpeg+ cells in contact with the pLL had increased to a mean of 6.36 ± 2.77 in Mtz-treated animals, compared to 3.13 ± 1.36 in control animals ($p = 0.0022$). The numbers of mpeg+ cells in contact with the pLL continued to increase at 3d post-treatment and 4d post-treatment in both control and Mtz-treated animals (5.60 ± 2.07 and 6.25 ± 3.95 cells in control animals 10.33 ± 2.31 and 10.50 ± 3.11 cells in Mtz-treated animals, $p = 0.0042$ and $p = 0.0078$, respectively). By 5d post-treatment, the number of mpeg+ cells in the PNS of Mtz-treated animals had descended to the level of controls, (a mean of 6.67 ± 1.21 cells in control animals, compared to 9.33 ± 2.08 in Mtz-treated animals, $p = 0.089$) suggesting that the immune invasion was over. This was not altogether surprising, given that only two days later, the peripheral nerve is fully remyelinated and that Schwann cell numbers have been restored to control levels at this point.

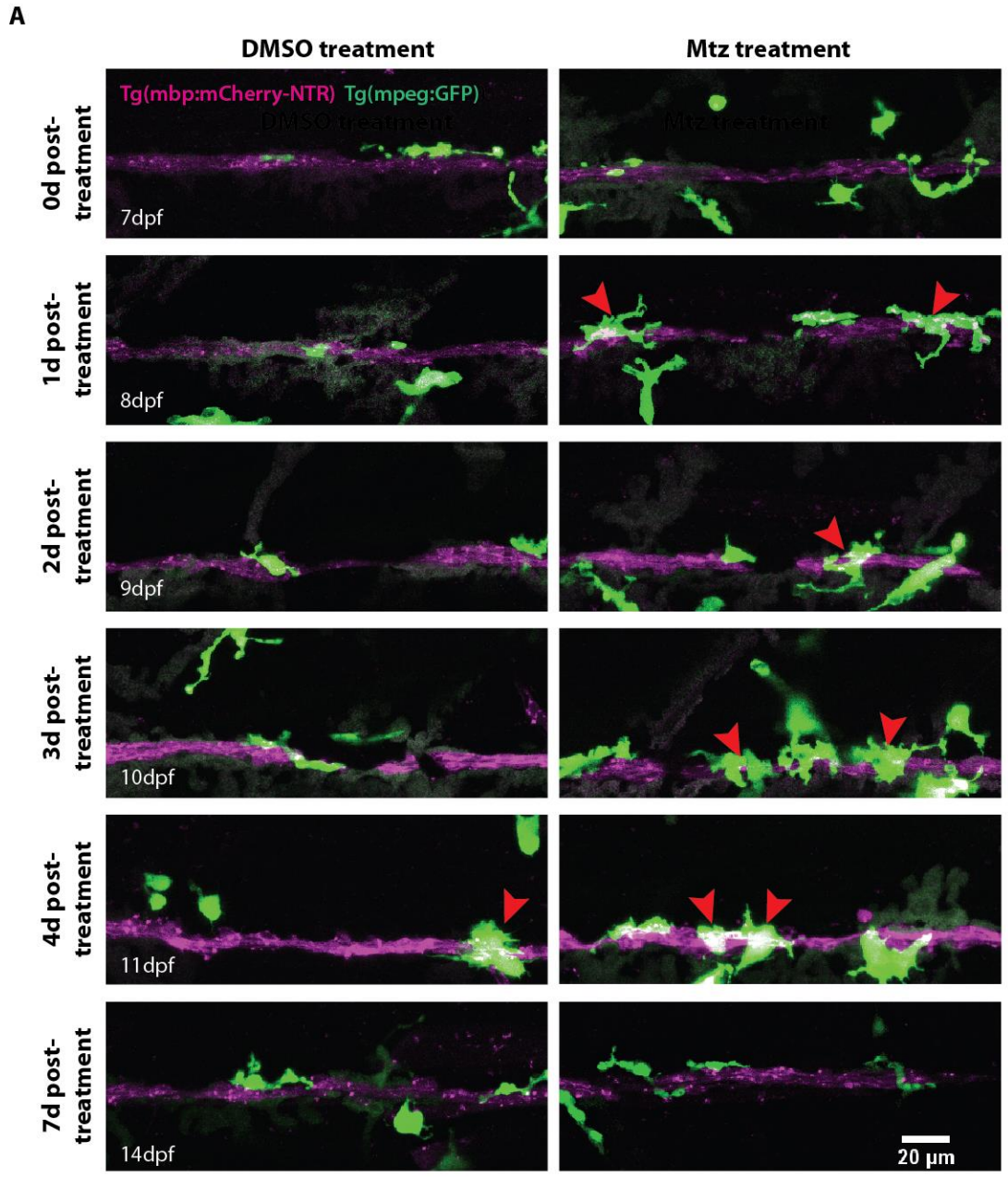

Quantification overleaf

B

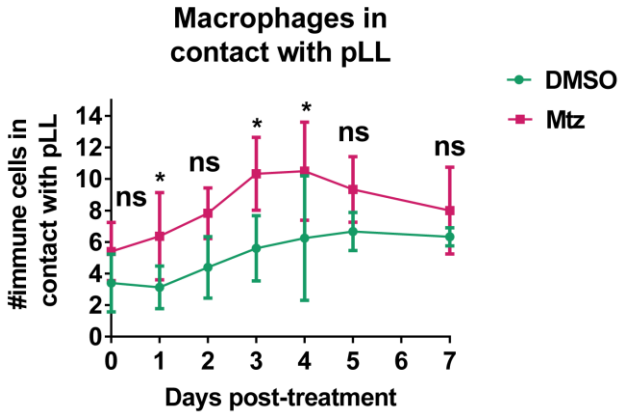

Figure 44. A macrophage response to Schwann cell death is observed immediately after Mtz-treatment and is over by 5d post-treatment. A. Confocal images from peripheral nerves of larvae at 7-14dpf, treated with either DMSO or Mtz, as indicated, showing mpeg-expressing macrophages in green, and mbp-expressing Schwann cells and myelin sheaths in magenta. At 1-4d post-treatment, there are more mpeg+ cells in Mtz-treated than in DMSO-treated animals. **B**. Quantification shows that at 0d post-treatment, there is a mean of 3.40 ± 1.84 mpeg+ cells in contact with the pLL in control animals and 5.40 ± 1.84 in Mtz-treated animals, p = 0.045. At 1d post-treatment, the number of mpeg+ cells in contact with the pLL increases to a mean of 6.36 ± 2.77 in Mtz-treated animals, compared to 3.13 ± 1.36 in control animals (p = 0.0022). The numbers of mpeg+ cells in contact with the pLL continued to increase at 3d post-treatment and 4d post-treatment in both control and Mtz-treated animals (5.60 ± 2.07 and 6.25 ± 3.95 cells in control animals 10.33 ± 2.31 and 10.50 ± 3.11 cells in Mtz-treated animals, p = 0.0042 and p = 0.0078, respectively; both significant). By 5d post-treatment, the number of mpeg+ cells in the PNS of Mtz-treated animals had descended to the level of controls, (a mean of 6.67 ± 1.21 cells in control animals, compared to 9.33 ± 2.08 in Mtz-treated animals, p = 0.089) n = no less than 3.

5.8.2. Macrophages containing mCherry+ material are seen from 1d post-treatment

Having observed the rapid response of the innate immune system to Schwann cell ablation, I next investigated whether macrophages also phagocytosed myelin debris in the peripheral nerve, as I had seen them do in the spinal cord. To this end, I reanalysed the data set from **Figure 44**, and counted only those mpeg+ cells that clearly contained within them mbp+ material (examples are highlighted with red arrowheads in Figure **45A**). This analysis suggested that at every time point examined, there seemed to be more mpeg+ cells containing mbp+ material in Mtz-treated than control animals, but

at no time point did this difference reach statistical significance: at 1d post-treatment, there was a mean of 0 mpeg+ cells containing mbp+ material in control larvae and 1.5 ± 1.29 in Mtz-treated larvae, p = 0.451. At 2d post-treatment, there were 0.75 ± 0.96 such cells in control animals and 1.0 ± 2.0 in Mtz-treated, p = 0.81. At 3d post-treatment, there were 0.75 ± 0.96 in control animals and 2.0 ± 3.46 in Mtz-treated animals, p = 0.272. At 4d post-treatment, there were 1.5 ± 1.29 in control animals and 2.5 ± 1.73 in Mtz-treated animals, p = 0.342. At 5d post-treatment, there were 0.67 ± 0.52 in control animals and 2.33 ± 2.08 in Mtz-treated animals, p = 0.116. At 7d post-treatment, there were 1.67 ± 2.08 in control animals and 2.33 ± 1.37 in Mtz-treated animals, p = 0.525 (**Figure 45B**).

It is likely that the high level of variability in both the DMSO and Mtz-treated conditions accounts for the lack of statistical significance. In addition, it is well established that Schwann cells themselves are able to perform phagocytosis of myelin debris (Vargas and Barres 2007; Gordon 2016) and it is possible that the some of the 47% of Schwann cells that was not ablated by the Mtz-treatment carried out phagocytosis, thus reducing the number of macrophages required for the task.

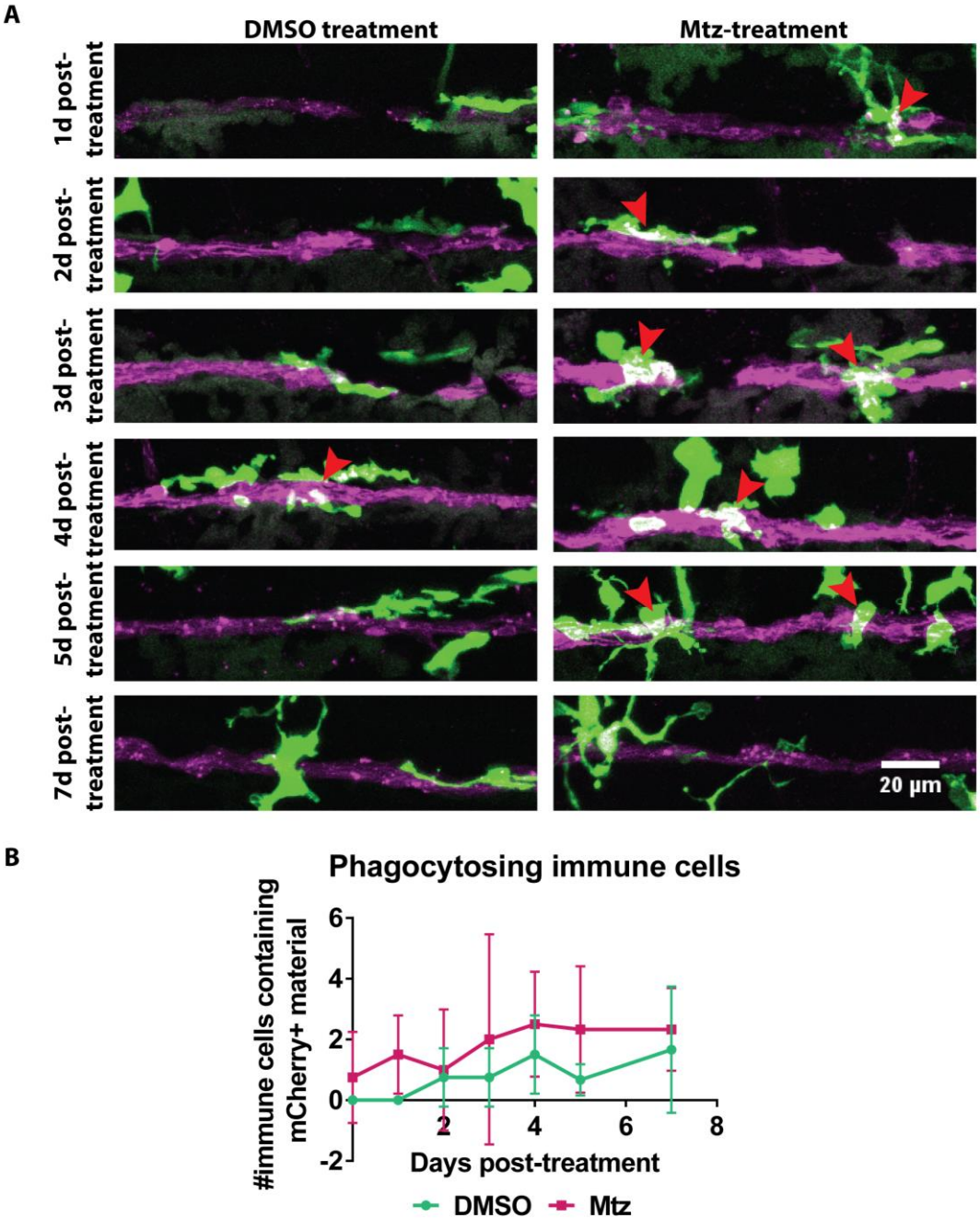
A
DMSO treatment
Mtz-treatment
1d post-treatment
2d post-treatment
3d post-treatment
4d post-treatment
5d post-treatment
7d post-treatment
20 µm
B
Phagocytosing immune cells
#immune cells containing mCherry+ material
6
4
2
0
-2
2
4
6
8
Days post-treatment
DMSO
Mtz

Figure 45. Immune cells phagocytose mCherry+ material from 0d post-treatment. **A**. Confocal images from peripheral nerves of larvae at 8-14dpf, showing mpeg-expressing mpeg+ immune cells in contact with the pLL. Immune cells containing mbp+ material are indicated with red arrowheads. **B**. Quantification shows that there are mpeg+ cells containing mbp+ material in both control and Mtz-treated larvae, but there increase in Mtz-treated animals does not reach statistical significance at any time point. At 1d post-treatment, there was a mean of 0 mpeg+ cells containing mbp+ material in control larvae and 1.5 ± 1.29 in Mtz-treated larvae, p = 0.451. At 2d post-treatment, there were 0.75 ± 0.96 such cells in control animals and 1.0 ± 2.0 in Mtz-treated, p = 0.81. At 3d post-treatment, there were 0.75 ± 0.96 in control animals and 2.0 ± 3.46 in Mtz-treated animals, p = 0.272. At 4d post-treatment, there were 1.5 ± 1.29 in control animals and 2.5 ± 1.73 in Mtz-treated animals, p = 0.342. At 5d post-treatment, there were 0.67 ± 0.52 in control animals and 2.33 ± 2.08 in Mtz-treated animals, p = 0.116. At 7d post-treatment, there were 1.67 ± 2.08 in control animals and 2.33 ± 1.37 in Mtz-treated animals, p = 0.525. n = no less than 3.

5.9 Peripheral nerve remyelination in irf8 mutant animals

5.9.1. Irf8 null larvae are able to remyelinate their peripheral nerves.

Having seen that macrophages respond swiftly to Schwann cell ablation, I wished to determine whether animals where this response is impaired could remyelinate their axons. In order to investigate this, I used the same dataset as in **Chapter 4**. Thus, the animals were 23dpf, well above the age where I see remyelination in the peripheral nerves. This was because the experiments using the irf8 mutant fish were performed very late during my studies, and I was not able to carry out a specific experiment to examine the effects of the irf8 mutation on PNS remyelination.

Representative peripheral nerves from DMSO-treated non-mutants, Mtz-treated non-mutants and Mtz-treated irf8 mutants are presented in **Figure 46A**; they appear indistinguishable from each other.

To quantify the apparent remyelination in these peripheral nerves, I counted the total number of myelinated axons, calculated the percentage of all axons that was myelinated, and the percentage of large-calibre axons that was myelinated. This

analysis, shown in **Figure 46B – D**) indicated that there were no differences between the groups in any of the parameters: in the total number of myelinated axons there was a mean of 38.33 ± 7.37 myelinated axons in DMSO-treated non-mutants, 43.33 ± 7.97 in Mtz-treated non-mutants and 39.20 ± 5.07 in Mtz-treated mutants. A one-way ANOVA found the difference between the groups non-significant ($p = 0.507$). Quantification of the percentage of all axons that is myelinated showed that a mean of 33.17 ± 0.67% of all axons was myelinated in DMSO-treated non-mutants, 33.85 ± 4.61% in Mtz-treated non-mutants, and 31.06 ± 1.82% in Mtz-treated mutants. A one-way ANOVA found the difference between the groups non-significant ($p = 0.370$). Finally, quantification of the percentage of large-calibre axons that is myelinated showed that 95.17 ± 6.33% of large-calibre axons is myelinated in DMSO-treated non-mutants, 97.40 ± 2.34% in Mtz-treated non-mutants, and 96.80 ± 2.51% in Mtz-treated mutants. A one-way ANOVA found the difference between the groups non-significant ($p = 0.658$).

A

DMSO (WT)
16d post-treatment

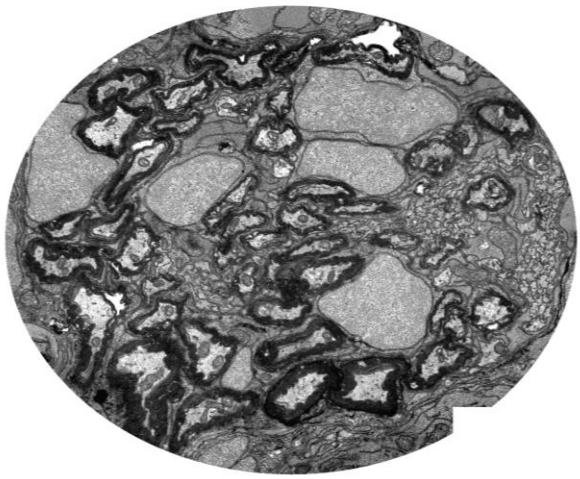

Mtz (WT)
16d post-treatment

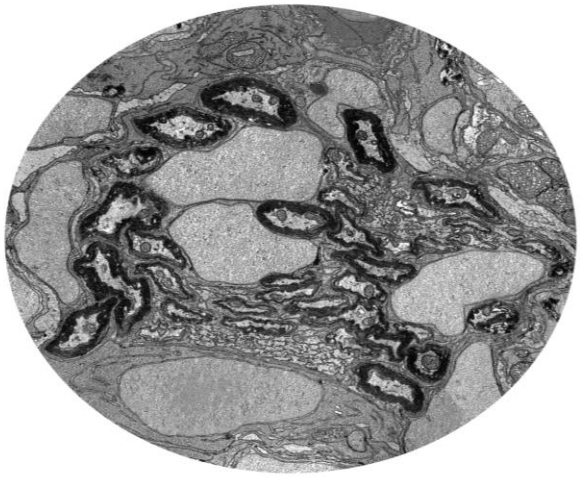

Mtz (mutant)
16d post-treatment

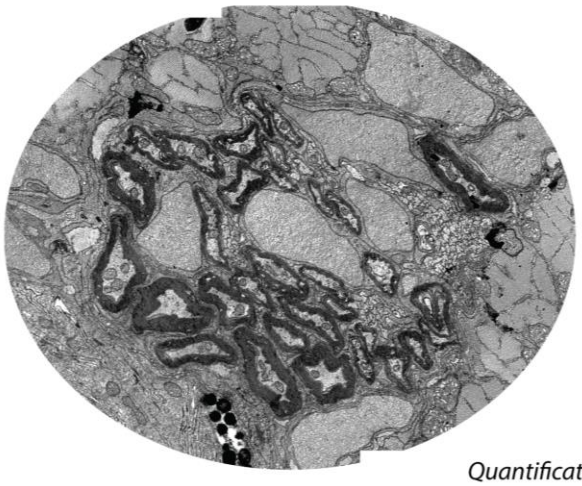

Quantification overleaf

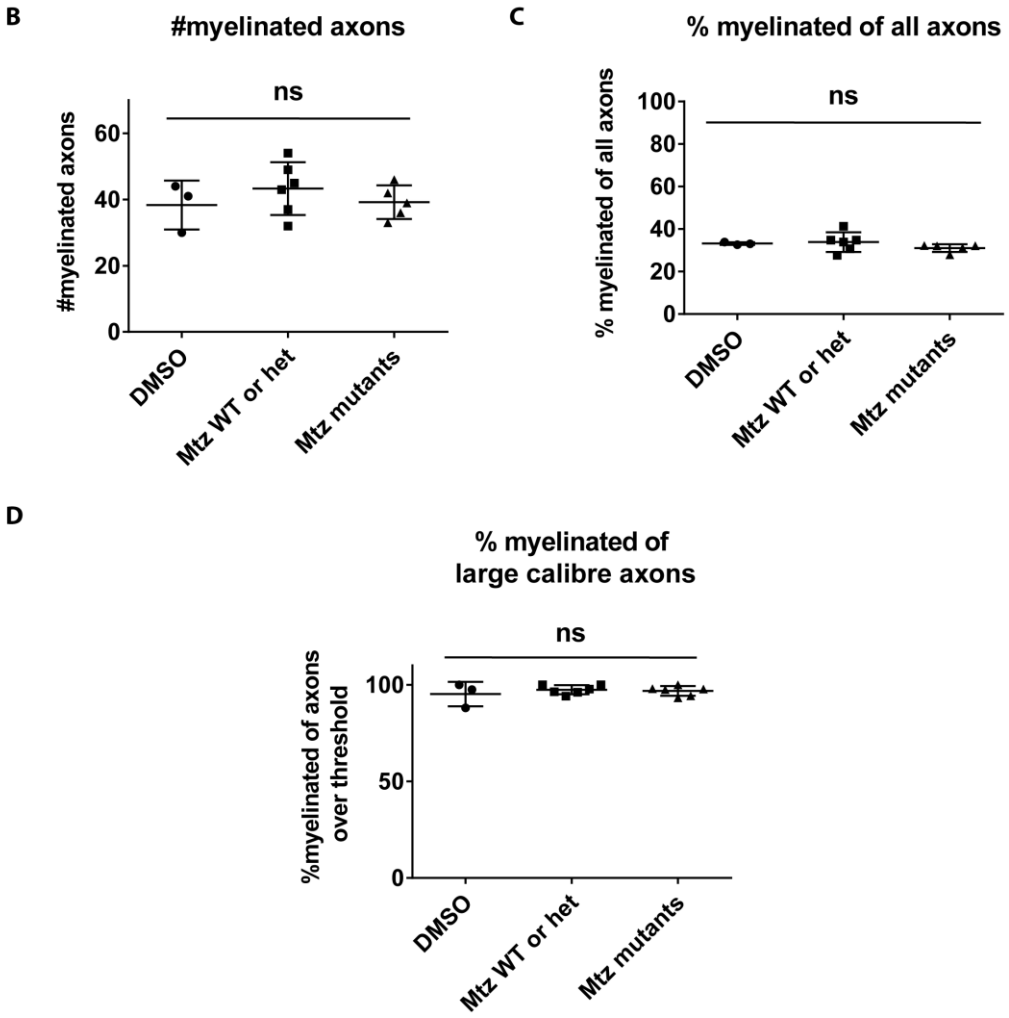

Figure 46. Irf8 mutants have remyelinated their peripheral nerves by 16d post-treatment. **A**. TEM images of peripheral nerves of 23dpf larvae, treated with DMSO or Mtz, and carrying wild-type or mutant alleles of irf8, as indicated. All three nerves appear indistinguishable from each other. **B**. Quantification of the total number of myelinated axons shows that there is a mean of 38.33 ± 7.37 myelinated axons in DMSO-treated non-mutants, 43.33 ± 7.97 in Mtz-treated non-mutants and 39.20 ± 5.07 in Mtz-treated mutants. A one-way ANOVA found the difference between the groups non-significant ($p = 0.507$). **C**. Quantification of the percentage of all axons that is myelinated shows that a mean of 33.17 ± 0.67% of all axons are myelinated in DMSO-treated siblings, 33.85 ± 4.61% in Mtz-treated non-mutants, and 31.06 ± 1.82% in Mtz-treated mutants. A one-way ANOVA found the difference between the groups non-significant ($p = 0.370$). **D**. Quantification of the percentage of large-calibre axons that is myelinated shows that 95.17 ± 6.33% of large-calibre axons is myelinated in DMSO-treated non-mutants, 97.40 ± 2.34% in Mtz-treated non-mutants, and 96.80 ± 2.51% in Mtz-treated mutants. A one-way ANOVA found the difference between the groups non-significant ($p = 0.658$). n = 3 for DMSO-treated non-mutants, 6 for Mtz-treated non-mutants and 5 for Mtz-treated mutants.

These data demonstrate that irf8 mutant larvae are not impaired at remyelinating their peripheral nerves, just as they are not impaired at remyelinating their spinal cords

(**Figures 27** and **28**). It is essential to note, however, that this analysis was made at 16d post-treatment, so remains possible that irf8 null larvae experienced a delay in the remyelination of their peripheral nerves, compared to wild-type larvae which show full remyelination at 7d post-treatment, but had achieved the task by 16d post-treatment. This possibility should be investigated in the future.

5.10. Discussion

In this chapter, I described how the Tg(mbp:mCherry-NTR) line induced Schwann cell ablation and subsequent PNS demyelination and remyelination using the posterior lateral line nerve (pLL) as a model. I showed that a two-day treatment with 5mM metronidazole from 5 to 7 days post-fertilisation ablates approximately half (53%) of the myelinating Schwann cells of the pLL, and this results in approximately half (56%) of the large-calibre axons in the nerve at 7dpf becoming demyelinated. By 5d post-treatment, Schwann cell numbers have been restored to control levels, and by 7d post-treatment, full remyelination of the peripheral nerve is seen, complete with normal thickness of myelin sheaths relative to control.

I did not observe any changes in mitochondria numbers or size between control and Mtz-treated animals at either the demyelinated (1d and 3d post-treatment) or the remyelinated (7d post-treatment) stage. There are also no differences in axon calibre either between control and treated at any stage throughout my analysis.

A macrophage response to Schwann cell ablation was observed from 1d post-treatment, which peaked at 3d and 4d post-treatment, and resolved by 5d post-treatment, at which time macrophage numbers associated with the pLL nerve had returned to control levels.

Thus, the response to primary Schwan cell ablation in this model seems to be rapid demyelination followed by rapid restoration of Schwann cells and rapid remyelination, without adaptive changes to axons, at least at the stages examined.

5.10.1. Demyelination and remyelination occur more rapidly in the PNS than in the CNS

It is notable that at 7d post-treatment, when the spinal cord is in its peak demyelination stage, the pLL nerve has already undergone complete remyelination. In addition, the numbers of Schwann cells are restored to control levels within five days following

ablation, whereas oligodendrocyte cell numbers in Mtz-treated larvae do not reach control levels at any stage I have examined so far.

This efficient time course of Schwann cell and myelin regeneration was not altogether unexpected, given that the PNS is well known to possess a greater capacity for repair and regeneration than the CNS (Vargas and Barres, 2007; Gordon, 2016). I will discuss the results presented in this chapter in the context of the speed of the regenerative response, discuss potential reasons which contribute to such fast regeneration, and the consequences of the speed to axon health and future usefulness of the model.

A key reason for the rapidity of the time course of PNS regeneration in this model is that the pLL is in a relatively early stage of normal development and myelination at the stages that demyelination and remyelination occurred. This is evident from the rates of growth observed in both the control and Mtz-treated animals: ultrastructural analyses of the pLL nerve show that in control animals, the mean total number of all axons (with a perimeter of over 1.2µm) increases from 42.25 ± 20.39 at 1d post-treatment (8dpf) to 91.17 ± 29.28 at 7d post-treatment (14dpf). In Mtz-treated animals, too, the mean total number of axons rises from 45.0 ± 12.44 at 1d post-treatment to 100.80 ± 41.95 at 7d post-treatment. These increases in total axon numbers in both control and treated animals reflect the rapid ongoing growth of the pLL nerve over the time points examined, irrespective of the Mtz-treatment.

Importantly, the number of myelinated axons also increases significantly in both control and Mtz-treated pLLs over the course of the remyelination period: in control animals, from a mean of 9.0 ± 4.69 at 1d post-treatment to 26.33 ± 8.47 at 7d post-treatment, and in Mtz-treated animals, from a mean of 4.0 ± 1.67 at 1d post-treatment to 25.0 ± 15.28 at 7d post-treatment. Thus, the majority of the myelinated axons present in the pLL at 7d post-treatment were born and myelinated after the Mtz-treatment, and thus only a minority actually represent remyelinated axons, or remyelinated segments of axon. With first-time myelination so prevalent in the pLL, those axons that were demyelinated as a result of Schwann cell ablation, were likely quickly remyelinated alongside the newly myelinated axons.

Very interestingly, however, myelinating Schwann cell numbers do not increase as sharply over the same time period: in control animals they go from 36.36 ± 4.72 at 0d post-treatment to 47.77 ± 13.56 at 7d post-treatment, and in Mtz-treated animals, Schwann cells go from 16.53 ± 5.18 at 0d post-treatment to 50.57 ± 9.62 at 7d post-treatment. This apparent discrepancy is likely explained by the fact that individual myelinating Schwann cells grow significantly in length over this period of maturation. EM analyses are made from cross-sections that do not capture how Schwann cells contribute to myelination along the length of the nerve. In the future, it will be important to assess myelinating Schwann cell growth over this period of time, as well as to investigate how individual axons are myelinated over time. This could be achieved by using the GFP-Contactin1A reporter developed by our lab that allows analysis of myelin sheath number and length along axons over time, as described in **Chapter 3** discussion (Koudelka et al. 2016).

Given the strong influence that the background of ongoing normal development is likely to have on remyelination in the PNS, it may be beneficial to begin the Mtz-treatment at a later stage, perhaps at nearer to 23dpf, since I still observed a notable increase in the numbers of myelinated axons between 14dpf and 23dpf (the age when I analysed the peripheral nerves of irf8 mutants and their siblings; **Figure 5.16**). In this way, one would be much better able to assess the regenerative response in the pLL nerve without such a prominent confound of ongoing development. Live imaging of the pLL nerve in older larvae may be more feasible than live imaging of the spinal cord in older larvae, since the pLL nerve is located on the surface of the animal.

However, the fact remains that half of the axons that were already myelinated by 8dpf were demyelinated as a result of Schwann cell ablation. This comprises on average 5 axons per Mtz-treated pLL nerve (based on a mean of 9 myelinated axons in control animals and 4 in Mtz-treated animals at 1d post-treatment), so approximately 1/5 of the myelinated axons seen in Mtz-treated animals at 7d post-treatment (5/25) are remyelinated, rather than myelinated for the first time. It is therefore interesting to consider how these axons come to be remyelinated so rapidly.

5.10.2. Schwann cell ablation does not result in vacuolation

A striking difference between the ablation of oligodendrocytes and Schwann cells in the Tg(mbp:mCherry-NTR) model is that Schwann cell ablation does not result in vacuoles. As depicted in **Figure 33A**, Schwann cells in Mtz-treated animals exhibit a disrupted, occasionally fragmenting morphology following Mtz-treatment, and the myelin sheaths, as visualised by the Tg(mbp:EGFP-CAAX) line (**Figure 34**), seem to be fainter and more disorganised than in controls. Both the Schwann cell and myelin sheath morphology in the pLL contrasts sharply with the extensive vacuolation observed in the spinal cord.

Since the Tg(mbp:mCherry-NTR) model is, to my knowledge, the first system to genetically ablate Schwann cells, it is not currently known whether the mode of Schwann cell death typically differs from that of oligodendrocyte cell death. Similarly, primary PNS demyelination in the absence of axon injury has not been demonstrated before, so it is not known whether PNS demyelination typically results in vacuolated tissue such as that seen in CNS demyelination following genetic ablation of oligodendrocytes. Be that as it may, the difference in timing/nature of death may help to explain the different time course of the immune response between the PNS and CNS: if my speculation in the Discussion of **Chapter 4** is correct and oligodendrocyte cell bodies swell up prior to entering a cell death programme, the lack of swelling seen in Schwann cells suggests that they proceed to cell death at a faster rate. This, then, may account for the more rapid onset of the macrophage response observed in the PNS, commencing at 1d post-treatment and diminishing to control levels by 5d post-treatment, and as such, contribute to the speed of the regenerative response in the PNS.

It is not clear why the natures of death appear to be so different between Schwann cells and oligodendrocytes. Continuous time-lapse monitoring of oligodendrocytes and Schwann cells during the period of Mtz-treatment may provide important insights into the mechanics of cell death in the two cell types. In addition, it would be interesting to stain both oligodendrocytes and Schwann cells with different markers of cell death at different time points, to see whether cell death pathways are differentially upregulated.

5.10.3. Less phagocytic activity by mpeg+ cells is seen in the PNS than CNS

Another interesting difference between the CNS and PNS responses to glial ablation is that the numbers of microglia/macrophages seen phagocytosing mCherry+ material are higher in the CNS than the PNS: at the peak of phagocytosis in the spinal cord, there are on average 1.0 ± 0.89 mpeg+ cells containing mCherry+ material in control animals, compared to a mean of 9.23 + 4.02 in Mtz-treated animals. By contrast, in the pLL, the numbers of mpeg+ cells containing mCherry+ material do not exhibit a similar peaked curve in their time course, and the highest number of mpeg+ cells containing mCherry+ material seen in Mtz treated animals is 2.5 ± 1.73 at 4d post-treatment (1.5 ± 1.29 in controls at the same time point).

It is likely that the less pronounced phagocytic activity in the PNS is due to the fact that fewer Schwann cells are ablated than oligodendrocytes (one-half versus one-third, respectively). This, combined with the lower basal numbers of Schwann cells (a four-somite stretch of the pLL contains a mean of 35.36 ± 4.72 Schwann cells at 7dpf, whereas a four-somite stretch of the spinal cord contains a mean of 85.71 ± 2.1 oligodendrocytes at 7dpf) means that the cell ablation generates much smaller amounts of debris in the pLL compared to the spinal cord, and thus fewer phagocytic cells are required to clear the debris. In addition, it is possible that some of the remaining Schwann cells can assume the "repair" phenotype seen following peripheral nerve injury, and clear some of the debris left by the ablated Schwann cells (Jessen and Mirsky 2016). To check whether this is the case, it would be very interesting to stain pLL nerves of Mtz-treated animals for markers of this "repair" phenotype, including c-Jun, glia-derived neurotrophic factor (GDNF), brain derived neurotrophic factor (BDNF) and vascular endothelial growth factor (VEGF; Jessen and Mirsky 2016). If such immunostains indeed revealed evidence that the remaining Schwann cells are able take on a "repair" phenotype following primary Schwann cell ablation, that may constitute another reason for the faster time course of PNS remyelination compared to CNS in this model. Also, as discussed in **Chapter 4**, it is possible that neutrophils engage in phagocytosis in the pLL nerve; this interesting possibility could also be investigated in the future.

5.10.4. No evidence of mitochondrial adaptation is seen in the PNS

As in the spinal cord, I saw no changes to mitochondrial numbers during the demyelinated stages in the PNS, but in contrast to the CNS, there were also no differences in mitochondrial numbers, or sizes, between control and Mtz-treated animals at the remyelinated stage. One reason for this lack of mitochondrial response to demyelination may again be that remyelination occurs so rapidly in the PNS that the demyelinated axons do not begin to suffer from energy shortages before they are remyelinated. Furthermore, since only half of Schwann cells are ablated, I would expect only half of the internodes on a specific axon to be disrupted, and thus each individual axon to be on average half demyelinated. It is possible that the remaining half of the internodes were sufficient to sustain the energy needs the axons for the relatively short period of time before they were remyelinated.

Additionally, and likely the main reason for the seeming lack of effect of the Mtz-treatment on mitochondria numbers is that the majority of the axons in the pLL nerve analysed at 7d post-treatment had not undergone demyelination due to their later development. These axons would naturally have no need for increased numbers of mitochondria. As noted above, it would be advisable to ablate Schwann cells at a later time point, once a larger proportion of pLL nerve axons are already myelinated.

5.10.5. Does axon calibre growth stimulate myelin thickness growth in the PNS?

Given the evidence for rapid growth of both control and Mtz-treated larvae between 1d post-treatment and 7d post-treatment, it seems likely that peripheral axons also grow in calibre during this time. As I discussed extensively in **Chapter 3**, one possible reason for restoration of full myelin thickness on axons during development and remyelination (of zebrafish reticulospinal axons) may well be that axons are growing in calibre during the relevant period. It would be highly interesting to investigate whether this could also be the case in the PNS.

In order to test that possibility, one should determine the stage when pLL axons finish growing in calibre, by measuring axon calibres at multiple time points throughout the development of the larva into a juvenile animal and beyond. Then one could induce Schwann cell ablation at a stage when the axons were no longer growing radially and examine whether remyelination still resulted in normal g ratios. Alternatively, a previous study by Voyvodic (1989) found that increasing the size of the target of the axons (the author made the submandibular salivary glands larger than normal by cutting one branch of a sympathetic nerve innervating the gland at birth) caused axons to grow in calibre. Thus, manipulating the size of the pLL axons (the neuromasts) may be one way to experimentally alter axon calibre and subsequently test the effects of the alteration on myelin sheath thickness during remyelination.

5.10.6. Future experiments

In this chapter, I have shown that primary ablation of half of Schwann cells results in rapid demyelination of approximately half the axons present at that stage, and that remyelination is seen at 7d post-treatment. I have discussed the reasons for the rapidity of this remyelination, and suggested that many of the axons present at 7d post-treatment were in fact born after the Mtz-treatment and do not represent remyelinated axons. I proposed that the environment of ongoing normal development was likely to be conducive for remyelination of those axons that had been (partially) demyelinated as a result of Schwann cell ablation.

In order to assess the effect of long-term demyelination on pLL axons, it would be interesting to inhibit remyelination by preventing Schwann cell development (for example, by the pharmacological ErbB inhibitor AG1478) and observe the consequences on peripheral axon health, in terms of organelle transport, calibre, and degeneration.

As I have mentioned, it may be beneficial to begin the Mtz-treatment at a later stage. In order to determine what would be a suitable time point to ablate Schwann cells, it should be established when the number of myelinated axons in the pLL nerve plateaus, when the axons cease to grow in calibre, and when Schwann cells cease to elongate

along axons. At this point, the background of ongoing development would be less prominent, and the majority of denuded axons observed following Mtz-treatment could be interpreted as demyelinated axons, and by the same token, the majority of myelinated axons at the remyelinated stage could be interpreted as remyelinated axons. Thus, by inducing Schwann cell ablation at a later stage, I will be better able to assess the potential for Schwann cell regeneration and remyelination of PNS axons without the aid of ongoing normal development.

Chapter 6:
Discussion

6.1. Summary of thesis

In this thesis, I have characterised the Tg(mbp:mCherry-NTR) larval zebrafish model of myelinating glial cell ablation, demyelination and remyelination. In this model, a treatment with 5mM metronidazole (Mtz) between 5 and 7 days post-fertilisation ablates two-thirds of myelinating oligodendrocytes and one-half of myelinating Schwann cells. Oligodendrocyte ablation results in vacuolation of the spinal cord tissue, which subsides by 5-7d post-treatment, whereas Schwann cell ablation does not elicit the same effect around the posterior lateral line nerve (pLL). Approximately two-thirds of large-calibre axons in the ventral spinal cord are found to be demyelinated at 5d post-treatment, and this persists through to 11d post-treatment. After this, remyelination occurs, such that by 16d post-treatment, control and Mtz-treated spinal cords are indistinguishable from each other in terms of total axon number, the percentage of myelinated axons, and the thickness of myelin sheaths. At this time point of complete remyelination, oligodendrocyte numbers in Mtz-treated animals are also restored to control levels.

At the remyelinated stage, axons in the ventral spinal cord of Mtz-treated animals have more and smaller mitochondria than control animals, suggesting accumulating dysregulation of mitochondria during the period of demyelination and remyelination. In addition, myelinated axons grow in calibre during the period analysed, raising the possibility that radial growth of axons contributes to the generation of thick myelin sheaths during remyelination in this model.

In the pLL, approximately half of the large-calibre axons are demyelinated by 1d post-treatment, a situation which prevails at 3d post-treatment but is resolved by 7d post-treatment, when control and Mtz-treated pLL nerves have equivalent numbers and percentages of myelinated axons and g ratios. Schwann cell numbers in Mtz-treated animals are restored to control levels by 5d post-treatment. The rapid regenerative response in the pLL is likely due to ongoing normal development, which is evident in greatly increased numbers of myelinated axons between 1d and 7d post-treatment in both control and cell-ablated animals.

I also sought to study the role of the innate immune system, specifically microglia and macrophages, in the response to oligodendrocyte and Schwann cell ablation. Oligodendrocyte ablation is followed by a drastic increase in the numbers of microglia/macrophages in the spinal cord, beginning at 3d post-treatment, peaking at 4d post-treatment, and then declining gradually until 9d post-treatment. The microglia and macrophages are seen phagocytosing myelin material. In irf8 mutant fish which do not develop microglia and macrophages, a delay in oligodendrocyte number regeneration is seen at 14d post-treatment, but by 16d post-treatment, mutant fish have achieved full remyelination with normal thickness myelin. Further analyses are required to determine more precisely if and when irf8 mutants have a delay in remyelination itself.

Schwann cell ablation results in an increase in macrophage numbers in the pLL nerve, which begins at 1d post-treatment and returns to control levels by 5d post-treatment. Fewer macrophages are seen ingesting myelin material than in the spinal cord, likely due to smaller quantities of debris to be cleared. Analysis of irf8 mutants coincident with remyelination will be required in the future, to determine how macrophages might regulate the rapid remyelination response observed in the PNS.

The timeline of events in the Tg(mbp:mCherry-NTR) model is summarised in **Figure 47**. below.

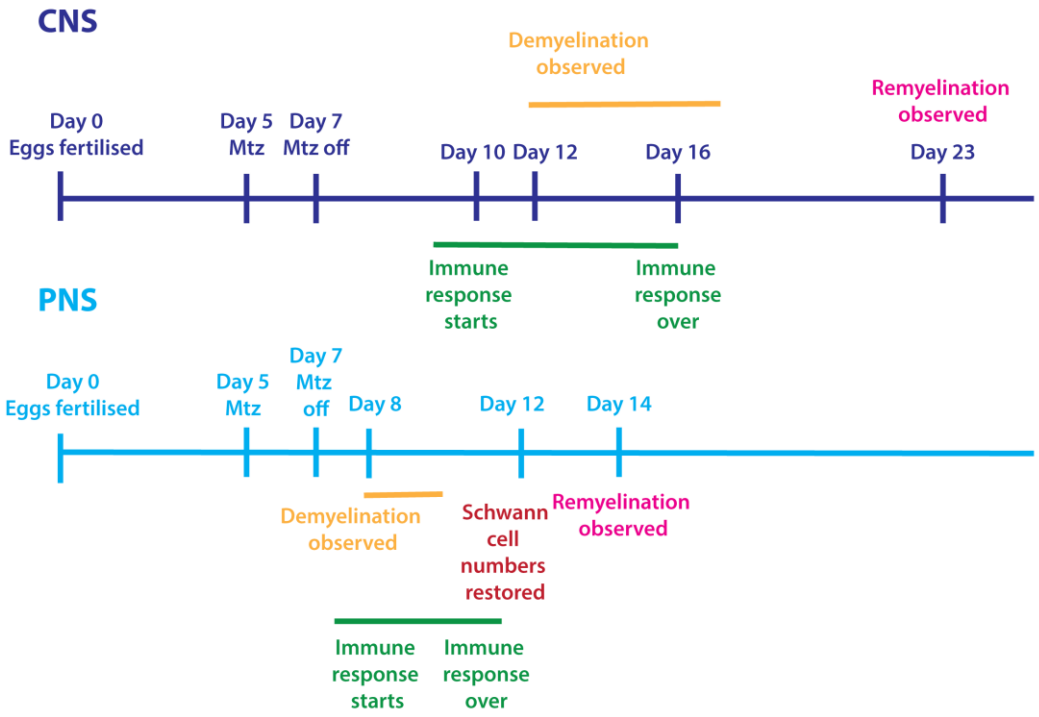

Figure 47. Summary of the timeline of events in Tg(mbp:mCherry-NTR) model.

6.1.1. How useful is the Tg(mbp:mCherry-NTR) model?

Having characterised the main features of demyelination and remyelination in the Tg(mbp:mCherry-NTR) model, I will now turn to evaluating its general suitability for future studies of demyelination and remyelination. To do this, I will consider the purposes, outlined in the introductions to the chapters, for which the Tg(mbp:mCherry-NTR) line was developed, and predict how well the line will serve those purposes.

6.2. Assessment of Tg(mbp:mCherry-NTR) model

6.2.1. Suitability for live imaging of demyelination and remyelination events

One of the main reasons why we felt a larval zebrafish model would be valuable to the field of demyelination and remyelination research was that such a model could enable sophisticated *in vivo* analyses of cellular interactions during demyelination and remyelination. Such analyses included detailed study of an axon's health, in terms of organelle transport, mitochondrial activity and calibre, and how these would be affected by demyelination, and how in turn remyelination may reverse any effects of demyelination. I will use this study of axon health as an example to evaluate how well live imaging experiments of demyelination and remyelination events in general might work in the Tg(mbp:mCherry-NTR) model. Given that live imaging is easiest at embryonic and early larval stages, due to natural transparency and small size of the animals at these stages, we aimed to carry out demyelination as early as possible. We therefore chose to induce oligodendrocyte ablation from 5 days post-fertilisation, as we knew from previous studies that this ought to demyelinate the well-defined set of early-myelinated reticulospinal axons in the ventral spinal cord.

The first aspect to consider is the timing of remyelination: axons remain demyelinated for a maximum of sixteen days, and in general less, as extensive demyelination is predominantly observed from 5d through 11 d post-treatment. In this time, I have not observed any axon loss or signs of pathology by EM, despite ablation of approximately two-thirds of oligodendrocytes and demyelination of two-thirds of axons (as seen in cross-section, although most likely I have ablated on average two-thirds of the internodes along the length of each axon). My preliminary analyses of mitochondrial content in demyelinated axons found subtle effects on mitochondrial number and size, suggestive of increases levels of mitochondrial fission in Mtz-treated larvae, but these were only present at the remyelinated stage, implying that they had accumulated over time. While more detailed analyses of axon health, by use of transgenic lines that label single axons, or immunostains for markers of axon pathology such as SMI-32 or APP, may still reveal signs of pathology during demyelination, it is also possible that the axons are simply not demyelinated for long enough to trigger pathological responses.

Moreover, the fact that very few axons are likely to be completely demyelinated, but rather most are two-thirds demyelinated on average, means that remaining myelin sheaths may also to maintain the axons' general health until they become remyelinated.

As I mentioned in **Chapter 3,** it would be possible to study the effects of long-term demyelination on axon health if a manipulation was performed to inhibit remyelination in this model; I suggested the options of repeated treatments with Mtz, disrupting of wnt signalling, upregulating hyaluronan, or administering cyclopamine, but many others could also be considered. Unfortunately, however, such studies are associated with other problems, chiefly related to the increasing age and, consequently, size of the larvae, which begins to limit the advantages of using zebrafish for the most facile live imaging studies.

One important point to make with respect to analysing single axons over time using this model is that it is prudent to wait until the presence of vacuolated myelin in the spinal cord has subsided, because the presence of large vacuoles themselves may compress axons and some cases, cause them to bend (data not shown). In addition, it is also advisable to wait until the numbers of microglia and macrophages have returned to normal levels, as the potential demyelinating effects of microglia and macrophages (which have been observed in many rodent systems and MS; Yamasaki et al. 2014; Ajami et al. 2011; Lucchinetti et al. 2000) may confound the analysis of the relationship between an axon's health and its myelination status.

Waiting until the immune response and vacuoles have declined, however, would mean starting an intervention to prolong demyelination at 7d or 9d post-Mtz-treatment, when the animals are 14 or 16 days of age, and consequently carrying out the subsequent analyses at even later ages than I analysed here. Larval zebrafish grow considerably in size at about three weeks post-fertilisation as they become juvenile animals; this general increase, with the associated increased thickness and opacity of muscle tissue separating the microscope lens from the spinal cord, renders high-resolution sub-cellular live imaging difficult. This difficulty is exemplified by my decision to quantify oligodendrocyte numbers most accurately by preparing cryosections from 7d treatment (14dpf) onwards.

The fact that live imaging becomes more challenging as the larvae become older and larger is a pervasive problem which must be taken into account when planning any experiments using the Tg(mbp:mCherry-NTR) model. In addition, larvae at the post-embryonic stages are more sensitive to repeating the procedure of being anaesthetised, mounted and imaged. This is inconvenient, as it limits the number of time points that can be analysed in the same animal.

Of course, some of the issues relating to the difficulties of live imaging of older larvae can be circumvented by immunostaining, either whole-mount larvae of transverse sections, and indeed I have suggested many such experiments throughout this thesis. However, since the advantages of the zebrafish for live imaging were a major reason for wishing to develop a zebrafish model of demyelination and remyelination in the first place, it is also helpful to seek ways to improve live imaging in older larvae.

One pertinent point to make is that the vast majority of the imaging I have performed during my studies was done on a conventional point scanning confocal microscope (a Zeiss LSM 710), which is not an ideal system for deep tissue imaging. To that end, it would be preferable to use a multi-photon microscope (Denk et al. 1990). In addition, towards the end of my studies, our lab acquired a Zeiss LSM 880 confocal microscope with Airyscan, which enables higher resolution imaging by use of multiple pinholes and *post hoc* image deconvolution.

As for the older larvae being less tolerant of repeated rounds of mounting and imaging, one could explore alternative methods of mounting, such as using methycellulose instead of agarose, and not embedding the head of the larva in the mounting medium; both of which have been suggested to improve survival of mounted larvae (C. Becker, and D. Lyons, pers. comm.).

In addition, several mutant zebrafish exist which have reduced or absent pigment, including *golden*, *casper*, and *nacre* (Lamason et al. 2005; Lister et al. 1999; White et al. 2008). Crossing the Tg(mbp:mCherry-NTR) line with one of these could considerably prolong the period during which live imaging is feasible, and therefore should certainly be attempted. However, when working with pigment mutants, it is

important to control for any effects the mutation may have on myelination by rigorous comparison of the pattern and timing of myelination between mutants and wild-types.

Finally, as I discussed at length in **Chapter 4**, the fact that the larvae are growing during the period of demyelination and remyelination, and indeed may grow at widely varying rates, can complicate the interpretation of results acquired using this model, for example meaning that remyelination may be achieved at earlier or later chronological time points, depending on the overall growth of the animal. This means that it is imperative to normalise results to a proxy indicator of the overall developmental stage of the larvae, in addition to chronological age.

As I have mentioned, throughout my studies I have striven to analyse similar-sized animals within experiments. There are also well-defined post-embryonic staging series to help researchers define the developmental stage their specimens are at (Parichy et al. 2009). Making use of such staging series will be very important in interpreting results from live imaging experiments made in older larvae.

However, importantly, the fact that demyelination is induced in a still-developing animal in the Tg(mbp:mCherry-NTR) model can be seen an advantage as well as a disadvantage. For example, if the larvae were not developing during the period of remyelination, I would not have been able to note the potential relationship between radial growth of axons and regeneration of thick myelin sheaths, which may turn out to be a very interesting insight into the regulation of myelin thickness during remyelination. In addition, the robust remyelination observed in this model allows researchers to identify factors that are *required* for remyelination, by seeking factors that impair remyelination and analysing their targets.

Thus, with appropriate adaptations to imaging protocols, and using the knowledge I have presented in this thesis regarding the timeline of demyelination and remyelination, the Tg(mbp:mCherry-NTR) model could still be a highly useful tool for live imaging of demyelination and remyelination events.

6.2.2. Chemical screening for compounds that regulate remyelination

Another major purpose for establishing a larval zebrafish model of demyelination was the possibility to use it as a platform for chemical screening of compounds that may regulate remyelination. Naturally, given that Mtz-treated Tg(mbp:mCherry-NTR) larvae achieve full remyelination, with normal thickness myelin, means that the end stage of remyelination can hardly be enhanced. However, the model may still be helpful for discovering compounds to *accelerate* remyelination, or, as noted above, *impair* remyelination, which would provide insight into mechanisms of normal remyelination. One of the benefits of the Tg(mbp:mCherry-NTR) model is that there is a clear temporal separation between demyelination and remyelination, and thus effects on the two processes can be easily distinguished. Furthermore, since oligodendrocyte numbers are not restored to control levels by the time of remyelination, the system can be used to identify compounds which increase oligodendrocyte numbers in the context of demyelination.

From a screening point of view, the rather large size of larvae during demyelination and remyelination might present a problem. As part of a primary screen for remyelinating compounds, in order to test large numbers of compounds in a high-throughput manner, it would be paramount to rapidly and quantitatively assess the numbers of oligodendrocytes or the extent of remyelination at specific time points. However, as I have explained above, live imaging of larvae at the ages of interest here is not simple and straightforward in this model, and oligodendrocyte numbers and remyelination are best quantified from fixed tissue, or else with alternative imaging modalities such as multiphoton imaging. Both approaches would considerably slow down the screening process (it is worthwhile to note for context that our laboratory currently uses high-speed spinning disk confocal imaging for screens of myelination at earlier developmental stages, which is not a modality compatible with deep tissue imaging).

Thus, without major investment in new screening technologies to accommodate larger specimens, a better use for the model would be as a *secondary* screening/validation assay. That is, after a primary screen to identify compounds that, for example, increase

oligodendrocyte numbers or myelination in normal development, the Tg(mbp:mCherry-NTR) model could be used to test whether the same compounds could also increase oligodendrocyte numbers and/or remyelination following oligodendrocyte ablation. Thus employed, I believe the model could be a highly valuable tool, as the context for oligodendrocyte development in Mtz-treated Tg(mbp:mCherry-NTR) animals is markedly different from that found in normal developing larvae before 5dpf, when current developmental screens are carried out. First, there is the presence of debris, and high numbers of microglia and macrophages, which significantly alter the molecular environment in which oligodendrocyte development occurs and could affect its rate and overall success. Second, the majority axons to be remyelinated are genuinely demyelinated, rather than new and never-before myelinated, which may alter the signals required to myelinate them. Third, at older ages, the larvae have developed a mature blood-brain barrier (Fleming et al. 2013), and thus any compounds which do not penetrate this can be eliminated. In this way, the Tg(mbp:mCherry-NTR) line can provide a more disease-relevant context in which to test compounds previously found to affect oligodendrocyte numbers and myelination during development.

Furthermore, if it proved difficult to identify compounds to accelerate remyelination, with the spontaneous process occurring so rapidly once it has begun, it would be possible to lengthen the Mtz-treatment regime, or administer repeated treatments, in order to prolong the demyelinated period and make it easier to capture effects of compounds that shorten it. With a small number of candidate compounds discovered in a primary screen, more detailed analyses of the effects of compounds on oligodendrocyte numbers and remyelination can feasibly be carried out. Furthermore, by using the Tg(mpeg:GFP) line, it will also be possible to identify compounds which specifically affect the rate and extent of the microglia/macrophage response to demyelination, and the effects of such compounds on oligodendrocyte regeneration and remyelination. Thus, as secondary testing platform for compounds that regulate remyelination and oligodendrocyte regeneration and the immune response to demyelination, I am confident that the Tg(mbp:mCherry-NTR) model will be extremely helpful, and will be used in this capacity in our lab.

6.2.3. Testing the effects of genetic manipulations on remyelination

In **Chapter 1**, I explained how the zebrafish is commonly used to discover novel genes regulating developmental events of interest, such as myelination, and how recent advances in genome editing technology have made it relatively straightforward to knock genes out, or in, and assess the effects on the phenomenon of interest. Both large-scale forward genetic screens and precise genome editing techniques such as crisp-cas are now well-established activities in our lab. Thus, when novel genes found to regulate myelination are found, the Tg(mbp:mCherry-NTR) model can be used to test whether the gene has similar effects on remyelination. Such studies are important, as it is well documented that the genetic control of developmental myelination and remyelination, while sharing common features, is not the same (Fancy et al. 2011). For instance, others in the lab have discovered mutants which show severe hypomyelination in the CNS during normal development, and it would be very interesting to test whether this mutant would, for example, fail to restore full thickness myelin during remyelination. Indeed, a mutant has been identified that has a defect in the growth of calibre in some CNS axons, which may allow us to test the possibility that growth in calibre regulates the generation of thick myelin sheaths during remyelination. In this way, genetic analyses using the Tg(mbp:mCherry-NTR) model may help to identify methods to enhance myelin sheath thickness in remyelination in mammals.

6.2.4. Possible Schwann cell remyelination in the CNS

An interesting question to consider is whether Schwann cells contribute to remyelination in the CNS in the Tg(mbp:mCherry-NTR) model, as Schwann cell remyelination of demyelinated CNS lesions is frequently observed in both experimental models of demyelination and MS (Dusart et al. 1992; Itoyama et al. 1983; Woodruff and Franklin 1999). Since in my experiments, I have visualised both oligodendrocytes and Schwann cells using transgenic lines where reporter proteins are expressed under the mbp promoter, it is possible that there have been Schwann cells in the spinal cord which I have counted as oligodendrocytes.

In order to resolve this, it would be important to use different markers for Schwann cells and oligodendrocytes and observe whether Schwann cells do play a role in CNS remyelination. To this end, I could use the Tg(foxd3:GFP) line which labels a subtype of neural crest-derived peripheral glia (Gilmour et al. 2002). By crossing these fish with Tg(mbp:mCherry-NTR) fish and imaging the progeny at frequent intervals following Mtz-treatment, I could detect Schwann cells entering the spinal cord, assess the their numbers and timing of their appearance (for instance, do they arrive during the immune response or after it?) and the contribution they may make to remyelination. In addition, it would be interesting to inhibit remyelination by preventing Schwann cell development (for example by the pharmacological ErbB inhibitor AG1478) and observe the consequences on CNS remyelination. If this were impaired following specific Schwann cell inhibition, that would provide direct evidence that Schwann cells contribute to CNS remyelination in this model.

However, since Schwann cells are also ablated by the Mtz-treatment it is possible that their ability to enter the spinal cord is impaired. I would predict that such an impairment is unlikely, since Schwann cell numbers are restored to control levels before remyelination in the CNS begins, but naturally, the presence and extent of any impairment would depend on when (if at all) during the course of demyelination and remyelination Schwann cells enter the CNS. In order to resolve the issue of both Schwann cells and oligodendrocytes being ablated in this model, it may be beneficial to generate alternative ablation systems whereby nitroreductase is expressed under oligodendrocyte and Schwann cell specific promoters.

6.3. Conclusion

Based on my characterisation of the Tg(mbp:mCherry-NTR) model, I believe it will be a very useful secondary assay for testing the effects of novel compounds or genes on oligodendrocyte regeneration and remyelination. In addition, we have available to us an extensive collection of transgenic tools with which to visualise oligodendrocytes and axons as well as immune cells during demyelination and remyelination, and I believe that combining these tools with the Tg(mbp:mCherry-NTR) model will yield

many important insights into the cellular events that underpin demyelination and remyelination. Although high-resolution of live imaging is more challenging during remyelination than during developmental myelination, due to the increasing size and opacity of the larvae, I have no doubt that with proper adjustments to imaging protocols, such as using more suitable microscopes and mutants with reduced pigment, live imaging of Tg(mbp:mCherry-NTR) larvae during remyelination will be eminently feasible.

Furthermore, the model will be a useful tool for studying potential influences on the overall timing and extent of oligodendrocyte regeneration and remyelination, such as impairing the development of microglia and macrophages, role of Schwann cells, or the role of axon calibre growth on myelin sheath thickness.

Thus, I propose that, as long as experiments are carefully designed and interpreted to take into account the influence of ongoing normal development, the Tg(mbp:mCherry-NTR) model will be a valuable tool demyelination and remyelination research.

References

Aharoni, R., 2013. The mechanism of action of glatiramer acetate in multiple sclerosis and beyond. *Autoimmunity Reviews*, 12(5), 543–53.

Ajami, B., Bennett, J.L., Krieger, C., McNagny, K.M. and Rossi, F.M.V., 2011. Infiltrating monocytes trigger EAE progression, but do not contribute to the resident microglia pool. *Nature Neuroscience*, 14(9), 1142–9.

Ajami, B., Bennett, J.L., Krieger, C., Tetzlaff, W. and Rossi, F.M.V., 2007. Local self-renewal can sustain CNS microglia maintenance and function throughout adult life. *Nature Neuroscience*, 10(12), 1538-43.

Almeida, R.G., Czopka, T., ffrench-Constant, C. and Lyons, D.A., 2011. Individual axons regulate the myelinating potential of single oligodendrocytes *in vivo*. *Development*, 138(20), 4443–4450.

Andrews, H., White, K., Thomson, C., Edgar, J., Bates, D., Griffirth, I., Turnbull, D. and Nichols, P., 2006. Increased axonal mitochondrial activity as an adaptation to myelin deficiency in the Shiverer mouse. *Journal of Neuroscience Research*, 83(8), 1533–9.

Arthur-Farraj, P.J., Latouche, M., Wilton, D.K., Quintes, S., Chabrol, E., Banerjee, A., Woodhoo, A., Jenkins, B., Rahman, M., Turmaine, M., Wicher, G.K., Mitter, R., Greensmith, L., Behrens, A., Raivich, G., Mirsky, R. and Jessen, K., 2012. c-Jun reprograms Schwann cells of injured nerves to generate a repair cell essential for regeneration. *Neuron*, 75(4), 633–47.

Avila, R.L., Lees, J.P., Inouye, H. and Kirschner, D.A., 2007. Myelin Structure and Composition in Zebrafish. *Neurochemical Research*, 32(2), 211–12.

Back, S.A., Tuohy, T.M.F., Chen, H., Wallingford, N., Craig, A., Struve, J., Luo, N.L., Banine, F., Liu, Y., Chang, A., Trapp, B., Bebo, B.F., Rao, M.S. and Sherman, L.S., 2005. Hyaluronan accumulates in demyelinated lesions and inhibits oligodendrocyte progenitor maturation. *Nature Medicine*, 11(9), 966–72.

Bai, C.B., Suna, S., Roholt, A., Bensona, E., Edberga, D., Medicetty, S., Dutta, R., Kidd, G., Macklin, W. and Trapp, B. 2016. A mouse model for testing remyelinating therapies. *Experimental Neurology*, 283(Pt A), 330–340.

Bai, Q., Sun, M., Stolz, D.B. and Burton, E.A. 2011. Major isoform of zebrafish P0 is a 23.5 kDa myelin glycoprotein expressed in selected white matter tracts of the central nervous system. *The Journal of Comparative Neurology*, 519(8), 1580–96.

Barnett, M. and Prineas, J., 2004. Relapsing and remitting multiple sclerosis: pathology of the newly forming lesion. *Annals of Neurology*, 55(4), 458–68.

Barron, M.J., Griffith, I., Turnbull, D.M., Bates, D. and Nichols, P., 2004. The distributions of mitochondria and sodium channels reflect the specific energy requirements and conduction properties of the human optic nerve head. *The British Journal of Ophthalmology*, 88(2), 286–90.

Baxter, A.G., 2007. The origin and application of experimental autoimmune encephalomyelitis. *Nature Reviews. Immunology*, 7(11), 904–12.

Becker, T. and Becker, C.G., 2014. Axonal regeneration in zebrafish. *Current Opinion in Neurobiology*, 27, 186–91.

Beirowski, B., Babetto, B., Golden, J.P., Chen, Y., Yang, K., Gross, R.W., Patti, G.J., and Milbrandt, J., 2014. Metabolic regulator LKB1 is crucial for Schwann cell-mediated axon maintenance. *Nature Neuroscience*, 17(10), 1351–61.

Beirowski, B., Adalbert, R, Wagner, D., Grumme, D.S., Addicks, K., Ribchester, R.R. and Coleman, M.P., 2005. The progressive nature of Wallerian degeneration in wild-type and slow Wallerian degeneration (WldS) nerves. *BMC Neuroscience*, 6, 6-33.

Bennett, M.L., Bennett, F.C., Liddelow, S.A., Ajami, B., Zamanian, J.L., Fernhoff, N.B., Mulinyawe, S.B., Bohlen, C.J., Adil, A., Tucker, A., Weissman, I.L, Chang, E.F., Li, G., Grant, G.A., Hayden Gerphart, M.G. and Barres, B.A., 2016. New tools for studying microglia in the mouse and human CNS. *Proceedings of the National Academy of Sciences of the United States of America*, 113(12), E1738–46.

Bin, J.M. and Lyons, D.A., 2016. Imaging myelination *in vivo* using transparent animal models. *Brain Plasticity*, 2(1), 3-29.

Bjartmar, C., Kidd, G., Mörk, S., Rudick, R. and Trapp, B.D., 2000. Neurological disability correlates with spinal cord axonal loss and reduced N-acetyl aspartate in chronic multiple sclerosis patients. *Annals of Neurology*, 48(6), 893-901.

Blakemore, W., 1972. Observations on oligodendrocyte degeneration, the resolution of status spongiosus and remyelination in cuprizone intoxication in mice. *Journal of Neurocytology*, 1(4), 413-26.

Blakemore, W. and Franklin, R.J.M., 2008. Remyelination in experimental models of toxin-induced demyelination. *Curr Top Microbiol Immunol*, 318, 193-212.

Blakemore, W. and Murray, J., 1981. Quantitative examination of internodal length of remyelinated nerve fibres in the central nervous system. *Journal of the Neurological Sciences*, 49(2), 273–84.

Blakemore, W.F., 1974. Pattern of remyelination in the CNS. *Nature*, 249(457), 577–8.

Blakemore, W.F., 1973. Remyelination of the superior cerebellar peduncle in the mouse following demyelination induced by feeding cuprizone. *Journal of the Neurological Sciences*, 20(1), 73–83.

Booss, J., Esiri, M.M., Tourtellotte, W.W. and Mason, D.Y., 1983. Immunohistological analysis of T lymphocyte subsets in the central nervous system in chronic progressive multiple sclerosis. *Journal of the Neurological Sciences*, 62(1-3), 219–32.

Bornstein, M.B., Miller, A., Slagle, S., Weitzman, M., Crystal, H., Drexler, E., Keilson, M., Merriam, A., Wassertheil-Smoller, S., Spada, V., Weiss, W., Arnon, R., Jacobsohn, I., Teitelbaum, D. and Sela, M., 1987. A pilot trial of Cop 1 in exacerbating-remitting multiple sclerosis. *The New England Journal of Medicine*, 317(7), 408–14.

Bouhy, D. and Timmerman, V., 2013. Animal models and therapeutic prospects for Charcot-Marie-Tooth disease. *Annals of Neurology*, 74(3), 391–6.

Boyd, A., Zhang, H. and Williams, A., 2013. Insufficient OPC migration into demyelinated lesions is a cause of poor remyelination in MS and mouse models. *Acta Neuropathologica*, 125(6), 841–59.

Breij, E.C.W., Brink, B.P., Veerhuis, R., van den Berg, C., Vloet, R., Yan, R., Dijkstra, C.D., van der Valk, P. and Bö, L., 2008. Homogeneity of active demyelinating lesions in established multiple sclerosis. *Annals of Neurology*, 63(1), 16–25.

Bridge, P.M., Ball, D.J., Mackinnon, S.E., Nakao, Y., Brandt, K., Hunter, D.A. and Hertl, C., 1994. Nerve crush injuries--a model for axonotmesis. *Experimental Neurology*, 127(2), 284–90.

Brinkmann, B.G., Agarwal, A., Sereda, M.W., Garratt, A.N., Müller, T., Wende, H., Stassart, R.M., Nawaz, S., Humml, C., Velanac, V., Radyshkin, K., Goebbels, S., Fischer, T.M., Franklin, R.J.M., Lai, C., Ehrenreich, H., Birchmeier, C., Schwab, M.H., and Nave, K-A., 2008. Neuregulin-1/ErbB Signaling Serves Distinct Functions in Myelination of the Peripheral and Central Nervous System. *Neuron*, 59(4), 581–95.

Britsch, S., Li, L., Kirchhoff, S., Theuring, F., Brinkmann, V., Birchmeier, C. and Riethmacher, D., 1998. The ErbB2 and ErbB3 receptors and their ligand, neuregulin-1, are essential for development of the sympathetic nervous system. *Genes and Development*, 12(12), 1825–36.

Brösamle, C. and Halpern, M.E., 2002. Characterization of myelination in the developing zebrafish. *Glia*, 39(1), 47–57.

Buckley, C.E., Marguerie, A., Alderton, W.K., and Franklin, R.J.M., 2010. Temporal dynamics of myelination in the zebrafish spinal cord. *Glia*, 58(7), 802-12.

Buckley, C.E., Marguerie, A., Roach, A.G., Goldsmith, P., Fleming, A., Alderton, W.K. and Franklin, R.J.M., 2010. Drug reprofiling using zebrafish identifies novel compounds with potential pro-myelination effects. *Neuropharmacology*, 59(3), 149–59.

Bugiani, M., Boor, I., Powers, J.M., Scheper, G.C. and van der Knaap, M., 2010. Leukoencephalopathy with vanishing white matter: a review. *Journal of Neuropathology and Experimental Neurology*, 69(10), 987–96.

Butovsky, O., Jedrychowski, M.P., Moore, C.S., Cialic, R., Lanser, A.J., Gabriely, G., Koeglsperger, T., Dake, B., Wu, P.M., Doykan, C.E., Fanek, Z., Liu, L., Chen, Z., Rothstein, J.D., Ransohoff, R.M., Gygi, S.P., Antel, J.P. and Weiner, H., 2014. Identification of a unique TGF-β-dependent molecular and functional signature in microglia. *Nature Neuroscience*, 17(1), 131–43.

Casano, A.M., Albert, M. and Peri, F., 2016. Developmental Apoptosis Mediates Entry and Positioning of Microglia in the Zebrafish Brain. *Cell Reports*, 16(4), 897–906.

Cattin, A.-L. and Lloyd, A.C., 2016. The multicellular complexity of peripheral nerve regeneration. *Current Opinion in Neurobiology*, 39, 38–46.

Cattin, A.-L., Burden, J.J., van Emmenis, L., Mackenzie, F.E., Hoving, J.J., Garcia Calavia, N., Guo, Y., McLaughlin, M., Rosenberg, L.H., Quereda, V., Jamecna, D., Napoli, I., Parrinello, S., Enver, T., Ruhrberg, C. and Lloyd, A., 2015. Macrophage-Induced Blood Vessels Guide Schwann Cell-Mediated Regeneration of Peripheral Nerves. *Cell*, 162(5), 1127-39.

Ceci, M.L., Mardones-Krsulovic, C., Sanchez, M., Valdivia, L.E. and Allende, M.L., 2014. Axon-Schwann cell interactions during peripheral nerve regeneration in zebrafish larvae. *Neural Development*, 9, 22.

Chang, A., Tourtellotte, W.W., Rudick, R., Trapp, B.D., 2002. Premyelinating oligodendrocytes in chronic lesions of multiple sclerosis. *New England Journal of Medicine*, 346(3), 165-73.

Chari, D.M., Zhao, C., Kotter, M.R., Blakemore, W.F. and Franklin, R.J.M., 2006. Corticosteroids delay remyelination of experimental demyelination in the rodent central nervous system. *Journal of Neuroscience Research*, 83(4), 594–605.

Charles, P., Reynolds, R., Seilhean, D., Rougon, G., Aigrot, M.S., Niezgoda, A., Zalc, B. and Lubetzki, C., 2002. Re-expression of PSA-NCAM by demyelinated axons: an inhibitor of remyelination in multiple sclerosis. *Brain*, 125(9), 1972–9.

Chastain, E.M.L. and Miller, S.D., 2012. Molecular mimicry as an inducing trigger for CNS autoimmune demyelinating disease. *Immunological Reviews*, 245(1), 227–38.

Choi, R.Y., Engbretson, G.A., Solessio, E.C., Jones, G.A., Coughlin, A., Aleksic, I. and Zuber, M.E., 2011. Cone degeneration following rod ablation in a reversible model of retinal degeneration. *Investigative Ophthalmology and Visual Science*, 52(1), 364–73.

Chung, A.-Y., Kim, P.-S., Kim, S., Kim, E., Kim, D., Jeong, I., Kim, H.-K., Ryu, J.-H., Kim, C.-H., Choi, J., Seo, J.-H. and Park, H.-C., 2013. Generation of demyelination models by targeted ablation of oligodendrocytes in the zebrafish CNS. *Molecules and Cells*, 36(1), 82-7.

Clegg, A. and Bryant, J., 2001. Immunomodulatory drugs for multiple sclerosis: a systematic review of clinical and cost effectiveness. *Expert Opinion on Pharmacotherapy*, 2(4), 623-39.

Cole, L.K. and Ross, L.S., 2001. Apoptosis in the Developing Zebrafish Embryo. *Developmental Biology*, 240(1), 123–42.

Compston, A., 1999. The genetic epidemiology of multiple sclerosis. *Philosophical Transactions of the Royal Society B: Biological Sciences*, 354(1390), 1623–34.

Compston, A., 2000. The genetics of multiple sclerosis. *Journal of Neurovirology*, 6(2), S5–9.

Compston, A. and Coles, A., 2008. Multiple sclerosis. *Lancet*, 372(9648), 1502–17.

Confavreux, C., Vukusic, S., Moreau, T. and Adeleine, P., 2000. Relapses and progression of disability in multiple sclerosis. *The New England Journal of Medicine*, 343(20), 1430–8.

Conforti, L., Gilley, J. and Coleman, M.P., 2014. Wallerian degeneration: an emerging axon death pathway linking injury and disease. *Nature Reviews. Neuroscience*, 15(6), 394–409.

Craner, M., Newcombe, J., Black, J., Hartle, C., Cuzner, M.L. and Waxman, S.G., 2004. Molecular changes in neurons in multiple sclerosis: altered axonal expression of Nav1. 2 and Nav1. 6 sodium channels and Na+/Ca2+ exchanger. *Proceedings of the National Academy of Sciences of the United States of America*, 101(21) 8168–73.

Crawford, A.H, Tripathi, R.B., Foerster, S., McKenzie, I., Kougioumtzidou, E., Grist, M., Richardson, W.D. and Franklin, R.J.M., 2016. Pre-Existing Mature Oligodendrocytes Do Not Contribute to Remyelination following Toxin-Induced Spinal Cord Demyelination. *The American journal of Pathology*, 186(3), 511-16.

Curado, S., Anderson, R.M., Jungblut, B., Mumm. J., Schroeter, E. and Stainier, D.Y.R., 2007. Conditional targeted cell ablation in zebrafish: A new tool for regeneration studies. *Developmental Dynamics*, 236(4), 1025–35.

Cutler, C., Multane, P., Robbins, D., Kim, H.T., Le, T., Hoggatt, J., Pelus, L.M., Desponts, C., Chen. Y.-B., Rezner, B., Arman, P., Koreth, J., Glotzbecker, B., Ho, V.T., Alyea, E., Isom, M., Kao, G., Armant, M., Silberstein, L., Hu, P., Soiffer, R.J., Scadden, D.T., Ritz, J., Goessling, W., North, T.E., Mendlein, J., Ballen, K., Zon, L.I, Antin, J.H. and Shoemaker, D.D., 2013. Prostaglandin-modulated umbilical cord blood hematopoietic stem cell transplantation. *Blood*, 122, 3074-81.

Czopka, T., ffrench-Constant, C. and Lyons, D., 2013. Individual oligodendrocytes have only a few hours in which to generate new myelin sheaths *in vivo*. *Developmental Cell*, 25(6), 599–609.

D'Amico, E., Messina, S., Caserta, C. and Patti, F., 2015. A critical appraisal of daclizumab use as emerging therapy in multiple sclerosis. *Expert Opinion on Drug Safety*, 14(7), 1157–68.

Dang, M., Fogley, R. and Zon, L.I., 2016. Identifying Novel Cancer Therapies Using Chemical Genetics and Zebrafish. *Advances in Experimental Medicine and Biology*, 916, 103–24.

David, S. and Lacroix, S., 2003. Molecular approaches to spinal cord repair. *Annual Review of Neuroscience*, 26, 411–40.

Davison, J.M., Akitake, C.M., Goll, M.G., Rhee, J.M., Gosse, N., Baier, H., Halpern, M.E., Leach, S.D. and Parsons, M.J., 2007. Transactivation from Gal4-VP16 transgenic insertions for tissue-specific cell labeling and ablation in zebrafish. *Developmental Biology*, 304(2), 811–824.

Dawson, M.R., Polito, A., Levine, J.M. and Reynolds, R., 2003. NG2-expressing glial progenitor cells: an abundant and widespread population of cycling cells in the adult rat CNS. *Molecular and Cellular Neurosciences*, 24(2), 476–88.

Degterev, A., Hitomi, J., Germscheid, M., Ch'en, I.L., Korkina, O., Teng, X., Abbott, D., Cuny, G.D., Yuan, C., Wagner, G., Hedrick, S.M., Gerber, S.A., Lugovsky, A. and Yuan, J., 2008. Identification of RIP1 kinase as a specific cellular target of necrostatins. *Nature Chem Biol*,4(5), 313-21.

Demerens, C., Stankoff, B., Logak, M., Anglade, P., Allinquant, B., Couraud, F., Zalc, B. and Lubetzki, C., 1996. Induction of myelination in the central nervous system by electrical activity. *Proceedings of the National Academy of Sciences. National Acad Sciences*, 93(18), 9887–92.

Denarier, E., Forghani, R., Farhadi, H.F., Dib, S., Dionne, N., Friedman, H.C., Lepage, P., Hudson, T.J., Drouin, R. and Peterson, A., 2005. Functional organization of a Schwann cell enhancer. *The Journal of Neuroscience*, 25(48), 11210–7.

Denk, W., Strickler, J.H. and Webb, W.W., 1990. Two-photon laser scanning fluorescence microscopy. *Science*, 248(4951), 73–76.

Deoni, S.C.L., Zinkstok, J.R., Daly, E., Ecker, C., Williams, S.C.R. and Murphy, D.G.M., 2015. White-matter relaxation time and myelin water fraction differences in young adults with autism. *Psychological Medicine*, 45(4), 795–805.

Deshmukh, V.A., Tardif, V., Lyssiotis, C.A., Green, C.C., Kerman, B., Kim, H.J., Padmanabhan, K., Swoboda, J.G., Ahmad, I., Kndo, T., Gage, F.H., Theofilopoulos, A.B., Lawson. B.R., Schultz, P.G. and Lairson, L., 2013. A regenerative approach to the treatment of multiple sclerosis. *Nature*, 502(7471), 327–32.

de Stefano, N., Matthews, P.M., Fu, L., Narayanan, S., Stanley, J., Francis, G.S., Antel, J.P. and Arnold, D.L., 1998. Axonal damage correlates with disability in patients with relapsing-remitting multiple sclerosis. Results of a longitudinal magnetic resonance spectroscopy study. *Brain*, 121(8), 1469–77.

de Vos, A.F., van Meurs, M., Brok, H.P., Boven, L.A., Hintzen, R.Q., van der Valk, P., Ravid, R., Rensing, S., Boon, L., Hart, B.A. and Laman, J.D., 2002. Transfer of central nervous system autoantigens and presentation in secondary lymphoid organs. *Journal of Immunology*, 169(10), 5415–23.

Dhib-Jalbut, S. and Marks, S., 2010. Interferon-β mechanisms of action in multiple sclerosis. *Neurology*, 74(1), 17-24.

Driever, W., Solnica-Krezel, L., Schier, A.F., Neuhauss, S.C., Malicki, J., Stemple, D.L., Stainier, D.Y., Zwartkruis, F., Abdelilah, S., Rangini, Z., Belak, J. and Boggs, C., 1996. A genetic screen for mutations affecting embryogenesis in zebrafish. *Development*, 123, 37–46.

Dubois-Dalcq, M., ffrench-Constant, C. and Franklin, R.J.M., 2005. Enhancing central nervous system remyelination in multiple sclerosis. *Neuron*, 48(1), 9–12.

Dusart, I., Marty, S. and Peschanski, M., 1992. Demyelination, and remyelination by Schwann cells and oligodendrocytes after kainate-induced neuronal depletion in the central nervous system. *Neuroscience*, 51(1), 137–48.

Dutta, R. and Trapp, B.D., 2014. Relapsing and progressive forms of multiple sclerosis: insights from pathology. *Current Opinion in Neurology*, 27(3), 271–8.

Dutta, R., McDonough, J., Yin, X., Peterson, J., Chang, A., Torrest, T., Gudz, T., Macklin, W.B., Lewis, D.A., Fox, R.J., Rudick, R., Mirnics, K. and Trapp, B.D., 2006.

Mitochondrial dysfunction as a cause of axonal degeneration in multiple sclerosis patients. *Annals of Neurology*, 59(3), 478-89.

Duvezin-Caubet, S., Jagasia, R., Wagener, J., Hofmann, S., Trifunovic, A., Hansson, A., Chomyn, A., Bauer, M.F., Attardi, G., Larsson, N.G., Neupert, W., and Reichert, A.S., 2006. Proteolytic processing of OPA1 links mitochondrial dysfunction to alterations in mitochondrial morphology. *The Journal of Biological Chemistry*, 281(49), 37972–9.

Ellett, F., Pase, L., Hayman, J.W., Andrianopoulos, A. and Lieschke, G.J., 2011. mpeg1 promoter transgenes direct macrophage-lineage expression in zebrafish. *Blood*, 117(4), e49–56.

Emery, B., 2010. Regulation of oligodendrocyte differentiation and myelination. *Science*, 330(6005), 779-82.

Emery, B. and Lu, Q.R., 2015. Transcriptional and epigenetic regulation of oligodendrocyte development and myelination in the central nervous system. *Cold Spring Harbor Perspectives in Biology*, 7(9), p.a020461.

Etxeberria, A., Hokanson, K.C., Dao, D.Q., Mayoral, S.R., Mei, F., Redmond, S.A., Ullian, E.M. and Chan, J.R., 2016. Dynamic modulation of myelination in response to visual stimuli alters optic nerve conduction velocity. *The Journal of Neuroscience*, 36(26), 6937–48.

Etxeberria, A., Mangin, J.M., Aguirre, A. and Gallo, V., 2010. Adult-born SVZ progenitors receive transient synapses during remyelination in corpus callosum. *Nature Neuroscience*, 13(3), 287–89.

Fabriek, B.O., Zwemmer, J.N., Teunissen, C.E., Dijkstra, C.D., Polman, C.H., Laman, J.D. and Casteljins, J.A., 2005. *In vivo* detection of myelin proteins in cervical lymph nodes of MS patients using ultrasound-guided fine-needle aspiration cytology. *The Journal of Neuroimmunology*, 161(1-2), 190–4.

Fadok, V.A., Bratton, D.L., Konowal, A., Freed, P.W., Westcott, J.Y. and Henson, P.M., 1998. Macrophages that have ingested apoptotic cells *in vitro* inhibit

proinflammatory cytokine production through autocrine/paracrine mechanisms involving TGF-beta, PGE2, and PAF. *The Journal of Clinical Investigation*, 101(4), 890–98.

Fancy, S.P., Chan, J.R., Baranzini, S.E., Franklin, R.J.M. and Rowitch, D.H., 2011. Myelin regeneration: a recapitulation of development? *Annual Review of Neuroscience*, 34, 21–43.

Fancy, S.P., Baranzini, S.E., Zhao, C., Yuk, D.I., Irvine, K.A., Kaing, S., Sanai, N., Franklin, R.J.M. and Rowitch, D.H., 2009. Dysregulation of the Wnt pathway inhibits timely myelination and remyelination in the mammalian CNS. *Genes and Development*, 23(13), 1571–85.

Fancy, S.P., Zhao, C. and Franklin, R.J.M., 2004. Increased expression of Nkx2.2. and Olig2 identifies reactive oligodendrocye progenitor cells responding to demyelination in the adult CNS. *Molecular and Cellular Neurosci*, 27(3), 247-54.

Fang, Y., Lei, X., Li, X., Chen, Y., Xu, F., Feng, X.,, Wei, S. and Li, Y., 2014. A novel model of demyelination and remyelination in a GFP-transgenic zebrafish. *Biology Open*, 4(1), 62–8.

Fennema-Notestine, C., Archibald, S.L., Jacobson, M.W., Corey-Bloom, J., Paulsen, J.S., Peavy, G.M., Gamst, A.C., Hamilton, J.M., Salmon, D.P. and Jernigan, T.L., 2004. *In vivo* evidence of cerebellar atrophy and cerebral white matter loss in Huntington disease. *Neurology*, 63(6), 989–95.

Ferguson, B., Matyszak, M.K., Esiri, M.M. and Perry, V.H., 1997. Axonal damage in acute multiple sclerosis lesions. *Brain*, 120(3), 393–9.

Fife, B.T., Huffnagle, G.B., Kuziel, W.A. and Karpus, W.J., 2000. CC chemokine receptor 2 is critical for induction of experimental autoimmune encephalomyelitis. *J Exp Med*, 192(6), 899-905.

Fleming, A., Diekmann, H. and Goldsmith, P., 2013. Functional characterisation of the maturation of the blood-brain barrier in larval zebrafish. *PloS one*, 8(10), e77548.

Franklin, R.J.M. and Gallo, V., 2014. The translational biology of remyelination: past, present, and future. *Glia*, 62(11), 1905–15.

Franklin, R.J.M., 2002. Why does remyelination fail in multiple sclerosis? *Nature Reviews Neuroscience*, 3(9), 705–714.

Franklin, R.J.M. and ffrench-Constant, C., 2008. Remyelination in the CNS: from biology to therapy. *Nature Reviews Neuroscience*, 9(11), 839–855.

Franklin, R.J.M., ffrench-Constant, C., Edgar, J.M. and Smith, K.J., 2012. Neuroprotection and repair in multiple sclerosis. *Nature Reviews Neurology*, 8(11), 624–634.

ffrench-Constant, C. and Raff, M., 1986. Proliferating bipotential glial progenitor cells in adult rat optic nerve. *Nature*, 319(6053), 499–502.

Frischer, J.M., Bramow, S., Dal-Bianco, A., Lucchinetti, C.F., Rauschka, H., Schmidbauer, M., Laursen, H,m Sorensen., P.S. and Lassmann, H., 2009. The relation between inflammation and neurodegeneration in multiple sclerosis brains. *Brain*, 132(5), 1175–89.

Fryer, A.E., 1998. Goldberg-Shprintzen syndrome: report of a new family and review of the literature. *Clinical Dysmorphology*, 7(2), 97–101.

Fyffe-Maricich, S.L., Schott, A., Karl, M., Krasano, J. and Miller, R.H., 2013. Signaling through ERK1/2 controls myelin thickness during myelin repair in the adult central nervous system. *The Journal of Neuroscience*, 33(47), 18402–8.

Fünfschilling, U., Supplie, L.M., Mahad, D., Boretius, S., Saab, A.S., Edgar, J., Brinkmann, B.G., Kassmann, C.M., Tzvetanova, I.D., Möbius, W., Diaz, F., Meijer, D., Suter, U., Hamprecht, B., Sereda, M.W., Moraes, C.T., Frahm, J., Goebbels, S. and Nave, K.-A., 2012. Glycolytic oligodendrocytes maintain myelin and long-term axonal integrity. *Nature*, 485(7399), 517-21.

Gautier, H.O., Evans, K.A., Volbracht, K., James, R., Sitniknov, S., Lungaard, I., James, F., Lao-Peregrin, C., Reynolds, R., Franklin, R.J.M. and Kárádóttir, R.T., 2015.

Neuronal activity regulates remyelination via glutamate signalling to oligodendrocyte progenitors. *Nature Communications*, 6, 8518.

Gay, F.W., Drye, T.J., Dick, G.W. and Esiri, M.M., 1997. The application of multifactorial cluster analysis in the staging of plaques in early multiple sclerosis. Identification and characterization of the primary demyelinating lesion. *Brain*, 120(8), 1461–83.

Ge, Y., Grossman, R.I., Udupa, J.K., Wei, L., Mannon, L.J., Polansky, M. and Kolson, D.L., 2000. Brain atrophy in relapsing-remitting multiple sclerosis and secondary progressive multiple sclerosis: longitudinal quantitative analysis. *Radiology*, 214(3), 665–670.

Ghysen, A. and Dambly-Chaudière, C., 2007. The lateral line microcosmos. *Genes and Development*, 21(17), 2118–30.

Gilmour, D.T., Maischein, H.-M. and Nüsslein-Volhard, C., 2002. Migration and function of a glial subtype in the vertebrate peripheral nervous system. *Neuron*, 34(4), 577–588.

Gilson, J. and Blakemore, W.F, 1993. Failure of remyelination in areas of demyelination produced in the spinal cord of old rats. *Neuropathol Appl Neurobiol*, 19(2), 173-81.

Glenn, T.D. and Talbot, W.S., 2013. Signals regulating myelination in peripheral nerves and the Schwann cell response to injury. *Current Opinion in Neurobiology*, 23(6), 1041-8.

Goessling, W., Allen, R.S., Guan, X., Jin, P., Uchida, N., Dovey, M., Harris, J.M., Metzger, M.E., Bonifacino, A.C., Stroncek, D., Stegner, J., Armant, M., Schlaeger, T., Tisdale, J.F., Zon, L.I., Donahue, R.E. and North, T.E., 2011. Prostaglandin E2 enhances human cord blood stem cell xenotransplants and shows long-term safety in preclinical nonhuman primate transplant models. *Cell Stem Cell*, 8(4), 445-58.

Goldschmidt, T., Antel, J., König, F., Brück, W., and Kuhlmann, T., 2009. Remyelination capacity of the MS brain decreases with disease chronicity. *Neurology*, 72(22), 1914-21.

Gomez-Sanchez, J.A., Carty, L., Iruarrizaga-Lejarreta, M., Palomo-Irigoyen, M., Varela-Rey, M., Griffith, M., Hantke, J., Macias-Camara, N., Azkargorta, M., Aurrekoetxea, I., De Juan, V.G., Jefferies, H.B., Aspichueta, P., Elortza, F., Aransay, A.M., Martinez-Chantar, M.L., Baas, F., Mato, J.M., Mirsky, R., Woodhoo, A. and Jessen, K.R., 2015. Schwann cell autophagy, myelinophagy, initiates myelin clearance from injured nerves. *The Journal of Cell Biology*, 210(1), 153–68.

Gordon, H.B., Letsou, A. and Bonkowsky, J.L., 2014. The leukodystrophies. *Seminars in Neurology*, 34(3), 312–20.

Gordon, T., 2016. Nerve regeneration in the peripheral and central nervous systems. *The Journal of Physiology*, 594(13), 3517–20.

Granato, M. and Nüsslein-Volhard, C., 1996. Fishing for genes controlling development. *Current Opinion in Genetics and Development*, 6(4), 461–468.

Grandel, H. and Brand, M., 2013. Comparative aspects of adult neural stem cell activity in vertebrates. *Development Genes and Evolution*, 223(1-2), 131–47.

Griffiths, I., Klugmann, M., Anderson, T., Yool, D., Thomson, C., Schwab, M.H., Schneider, A., Zimmermann, F., McCulloch, M., Nadon, N. and Nave, K.-A., 1998. Axonal swellings and degeneration in mice lacking the major proteolipid of myelin. *Science*, 280(5369), 1610–3.

Haffter, P. and Nüsslein-Volhard, C., 1996. Large scale genetics in a small vertebrate, the zebrafish. *The International Journal of Developmental Biology*, 40(1), 221–227.

Haffter, P., Odenthal, J., Mullins, M.C., Lin, S., Farrell, M.J., Vogelsang, E., Haas, F., Brand, M., van Eeden, F.J., Furutani-Seiki, M., Granato, M., Hammerschmidt, M., Heisenberg, C.P., Jiang, Y.J., Kane, D.A., Kelsh, R.N., Hopkins, N. and Nüsslein-Volhard, C., 1996. Mutations affecting pigmentation and shape of the adult zebrafish. *Development Genes and Evolution*, 206(4), 260–276.

Hahn, R., 1978. Relation between myelin sheath thickness and axon size in spinal cord white matter of some vertebrate species. *Journal of the Neurological Sciences*, 38(3), 421–434.

Hambleton, S., Salem, S., Bustamante, J., Bigley, V., Boisson-Dupuis, S., Azevedo, J., Fortin, A., Haniffa, M., Ceron-Gutierrez, L., Bacon, C.M., Menon, G., Trouillet, C., McDonald, D., Carey, P., Ginhoux, F., Alsina, L., Zumwalt, T.J., Kong, X.F., Kumaratatne, D., Butler, K., Hubeau, M., Feinberg, J., Al-Muhsen, S., Cant, A., Abel, L., Chaussabel, D., Doffinger, R., Talesnik, E., Grumach, A., Duarte, A., Abarca, K., Moraes-Vasconcelos, D., Burk, D., Berghuis, A., Geissmann, E., Collin, M., Casanova, J.L. and Gros, P., 2011. IRF8 mutations and human dendritic-cell immunodeficiency. *The New England Journal of Medicine*, 365(2), 127–38.

Hammerschmidt, M., Pelegri, F., Mullins, M.C., Kane, D.A., van Eeden, F.J., Granato, M., Brand, M., Furutani-Seiki, M., Haffter, P., Heisenberg, C.P., Jiang, Y.J., Kelsh, R.N., Odenthal, J., Warga, R.M. and Nüsslein-Volhard, C., 1996. dino and mercedes, two genes regulating dorsal development in the zebrafish embryo. *Development*, 123, 95–102.

Hampton, D.W., Serio, A., Pryce, G., Al-Izki, S., Franklin, R.J.M., Giovannoni, G., Baker, D. and Chandran, S., 2013. Neurodegeneration progresses despite complete elimination of clinical relapses in a mouse model of multiple sclerosis. *Acta Neuropathologica Communications*, 1(84), 1-17.

Harding, A.E. and Thomas, P.K., 1980. The clinical features of hereditary motor and sensory neuropathy types I and II. *Brain*, 103(2), 259–80.

Hartline, D.K. and Colman, D.R., 2007. Rapid conduction and the evolution of giant axons and myelinated fibers. *Current Biology*, 17(1), R29–35.

Hashimoto, D., Chow, A., Noizat, C., Teo, P., Beasley, M.B., Leboeuf, M., Becker, C.D., See, P., Price, J., Lucas, D., Gretrer, M., Mortha, A., Boyer, S.W., Forsberg, E.C., Tanaka, M., van Rooijen, N., García-Sastre, A., Stanley, E.R., Ginhoux, F., Frenette, P.S. and Merad, M., 2013. Tissue-resident macrophages self-maintain locally

throughout adult life with minimal contribution from circulating monocytes. *Immunity*, 38(4), 792–804.

He, D., Zhang, C., Zhao, X., Zhang, Y., Dai, Q., Li, Y. and Chu, L., 2016. Teriflunomide for multiple sclerosis. *The Cochrane Database of Systematic Reviews*, 3, p.CD009882.

Heppner, F.L., Greter, M., Marino, D., Falsig, J., Raivich, G., Hövelmeyer, N., Waisman, A., Rülicke, T., Prinz, M., Priller, J., Becher, B. and Aguzzi, A., 2005. Experimental autoimmune encephalomyelitis repressed by microglial paralysis. *Nature Medicine*, 11(2), 146-52

Herbomel, P., Thisse, B. and Thisse, C., 2001. Zebrafish early macrophages colonize cephalic mesenchyme and developing brain, retina, and epidermis through a M-CSF receptor-dependent invasive process. *Developmental Biology*, 238(2), 274–288.

Herbomel, P. and Levraud, J.-P., 2005. Imaging early macrophage differentiation, migration, and behaviors in live zebrafish embryos. *Methods in Molecular Medicine*, 105, 199–214.

Herbomel, P., Thisse, B. and Thisse, C., 1999. Ontogeny and behaviour of early macrophages in the zebrafish embryo. *Development*, 126(17), 3735–45.

Hickman, S.E., Kingery, N.D., Ohsumi, T.K., Borowsky, M.L., Wang, L.C., Means, T.K. and El Khoury, J., 2013. The microglial sensome revealed by direct RNA sequencing. *Nature Neuroscience*, 16(12), 1896–1905.

Hinks, G.L. and Franklin, R.J.M., 2000. Delayed changes in growth factor gene expression during slow remyelination in the CNS of aged rats. *Molecular and Cellular Neurosciences*, 16(5), 542–56.

Hochreiter-Hufford, A. and Ravichandran, K.S., 2013. Clearing the dead: apoptotic cell sensing, recognition, engulfment, and digestion. *Cold Spring Harbor Perspectives in Biology*, 5(1), a008748.

Hsu, C.-C., Hou, M.F., Hong, J.R., Wu, J.L. and Her, G.M., 2010. Inducible male infertility by targeted cell ablation in zebrafish testis. *Marine Biotechnology*, 12(4), 466–78.

Huang, B., Wei, W., Wang, G., Gaertig, M.A., Feng, Y., Wang, W., Li, X.J. and Li, S., 2015. Mutant huntingtin downregulates myelin regulatory factor-mediated myelin gene expression and affects mature oligodendrocytes. *Neuron*, 85(6), 1212–26.

Huang, J.K., Jarjour, A.A., Nait-Oumesmar, B., Kerninon, C., Williams, A., Krezel, W., Kagechika, H., Bauer, J., Zhao, C., Baron-van Evercooren, A., Chambon, P., ffrench-Constant, C. and Franklin, R.J.M., 2011. Retinoid X receptor gamma signaling accelerates CNS remyelination. *Nature Neuroscience*, 14(1), 45–53.

Hughes, E.G., Kang, S.H., Fukaya, M. and Bergles, D.E., 2013. Oligodendrocyte progenitors balance growth with self-repulsion to achieve homeostasis in the adult brain. *Nature Neuroscience*, 16(6), 668-76.

Irvine, K.A. and Blakemore, W.F., 2008. Remyelination protects axons from demyelination-associated axon degeneration. *Brain*, 131(6), 1464–77.

Itoyama, Y., Webster, H.D., Richardson, E.P. Jr. and Trapp, B.D. Schwann cell remyelination of demyelinated axons in spinal cord multiple sclerosis lesions. *Annals of Neurology*, 14(3), 339–346.

Jeffery, N.D. and Blakemore, W.F., 1997. Locomotor deficits induced by experimental spinal cord demyelination are abolished by spontaneous remyelination. *Brain*, 120(1), 27–37.

Jersild, C., Svejgaard, A. and Fog, T., 1972. HL-A antigens and multiple sclerosis. *Lancet*, 1(7762), 1240–1.

Jessen, K.R. and Mirsky, R., 2016. The repair Schwann cell and its function in regenerating nerves. *The Journal of Physiology*, 594(13), 3521–31.

Jessen, K.R. and Mirsky, R., 2005. The origin and development of glial cells in peripheral nerves. *Nature Reviews. Neuroscience*, 6(9), 671–82.

Johnson, K.P., 2014. Glatiramer acetate for treatment of relapsing–remitting multiple sclerosis. *Expert Review of Neurotherapeutics*, 12(4), 371–384.

Johnson, K.P., Brooks, B.R., Cohen, J.A., Ford, C.C., Goldstein, J., Lisak, R.P., Myers, L.W., Panitch, H.S., Rose, J.W. and Schiffer, R.B., 1995. Copolymer 1 reduces relapse rate and improves disability in relapsing-remitting multiple sclerosis: results of a phase III multicenter, double-blind placebo-controlled trial. The Copolymer 1 Multiple Sclerosis Study Group. *Neurology*, 45(7), 1268–76.

Johnson, K.P., Brooks, B.R., Cohen, J.A., Ford, C.C., Goldstein, J., Lisak, R.P., Myers, L.W., Panitch, H.S., Roe, J.W., Schiffer, R.B., Vollmer, T., Weiner, L.P. and Wolinsky, J.S., 1998. Extended use of glatiramer acetate (Copaxone) is well tolerated and maintains its clinical effect on multiple sclerosis relapse rate and degree of disability. Copolymer 1 Multiple Sclerosis Study Group. *Neurology*, 50(3), 701–8.

Johnston, M.V. and Hoon, A.H. Jr., 2006. Cerebral palsy. *Neuromolecular Medicine*, 8(4), 435–50.

Kang, H. and Lichtman, J.W., 2013. Motor axon regeneration and muscle reinnervation in young adult and aged animals. *The Journal of neuroscience*, 33(50), 19480–91.

Kang, S.H., Li, Y., Fukaya, M., Lorenzini, I., Cleveland, D.W., Ostrow, L.W., Rothstein, J.D. and Bergles, D.E., 2013. Degeneration and impaired regeneration of gray matter oligodendrocytes in amyotrophic lateral sclerosis. *Nature Neuroscience*, 16(5), 571–9.

Káradóttir, R., Cavelier, P., Bergersen, L.H. and Attwell, D., 2005. NMDA receptors are expressed in oligodendrocytes and activated in ischaemia. *Nature*, 438(7071), 1162–1166.

Kaya, F., Mannioui, A., Cheseneau, A., Sekizar, S., Maillard, E., Ballagny, C., Houel-Renault, L., Dupasquier, D., Bronchain, O., Holzmann, I., Desmazieres, A., Thomas, J.L., Demeinex, B.A., Brophy, P.J., Zalc, B. and Mazabraud, A., 2012. Live imaging

of targeted cell ablation in Xenopus: a new model to study demyelination and repair. *Journal of Neuroscience*, 32(37), 12885–12895.

Keightley, M.-C., Wang, C.H., Pazhakh, V. and Lieschke, G.J., 2014. Delineating the roles of neutrophils and macrophages in zebrafish regeneration models. *The International Journal of Biochemistry and Cell Biology*, 56, 92–106.

Khajavi, M., Shiga, K., Wiszniewski, W., He, F., Shaw, C.A., Yan, J., Wensel, T.G., Snipes, G.J. and Lupski, J.R., 2007. Oral curcumin mitigates the clinical and neuropathologic phenotype of the Trembler-J mouse: a potential therapy for inherited neuropathy. *American Journal of Human Genetics*, 81(3), 438–453.

Kierdorf, K., Erny, D., Goldmann, T., Sander, V., Schulz, C., Perdiguero, E.G., Wieghofer, P., Heinrich, A., Riemke, P., Hölscher, C., Müller, D.N., Luckow, B., Brocker, T., Debowski, K., Fritz, G., Opdenakker, G., Diefenbach, A., Biber, K., Heikenwalder, M., Geissmann, F., Rosenbauer, F. and Prinz, M., 2013. Microglia emerge from erythromyeloid precursors via Pu. 1-and Irf8-dependent pathways. *Nature Neuroscience*, 16(3), 273-80.

Kim, S., Lee, Y.I., Chang, K.Y., Lee, D.W., Cho, S.C., Ha, Y.W., Na, J.E., Rhyu, I.J., Park, S.C. and Park, H.C., 2015. Promotion of remyelination by sulfasalazine in a transgenic zebrafish model of demyelination. *Molecules and Cells*, 38(11), 1013–21.

Kimmel, C.B., Powell, S.L. and Metcalfe, W.K., 1982. Brain neurons which project to the spinal cord in young larvae of the zebrafish. *The Journal of Comparative Neurology*, 205(2), 112–27.

Kirby, B.B., Takada, N., Latimer, A.J., Shin, J., Carney, T.J., Kelsh, R.N. and Appel, B., 2006. *In vivo* time-lapse imaging shows dynamic oligodendrocyte progenitor behavior during zebrafish development. *Nature Neuroscience*, 9(12), 1506–1511.

Kiryu-Seo, S., Ohno, N., Kidd, G.J., Komuro, H. and Trapp, B.D., 2010. Demyelination increases axonal stationary mitochondrial size and the speed of axonal mitochondrial transport. *The Journal of Neuroscience*, 30(19), 6658–66.

Klugmann, M., Schwab, M.H., Pühlhofer, A., Schneider, A., Zimmermann, F., Griffiths, I.R. and Nave, K.-A., 1997. Assembly of CNS myelin in the absence of proteolipid protein. *Neuron*, 18(1), 59–70.

Kornek, B., Storch, M.K., Weissert, R., Wallström, E., Stefferl, A., Olsson, T., Linington, C., Schmidbauer, M. and Lassmann, H., 2000. Multiple sclerosis and chronic autoimmune encephalomyelitis: a comparative quantitative study of axonal injury in active, inactive, and remyelinated lesions. *The American Journal of Pathology*, 157(1), 267–76.

Kotter, M.R., Stadelmann, C. and Hartung, H.-P., 2011. Enhancing remyelination in disease - can we wrap it up? *Brain*, 134(7), 1882–1900.

Kotter, M.R., Li, W.W., Zhao, C. and Franklin, R.J.M., 2006. Myelin impairs CNS remyelination by inhibiting oligodendrocyte precursor cell differentiation. *The Journal of Neuroscience*, 26(1), 328–32.

Kotter, M.R., Zhao, C., van Rooijen, N. and Franklin, R.J.M., 2005. Macrophage-depletion induced impairment of experimental CNS remyelination is associated with a reduced oligodendrocyte progenitor cell response and altered growth factor expression. *Neurobiology of Disease*, 18(1), 166–175.

Kotter, M.R., Setzu, A., Sim, F.J., van Rooijen, N. and Franklin, R.J.M., 2001. Macrophage depletion impairs oligodendrocyte remyelination following lysolecithin-induced demyelination. *Glia*, 35(3), 204–212.

Koudelka, S., Voas, M.G., Almeida, R.G., Baraban, M., Soetaert, J., Meyer, M.P., Talbot, W.S. and Lyons, D.A., 2016. Individual neuronal subtypes exhibit diversity in CNS myelination mediated by synaptic vesicle release. *Current Biology*, 26(11), 1447–55.

Krajewski, K.M., Lewis, R.A., Fuerst, D.R., Turansky, C., Hinderer, S.R., Garbern, J., Kamholz, J. and Shy, M.E., 2000. Neurological dysfunction and axonal degeneration in Charcot-Marie-Tooth disease type 1A. *Brain*, 123(7), 1516–27.

Kremer, D., Küry, P. and Dutta, R., 2015. Promoting remyelination in multiple sclerosis: current drugs and future prospects. *Multiple sclerosis*, 21(5), 541–9.

Kroehne, V., Freudenreich, D., Hans, S., Kaslin, J. and Brand, M., 2011. Regeneration of the adult zebrafish brain from neurogenic radial glia-type progenitors. *Development*, 138(22), 4831–41.

Küffer, A., Lakkaraju, A.K., Mogha, A., Petersen, S.C., Airich, K., Doucerain, C., Marpakwar, R., Bakirci, P., Senatore, A., Monnard, A., Schiavi, C., Nuvolone, M., Grosshans, B., Hornemann, S., Bassilana, F., Monk, K.R. and Aguzzi, A., 2016. The prion protein is an agonistic ligand of the G protein-coupled receptor Adgrg6. *Nature*, 536(7617), 464-8.

Kuhlmann, T., Miron, V., Cui, Q., Wegner, C., Antel, J. and Brück, W., 2008. Differentiation block of oligodendroglial progenitor cells as a cause for remyelination failure in chronic multiple sclerosis. *Brain*, 131(7), 1749–58.

Kuhlmann, T., Lingfeld, G., Bitsch, A., Shuchardt, J. and Brück, W., 2002. Acute axonal damage in multiple sclerosis is most extensive in early disease stages and decreases over time. *Brain*, 125(P10), 2202–12.

Kukley, M., Capetillo-Zarate, E. and Dietrich, D., 2007. Vesicular glutamate release from axons in white matter. *Nature Neuroscience*, 10(3), 311–320.

Kurimoto, T., Yin, Y., Habboub, G., Gilbert, H.Y., Li, Y., Nakao, S., Hafezi-Moghadam, A. and Benowitz, L.I., 2013. Neutrophils express oncomodulin and promote optic nerve regeneration. *The Journal of Neuroscience*, 33(37), 14816–24.

Kwan, K.M., Fujimoto, E., Grabher, C., Mangum, B.D., Hardy, M.E., Campbell, D.S., Parant, J.M., Yost, H.J., Kanki, J.P. and Chien, C.B., 2007. The Tol2kit: A multisite gateway-based construction kit forTol2 transposon transgenesis constructs. *Developmental Dynamics*, 236(11), 3088–3099.

Kyritsis, N., Kizil, C., Zocher, S., Kroehne, V., Kaslin, J., Freudenreich, D., Iltzsche, A. and Brand, M., 2012. Acute inflammation initiates the regenerative response in the adult zebrafish brain. *Science*, 338(6112), 1353-6.

La Mantia, L., Tramacere, I., Firwana, B., Pacchetti, I., Palumbo, R. and Filippini, G., 2016. Fingolimod for relapsing-remitting multiple sclerosis. *The Cochrane Database of Systematic Reviews*, 4, p.CD009371.

Lamason, R., Mohideen, M., Mest, J., Wong, A.C., Norton, H.L., Aros, M.C., Jurynec, M.J., Mao, X., Humphreville, V.R., Humbert, J.E., Sinha, S., Moore, J.L., Jagadeeswaran, P., Zhao, W., Ning, G., Makalowska, I., McKeigue, P.M., O'Donnell, D., Kittles, R., Parra, E.J., Mangini, N.J., Grunwald, D.J., Shriver, M.D., Canfield, V.A. and Cheng, K.C., 2005. SLC24A5, a putative cation exchanger, affects pigmentation in zebrafish and humans. *Science*, 310(5755), 1782-6.

Lampert, P.W. and Kies, M.W., 1967. Mechanism of demyelination in allergic encephalomyelitis of guinea pigs. An electron microscopic study. *Experimental Neurology*, 18(2), p.210-23.

Lampron, A., Larochelle, A. and Laflamme, N., Préfontaine, P., Plante, M.M., Sánchez, M.G., Yong, V.W., Stys, P.K., Tremblay, M.È. and Rivest, S., 2015. Inefficient clearance of myelin debris by microglia impairs remyelinating processes. *J Exp Med*., 212(4), 481-95.

Lappe-Siefke, C., Goebbels, S., Gravel, M., Nicksch, E., Lee, J., Braun, P.E., Griffiths, I.R. and Nave, K.-A., 2003. Disruption of Cnp1 uncouples oligodendroglial functions in axonal support and myelination. *Nature Genetics*, 33(3), 366–374.

Lassmann, H., 1983. Comparative neuropathology of chronic experimental allergic encephalomyelitis and multiple sclerosis. *Schriftenreihe Neurologie*, 25, 1–135.

Lassmann, H., 2012. Cortical lesions in multiple sclerosis: inflammation versus neurodegeneration. *Brain*, 135(10), 2904–2905.

Lassmann, H., van Horssen, J. and Mahad, D., 2012. Progressive multiple sclerosis: pathology and pathogenesis. *Nature Reviews. Neurology*, 8(11), 647–56.

Lassmann, H., Brück, W. and Lucchinetti, C.F., 2007. The immunopathology of multiple sclerosis: an overview. *Brain Pathology*, 17(2), 210–8.

Lassmann, H., Brück, W. and Lucchinetti, C., 2001. Heterogeneity of multiple sclerosis pathogenesis: implications for diagnosis and therapy. *Trends in Molecular Medicine*, 7(3), 115–21.

Lee, S., Leach, M.K., Redmond, S.A., Chong, S.Y., Mellon, S.H., Tuck, S.J., Feng, Z.Q., Corey, J.M. and Chan, J.R., 2012. A culture system to study oligodendrocyte myelination processes using engineered nanofibers. *Nature Methods*, 9(9), 917-22.

Lee, Y., Morrison, B.M., Li, Y., Lengacher, S., Farah, M.H., Hoffman, P.N., Liu, Y., Tsingalia, A., Jin, L., Zhang, P.W., Pellerin, L., Magistretti, P.J. and Rothstein, J.D., 2012. Oligodendroglia metabolically support axons and contribute to neurodegeneration. *Nature*, 487(7408), 443–8.

Lee, S.M., Rosen, S., Weinstein, P., van Rooijen, N. and Noble-Haeusslein, L.J., 2011. Prevention of both neutrophil and monocyte recruitment promotes recovery after spinal cord injury. *Journal of Neurotrauma*, 28(9), 1893–907.

Li, Y., Du, X.F., Liu, C.S., Wen, Z.L. and Du, J.L., 2012. Reciprocal regulation between resting microglial dynamics and neuronal activity *in vivo*. *Developmental Cell*, 23(6), 1189–202.

Li, L., Jin, H., Xu, J., Shi, Y. and Wen, Z., 2011. Irf8 regulates macrophage versus neutrophil fate during zebrafish primitive myelopoiesis. *Blood*, 117(4), 1359–69.

Liang, X., Draghi, N.A. and Resh, M.D., 2004. Signaling from integrins to Fyn to Rho family GTPases regulates morphologic differentiation of oligodendrocytes. *The Journal of Neuroscience*, 24(32), 7140–9.

Lindner, M., Thümmler, K., Arthur, A., Brunner, S., Elliott, C., McElroy, D., Mohan, H., Williams, A., Edgar, J.M., Schuh, C., Stadelmann, C., Barnett, S., Lassmann, H., Mücklish, S., Mudaliar, M., Schaeren-Wiemers, N., Meinl, E. and Linington, C., 2015.

Fibroblast growth factor signalling in multiple sclerosis: inhibition of myelination and induction of pro-inflammatory environment by FGF9. *Brain*, 138(7), 1875-93.

Linker, R.A. and Haghikia, A., 2016. Dimethyl fumarate in multiple sclerosis: latest developments, evidence and place in therapy. *Therapeutic Advances in Chronic Disease*, 7(4), 198–207.

Lister, J., Robertson, C.P., Lepage, T., Johnson, S.L. and Raible, D.W., 1999. Nacre encodes a zebrafish microphthalmia-related protein that regulates neural-crest-derived pigment cell fate. *Development*, 126(17), 3757-67.

Liu, J., Dietz, K., DeLoyht, J.M., Pedre, X., Kelkar, D., Kaur, J., Vialou, V., Lobo, M.K., Dietz, D.M., Nestler, E.J., Dupree, J. and Casaccia, P., 2012. Impaired adult myelination in the prefrontal cortex of socially isolated mice. *Nature Neuroscience*, 15(12), 1621–3.

Locatelli, G., Wörtge, S., Buch, T., Ingold, B., Frommer, F., Sobottka, B., Krüger, M., Karram, K., Bühlmann, C., Bechmann, I., Heppner, F.L., Waisman, A. and Bechler, B., 2012. Primary oligodendrocyte death does not elicit anti-CNS immunity. *Nature Neuroscience*, 15(4), 543-50.

Lovas, G., Szilágyi, N., Majtényi, K., Palkovitz, M. and Komoly, S., 2000. Axonal changes in chronic demyelinated cervical spinal cord plaques. *Brain*, 123(2), 308–17.

Lublin, F.D., Reingold, S.C., Cohen, J.A., Cutter, G.R., Sørensen, P.S., Thompson, A.J., Wolinsky, J.S., Balcer, L.J., Banwell, B., Barkhof, F., Bebo, B. Jr., Calabresi, P.A., Clanet, M., Comi, G., Fox, R.J., Freedman, M.S., Goodman, A.D., Inglese, M., Kappos, L., Kieseier, B.C., Lincoln, J.A., Lubetzki, C., Miller, A.E., Montalban, X., O'Connor, P.W., Petkau, J., Pozzilli, C., Rudick, R.A., Sormani, M.P., Stüve, O., Waubant, E. and Polman, C.H., 2014. Defining the clinical course of multiple sclerosis: the 2013 revisions. *Neurology*, 83(3), 278–86.

Lublin, F.D. and Reingold, S.C., 1996. Defining the clinical course of multiple sclerosis: results of an international survey. National Multiple Sclerosis Society (USA)

Advisory Committee on Clinical Trials of New Agents in Multiple Sclerosis. *Neurology*, 46(4), 907–11.

Lucchinetti, C., Brück, W., Parisi, J., Scheithauer, B., Rodriguez, M. and Lassmann, H., 2000. Heterogeneity of multiple sclerosis lesions: implications for the pathogenesis of demyelination. *Annals of Neurology*, 47(6), 707-17.

Lucchinetti, C., Brück, W., Parisi, J., Scheithauer, B., Rodriguez, M. and Lassmann, H., 1999. A quantitative analysis of oligodendrocytes in multiple sclerosis lesions. *Brain*, 122(12), 2279-95.

Ludwin, S.K. and Sternberger, N.H., 1984. An immunohistochemical study of myelin proteins during remyelination in the central nervous system. *Acta Neuropathologica*, 63(3), 240–8.

Lundgaard, I., Luzhynskaya, A., Stockley, J.H., Wang, Z., Evans, K.A., Swire, M., Volbracht, K., Gautier, H.O., Franklin, R.J.M., ffrench-Constant, C., Attwell, D. and Kárádóttir, R.T., 2013. Neuregulin and BDNF induce a switch to NMDA receptor-dependent myelination by oligodendrocytes. *PLoS Biol*, 11(12), e1001743.

Lyons, D.A. and Talbot, W.S., 2015. Glial cell development and function in zebrafish. *Cold Spring Harbor Perspectives in Biology*, 7(2), a020586.

Lyons, D.A., Naylor, S.G., Mercurio, S., Dominiguez, C. and Talbot, W.S., 2008. KBP is essential for axonal structure, outgrowth and maintenance in zebrafish, providing insight into the cellular basis of Goldberg-Shprintzen syndrome. *Development*, 135(3), 599–608.

Lyons, D.A., Pogoda, H.M., Voas, M.G., Woods, I.G., Diamond, B., Nix, R., Arana, N., Jacobs, J. and Talbot, W.S., 2005. erbb3 and erbb2 are essential for schwann cell migration and myelination in zebrafish. *Current Biology*, 15(6), 513–24.

MacRae, C.A. and Peterson, R.T., 2015. Zebrafish as tools for drug discovery. *Nature Reviews Drug Discovery*, 14(10), 721–731.

Maeda, Y., Solanky, M., Menonna, J., Chapin, J., Li, W. and Dowling, P., 2001. Platelet-derived growth factor-α receptor-positive oligodendroglia are frequent in multiple sclerosis lesions. *Annals of Neurology*, 49(6), 776-85.

Mahad, D., Ziabreva, I., Campbell, G., Lax, N., White, K., Hanson, P.S., Lassmann, H. and Turnbull, D.M., 2009. Mitochondrial changes within axons in multiple sclerosis. *Brain*, 132(5), 1161-74.

Mahad, D., Ziabreva, I., Lassmann, H. and Turnbull, D., 2008. Mitochondrial defects in acute multiple sclerosis lesions. *Brain*, 131(7), 1722-1735.

Makinodan, M., Rosen, K.M., Ito, S. and Corfas, G., 2012. A critical period for social experience-dependent oligodendrocyte maturation and myelination. *Science*, 337(6100), 1357–60.

Manrique-Hoyos, N., Jürgens, T., Grønborg, M., Kreutzfeldt, M., Schedensack, M., Kuhlmann, T., Schrick, C., Brück, W., Urlaub, H., Simons, M. and Merkler, D., 2012. Late motor decline after accomplished remyelination: impact for progressive multiple sclerosis. *Annals of Neurology*, 71(2), 227–44.

Martini, R. and Willison, H., Neuroinflammation in the peripheral nerve: Cause, modulator, or bystander in peripheral neuropathies? *Glia*, 64(4), 475–486.

Martini, R., Fischer, S., López-Vales, R. and David, S., 2008. Interactions between Schwann cells and macrophages in injury and inherited demyelinating disease. *Glia*, 56(14), 1566–77.

Mathews, E.S. and Appel, B., 2016. Oligodendrocyte differentiation. *Methods in Cell Biology*, 134, 69–96.

Matsushima, G.K. and Morell, P., 2001. The neurotoxicant, cuprizone, as a model to study demyelination and remyelination in the central nervous system. *Brain Pathology*, 11(1), 107–16.

Mayadas, T.N., Cullere, X. and Lowell, C.A., 2014. The multifaceted functions of neutrophils. *Annual Review of Pathology*, 9, 181–218.

McDonald, W.I., Compston, A., Edan, G., Goodkin, D., Hartung, H.P., Lublin, F.D., McFarland, H.F., Paty, D.W., Polman, C.H., Reingold, S.C., Sandberg-Wollheim, M., Sibley, W., Thompson, A., van den Noort, S., Weinshenker, B.Y. and Wolinsky, J.S., 2001. Recommended diagnostic criteria for multiple sclerosis: guidelines from the International Panel on the diagnosis of multiple sclerosis. *Annals of Neurology*, 50(1), 121–7.

McKenzie, I.A., Ohayon, D., Li, H., de Faria, J.P., Emery, B., Tohyama, K. and Richardson, W.D., 2014. Motor skill learning requires active central myelination. *Science*, 346(6207), 318–322.

McMenamin, S.K., Chandless, M.N. and Parichy, D.M., 2016. Working with zebrafish at postembryonic stages. *Methods in Cell Biology*, 134, 587–607.

McMurran, C.E., Jones, C.A., Fitzgerald, D.C. and Franklin, R.J.M., 2016. CNS Remyelination and the innate immune system. *Frontiers in Cell and Developmental Biology*, 4, 38.

Mei, F., Fancy, S.P., Shen, Y.A., Niu, J., Zhao, C., Presley, B. Miao, E., Lee, S., Mayoral, S.R., Redmond, S.A., Etxeberria, A., Xiao, L., Franklin, R.J.M., Green, A., Hauser, S.L. and Chan, J.R., 2014. Micropillar arrays as a high-throughput screening platform for therapeutics in multiple sclerosis. *Nature Medicine*, 20(8), 954–60.

Mensch, S., Baraban, M., Almeida, R., Czopka, T., Ausborn, J., El Manira, A. and Lyons, D.A., 2015. Synaptic vesicle release regulates myelin sheath number of individual oligodendrocytes *in vivo*. *Nature Neuroscience*, 18(5), 628–30.

Merkler, D., Ernsting, T., Kerschensteiner, M., Brück, W. and Stadelmann, C., 2006. A new focal EAE model of cortical demyelination: multiple sclerosis-like lesions with rapid resolution of inflammation and extensive remyelination. *Brain*, 129(8), 1972–83.

Mi, S., Pepinsky, R.B. and Cadavid, D., 2013. Blocking LINGO-1 as a therapy to promote CNS repair: from concept to the clinic. *CNS Drugs*, 27(7), 493–503.

Mi, S., Miller, R.H., Tang, W., Lee, X., Hu, B., Wu, W., Zhang, Y., Shields, C.B., Zhang, Y., Miklasz, S., Shea, D., Mason, J., Franklin, R.J.M., Ji, B., Shao, Z., Chédotal, A., Bernard, F., Roulois, A., Xu, J., Jung, V. and Pepinsky, B., 2009. Promotion of central nervous system remyelination by induced differentiation of oligodendrocyte precursor cells. *Annals of Neurology*, 65(3), 304–15.

Mi, S., Hu, B., Hahm, K., Luo, Y., Kam Hui, E.S., Yuan, Q., Wong, W.M., Wang, L., Su, H., Chu, T.H., Guo, J., Zhang, W., So, K.F., Pepinsky, B., Shao, Z., Graff, C., Garber, E., Jung, V., Wu, E.X. and Wu, W., 2007. LINGO-1 antagonist promotes spinal cord remyelination and axonal integrity in MOG-induced experimental autoimmune encephalomyelitis. *Nature Medicine*, 13(10), 1228–33.

Mi, S., Miller, R.H., Lee, X., Scott, M.L., Shulang-Morskaya, S., Shao, Z., Chang, J., Thill, G., Levesque, M., Zhang, M., Hession, C., Sah, D., Trapp, B., He, Z., Jung, V., McCoy, J.M. and Pepinsky, R.B., 2005. LINGO-1 negatively regulates myelination by oligodendrocytes. *Nature Neuroscience*, 8(6), 745–51.

Mi, S., Lee, X., Shao, Z., Thill, G., Ji, B., Relton, J., Levesque, M., Allaire, N., Perrin, S., Sands, B., Crowell, T., Cate, R.L., McCoy, J.M. and Pepinsky, R.B. 2004. LINGO-1 is a component of the Nogo-66 receptor/p75 signaling complex. *Nature Neuroscience*, 7(3), 221–8.

Michailov, G.V., Sereda, M.W., Brinkmann, B.G., Fischer, T.M., Haung, B., Birchmeier, C., Role, L., Lai, C., Schwab, M.H. and Nave, K.-A., 2004. Axonal neuregulin-1 regulates myelin sheath thickness. *Science*, 304(5671), 700–3.

Miron, V.E. and Franklin, Robin J M, 2014. Macrophages and CNS remyelination. *Journal of Neurochemistry*, 130(2), 165–71.

Miron, V.E., Boyd, A., Zhao, J.W., Yuen, T.J., Ruckh, J.M., Shadrach, J.L., van Wijngaarden, P., Wagers, A.J., Williams, A., Franklin, R.J.M. and ffrench-Constant, C., 2013. M2 microglia and macrophages drive oligodendrocyte differentiation during CNS remyelination. *Nature Neuroscience*, 16(9), 1211-8.

Miron, V.E., Kuhlmann, T. and Antel, J.P., 2011. Cells of the oligodendroglial lineage, myelination, and remyelination. *Biochimica et Biophysica Acta*, 1812(2), 184–193.

Monk, K.R., Oshima, K., Jörs, S., Heller, S. and Talbot, W.S., 2011. Gpr126 is essential for peripheral nerve development and myelination in mammals. *Development*, 138(13), 2673–80.

Monk, K.R. and Talbot, W.S., 2009. Genetic dissection of myelinated axons in zebrafish. *Current Opinion in Neurobiology*, 19(5), 486–490.

Monk, K.R., Naylor, S.G., Glenn, T.D., Mercurio, S., Perlin, J.R., Dominiguez, C., Moens, C.B. and Talbot, W.S., 2009. A G protein-coupled receptor is essential for Schwann cells to initiate myelination. *Science*, 325(5946), 1402–5.

Morris, J.K., Lin, W., Hauser, C., Marchuk, Y., Getman, D. and Lee, K.F., 1999. Rescue of the cardiac defect in ErbB2 mutant mice reveals essential roles of ErbB2 in peripheral nervous system development. *Neuron*, 23(2), 273–83.

Mutsaers, S.E. and Carroll, W.M., 1998. Focal accumulation of intra-axonal mitochondria in demyelination of the cat optic nerve. *Acta Neuropathologica*, 96(2), 139–43.

Münzel, E.J., Becker, C.G., Becker, T. and Williams, A., 2014. Zebrafish regenerate full thickness optic nerve myelin after demyelination, but this fails with increasing age. *Acta Neuropathologica Communications*, 2, 77.

Münzel, E.J. and Williams, A., 2013. Promoting remyelination in multiple sclerosis - recent advances. *Drugs*, 73(18), 2017–29.

Najjar, S. and Pearlman, D.M., 2015. Neuroinflammation and white matter pathology in schizophrenia: systematic review. *Schizophrenia Research*, 161(1), 102–12.

Natrajan, M.S., de la Fuente, A.G., Crawford, A.H., Linehan, E., Nuñes, V., Johnson, K.R., Wu, T., Fitzgerald, D.C., Ricote, M., Bielekova, B. and Franklin, R.J.M., 2015. Retinoid X receptor activation reverses age-related deficiencies in myelin debris phagocytosis and remyelination. *Brain*, 138(12), 3581–97.

Nave, K.-A., 2010. Myelination and support of axonal integrity by glia. *Nature*, 468(7321), 244–252.

Nave, K.-A. and Salzer, J.L., 2006. Axonal regulation of myelination by neuregulin 1. *Current Opinion in Neurobiology*, 16(5), 492–500.

Nave, K.-A. and Trapp, B.D., 2008. Axon-glial signaling and the glial support of axon function. *Annual Review of Neuroscience*, 31, 535–61.

Nawaz, S., Schweitzer, J., Jahn, O. and Werner, H.B., 2013. Molecular evolution of myelin basic protein, an abundant structural myelin component. *Glia*, 61(8), 1364–1377.

Newbern, J. and Birchmeier, C., 2010. Nrg1/ErbB signaling networks in Schwann cell development and myelination. *Seminars in Cell and Developmental Biology*, 21(9), 922-8.

Nikić, I., Merkler, D., Sorbara, C., Brinkoetter, M., Kreutzfeldt, M., Bareyre, F.M., Brück, W., Bishop, D., Misgeld, T., Kerschensteiner, M., 2011. A reversible form of axon damage in experimental autoimmune encephalomyelitis and multiple sclerosis. *Nature Medicine*, 17(4), 495–9.

Nishiyama, A., Suzuki, R. and Zhu, X., 2014. NG2 cells (polydendrocytes) in brain physiology and repair. *Frontiers in Neuroscience*, 8, 133.

North, T.E., Goessling, W., Walkley, C.R., Lengerke, C., Kopani, K.R., Lord, A.M., Weber, G.J., Bowman, T.V., Jang, I.H., Grosser, T., Fitzgerald, G.A., Daley, G.Q., Orkin, S.H., Zon, L.I., 2007. Prostaglandin E2 regulates vertebrate haematopoietic stem cell homeostasis. *Nature*, 447(7147), 1007-11.

Ofengeim, D., Ito, Y., Najafov, A., Zhang, Y., Shan, B., DeWitt, J.P., Ye, J., Zhang, X., Chang, A., Vakifahmetoglu-Norberg, H., Geng, J., Py, B., Zhou, W., Amin, P., Berlink Lima, J., Qi, C., Yu, Q., Trapp, B. and Yuan, J. 2015. Activation of necroptosis in multiple sclerosis. *Cell Reports*, 10(11), 1836–49.

Ohnmacht, J., Yang, Y., Maurer, G.W., Barreiro-Iglesias, A., Tsarouchas, T.M., Wehner, D., Sieger, D., Becker, C.G. and Becker, T., 2016. Spinal motor neurons are regenerated after mechanical lesion and genetic ablation in larval zebrafish. *Development*, 143(9), 1464–74.

Oksenberg, J.R., Barcellos, L.F., Cree, B.A., Baranzini, S.E., Bugawan, T.L., Khan, O., Lincoln, R.R., Swerdlin, A., Mignot, E., Lin, L., Goodin, D., Erlich, H.A., Schmidt, S., Thomson, G., Reich, D.E., Pericak-Vance, M.A., Haines, J.L. and Hauser, S.L., 2004. Mapping multiple sclerosis susceptibility to the HLA-DR locus in African Americans. *American Journal of Human Genetics*, 74(1), 160–7.

Oluich, L.J., Stratton, J.A., Xing, Y.L., Ng, S.W., Cate, H.S., Sah, P., Windels, F., Kilpatrick, T.J. and Merson, T.D., 2012. Targeted ablation of oligodendrocytes induces axonal pathology independent of overt demyelination. *The Journal of Neuroscience*, 32(24), 8317–30.

Ousman, S.S. and David, S., 2000. Lysophosphatidylcholine induces rapid recruitment and activation of macrophages in the adult mouse spinal cord. *Glia*, 30(1), 92–104.

Paquet, D., Bhat, R., Sydow, A., Mandelkow, E.M., Berg, S., Hellberg, S., Fälting, J., Distel, M., Köster, R.W., Schmid, B. and Haass, C., 2009. A zebrafish model of tauopathy allows *in vivo* imaging of neuronal cell death and drug evaluation. *The Journal of Clinical Investigation*, 119(5), 1382–1395.

Pareyson, D., Reilly, M.M., Schenone, A., Fabrizi, G.M., Cavallaro, T., Santoro, L., Vita, G., Quattrone, A., Padua, L., Gemignani, F., Visioli, F., Laurà, M., Radice, D., Calabrese, D., Hughes, R.A., Solari, A., CMT-TRIAAL; CMT-TRAUK groups, 2011. Ascorbic acid in Charcot-Marie-Tooth disease type 1A (CMT-TRIAAL and CMT-TRAUK): a double-blind randomised trial. *The Lancet. Neurology*, 10(4), 320–8.

Parichy, D.M., Elizondo, M.R., Mills, M.G., Gordon, T.N. and Engeszer, R.E., 2009. Normal table of postembryonic zebrafish development: staging by externally visible anatomy of the living fish. *Developmental Dynamics*, 238(12), 2975-3015.

Park, H.-C., Shin, J., Roberts, R.K. and Appel, B., 2007. An olig2 reporter gene marks oligodendrocyte precursors in the postembryonic spinal cord of zebrafish. *Developmental Dynamics*, 236(12), 3402–7.

Passage, E., Norreel, J.C., Noack-Fraissignes, P., Sanguedolce, V., Pizant, J., Thirion, X., Robaglia-Schlupp, A., Pellissier, J.F. and Fontés, M., 2004. Ascorbic acid treatment corrects the phenotype of a mouse model of Charcot-Marie-Tooth disease. *Nature Medicine*, 10(4), 396–401.

Patani, R., Balaratnam, M., Vora, A. and Reynolds, R., 2007. Remyelination can be extensive in multiple sclerosis despite a long disease course. *Neuropathology and Applied Neurobiology*, 33(3), 277–87.

Patrikios, P., Stadelmann, C., Kutzelnigg, A., Rauschka, H., Schmidbauer, M., Laursen, H., Sorensen, P.S., Brück, W., Lucchinetti, C. and Lassmann, H., 2006. Remyelination is extensive in a subset of multiple sclerosis patients. *Brain*, 129(12), 3165–72.

Payne, S.C., Bartlett, C.A., Harvey, A.R., Dunlop, S.A. and Fitzgerald, M., 2012. Myelin sheath decompaction, axon swelling, and functional loss during chronic secondary degeneration in rat optic nerve. *Investigative Ophthalmology and Visual Science*, 53(10), 6093–6101.

Pellerin, L. and Magistretti, P.J., 2012. Sweet sixteen for ANLS. *Journal of Cerebral Blood Flow and Metabolism*, 32(7), 1152–66.

Pennuto, M., Tinelli, E., Malaguti, M., Del Carro, U., D'Antonio, M., Ron, D., Quattrini, A., Feltri, M.L. and Wrabetz, L., 2008. Ablation of the UPR-mediator CHOP restores motor function and reduces demyelination in Charcot-Marie-Tooth 1B mice. *Neuron*, 57(3), 393–405.

Peri, F. and Nüsslein-Volhard, C., 2008. Live imaging of neuronal degradation by microglia reveals a role for v0-ATPase a1 in phagosomal fusion *in vivo*. *Cell*, 133(5), 916–27.

Perlin, J.R., Lush, M.E., Stephens, W.Z., Piotrowski, T. and Talbot, W.S., 2011. Neuronal Neuregulin 1 type III directs Schwann cell migration. *Development*, 138(21), 4639–48.

Perry, V.H., Tsao, J.W., Fearn, S. and Brown, M.C., 1995. Radiation-induced reductions in macrophage recruitment have only slight effects on myelin degeneration in sectioned peripheral nerves of mice. *The European Journal of Neuroscience*, 7(2), 271–80.

Piaton, G., Aigrot, M.S., Williams, A., Moyon, S., Tepavcevic, V., Moutkine, I., Gras, J., Matho, K.S., Schmitt, A., Soellner, H., Huber, A.B., Ravassard, P. and Lubetzki, C., 2011. Class 3 semaphorins influence oligodendrocyte precursor recruitment and remyelination in adult central nervous system. *Brain*, 134(4), 1156–67.

Pisharath, H., 2007. Validation of nitroreductase, a prodrug-activating enzyme, mediated cell death in embryonic zebrafish (Danio rerio). *Comparative Medicine*, 57(3), 241–6.

Pogoda, H.-M., Sternheim, N., Lyons, D.A., Diamond, B., Hawkins, T.A., Woods, I.G., Bhatt, D.H., Franzini-Armstrong, C., Dominiguez, C., Arana, N., Jacobs, J., Nix, R., Fetcho, J.R. and Talbot, W.S., 2006. A genetic screen identifies genes essential for development of myelinated axons in zebrafish. *Developmental Biology*, 298(1), 118–31.

Pohl, H.B., Porcheri, C., Mueggler, T., Bachmann, L.C., Martino, G., Riethmacher, D., Franklin, R.J.M., Rudin, M. and Suter, U., 2011. Genetically induced adult oligodendrocyte cell death is associated with poor myelin clearance, reduced remyelination, and axonal damage. *The Journal of Neuroscience*, 31(3), 1069–80.

Powers, B., Sellers, D.L., Lovelett, E.A., Cheung, W., Aalami, S.P., Zapertov, N., Maris, D.O. and Horner, P.J., 2013. Remyelination reporter reveals prolonged refinement of spontaneously regenerated myelin. *Proceedings of the National Academy of Sciences of the United States of America*, 110(10), 4075–80.

Preston, M.A. and Macklin, W.B., 2014. Zebrafish as a model to investigate CNS myelination. *Glia*, 63(2), 177-93.

Prineas, J. and Parratt, J.D., 2012. Oligodendrocytes and the early multiple sclerosis lesion. *Annals of Neurology*, 72(1), 18–31.

Prineas, J.W. and Connell, F., 1979. Remyelination in multiple sclerosis. *Annals of Neurology*, 5(1), 22–31.

Prineas, J., 1975. Pathology of the early lesion in multiple sclerosis. *Human Pathology*, 6(5), 531-54.

Pringle, N.P., Mudhar, H.S., Collarini, E.J. and Richardson, W.D., 1992. PDGF receptors in the rat CNS: during late neurogenesis, PDGF alpha-receptor expression appears to be restricted to glial cells of the oligodendrocyte lineage. *Development*, 115(2), 535–51.

Proudfoot, N.J., 2011. Ending the message: poly(A) signals then and now. *Genes and Development*, 25(17), 1770–1782.

Love, S., 2006. Demyelinating diseases. *Journal of Clinical Pathology*, 59(11), 1151–1159.

Ransohoff, R.M., 2016. A polarizing question: do M1 and M2 microglia exist? *Nature Neuroscience*, 19(8), 987–91.

Rushton, W.A., 1951. A theory of the effects of fibre size in medullated nerve. *The Journal of physiology*, 115(1), 101–22.

Raphael, A.R. and Talbot, W.S., 2011. New insights into signaling during myelination in zebrafish. *Current Topics in Developmental Biology*, 97, 1–19.

Raphael, A.R., Lyons, D.A. and Talbot, W.S., 2011. ErbB signaling has a role in radial sorting independent of Schwann cell number. *Glia*, 59(7), 1047–1055.

Readhead, C. and Hood, L., 1990. The dysmyelinating mouse mutations shiverer (shi) and myelin deficient (shimld). *Behavior Genetics*, 20(2), 213–34.

Renshaw, S.A., Loynes, C.A., Elworthy, S., Ingham, P.W. and Whyte, M.K., 2007. Modeling inflammation in the zebrafish: how a fish can help us understand lung disease. *Experimental Lung Research*, 33(10), 549–54.

Richardson, W., Tripathi, R.B. and McKenzie, I., 2011. NG2-glia as multipotent neural stem cells: fact or fantasy? *Neuron*, 70(4), 661-73.

Riethmacher, D., Sonnenberg-Riethmacher, E., Brinkmann, B., Yamaai, T., Lewin, G.R. and Birchmeier, C., 1997. Severe neuropathies in mice with targeted mutations in the ErbB3 receptor. *Nature*, 389(6652), 725–30.

Rittchen, S., Boyd, A., Burns, A., Park, J., Fahmy, T.M., Metcalfe, S. and Williams, A., 2015. Myelin repair *in vivo* is increased by targeting oligodendrocyte precursor cells with nanoparticles encapsulating leukaemia inhibitory factor (LIF). *Biomaterials*, 56, 78–85.

Rivers, L.E., Young, K.M., Rizzi, M., Jamen, F., Psachoulia, K., Wade, A., Kessaris, N. and Richardson, W.D., 2008. PDGFRA/NG2 glia generate myelinating oligodendrocytes and piriform projection neurons in adult mice. *Nature Neuroscience*, 11(12), 1392–401.

Robinson, A.P., Harp, C.T., Noronha, A. and Miller, S.D., 2014. The experimental autoimmune encephalomyelitis (EAE) model of MS: utility for understanding disease pathophysiology and treatment. *Handbook of Clinical Neurology*, 122, 173–89.

Rosenberg, A.F., Wolman, M.A., Franzini-Armstrong, C. and Granato, M., 2012. *In vivo* nerve-macrophage interactions following peripheral nerve injury. *The Journal of Neuroscience*, 32(11), 3898–909.

Rosenberg, S.S., Kelland, E.E., Tokar, E., de la Torre, A.R. and Chan, J.R., 2008. The geometric and spatial constraints of the microenvironment induce oligodendrocyte differentiation. *Proceedings of the National Academy of Sciences of the United States of America*, 105(38), 14662–7.

Ruckh, J.M., Zhao, J.W., Shadrach, J.L., van Wijngaarden, P., Rao, T.N., Wagers, A.J. and Franklin, R.J.M., 2012. Rejuvenation of regeneration in the aging central nervous system. *Cell Stem Cell*, 10(1), 96–103.

Rudick, R.A., Stuart, W.H., Calabresi, P.A., Confavreux, C., Galetta, S.L., Radue, E.W., Lublin, F.D., Weinstock-Guttman, B., Wynn, D.R., Lynn, F., Panzara, M.A., Sandrock, A.W; SENTINEL Investigators, 2006. Natalizumab plus interferon beta-1a for relapsing multiple sclerosis. *New England Journal of Medicine*, 354(9), 911-23.

Saab, A.S., Tzvetavona, I.D., Trevisiol, A., Baltan, S., Dibaj, P., Kusch, K., Möbius, W., Goetze, B., Jahn, H.M., Huang, W., Steffens, H., Schombug, E.D., Pérez-Samartín, A., Péres-Cerdá, F., Bakhtiari, D., Matute, C., Löwel, S., Griesinger, C., Hirrlinger, J., Kirchhoff, F. and Nave, K.-A., 2016. Oligodendroglial NMDA receptors regulate glucose import and axonal energy metabolism. *Neuron*, 91(1), 119–32.

Sachs, H.H., Bercury, K.K., Popescu. D.C., Narayanan, S.P. and Macklin, W.B., 2014. A new model of cuprizone-mediated demyelination/remyelination. *ASN Neuro*, 6(5), 1-16.

Safaiyan, S., Kannaiyan, N., Snaidero, N., Brioschi, S., Biber, K., Yona, S., Edinger, A.L., Jung, S., Rossner, M.J. and Simons, M., 2016. Age-related myelin degradation burdens the clearance function of microglia during aging. *Nature Neuroscience*, 19(8), 995–8.

Sawcer, S., Hellenthal, G., Pirinen, M., Spencer, C.C., Patsopoulos, N.A., Moutsianas, L., Dilthey, A., Su, Z., Freeman, C., Hunt, S.E., Edkins, S., Gray, E., Booth, D.R., Potter, S.C., Goris, A., Band, G., Oturai, A.B., Strange, A., Saarela, J., Bellenguez, C,. Fontaine, B., Gillman, M., Hemmer, B., Gwilliam, R., Zipp, F., Jayakumar, A., Martin, R., Leslie, S., Hawkins, S., Giannoulatou, E., D'alfonso, S., Blackburn, H., Martinelli Boneschi, F., Liddle, J., Harbo, H.F., Perez, M.L., Spurkland, A., Waller, M.J., Mycko, M.P., Ricketts, M., Comabella, M., Hammond, N., Kockum, I., McCann, O.T., Ban, M., Whittaker, P., Kemppinen, A., Weston, P., Hawkins, C., Widaa, S., Zajicek, J., Dronov, S., Robertson, N., Bumpstead, S.J., Barcellos, L.F., Ravindrarajah, R., Abraham, R., Alfredsson,

L., Ardlie, K., Aubin, C., Baker, A., Baker, K., Baranzini, S.E., Bergamaschi, L, Bergamaschi R, Bernstein A, Berthele A, Boggild M, Bradfield JP, Brassat D., Broadley, S.A., Buck, D., Butzkueven, H., Capra, R., Carroll, W.M., Cavalla, P., Celius, E.G., Cepok, S., Chiavacci, R., Clerget-Darpoux, F., Clysters, K., Comi, G., Cossburn, M., Cournu-Rebeix, I., Cox, M.B., Cozen, W., Cree, B.A., Cross, A.H., Cusi, D., Daly, M.J., Davis, E., de Bakker, P.I., Debouverie, M., D'hooghe, M.B., Dixon, K., Dobosi, R., Dubois, B., Ellinghaus, D., Elovaara, I., Esposito, F., Fontenille, C., Foote, S., Franke, A., Galimberti, D., Ghezzi, A., Glessner, J., Gomez, R., Gout, O., Graham, C., Grant, S.F., Guerini, F.R., Hakonarson, H., Hall, P., Hamsten, A., Hartung, H.P., Heard, R.N., Heath, S., Hobart, J., Hoshi, M., Infante-Duarte, C., Ingram, G., Ingram, W., Islam, T., Jagodic, M., Kabesch, M., Kermode, A.G., Kilpatrick, T.J., Kim, C., Klopp, N., Koivisto, K., Larsson, M., Lathrop, M., Lechner-Scott, J.S., Leone, M.A., Leppä, V., Liljedahl, U., Bomfim, I.L., Lincoln, R.R., Link, J., Liu, J., Lorentzen, A.R., Lupoli, S., Macciardi, F., Mack, T., Marriott, M., Martinelli, V., Mason, D., McCauley, J.L., Mentch, F., Mero, I.L., Mihalova, T., Montalban, X., Mottershead, J., Myhr, K.M., Naldi, P., Ollier, W., Page, A., Palotie, A., Pelletier, J., Piccio, L., Pickersgill, T., Piehl, F., Pobywajlo, S., Quach, H.L., Ramsay, P.P., Reunanen, M., Reynolds, R., Rioux, J.D., Rodegher, M., Roesner, S., Rubio, J.P., Rückert, I.M., Salvetti, M., Salvi, E., Santaniello, A., Schaefer, C.A., Schreiber, S., Schulze, C., Scott, R.J., Sellebjerg, F., Selmaj, K.W., Sexton, D., Shen, L., Simms-Acuna, B., Skidmore, S., Sleiman, P.M., Smestad, C., Sørensen, P.S., Søndergaard, H.B., Stankovich, J., Strange, R.C., Sulonen, A.M., Sundqvist, E., Syvänen, A.C., Taddeo, F., Taylor, B., Blackwell, J.M., Tienari, P., Bramon, E., Tourbah, A., Brown, M.A., Tronczynska, E., Casas, J.P., Tubridy, N., Corvin. A., Vickery, J., Jankowski, J., Villoslada, P., Markus, H.S., Wang, K., Mathew, C.G., Wason, J., Palmer, C.N., Wichmann, H.E., Plomin, R., Willoughby, E., Rautanen, A., Winkelmann, J., Wittig, M., Trembath, R.C., Yaouanq, J., Viswanathan, A.C., Zhang, H., Wood, N.W., Zuvich, R., Deloukas, P., Langford, C., Duncanson, A., Oksenberg, J.R., Pericak-Vance, M.A., Haines, J.L., Olsson, T., Hillert, J., Ivinson, A.J., De Jager, P.L., Peltonen, L., Stewart, G.J., Hafler, D.A., Hauser, S.L., McVean, G., Donnelly, P.

and Compston, A., 2011. Genetic risk and a primary role for cell-mediated immune mechanisms in multiple sclerosis. *Nature*, 476(7359), 214–9.

Saxton, W.M. and Hollenbeck, P.J., 2012. The axonal transport of mitochondria. *Journal of Cell Science*, 125(9), 2095–2104.

Schafer, D., Lehrman, E.K., Kautzman, A.G., Koyama, R., Mardinly, A.R., Yamasaki, R., Ransohoff, R.M., Greenberg, M.E., Barres, B.A. and Stevens, B., 2012. Microglia sculpt postnatal neural circuits in an activity and complement-dependent manner. *Neuron*, 74(4), 691-705.

Scherer, S.S. and Wrabetz, L., 2008. Molecular mechanisms of inherited demyelinating neuropathies. *Glia*, 56(14), 1578–89.

Schlegel, A.A., Rudelson, J.J. and Tse, P.U., 2012. White matter structure changes as adults learn a second language. *Journal of Cognitive Neuroscience*, 24(8), 1664–70.

Scholz, J., Klein, M.C., Behrens, T.E. and Johansen-Berg, H., 2009. Training induces changes in white-matter architecture. *Nature Neuroscience*, 12(11), 1370–1.

Schweitzer, J., Becker, T., Schachner, M., Nave, K.-A. and Werner, H., 2006. Evolution of myelin proteolipid proteins: gene duplication in teleosts and expression pattern divergence. *Molecular and Cellular Neurosciences*, 31(1), 161–177.

Scolding, N., Franklin, R.J.M., Stevens, S., Heldin, C.H., Compston, A. and Newcombe, J., 1998. Oligodendrocyte progenitors are present in the normal adult human CNS and in the lesions of multiple sclerosis. *Brain*, 121 (12), 2221–8.

Sereda, M.W., Meyer zu Hörste, G., Suter, U., Uzma, N. and Nave, K.-A., 2003. Therapeutic administration of progesterone antagonist in a model of Charcot-Marie-Tooth disease (CMT-1A). *Nature Medicine*, 9(12), 1533–7.

Setzu, A., Lathia, J.D., Zhao, C., Wells, K., Rao, M.S., ffrench-Constant, C. and Franklin, R.J.M., 2006. Inflammation stimulates myelination by transplanted oligodendrocyte precursor cells. *Glia*, 54(4), 297–303.

Shen, S., Sandoval, J., Swiss, V.A., Li, J., Dupree, J., Franklin, R.J.M. and Casaccia-Bonnefil, P., 2008. Age-dependent epigenetic control of differentiation inhibitors is critical for remyelination efficiency. *Nature Neuroscience*, 11(9), 1024–34.

Shen, S., Li, J. and Casaccia-Bonnefil, P., 2005. Histone modifications affect timing of oligodendrocyte progenitor differentiation in the developing rat brain. *The Journal of Cell Biology*, 169(4), 577–89.

Sherman, D.L. and Brophy, P.J., 2005. Mechanisms of axon ensheathment and myelin growth. *Nature Reviews Neuroscience*, 6(9), 683–690.

Shiau, C.E., Kaufman, Z., Meireles, A.M. and Talbot, W.S., 2015. Differential requirement for irf8 in formation of embryonic and adult macrophages in zebrafish. *PloS One*, 10(1), e0117513.

Shields, S.A., Gilson, J.M., Blakemore, W.F. and Franklin, R.J.M., 1999. Remyelination occurs as extensively but more slowly in old rats compared to young rats following gliotoxin-induced CNS demyelination. *Glia*, 28(1), 77–83.

Shigemoto-Mogami, Y., Hoshikawa, K., Goldman, J.E., Sekino, Y. and Sato, K., 2014. Microglia enhance neurogenesis and oligodendrogenesis in the early postnatal subventricular zone. *The Journal of Neuroscience*, 34(6), 2231–43.

Shintaku, M., Hirano, A. and Llena, J.F., 1988. Increased diameter of demyelinated axons in chronic multiple sclerosis of the spinal cord. *Neuropathology and Applied Neurobiology*, 14(6), 505–510.

Sieger, D. and Peri, F., 2013. Animal models for studying microglia: The first, the popular, and the new. *Glia*, 61(1), 3–9.

Sieger, D., Moritz, C., Ziegenhals, T., Prykhozhij, S. and Peri, F., 2012. Long-range Ca2+ waves transmit brain-damage signals to microglia. *Developmental Cell*, 22(6), 1138–1148.

Sim, F.J., Zhao, C., Penderis, J. and Franklin, R.J.M., 2002. The age-related decrease in CNS remyelination efficiency is attributable to an impairment of both

oligodendrocyte progenitor recruitment and differentiation. *The Journal of Neuroscience*, 22(7), 2451–9.

Simons, M., Misgeld, T. and Kerschensteiner, M., 2014. A unified cell biological perspective on axon-myelin injury. *The Journal of Cell Biology*, 206(3), 335–345.

Smith, K.J., Blakemore, W.F. and McDonald, W.I., 1981. The restoration of conduction by central remyelination. *Brain*, 104(2), 383–404.

Snaidero, N., Möbius, W., Czopka, T., Hekking, L.H., Mathisen, C., Verkleij, D., Goebbels, S., Edgar, J., Merkler, D., Lyons, D.A., Nave, K.-A. and Simons, M., 2014. Myelin membrane wrapping of CNS axons by PI(3,4,5)P3-dependent polarized growth at the inner tongue. *Cell*, 156(1-2), 277–90.

Snyder, D.H, Valsamis, M.P., Stone, S.H and Raine, C.S., 1975. Progressive demyelination and reparative phenomena in chronic experimental allergic encephalomyelitis. *Journal of Neuropathology and Experimental Neurology*, 34(3), 209-21.

Soares, J.M., Marques, P., Alves, V. and Sousa, N., 2013. A hitchhiker's guide to diffusion tensor imaging. *Frontiers in Neuroscience*, 7(31), 1-14.

Stassart, R.M., Fledrich, R., Velanac, V., Brinkmann, B.G., Schwab, M.H., Meijer, D., Sereda, M.W. and Nave, K.-A., 2012. A role for Schwann cell-derived neuregulin-1 in remyelination. *Nature Neuroscience*, 16(1), 48-54.

Stoll, G., Griffin, J.W., Li, C.Y. and Trapp, B.D., 1989. Wallerian degeneration in the peripheral nervous system: participation of both Schwann cells and macrophages in myelin degradation. *Journal of Neurocytology*, 18(5), 671–83.

Suter, U. and Scherer, S.S., 2003. Disease mechanisms in inherited neuropathies. *Nature Reviews Neuroscience*, 4(9), 714–26.

Teitelbaum, D., Arnon, R. and Sela, M., 1997. Copolymer 1: from basic research to clinical application. *Cellular and Molecular Life Sciences*, 53(1), 24–8.

Teitelbaum, D., Meshorer, A., Hirshfeld, T., Arnon, R. and Sela, M., 1971. Suppression of experimental allergic encephalomyelitis by a synthetic polypeptide. *European Journal of Immunology*, 1(4), 242–8.

Tekki-Kessaris, N., Woodruff, R., Hall, A.C., Gaffield, W., Kimura, S., Stiles, C.D., Rowitch, D.H. and Richardson, W.D., 2001. Hedgehog-dependent oligodendrocyte lineage specification in the telencephalon. *Development*, 128(13), 2545–54.

Thöne, J. and Linker, R.A., 2016. Laquinimod in the treatment of multiple sclerosis: a review of the data so far. *Drug Design, Development and Therapy*, 10, 1111–8.

Traka, M., Podojil, J.R., McCarthy, D.P., Miller, S.D. and Popko, B., 2016. Oligodendrocyte death results in immune-mediated CNS demyelination. *Nature Neuroscience*, 19(1), 65–74.

Traka, M., Arasi, K., Avila, R.L., Podojil, J.R., Christakos, A., Miller, S.D., Soliven, B. and Popko, B., 2010. A genetic mouse model of adult-onset, pervasive central nervous system demyelination with robust remyelination. *Brain*, 133(10), 3017–29.

Trapp, B.D. and Stys, P.K., 2009. Virtual hypoxia and chronic necrosis of demyelinated axons in multiple sclerosis. *The Lancet Neurology*, 8(3), 280–91.

Trapp, B.D. and Nave, K.-A., 2008. Multiple sclerosis: an immune or neurodegenerative disorder? *Annual Review of Neuroscience*, 31, 247–69.

Trapp, B.D., Peterson, J., Ransohoff, R.M., Rudick, R., Mörk, S. and Bö, L., 1998. Axonal transection in the lesions of multiple sclerosis. *The New England Journal of Medicine*, 338(5), 278–85.

Ueno, M., Fujita, Y., Tanaka, T., Nakamura, Y., Kikuta, J., Ishii, M. and Yamashita, T., 2013. Layer V cortical neurons require microglial support for survival during postnatal development. *Nature Neuroscience*, 16(5), 543-51.

van Ham, T.J., Brady, C.A., Kalicharan, R.D., Oosterhof, N., Kuipers, J., Veenstra-Algra, A., Sjollema, K.A., Peterson, R.T., Kampinga, H.H. and Giepmans, B.N., 2014. Intravital correlated microscopy reveals differential macrophage and microglial

dynamics during resolution of neuroinflammation. *Disease Models and Mechanisms*, 7(7), 857–69.

van Ham, T.J., Kokel, D. and Peterson, R.T., 2012. Apoptotic cells are cleared by directional migration and elmo1- dependent macrophage engulfment. *Current Biology*, 22(9), 830–6.

Vargas, M. and Barres, A., 2007. Why is Wallerian degeneration in the CNS so slow? *Annual Review of Neuroscience*, 30, 153–79.

Vesterinen, H.M., Sena, E.S., ffrench-Constant, C., Williams, A., Chandran, S. and Macleod, M.R., 2010. Improving the translational hit of experimental treatments in multiple sclerosis. *Multiple Sclerosis*, 16(9), 1044-55.

Voas, M.G., Glenn, T.D., Raphael, A.R. and Talbot, W.S., 2009. Schwann cells inhibit ectopic clustering of axonal sodium channels. *The Journal of Neuroscience*, 29(46), 14408–14.

Voyvodic, J.T., 1989. Target size regulates calibre and myelination of sympathetic axons. *Nature*, 342(6248), 430–3.

Wake, H., Lee, P.R. and Fields, R.D., 2011. Control of local protein synthesis and initial events in myelination by action potentials. *Science*, 333(6049), 1647–51.

Wakselman, S., Béchade, C., Roumier, A., Bernard, D., Triller, A. and Bessis, A., 2008. Developmental neuronal death in hippocampus requires the microglial CD11b integrin and DAP12 immunoreceptor. *The Journal of Neuroscience*, 28(32), 8138-43.

Waxman, S.G., 2006. Axonal conduction and injury in multiple sclerosis: the role of sodium channels. *Nature Reviews Neuroscience*, 7(12), 932–41.

Weil, M.-T., Möbius, W., Winkler, A., Ruhwedel, T., Wrzos, C., Romanelli, E., Bennett, J.L., Enz, L., Goebels, N., Nave, K.-A., Schaeren-Wiemers, N., Stadelmann, C. and Simons, M., 2016. Loss of myelin basic protein function triggers myelin breakdown in models of demyelinating diseases. *Cell Reports*, 16(2), 314–22.

White, R.M., Cech, J., Ratanasirintrawoot, S., Lin, C.Y., Rahl, P.B., Burke, C.J., Langdon, E., Tomlinson, M.L., Mosher, J., Kaufman, C., Chen. F., Long, H.K., Kramer, M., Datta, S., Neuberg, D., Granter, S., Young, R.A., Morrison, S., Wheeler, G.N. and Zon, L.I., 2011. DHODH modulates transcriptional elongation in the neural crest and melanoma. *Nature*, 471(7339), 518-22.

White, R.M., Sessa, A., Burke, C., Bowman, T., LeBlanc, J., Ceol, C., Bourque, C., Dovey, M., Goessling, W., Burns, C.E. and Zon, L.I., 2008. Transparent adult zebrafish as a tool for *in vivo* transplantation analysis. *Cell Stem Cell*, 2(2), 183-9.

White, Y.A.R., Woods, D.C. and Wood, A.W., 2011. A transgenic zebrafish model of targeted oocyte ablation and de novo oogenesis. *Developmental Dynamics*, 240(8), 1929–37.

Wilkinson, R.N., Elworthy, S., Ingham, P.W., and van Eeden, F.J.M., 2013. A method for high-throughput PCR-based genotyping of larval zebrafish tail biopsies. *BioTechniques*, 55, 314-316.

Willer, C.J., Dyment, D.A., Risch, N.J., Sadovnick, A.D., Ebers, G.C. and Canadian Collaborative Study Group, 2003. Twin concordance and sibling recurrence rates in multiple sclerosis. *Proceedings of the National Academy of Sciences of the United States of America*, 100(22), 12877–82.

Williams, A., 2015. Remyelination in multiple sclerosis: what do we know and where are we going? *Neurodegenerative Disease Management*, 5(1), 49-59.

Willis, M.D. and Robertson, N.P., 2016. Alemtuzumab for multiple sclerosis. *Current Neurology and Neuroscience Reports*, 16(9), 84.

Witte, M.E., Bø, L., Rodenburg, R.J., Belien, J.A., Musters, R., Hazes, T., Wintjes, L.T., Smeitink, J.A., Geurts, J.J., De Vries, H.E., van der Valk, P. and van Horssen, J., 2009. Enhanced number and activity of mitochondria in multiple sclerosis lesions. *The Journal of Pathology*, 219(2), 193–204.

Woldeyesus, M.T., Britsch, S., Riethmacher, D., Xu, L., Sonnenberg-Riethmacher, E., Abou-Rebyeh, F., Harvey, R., Caroni, P. and Birchmeier, C., 1999. Peripheral nervous system defects in erbB2 mutants following genetic rescue of heart development. *Genes and Development*, 13(19), 2538–48.

Wolswijk, G., 2002. Oligodendrocyte precursor cells in the demyelinated multiple sclerosis spinal cord. *Brain*, 125(2), 338–49.

Wood, M.D., Kemp, S.W., Weber, C., Borscher, G.H. and Gordon, T., 2011. Outcome measures of peripheral nerve regeneration. *Annals of Anatomy*, 193(4), 321–33.

Woodruff, R. and Franklin, R.J.M., 1999. Demyelination and remyelination of the caudal cerebellar peduncle of adult rats following stereotaxic injections of lysolecithin, ethidium bromide, and complement/anti-galactocerebroside: a comparative study. *Glia*, 25(3), 216–28.

Xiao, L., Ohayon, D., McKenzie, I.A., Sinclair-Wilson, A., Wright, J.L., Fudge, A.D., Emery, B., Li, H. and Richardson, W.D., 2016. Rapid production of new oligodendrocytes is required in the earliest stages of motor-skill learning. *Nature Neuroscience*, 19(9), 1210-7.

Xiao, Y., Faucherre, A., Pola-Morell, L., Heddleston, J.M., Liu, T.L., Chew, T.L., Sato, F., Sehara-Fujisawa, A., Kawakami, K. and López-Schier, H., 2015. High-resolution live imaging reveals axon-glia interactions during peripheral nerve injury and repair in zebrafish. *Disease Models and Mechanisms*, 8(6), 553–64.

Yamasaki, R., Lu, H., Butovsky, O., Ohno, N., Rietsch, A.M., Cialic, R., Wu, P.M., Doykan, C.E., Lin, J., Cotleur, A.C., Kidd, G., Zorlu, M.M., Sun, N., Hu, W., Liu, L., Lee, J.C., Taylor, S.E., Uehlein, L., Dixon, D., Gu, J., Floruta, C.M., Zhu, M., Charo, I.F., Weiner, H.L. and Ransohoff, R.M., 2014. Differential roles of microglia and monocytes in the inflamed central nervous system. *The Journal of Experimental Medicine*, 211(8), 1533–49.

Yeung, M.S., Zdunek, S., Bergmann, O., Bernard, S., Salehpour, M., Alkass, K., Perl, S., Tisdale, J., Possnert, G., Brundin, L., Druid, H. and Frisén, J., 2014. Dynamics of oligodendrocyte generation and myelination in the human brain. *Cell*, 159(4), 766–74.

Young, K., Psachoulia, K., Tripathi, R.B., Dunn, S.J., Cossell, L., Attwell, D., Tohyama, K. and Richardson, W.D., 2013. Oligodendrocyte dynamics in the healthy adult CNS: evidence for myelin remodeling. *Neuron*, 77(5), 873–85.

Yuen, T.J., Johnson, K.R., Miron, V.E., Zhao, C., Quandt, J., Harrisingh, M.C., Swire, M., Williams, A., McFarland, H.F., Franklin, R.J. and ffrench-Constant, C., 2013. Identification of endothelin 2 as an inflammatory factor that promotes central nervous system remyelination. *Brain*, 136(4), 1035–1047.

Zambonin, J.L., Zhao, C., Ohno, N., Campbell, G.R., Engeham, S., Ziabreva, I., Schwarz, N., Lee, S.E., Frischer, J.M., Turnbull, D.M., Trapp, B.D., Lassmann, H., Franklin, R.J.M. and Mahad, D.J., 2011. Increased mitochondrial content in remyelinated axons: implications for multiple sclerosis. *Brain*, 134(7), 1901-13.

Zatorre, R.J., Fields, R.D. and Johansen-Berg, H., 2012. Plasticity in gray and white: neuroimaging changes in brain structure during learning. *Nature Neuroscience*, 15(4), 528–36.

Zawadzka, M., Rivers, L.E., Fancy, S.P., Zhao, C., Tripathi, R.B., Jamen, F., Young, K., Goncharevich, A., Pohl, H., Rizzi, M., Rowitch, D.H., Kessaris, N., Suter, U., Richardson, W.D. and Franklin, R.J.M., 2010. CNS-resident glial progenitor/stem cells produce Schwann cells as well as oligodendrocytes during repair of CNS demyelination. *Cell Stem Cell*, 6(6), 578–90.

Zhang, H., Jarjour, A.A., Boyd, A. and Williams, A., 2011. Central nervous system remyelination in culture - a tool for multiple sclerosis research. *Experimental Neurology*, 230(1), 138–48.

Ziemssen, T., de Stefano, N., Pia Sormani, M., van Wijmeersch, B., Wiendl, H. and Kieseier, B.C., 2015. Optimizing therapy early in multiple sclerosis: An evidence-based view. *Multiple sclerosis and Related Disorders*, 4(5), 460-9.

Zon, L., 2016. Modeling human diseases: an education in interactions and interdisciplinary approaches. *Disease Models and Mechanisms*, 9(6), 597–600.